University of Southampton
Faculty of Life Sciences
School of Biological Sciences

New insights into insulin signalling: The roles of 80K-H, PKCζ and munc18c in GLUT4 vesicle trafficking.

Natalie P. Smithers

Submitted for the qualification of Doctor of Philosophy, February 2008

UNIVERSITY OF SOUTHAMPTON

ABSTRACT

FACULTY OF MEDICINE, HEALTH AND LIFE SCIENCES
SCHOOL OF BIOLOGICAL SCIENCES

Doctor of Philosophy

NEW INSIGHTS INTO INSULIN SIGNALLING: THE ROLES OF 80K-H, PKCζ AND MUNC18C IN GLUT4 VESICLE TRAFFICKING.

By Natalie P Smithers

Insulin is the principal anabolic hormone and is responsible for a vast array of cellular and physiological processes. One of the most fundamental of insulin's actions is the maintenance of glucose homeostasis, primarily ahieved by the selective targeting of the GLUT4 (glucose tansporter 4) vesicle from intracellular stores to the plasma membrane. Insulin triggered signalling cascades activate kinases, notably PKCζ, which influence proteins required for GLUT4 vesicle targeting to the plasma membrane. These vesicle targeting proteins include syntaxin4, VAMP2 and munc18c. Munc18c is thought to preclude interaction between VAMP2, present in the GLUT4 vesicle, and syntaxin4 which is found in the plasma membrane, thus preventing GLUT4 vesicle exocytosis in the basal state. Previously, insulin action was thought to release munc18c from syntaxin4, thus enabling GLUT4 vesicle docking at the plasma membrane. 80K-H forms a complex with PKCζ and munc18c in response to insulin, thus acting as a bridge to enable the cell signalling to affect the GLUT4 vesicle trafficking machinery. In this thesis, a number of in vitro and in vivo techniques, including fluorescence correlation spectroscopy (FCS), were used to determine the nature and role of the protein:protein interactions in GLUT4 vesicle trafficking. The results show that insulin activated PKCζ acts on 80K-H to release it from a membrane tether. This un-tethering of 80K-H causes a repositioning of munc18c on syntaxin4. It is this repositioning of munc18c, rather than the release of this protein from syntaxin4, that enables VAMP2 to bind syntaxin4 thus facilitating the docking of the GLUT4 vesicle at the plasma membrane. This is the first time that it has been shown that munc18c isn't merely released from syntaxin4 in response to insulin. These results further elucidate the molecular mechanisms of insulin action, which will hopefully lead to treatments for diseases such as Type II diabetes in the future.

Contents

FIGURES

TABLES

Table 1: Diffusion coefficients for MFL pg 261

APENDICES

Apendix 1. Biochemical Journal Immediate Publication. Published on 24 Oct 2007 as manuscript BJ20070802. "Insulin triggered repositioning of munc18c on syntaxin-4 in GLUT4 signalling." Natalie P. Smithers, Conrad P. Hodgkinson, Matt Cuttle, Graham J. Sale.

Acknowledgements

Thank you to my superviser, Graham Sale.

Thank you so much to my mum and dad, who are most deffinately the best mum and dad in the world! Thanks for all the guidance, support and enthusiasm throughout both my undergraduate and postgraduate degrees. And thanks also to the most generous Royal Bank of Ma and Pa, without which I would be living under the bench in the lab! THANK YOU!!!

A massive great big thank you to Dr Conrad Hodgkinson, for his fantabulous supervision and great friendship throughout my PhD. I feel privilaged to have been able to get to know and work with him and wouldn't have a PhD if it wasn't for him! THANK YOU!!!!! Hope you enjoyed it as much as I did! (.....Why?!?!! Why, why, why?!!!)

Thank you to my gran for the support and encouragement....both emotionally and financially! Thank you!

A big thank you to Dr Steven Harrision.....for making the years spent doing my PhD so much fun.....and also for all the help, advice and intellectual stimulation! You're a genius! Thanks for keeping me grounded! And thanks for all the giggles!

Thanks to Dr Ann Mander for persuading me to do a PhD in the first place. Doing my 3rd year undergraduate project with you was a turning point. I wouldn't have even considered doing a PhD (or a career in research for that matter!) if it wasn't for Ann. Thank you.

Thank you to Dr Matt Cuttle for his help with the microscopy, for the hours and hours spent in the microscopy room hoping for the perfect FCS graph!

Thank you to Shaggy for looking after me!

Thank you to BBRSC for the lovely funding!

Abbreviations

ADP = adenosine diphosphate
ATP = adenosine triphosphate
AGEs = advanced glycation endproducts
CAP = Cbl associated protein
CFP = cyan fluorescent protein
ECFP = enhanced cyan fluorescent protein
ER = endoplasmic reticulum
YFP = yellow fluorescent protein
EYFP = enhanced yellow fluorescent protein
GFP = green fluorescent protein
GLUT4 = glucose transporter 4
IRS = insulin receptor substrate
PB1 domain = Phox and Bem1 domain
PDK1 = phosphoinositide dependent kinase 1
PH = plekstrin homology
PI3K = phosphatidylinositol-3-kinase
PIP_2 =phosphatidylinositol-4, 5-bisphosphate
PIP_3 = phosphatidylinositol-3, 4, 5-trisphosphate
PKB protein kinase B
PKC = protein kinase C
PTB = phosphotyrosine binding
SH2 = Shc homology 2
SH3 = Shc homology 3
siRNA = small interfering RNA
SM family of proteins = Sec1/Munc18 family of proteins
SNAP = soluble NSF attachment protein
SNARE = SNAP receptor
t-SNARE = target SNARE
VAMP2 = vesicle-associated membrane protein-2
v-SNARE = vesicle SNARE
SOEing = Splicing by overlap extension
IDDM = insulin dependent diabetes mellitus
NIDDM = non-insulin dependent diabetes mellitus
FFAs = free fatty acids
TNFα = tumour necrosis factor alpha
IL-6 = interleukin 6
DNA = deoxyribonucleic acid
RNA = ribonucleic acid
PBS = phosphate buffered saline
APS domain = adapter containing plekstrin homology domain
CHO cells = Chinese hamster ovary cells
SoHo domain = Sorbin homology domain

GDP = guanosine diphosphate
GTP = guanosine triphosphate
VASAP60 = Vacuolar system-associated protein-60
HDEL = His-Asp-Glu-Leu ER retrieval signal
FGF = fibroblast growth factor
KIF = kinesin superfamily
KAPs = kinesin-associated proteins

INTRODUCTION

1. INTRODUCTION

1.1. Overview of the Actions of Insulin

Insulin is the key anabolic hormone, and is responsible for a complex array of cellular and physiological processes. The effects of insulin are broad in scope, involve numerous organs and intracellular pathways, and are critical to metabolism. Insulin promotes the synthesis and storage of carbohydrates, lipids, and proteins, whilst inhibiting their degradation and release into the circulation (please refer to table 1.1 and figure 1.1.) It does this by stimulating the uptake of glucose, fatty acids, and amino acids into cells, and increasing the expression or activity of enzymes that catalyze glycogen, lipid, and protein synthesis, while inhibiting the activity or expression of those that catalyze their degradation. Insulin exerts these effects on muscle, adipose and liver cells, by triggering a complex array of signalling cascades, upon binding to its receptor. These signalling pathways ultimately lead to the phosphorylation or dephosphorylation (causing activation or deactivation) of key metabolic enzymes, and the production of mitogenic signals and transcription factors.

In the fasting state, insulin secretion is reduced and the body starts to mobilize the available food stores. Whilst fasting, approximately 90% of the glucose in the circulation is produced by the liver by both glycogenolysis and gluconeogenesis. Lipolysis is increased in adipose tissue to cause the release of free fatty acids from triacylglycerols. These free fatty acids can then be utilised by the liver and muscle in order to conserve glucose for use by the brain. Conversely, in the postprandial state, insulin is secreted from the pancreas so that the body can store the available energy supplies. The hepatic glucose output is suppressed in order to help limit the rise in plasma glucose levels, whilst glycogenesis is increased to enable the liver to store the glucose as glycogen. Insulin induces a rapid and dramatic increase in glucose uptake in liver, muscle and adipose cells. This occurs due to the insulin mediated translocation of the GLUT4 glucose transporter from intracellular stores to the plasma membrane, the mechanics of

which are the main focus of this thesis. For the actions of insulin on the metabolism in liver, muscle and adipose tissues, please refer to Table 1.1 and Figure 1.1.

	Liver	Muscle	Adipose
Stimulation of glucose uptake		✓	✓
Stimulation of cellular respiration	✓	✓	✓
Stimulation of glycogenesis	✓	✓	
Inhibition of glycogenolysis	✓	✓	
Stimulation of amino acid uptake		✓	
Stimulation of protein synthesis	✓	✓	✓
Inhibition of protein degradation	✓	✓	✓
Stimulation of fatty acid and triglyceride synthesis	✓		✓
Inhibition of lipolysis	✓		✓
Stimulation of lipoproteins uptake			✓

Table 1.1. Effects of insulin on liver, muscle and adipose.

Table showing the major actions of insulin on liver, muscle and adipose.

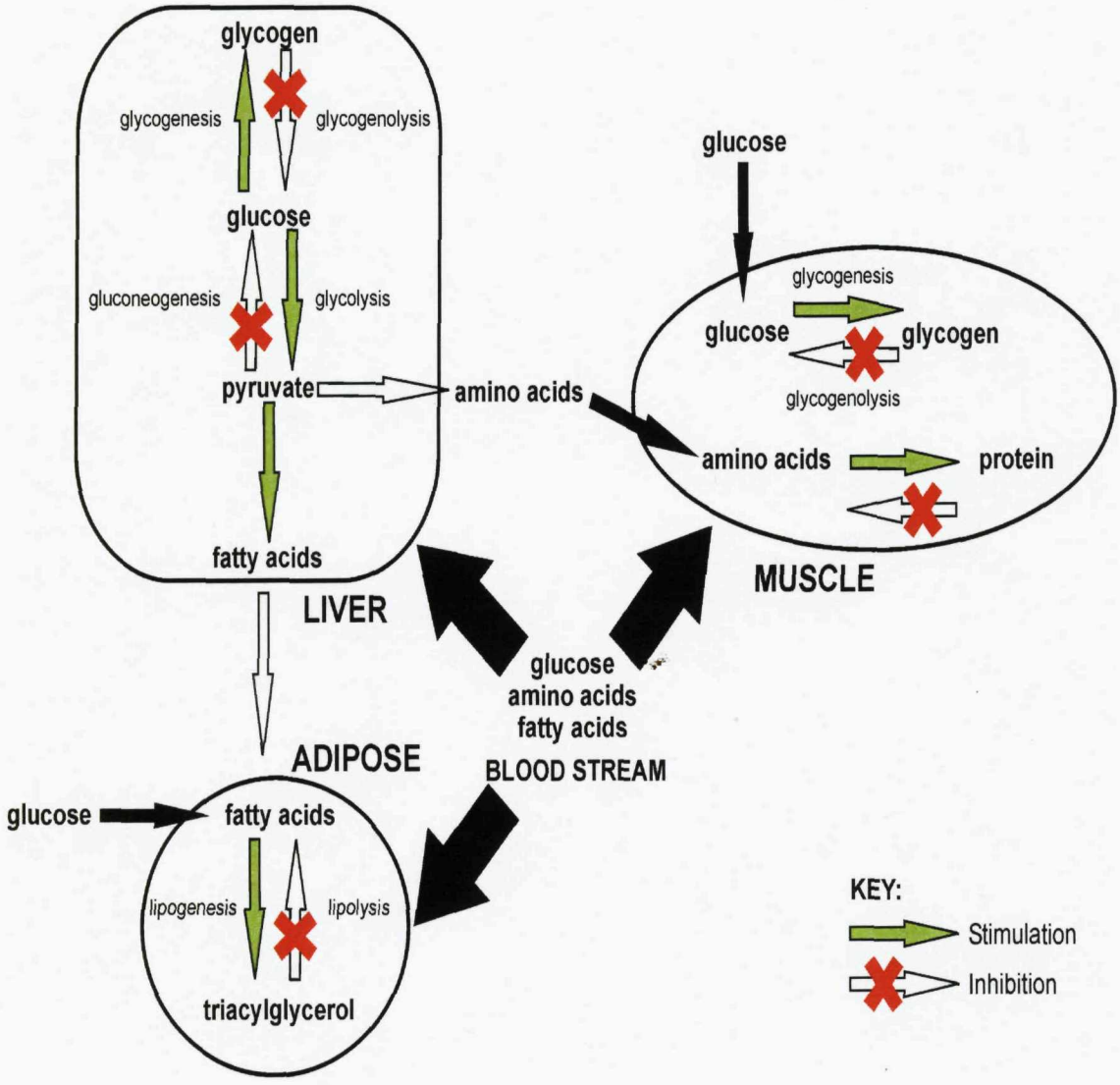

Figure 1.1. Effects of insulin on whole body metabolism

Insulin is the principle anabolic hormone. It causes the body to store available energy sources (glucose, fatty acids and amino acids) as glycogen, triglycerides and proteins.

1.2. Diabetes

1.2.1. Overview

Meticulous physiological control of glucose homeostasis ensures that plasma glucose concentrations are maintained between tight limits (between 4-7 mM in humans.) Deviations from this narrow range can have severe consequences. Low blood glucose levels can lead to seizures, coma and death, whilst prolonged high blood glucose levels (as occurs in diabetes) leads to complications such as renal failure, neuropathy, blindness and cardiovascular disease [Watson et al. 2004]. Diabetes Mellitus is not a single disease, but rather a family of diseases with the same outcome: an inability of the body to utilize glucose, resulting in dramatically and persistently high blood glucose levels. Type 1 diabetes results from complete insulin deficiency, usually as a result of autoimmune destruction of the β-cells of the islets of Langerhans. Type 2 diabetes (which accounts for ~90% of all cases) occurs when some kind of insulin defect means that the body cannot efficiently stimulate glucose uptake into muscle and fat. Whatever the exact cause of the diseased state, the outcomes are the same with severe consequences on whole body metabolism. The failure of normal insulin action causes an accumulation of glucose in the blood, with blood glucose levels exceeding 30 mM if left untreated. The cells become starved of nutrients, triggering metabolic responses similar to those seen when fasting. Gluconeogenesis is stimulated in the liver, the increased hepatic glucose production further escalating blood glucose levels. Most of the substrates for the increased rate of gluconeogenesis come from amino acids formed from uninhibited proteolysis of muscle proteins. Consequently, untreated diabetics loose a substantial amount of weight, despite consuming an adequate diet. The cells of the body attempt to generate usable energy sources by mobilizing fat stores through increased lipolysis. Uninhibited lipolysis and ketogenesis increase the levels of free fatty acids and strong carboxylic acids (acetoacetic and β-OH-butyric acids) in the blood, which may lead to blood pH levels falling below 6.8 and death from diabetic ketoacidosis. Such excessive concentrations of glucose in the blood generate other metabolic problems. When blood glucose levels exceed 10 mM, the kidneys are no longer able to reabsorb all of the glucose from the blood filtrate. This

means that an excessive amount of glucose remains in the urine. This creates an osmotic load and causes a large amount of water to be excreted as well, leading to severe dehydration.

Other long term medical complications that arise from diabetes include progressive neuropathy [Said 2007], retinopathy leading to blindness [Neely et al. 1998], nephropathy leading to chronic renal failure [Forbes et al. 2007] and atherosclerotic cardiovascular disease leading to stroke, myocardial infarction, and (in some cases) sudden death [Goldberg and Dansky 2006]. The major cause of these complications is the uncontrolled glycosylation of proteins [Nawale et al. 2006] and lipids [Actis Dato and Rebolledo 2000] due to the excessive amounts of glucose in the circulation. Prolonged hyperglycaemia causes the production of AGEs (advanced glycation endproducts) formed from the non-enzymatical glycosylation and oxidation of lipids and proteins [Sato et al. 2006]. The reaction that forms the AGEs is irreversible, so the AGEs accumulate in the vasculature, altering and perturbing cell structure and function and leading to the medical complications described above [Soldatos and Cooper 2006, Tan et al. 2007, Yamagishi et al. 2006, Yamagishi et al. 2007]

1.2.2. Type 1 Diabetes Mellitus

Type 1 Diabetes Mellitus, also referred to as juvenile onset diabetes or dependent diabetes mellitus (IDDM) often manifests itself in children and young adults. It is caused by a marked failure of the β islet cells of the pancreas to produce or release insulin. The cause of progressive pancreatic β-cell failure is not completely understood, but the most frequent cause of this is the autoimmune destruction of the β cells of the islets of Langerhans. This usually results from a genetic vulnerability that initiates the destructive autoimmune process, but it also appears to result from a number of factors, including chronic inflammation, glucotoxicity and the deleterious effects of elevated levels of free fatty acids on β-cell function. The only effective treatment of the disease is subcutaneous administration of insulin, hence the frequent designation of this form as insulin dependent diabetes mellitus (IDDM.) Patients control their blood glucose levels by injecting

modified insulin preparations at suitable times throughout the day, coupled with meticulous control of diet and exercise.

1.2.3. Type 2 Diabetes Mellitus

Type 2 diabetes, or maturity onset diabetes, tends to manifest itself in adults, especially if obese. The distinction between type 1 and type 2 diabetes and especially between type 2 diabetes and glucose intolerance/insulin resistance is often blurred. Very often, patients will first develop glucose intolerance/insulin resistance which eventually leads to type 2 diabetes. Type 2 diabetes is a metabolic disorder that results from complex interactions of multiple factors and is defined by an impaired glucose uptake and increased blood glucose levels. Sometimes this may occur due to decreased secretion of insulin by the pancreas, but often there is significant secretion of insulin, but for reasons not fully understood, this insulin is not fully effective. Type 2 diabetes may occur due to genetic mutations in the insulin or insulin receptor, faults in the regulation of insulin secretion from the β-islet cells or faults within the insulin signalling mechanisms which render the cells resistant to the effects of insulin. The development of type 2 diabetes often begins with cells becoming slightly less sensitive to the effects of insulin. This is known as glucose intolerance or insulin resistance. Early in the pathogenesis of glucose intolerance, the insulin-producing β cells are able to compensate for the cellular insulin resistance by increasing the amounts of insulin secreted. This compensatory hyperinsulinemia is able to maintain blood glucose levels in the normal range. Progression to type 2 diabetes occurs when this compensatory cell response fails to produce enough insulin required to maintain normal blood glucose levels. Often such increases in insulin secretion cause gradual deteriation of the pancreatic β cells, which further exacerbates the problem. Patients control their blood glucose levels by using one or more of a number of oral anti-diabetic treatments (see section 1.2.5), coupled with meticulous control of diet and exercise. Subcutaneous insulin treatment may also be used and is becoming increasingly popular.

1.2.4. Obesity

Obesity is a major worldwide health problem. It has reached epidemic proportions and remains to be on a steady yet dramatic increase. There are currently few European countries with obesity rates below 10%, with many reaching as high as 20%. The greatest increase in obesity rates in Europe were noted in England where obesity rates rose three-fold from 1980 to 2001 (with levels of morbid obesity increasing three-fold among men and doubling among women during the 1990s). In the United States, obesity affects a third of all adults, more than double the rate of 20 years ago. However, it is not just Western civilisation that is affected from increasing levels of obesity. Globally, more than 1.1 billion people are estimated to be overweight, with more than 320 million of these calculated to be obese. The International Obesity Task Force (IOTF) estimates that up to 1.7 billion people may be exposed to weight-related health risks and more than 2.5 million deaths each year are attributed to higher BMI*, a figure that is expected to double by the year 2030.

[* The body mass index (BMI) is globally used as a practical marker to assess obesity. It is calculated by dividing the weight in kilograms by the square of height in metres (kg/m^2). A BMI above 25 is classified as overweight, above 30 classified as obese and above 40 as morbidly obese.]

Source: World Health Organisation. Obesity: Preventing and Managing the Global Epidemic. Technical Report Series no. 894. WHO, Geneva, 2000.

Obesity is usually the result of a combination of factors, both genetic and environmental. Humans have developed inappropriate lifestyles, with diets rich in fats, high in calorific content and low in fibre. This, coupled with the lack of regular physical activity, is responsible for the levels of obesity seen in today's world. There is a close association between obesity and various vascular and metabolic diseases. These include type 2 diabetes, cardiovascular disease, hypertension and dislipidemia. It is widely believed that

the link between obesity and the above diseases is insulin resistance. The strong link between insulin resistance (and associated diseases) and obesity has been recognised for decades. In Western countries approximately 90% of cases of type 2 diabetes are attributable to weight gain [Diabetes Atlas 2nd Edition © international task force 2003]. Numerous studies (using animal models and humans) have shown a link between obesity and the development of diabetes [Bloomgarden 2000, Felber & Golay 2002, Finegood 2003]. So, how does obesity lead to insulin resistance and diabetes? The excess adipose tissue in the obese individual is to blame. Adipocytes are one of the most insulin responsive of cells. Not only are they responsible for the storage of energy in the form of triglycerides, but they also secrete a number of cytokines, peptides and free fatty acids (FFAs) that have local and widespread effects on glucose and lipid metabolism. In particular, cytokines such as tumour necrosis factor alpha (TNFα), interleukin (IL)-6, resistin and leptin are released by adipose tissue and have been shown to desensitize cells (most notably muscle) to the effects of insulin. [Kahn & Flier 2000, Pittas et al. 2004, Greenberg & McDaniel 2002]. Additionally, excessive adipose tissue has been associated with decreased levels of adiponectin, which has been shown to increase sensitivity of muscle and fat to insulin. The large excess of adipose tissue in the obese hence causes the body to be less sensitive to the effects of insulin, ultimately leading to insulin resistance and diabetes. It is this obesity-induced insulin resistance which is to blame for many of the other health defects associated with obesity, including cardiovascular disease. With the increase of diabetes, obesity and other related diseases hitting epidemic proportions, there is now more focus on their causes and effects than ever before and a greater need for research into the molecular mechanisms underlying them.

1.2.5. Treatments for Type 2 Diabetes

The number of different drugs available for treating type 2 diabetes has grown enormously over the last 10 years. The ever expanding population of overweight, obese and diabetics has spurred the pharmaceutical companies into spending billions of dollars

on the development of new therapies to treat these diseases. There are three ways in which these drugs work to improve glycaemic control:

1.) By increasing insulin secretion
These drugs are insulin secretagogues. Examples include the sulfonylureas. [Zimmerman 1997.]
2.) By increasing insulin action
These drugs are insulin sensitizers. Examples include biguanides [Kirpichnikov et al. 2002] and thiazolidinediones (TZDs) [Diamant and Heine 2003].
3.) By decreasing insulin need. These drugs are inhibitors of glucose absorption. Examples include the alpha-glucosidase inhibitors [Brewer 2006].

Despite the continual improvement of current therapies, these drugs still have a number of unpleasant short and long term side effects and more still needs to be done to research future therapies.

1.3. Models for researching insulin signalling and diabetes

There are a number of different animal models used for studying various aspects of diabetes and insulin action. However, most of our knowledge of the molecular mechanisms that govern insulin induced events comes from the use of cell lines. The two most widely used are 3T3-L1 adipocytes (mouse) and L6 myotubes (rat). These give a good representation of the responses of fat and muscle respectively. 3T3-L1 adipocytes have become the "gold standard" for studying insulin action, in particular GLUT4 mediated glucose uptake, showing up to a 10-fold increase in insulin stimulated glucose uptake. Although these cells give the best depiction of insulin's actions, they are often difficult to work with, mainly due to the difficulties encountered when trying to introduce DNA or inhibitory compounds into them. The other cell type used to study the actions of insulin is Chinese Hamster Overy (CHO) cells. CHO cells are responsive to insulin, but do not express the GLUT4 protein. CHO cells stably expressing the GLUT4 protein are often used as an alternative to 3T3-L1 adipocytes and show an insulin mediated

translocation of the GLUT4 protein to the plasma membrane and a corresponding increase in glucose uptake [Hodgkinon et al 2005]. However, the GLUT4 storage vesicle is less defined from the ER in these cells and they may lack various specialised cellular machinery found in the naturally GLUT4 expressing 3T3-L1 adipocytes.

1.4. The Insulin Receptor

Insulin exerts its actions by binding to the insulin receptor, found mainly on adipose and muscle cells. The insulin receptor is a transmembrane tyrosine kinase receptor, formed of 2 α, and 2 β subunits, disulphide linked into a $\alpha_2\beta_2$ heterotetrameric complex (see figure 1.2). Insulin binding to the α subunits activates the kinase activity of the β subunits, initiating their autophosphorylation and consequent activation of the insulin receptor. Once activated, the receptor is able to recruit numerous docking and signalling proteins, through the interaction of their SH2, SH3, or PTB (phosphotyrosine binding) domains, with the phosphorylated tyrosine residues on the receptor. Examples of these docking and signalling proteins are the IRS proteins which are discussed in section 1.5.2.2.1, and c-Cbl, which is discussed in section 1.5.2.3. Once these proteins are recruited, they themselves are activated by either tyrosine phosphorylation or induction of a conformational change, enabling the continuation of the signal to other proteins. The involvement of so many proteins and the inter-linking of different pathways provide insulin with the means to control such diverse cellular functions. Often the activation of more than one signal is required for a single effect within the cell. The phosphorylation state of proteins within these pathways is the key regulator of their activity, and controls the progression of a signal along its course. The phosphorylation and dephosphorylation of proteins must therefore be exquisitely controlled in order to maintain normal functioning of the signalling pathways. This is mediated by kinases (responsible for phosphorylations) and phosphatases (responsible for dephosphorylations).

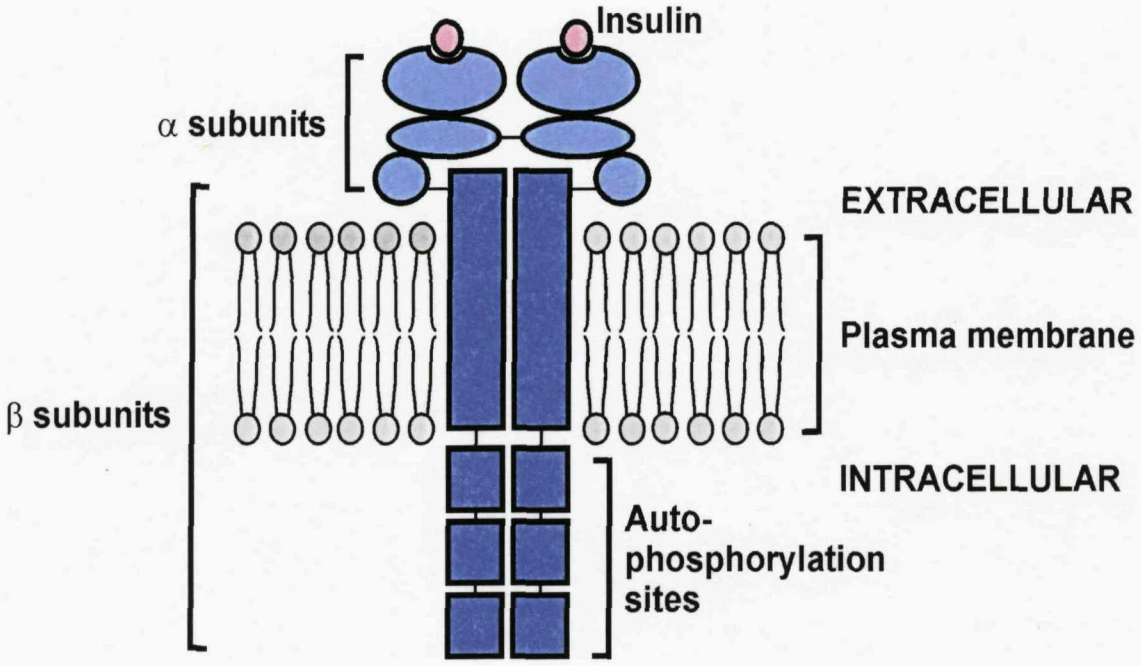

Figure 1.2. The Insulin Receptor

The insulin receptor consists of two α and two β subunits disulphide linked into an $\alpha_2\beta_2$ heterotetrameric complex. The extracellular α subunits contain the insulin binding domains, whilst the transmembrane β subunits contain the tyrosine kinase domains responsible for the autophosphorylation and activation of the receptor. Autophosphorylation of the β subunits provides the phosphorylated tyrosine residues essential for the docking of downstream signalling proteins

1.5. GLUT4 Vesicle Translocation

1.5.1. The GLUT4 Storage Compartment

Glucose is cleared from the bloodstream by facilitated diffusion through hexose transporters known as GLUT proteins. The GLUT family encompasses a wide variety of proteins (there are currently known to be 13 members of the GLUT family) in order to meet the specific metabolic needs of the various tissues of the body. Each of the GLUTs are highly related to each other, with 12 transmembrane spanning domains. Most is known about the Class I GLUT proteins which include GLUTs 1, 2, 3 and 4. GLUT1 is

constitutively expressed, and responsible for the low level of basal glucose uptake required for primary cellular functions. GLUT2 is present in liver, intestine, kidney and pancreatic β-cells, and functions to absorb glucose into the epithelia of the intestine, and as a glucose sensor system to the β-islet cells. GLUT3 is found mainly in neurons where (together with GLUT1) it functions to allow glucose to cross the blood-brain barrier. GLUT4 is the most characterized of the GLUT proteins. It is found primarily in adipose tissue and striated muscle, where it facilitates glucose uptake in an insulin-responsive manner. Unlike most other GLUT proteins, GLUT4 is found in specialized intracellular membrane compartments. In the basal state, more than 95% of the cell's GLUT4 protein is contained within these storage compartments. Upon insulin stimulation, there is a dramatic accumulation of GLUT4 protein at the plasma membrane, caused by a 10-20-fold increase in the rate of GLUT4 exocytosis, and a small decrease in GLUT4 endocytosis (see figure 1.3). This highly organized and complex trafficking of GLUT4 vesicles is orchestrated by the signalling pathways emanating from the activated insulin receptor. However, the exact mechanisms underlying the targeting, mobilization and redistribution of the GLUT4 vesicles still remain to be fully elucidated.

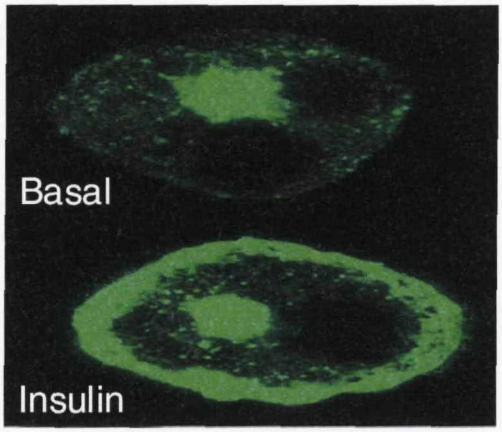

Figure 1.3. Cellular distribution of GLUT4 in the basal and insulin stimulated states

The picture shows adipocytes overexpressing GFP-tagged GLUT4. In the basal state (shown in the top section of the diagram) the GLUT4 is mainly found in intracellular storage compartments. Upon insulin stimulation (shown in the bottom section of the diagram) the GLUT4 is predominantly found at the plasma membrane.

1.5.2. The Insulin Signalling Pathway

1.5.2.1. Overview

As mentioned, the insulin receptor is a transmembrane tyrosine kinase receptor. Insulin binds to the extracellular α subunits. This induces a conformational change in the receptor that allosterically regulates the intrinsic catalytic activity of the kinase domain in the transmembrane β-subunits. Activation of, and subsequent trans-phosphorylation of the β-subunits provides docking sites for a number of downstream scaffolding and adaptor proteins. These adaptors are then able to recruit and/or activate further downstream signalling proteins. This provides the insulin receptor with the potential to activate a huge number of intricate and interlinking signalling pathways, which explains the complexity of this hormones action. Here I will just focus on two separate signalling pathways and their role in GLUT4 vesicle translocation to the plasma membrane. The first is the PI3K signalling pathway, and the second is the less well characterized TC10 pathway.

1.5.2.2. The PI3K Pathway

1.5.2.2.1. The Insulin Receptor Substrates

Phosphorylation of the β-subunits of the insulin receptor in response to insulin provides docking sites for the insulin receptor substrate (IRS) proteins. These are scaffolding proteins that play a fundamental role in insulin signalling. Although they themselves have no catalytic activity, their docking at the insulin receptor enables the necessary recruitment and regulation of various downstream signalling proteins. Four members of this family have been identified to date (IRS-1,-2,-3 and -4). All share a similar structure, but differ in their tissue distribution, subcellular localisation, and binding affinities for downstream proteins. All have a conserved plekstrin homology (PH) domain at the N-

terminus, followed by a phosphotyrosine binding (PTB) domain and a C-terminal domain containing several conserved tyrosine phosphorylation sites. The PTB domain interacts with the NPXYp motif of the active insulin receptor [Hers, I. et.al. (2002)]. This interaction enables tyrosine phosphorylation of the IRS proteins, providing docking sites for downstream proteins with Shc homology 2 (SH2) domains. One of the most important of these is a lipid kinase called PI3K (Phosphatidylinositol-3-Kinase).

1.5.2.2.2. PI-3-Kinase

PI-3-Kinase has a multifaceted and extensively characterised involvement in insulin action. Extensive experimental evidence (using the PI3K inhibitors wortmanin or LY29004, as well as the use of over-expression or dominant negative strategies) shows the requirement for this kinase in many effects of insulin, including GLUT4 translocation/glucose transport [Watson et al. 2004/ Tsakiridis et al. 1995/ Frevert et al.1997]. PI3K is composed of 2 subunits: the p85 regulatory subunit, and the p110 catalytic subunit. PI3K catalyses the phosphorylation of the 3'-OH moiety of membrane inositol phospholipids. Although it can phosphorylate several phospholipids, the most significant is the phosphorylation of phosphatidylinositol-4,5-bisphosphate (PIP_2) to generate phosphatidylinositol-3,4,5-trisphosphate (PIP_3). PIP_3 is a 2nd messenger produced by insulin stimulation, which is crucial for regulation of the downstream signalling proteins. Insulin stimulation results in tyrosine phosphorylation of the IRS proteins by the insulin receptor. These generate docking sites for the SH2 domains of the regulatory p85 subunit, which recruits the catalytic p110 subunit to the plasma membrane. This brings it into the vicinity of its primary substrate, PIP_2, therefore enabling the generation of PIP_3 at the plasma membrane (see figure 1.4.).

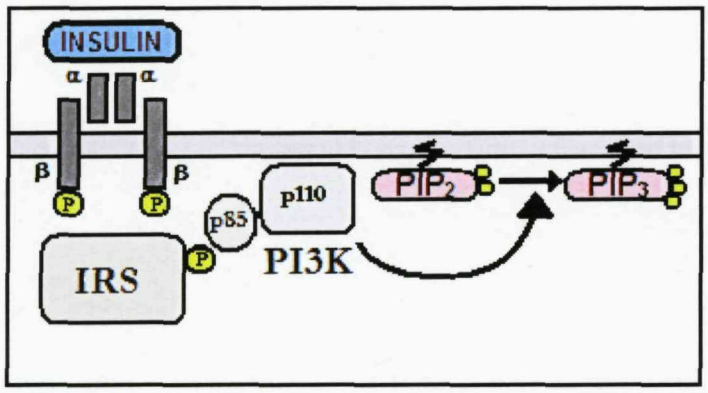

Figure 1.4. Insulin activation of the PI3K pathway

Insulin activation of the insulin receptor causes the tyrosine phosphorylation of the β subunits of the receptor. These phosphorylated tyrosines are docking sites for the insulin receptor substrates (IRS) which are then also phosphorylated. The p85 subunit of PI3K can then bind to IRS via its SH2 domain. This activates the p110 catalytic subunit of PI3K so that it can phosphorylate PIP_2. The PIP_3 produced then activates a number of downstream signalling proteins including PKB and PKCζ.

As mentioned, the production of PIP_3 is necessary for activation of downstream AGC kinases, two of the most important of which are Protein Kinase C Zeta (PKCζ) and Protein Kinase B (PKB). PIP_3 plays more than one role in activation of downstream proteins. Firstly, PIP_3 recruits proteins (such as PKB and PKCζ) to the plasma membrane through interaction with their PH domains. This brings them into the correct localisation for activating/activation by other signalling proteins. Secondly, the binding of PIP_3 to the AGC kinases induces a conformational change that enables them to be phosphorylated and activated by the kinase PDK1 (Phosphoinositide dependent kinase 1) [Milburn et al. 2003]. PIP_3 also binds to PDK1, but it is thought that this only activates PDK1 indirectly, colocalising it with its substrates [Currie et al. 1999].

1.5.2.2.3. Protein Kinase B

Protein Kinase B (PKB, also known as Akt) is a serine/threonine kinase shown to be rapidly activated in response to insulin. It has been shown to play important roles in both the long and short term effects of this hormone, though the exact mechanisms of its actions still remain to be clarified [Hanada et al. 2004/ Watson et al. 2004]. There are 3 isoforms of this kinase, PKBα, β and γ, all of which are activated by insulin. The generation of PIP_3 by insulin recruits PKB to the plasma membrane through specific interactions with its amino terminal PH domain. Once at the plasma membrane, PKB is activated by phosphorylation of two key residues, threonine 308 (T308) and serine 473 (S473). T308 is phosphorylated by PDK1 (as mentioned above) whilst the candidate for phosphorylating S473 remains to be identified. Possibilities include autophosphorylation and phosphorylation by a putative kinase, PDK2. Once both of these residues have been phosphorylated, PKB is fully active and can dissociate from the plasma membrane in order to phosphorylate its substrates. Extensive experimental evidence supports a role for PKB in GLUT4 translocation and glucose transport, and siRNA and mouse models show PKBβ to be the dominant isoform involved in glucose transport [Zhou et al. 2004)/ Watson et al. 2004].

1.5.2.2.4. PKCζ

1.5.2.2.4.1. Overview of the Protein Kinase C family

The Protein Kinase C family is a large family of serine/threonine kinases shown to play a role in a diverse number of cell signalling events including cell growth, differentiation, apoptosis, cell migration, cell polarity and metabolism and have been linked to a wide variety of pathological states including diabetes (and it's associated secondary complications), cancer, Alzheimer's disease, leukaemia and stroke [Chou and Messing 2005]. The Protein Kinase C family is divided into three major categories, based upon their

structurally distinct N-terminal regulatory domains: the conventional (consisting of α and β), novel (consisting of δ, ε, η, and θ) and atypical (consisting of λ/ι and ζ). The basic PKC structure consists of an N-terminal regulatory domain and a C-terminal catalytic domain. The regulatory domain consists of a pseudosubstrate domain, which blocks the substrate binding cavity of the kinase domain in an autoinhibitory fashion. There are also either one or two types of membrane targeting domains called C1 and C2. The C1 domain binds diacylglycerol or phorbol esters (potent functional analogues of diacylglycerol) whilst the C2 domain binds Ca^{2+} and acidic phospholipids. The highly conserved catalytic domain contains the C3 and C4 motifs required for ATP and substrate binding and catalytic activity. The kinase domain includes an ATP-binding region, an activation loop, a turn motif and a hydrophobic motif.

Activation of PKC family members requires release of the autoinhibitory pseudosubstrate domain from the catalytic core. The cellular and molecular processes that cause this release are highly complex. All of the PKC isoforms are activated by two or three consecutive phosphorylations in the catalytic domain, the sites for which are conserved amongst the family members. Both conventional and novel isoforms are activated by diacylglycerol, but only the former is sensitive to Ca^{2+}. The atypical PKCs lack a C2 domain and are activated by neither Ca^{2+} nor diacylglycerol, but are instead activated by a distinct set of phospholipid cofactors. They also contain a PB1 domain which binds to other PB1 domain-containing proteins and functions to regulate atypical PKC activity.

Protein kinase C is normally found within the cytosol and has little affinity for membranes. Activation of signalling pathways causes the generation of diacylglycerol, anionic phospholipids such as phosphatidylserine and various other phospholipid signalling molecules such as PIP_3. These activate PKCs in two ways. Firstly, their high affinity binding to the regulatory domain of PKCs induces a conformational change which causes the release of the pseudosubstrate from the active site of the enzyme. Secondly, the production of these signalling lipids causes a dramatic increase in PKC's affinity for membranes, resulting in the translocation of the enzyme to the site of the substrates at the plasma membrane. Additional interactions with proteins that bind protein

kinase C (for example via the PB1 domain of the atypical PKCs) may target the enzyme to specific membrane locations. Ca^{2+} causes activation of the conventional PKCs by increasing the affinity of PKC for anionic phospholipids.

The insulin responsive cell types, namely muscle, fat and liver, have been shown to express PKC isoforms from each of the conventional, novel and atypical categories. PKCs α, βI, βII, δ, ε, θ, ζ and λ/ι have all been shown to be activated by insulin or conditions important for effective insulin stimulation and have been shown to mimic or modify insulin's actions in one form or another. However, it is the atypical PKCs for which most comprehensive evidence has been found to link them to insulin mediated glucose transport.

1.5.2.2.4.2. The atypical Protein Kinase C family

The atypical Protein Kinase C (aPKC) subfamily includes PKCζ and PKCι/λ (PKCι is the human ortholog and PKCλ the mouse ortholog and the two share over 98% sequence homology). Much of the evidence linking the aPKCs to insulin-mediated events have shown that PKCζ and PKCλ/ι are highly interchangeable. This is likely due to the high degree of homology in the functional regions of the aPKCs in mouse, rat and human tissues, which also highlights the necessity and importance of the aPKCs in evolution. However, experimental evidence points towards PKCζ as the dominant isoform in insulin-mediated glucose transport and GLUT4 vesicle trafficking and is the focus of this study.

As shown in figure 1.5., as with the other PKCs, PKCζ consists of a regulatory domain consisting of the pseudosubstrate domain and a single C1 domain. It also contains the PB1 domain which is responsible for protein:protein interactions so critical for many of PKCζ's functions. The kinase domain includes an ATP-binding region, an activation loop, a turn motif and a hydrophobic motif. The ATP-binding region contains a Lysine residue crucial for catalytic activity (Lys-281), and the activation loop and turn motif

contain Threonine residues whose phosphorylation are crucial for PKCζ's catalytic activity (Thr-410 and Thr-560 respectively.) Unlike conventional or novel PKC isoforms, the atypical PKCs are not activated by diacylglycerol and lack PH domains, but are however activated by PIP_3. PIP_3 binds directly to the pseudosubstrate domain to relieve the autoinhibition. PIP_3 also activates PKCζ indirectly through PDK1, which phosphorylates Thr-410 in the activation loop [Chou et al. 1998/ Le Good et al. 1998/Braiman 2001]. Phosphorylation of this Thr-410 residue has been shown to be critical for PKCζ's enzymatic activity [Standaert et al. 1999 /Chou et al. 1998]. However, unlike PKB and the other families of PKCs, the atypical PKCs have an acidic residue at their PDK2 site which mimics phosphorylation.

Due to the differences in the regulatory domain of the atypical PKCs, they are resistant to activation by lipid metabolites. Instead, protein:protein interactions via the PB1 domain appear to compensate for this and add another level of complexity to the regulation of atypical PKC activity. Proteins such as ZIP/p62, Par6 or MAPK5 have been shown to interact with the atypical PKCs through a PB1–PB1 domain interaction and to play a significant role in their cellular function [Durán et al. 2004/Puls et al. 1997/ Corbalan-Garcia and Gomez-Fernandez. 2006]

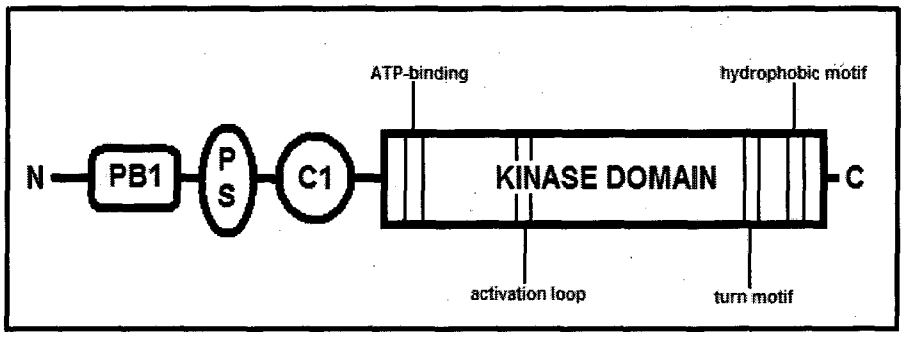

Figure 1.5. Structure of PKCζ

PKCζ is composed of a PB1 domain, a pseudosubstrate domain (PS), a C1 domain and a large C-terminal kinase domain.

1.5.2.2.4.3. Experimental evidence linking PKCζ to glucose transport

There is a vast amount of experimental evidence linking PKCζ to insulin action and diabetes and more specifically to insulin mediated glucose transport via GLUT4, including in vitro, in vivo and animal models. As has been previously mentioned, PKCζ is activated by PDK1 in response to insulin [Braiman et al. 2001]. It has been shown that insulin increases the activity of PKCζ [Bandyopadhyay et al. 1997] and induces its translocation to GLUT4 compartments in adipocytes [Bandyopadhyay et al. 1999]. Overexpression studies also support a role for PKCζ in insulin stimulated glucose transport. Overexpression of kinase dead PKCζ has been shown to inhibit insulin stimulated GLUT4 translocation and glucose transport in both 3T3-L1 adipocytes and L6 myotubes [Bandyopadhyay et al. 1997] whilst expression of constitutionally active PKCζ promoted glucose transport [Watson et al. 2004]. In addition, PKCζ activity has been shown to be impaired in muscle and adipocytes from individuals throughout the pathological spectrum of obesity and Type II diabetes [Kanoh et al 2003/Beeson et al. 2003/ Sajan et al. 2004] and well known anti-diabetic treatments (including TZDs) have been shown to increase PKCζ activity. There is however, some evidence to suggest that PKCζ is not involved in insulin mediated glucose transport. Work using PKCζ $^{(-/-)}$ mice and siRNA has shown that depletion of this protein has no effect on insulin stimulated glucose uptake [Zhou et. al. 2004/ Tsuru et al. 2002]. Much is still to be learnt of this proteins role in GLUT4 vesicle translocation and glucose uptake.

1.5.2.3. The TC10 Pathway

TC10 is a member of the Rho family of small GTP-binding proteins and has been implicated in GLUT4 vesicle trafficking. It appears to function independently of, yet in concert with, the IRS and PI3K mediated signalling pathway mentioned above. This second signalling cascade is functionally organised within caveolin-enriched lipid raft domains. Caveolae are a subset of lipid raft domains consisting of 50-100 nm invaginations of the plasma membrane. These localised regions contain the structural

proteins flotillin and caveolin and are enriched in lipid-modified signalling proteins, glycolipids, sphingolipids and cholesterol [Smart 1999].These lipid rafts are thought to spatially organise signalling cascades. It was shown that the insulin receptor was found in these microdomains of the plasma membrane [Gustavsson J et. al. 1999] and that the tyrosine kinase activity of the insulin receptor is enhanced when associated with caveolae [Yamamoto M et. al. 1998]. The discovery of another insulin receptor substrate, c-Cbl, within these caveolae led to further investigation into these plasma membrane microdomains. As is shown in figure 1.6, c-Cbl becomes tyrosine phosphorylated by the active insulin receptor through interactions with two adaptor proteins called CAP and APS. CAP contains three SH3 domains that stably interact with Cbl. The CAP/Cbl heterodimer is recruited to the plasma membrane (through interactions with APS) and Cbl phosphorylated by the insulin receptor. Once phosphorylated, the CAP/Cbl heterodimer dissociates from the insulin receptor and accumulates in lipid raft domains through interactions between the Sorbin homology (SoHo) domain of CAP and the caveolae resident protein flotillin. Once in the caveolae, Cbl then recruits a complex containing CrkII (an adaptor protein) and C3G (a guanine nucleotide exchange factor). This guanine nucleotide exchange factor is responsible for the conversion of the caveolae-resident TC10 from the GDP-bound inactive state to the GTP-bound active state. Putting together, insulin induces a signalling cascade involving the activation and recruitment of multiple molecules such as CAP, Cbl, CrkII and C3G, which leads to the activation of the Rho family GTPase protein TC10. It is not known exactly how TC10 is involved in GLUT4 vesicle trafficking, but it has been shown to directly interact with numerous effectors that modulate cytoskeletal function, which could lead to GLUT4 translocation [Ishikawa et al. 2005].

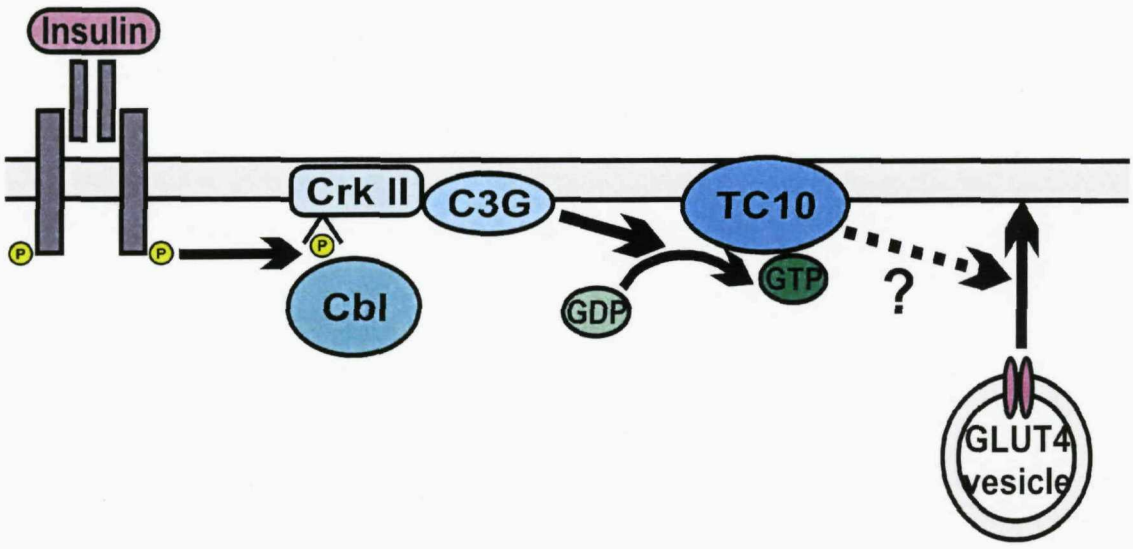

Figure 1.6. Insulin activation of the TC10 signalling pathway.

The activated insulin receptor phosphorylates c-Cbl. This then recruits CrkII along with the guanine nucleotide exchange factor C3G. C3G then activates TC10 by exchanging its bound GDP for GTP. Active GTP-bound TC10 then promotes GLUT4 vesicle trafficking by an as yet unidentified mechanism.

1.5.2.4. Rab Proteins

Rab proteins are members of the Ras superfamily of small GTPases, shown to be regulators of membrane transport. They function as molecular switches, by continually cycling between structurally distinct active GTP-bound, and inactive GDP-bound states. More than 60 genes encoding Rab proteins have been identified, and have been shown to regulate a number of cellular events. These include vesicle budding, interactions between vesicles and the cytoskeleton, organelle architecture and tethering and fusion of transport vesicles with target membranes [Deneka M et. al. 2003]. Active GTP-bound Rab proteins recruit soluble factors in order to transmit the GTPase signal to downstream effectors. These then mediate the subsequent steps in membrane transport. After a round of vesicle fusion, the Rab protein returns to its GDP-bound state and is recycled back to the donor

membrane for another round of membrane transport. Although many Rab proteins are expressed in insulin-responsive tissues, only three Rab proteins, Rab4, Rab5 and Rab11, have been suggested to play a role in the trafficking of GLUT4 vesicles. Rab4 has been shown to colocalise with GLUT4, and has been shown to redistribute from the microsome fraction to the cytosolic fraction in response to insulin and in a parallel fashion to GLUT4 redistribution to the plasma membrane [Cormont M et. al. 1993, Cormont M et. al. 1996]. Rab4 has also been shown to interact with syntaxin4 and to influence SNARE protein interactions in a GTP/GDP-dependent fashion [Li et al. 2001].

1.5.3. SNAREs

1.5.3.1. Overview

The trafficking of GLUT4 vesicles has been shown to have a great deal in common with the regulated exocytosis of synaptic vesicles in neurons. Regulated exocytosis of proteins at the plasma membrane involves the correct recognition of the target membrane by the vesicle and the correct coupling of proteins that direct the fusion of the two membranes. The proteins that direct these fusion steps are known as SNAREs (Soluble NSF attachment protein receptors). Vesicles contain integral membrane proteins, v-SNAREs, which bind to the cognate receptors, the t-SNAREs, on the plasma membrane. Binding of the v-SNARE to its t-SNARE allows the vesicle to dock and fuse with the plasma membrane, allowing the insertion of the proteins contained within the vesicle into the lipid bilayer. The SNARE proteins found to be associated with GLUT4 vesicle exocytosis are the v-SNARE VAMP2, the t-SNARE Syntaxin4, and SNAP23, a non-transmembrane t-SNARE (see figure 1.7). In the basal state, syntaxin4 and SNAP23 are associated at the plasma membrane, unable to bind to the VAMP2 protein in the GLUT4 vesicle membrane. Insulin stimulation enables VAMP2 to bind to the syntaxin4/SNAP23 complex thus allowing the docking and fusion of the GLUT4 vesicle with the plasma membrane.

Syntaxin4 is an ~32 kDa t-SNARE and the only syntaxin implicated in the role of GLUT4 vesicle trafficking. It is highly expressed in both muscle and adipose tissue and has been shown to redistribute from the low-density microsomes to the plasma membrane in response to insulin [Volchuk 1996]. Various approaches to inhibit syntaxin4 function (including introduction of inhibitory syntaxin4 antibodies) [Volchuk 1996] have caused inhibition of insulin-stimulated GLUT4 translocation, apparently by blocking the docking or fusion of GLUT4 vesicles with the plasma membrane.

VAMP2 has been shown to colocalise with GLUT4 in intracellular membrane compartments and to translocate to the plasma membrane in response to insulin [Malide et. al. 1997] and VAMP2 and syntaxin4 have been shown to interact *in vitro* [Macaulay 1997]. SNAP23 is highly expressed in insulin responsive tissues, and microinjection of cells with antibodies or peptides against SNAP23 inhibits insulin stimulated GLUT4 translocation [Macaulay 1997, Foster et. al. 1999].

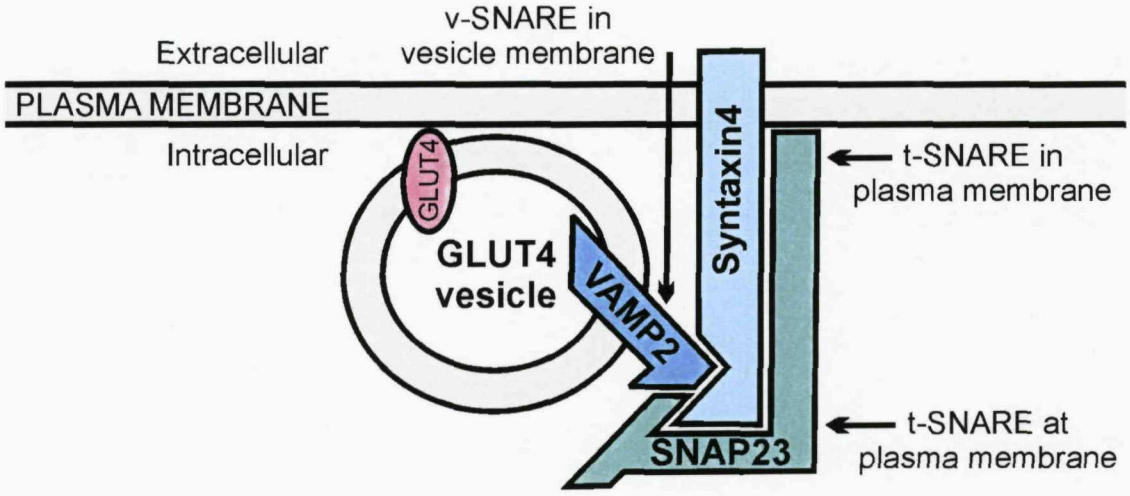

Figure 1.7. SNARE-mediated GLUT4 vesicle docking

The GLUT4 vesicle contains the v-SNARE, VAMP2. Two t-SNAREs are found at the target (plasma) membrane: the transmembrane syntaxin4 and the membrane-associated SNAP23. In the basal state, VAMP2 is unable to bind to syntaxin4 and SNAP23. Insulin stimulation enables VAMP2 to interact with the syntaxin4/SNAP23 complex, hence enabling the GLUT4 vesicle to dock and fuse with the plasma membrane. Glucose can then enter the cell through the GLUT4 protein.

1.5.3.2. SNARE protein structure and function

The first identification of SNARE proteins was in the late 1980's by Rothman and colleagues who identified a pair of soluble proteins that were required for successful fusion of Golgi vesicles with acceptor Golgi stacks. These proteins were designated NSF (*N*-ethylmaleimide-sensitive factor) and SNAP (soluble NSF attachment protein) on the basis of the sensitivity of the former to *N*-ethylmaleimide and the ability of both proteins to bind to each other. Later, four membrane proteins from brain extracts were found to act as receptors for NSF and SNAP and were termed SNAREs (for SNAP receptors)[Sollner et al. 2003].These SNARE proteins were then sub-classified depending on their topological localization in the presynaptic neuron. Those residing on the vesicle membrane were

classified as v-SNAREs, whilst those residing on the target membrane were classified as t-SNAREs. The proteins consisted of the v-SNARE VAMP-2 (vesicle-associated membrane protein-2) [Elferink et al. 1989] and the t-SNAREs syntaxins A and B [Bennett, M.K. et al. 1992] and SNAP25 (25-kDa synaptosome-associated proteins) [Oyler .et al. 1989]. Subsequent work by a number of groups established that members of the SNARE protein superfamily act not only in neurotransmitter release at the synapse, but also in most, if not every other intracellular trafficking pathway [Chen & Scheller 2001, Jahn and Grubmuller 2003, Kavalali 2002, Pelham 2001, Rizo & Sudhof 2002].

Membrane fusion in cells is an essential and fundamental requirement, occurring in many diverse cellular processes and in all life forms – from yeast to humans. Therefore, deciphering SNARE structure and function has been of intense interest to all in cell biology for many years. In general, SNAREs consist of a central, cytosolic 'SNARE motif' that is flanked by a C-terminal single transmembrane anchor and a variable N-terminal region encompassing one or two coiled-coil domains. Although they vary considerably in their structure, size and function, all share the homologous SNARE motif. This SNARE motif consists of ~60 amino acids which are capable of forming quaternary coiled-coil complexes with other SNARE motifs. In order for membrane fusion to occur, the complex must consist of four SNARE motifs, three from the target membrane and one from the vesicle bilayer [Sutton et al. 1998, Parlati et al. 2000].

The SNARE motif contains a repeating heptad pattern of hydrophobic residues. These are spaced such that the adoption of an α-helical structure places all the hydrophobic side chains on the same face of the helix. The burial of these hydrophobic helix faces in the bundle core are thought to stabilize the four-helix bundle when the SNARE motifs assemble [Antonin et al. 2002, Poirier et al. 1998, Sutton et al. 1998]. Monomeric SNARE motifs are disordered and the assembly of the four SNARE motifs into this four-helix bundle is accompanied by a dramatic increase in α-helical secondary structure [Fasshauer et al. 1997 and 1998, Rice et al. 1997]. The Formation of the SNARE complex is thought to involve zippering up of the helices of individual SNAREs from their membrane distal to membrane proximal ends. This brings the transmembrane anchors, and the two membranes, into

close proximity [Hanson et al. 1997] and is thought to be sufficient to overcome the energetic barrier of membrane fusion.

In most cases of exocytosis at the plasma membrane, each of the v- and t-SNAREs contribute one SNARE motif to the coiled-coil complex, whilst the other two SNARE motifs are from one of the SNAP23/25 family of proteins. These proteins are found at the target membrane, but unlike the other t-SNAREs, contain two SNARE motifs, one N- and one C-terminal. The SNAP proteins are not integral membrane proteins, like the other t-SNAREs, but associate with the plasma membrane through a central membrane binding motif.

It appears that the t-SNAREs syntaxins1-4 exist in one of two different conformations, either "open" or "closed" [Dulubova et al. 1999, Dulubova et al. 2003]. All t-SNAREs have a set of regulatory α-helices (Ha–Hb–Hc) that, in the closed conformation, fold back to interact with the SNARE motif. This conceals the SNARE motif so that it is unable to contribute to the quaternary coiled-coil responsible for t- and v-SNARE interaction. However, in the open conformation, the SNARE motif is exposed, allowing formation of the four-helix bundle. The events that lead to the transformation from the closed to the open conformation in syntaxins1-4 are not yet understood.

1.5.3.3. Specificity of membrane fusion

There are various stages of specificity during the process of targeted exocytosis. Once a transport vesicle approaches its destination, it is first loosely attached to the plasma membrane by tethering proteins. This is the first level of specificity, ensuring that the vesicle reaches the correct area of the target membrane. Next, the vesicle docks at the membrane, which secures the vesicle at the cell surface with greater affinity through interactions between SNAREs. Next these SNARE complexes must be "activated" before the vesicle membrane can finally fuse with the lipid bilayer of the plasma membrane.

Although there is a significant level of specificity achieved through the correct unison of complementary SNAREs, they do not account for the high levels of specificity that are seen in many exocytotic pathways. The hypothesis that SNAREs provided the precision needed for specific membrane fusion was challenged when SNARE proteins lacking their membrane anchors were produced. Soluble versions of v- and t-SNARES paired almost completely promiscuously, suggesting that pairing of specific SNAREs did not contribute to specificity [Fasshauer et al. 1999, Yang et al., 1999]. It has also been shown in the yeast vacuolar sorting pathway and *Drosophila* neurons that one SNARE can functionally replace the loss of another [Darsow et al. 1997, Gotte & Gallwitz 1997, Vilinsky et al. 2002], supporting the theory that the pairing of SNAREs is not the only level of specificity during the targeting of exocytosis.

The specificity of membrane trafficking is most probably defined at the vesicle targeting and tethering stages, during which vesicles are captured and tethered by long extended proteins from the target membrane. Small GTPases of the Rab family have been proposed to be important in the early stage of vesicle targeting and tethering, and many of them have been found to localize to distinct cellular compartments [Gurkan et al. 2005, Zerial and McBride 2001]. Evidence from genetic and biochemical studies suggests that Rabs may regulate the flux of membrane fusion pathways by activating appropriate SNAREs [Woodman 1998, Lian et al. 1994, Lupashin and Waters 1997]. However, the exact role of Rab proteins in the specificity of vesicle targeting remains unknown (For more information regarding the Rab GTPases, please refer to section 1.5.2.4.). Additionally, the SM family of proteins (for example munc18c) play a hugely significant role in the specificity and regulation of vesicular recognition and docking at the membrane. Munc18c was at first just thought to play an inhibitory role in GLUT4 vesicle trafficking by preventing the interaction between syntaxin4 and VAMP2 in the non-insulin stimulated state. However, there is now more evidence to suggest that it plays a far more intricate role in insulin mediated GLUT4 vesicle trafficking. Munc18c is discussed in detail below in section 1.5.4.

Synip and TUG are two other proteins shown to play a role in the specificity of insulin mediated GLUT4 trafficking. Synip was first identified as a syntaxin4 binding protein

and was found to interact with syntaxin4 in unstimulated, but not insulin stimulated, adipocytes [Min et al. 1999]. It is thought that synip binds to syntaxin4 in the basal state and that this inhibits an interaction from occurring between syntaxin4 and VAMP2 and hence prevents the GLUT4 vesicle from docking and fusing with the plasma membrane. Insulin stimulation is thought to release synip from syntaxin4, most probably due to phosphorylation of synip. There is evidence to suggest that Akt2/PKBβ is responsible for the insulin induced phosphorylation and release of synip from syntaxin4 [Yamada, E. et al. (2005)], though there is also evidence to contradict this [Sano, H. et al. (2005)]. TUG is a protein found to bind to GLUT4 and retains the GLUT4 protein within the intracellular storage compartments in the unstimulated state. Although not yet fully understood, it is thought that insulin stimulation disrupts the interaction between TUG and GLUT4 and hence allows the GLUT4 vesicle to enter the plasma membrane recycling pathway [Yu, C. et al. (2007)/Govers,R. et al. (2004)]

1.5.4. Munc18c

1.5.4.1. Overview

Insulin is able to affect the interaction between syntaxin4 and VAMP2 (and hence affect the ability of the GLUT4 vesicle to dock/fuse with the plasma membrane) by virtue of accessory proteins. One of the most important of these is munc18c. Munc18 proteins are mammalian homologs of the vesicle trafficking proteins found in yeast (Sec1) and C. elegans (UNC-18). This SM (Sec1/Munc18) family of proteins includes three eukaryotic members, munc18a, b, and c. Munc18a is expressed primarily in neurons and neuroendocrine cells, whereas Munc18b and Munc18c are ubiquitously expressed. Each play roles in inter-organelle trafficking, but munc18c is the only member shown to interact with syntaxin4, so has been the subject of much scrutiny with regards to insulin stimulated GLUT4 trafficking [Katagiri et al. 1995, Tellam et al. 1995 and 1997, Halachmi. and Lev 1996, Hata and Sudhof 1995]

Experimental evidence points towards an inhibitory role for munc18c in GLUT4 vesicle exocytosis. The simplest model is as follows: In the absence of insulin, munc18c binds to syntaxin4 and holds it in its closed conformation, thus inhibiting GLUT4 vesicle docking/fusion at the plasma membrane. Upon insulin stimulation, munc18c dissociates from syntaxin4, allowing it to adopt the open conformation and enabling syntaxin4/VAMP2 interaction and GLUT4 vesicle docking/fusion [Tamori Y (1998)/ Thurmond DC et. al. (1998), Macaulay SL et. al. (2002), Thurmond DC et. al. (1998), Kanda H et. al. (2005)]. Although this is an attractive and well characterised model, it is almost certainly an over-simplistic depiction of the role of munc18c in insulin-mediated GLUT4 vesicle trafficking.

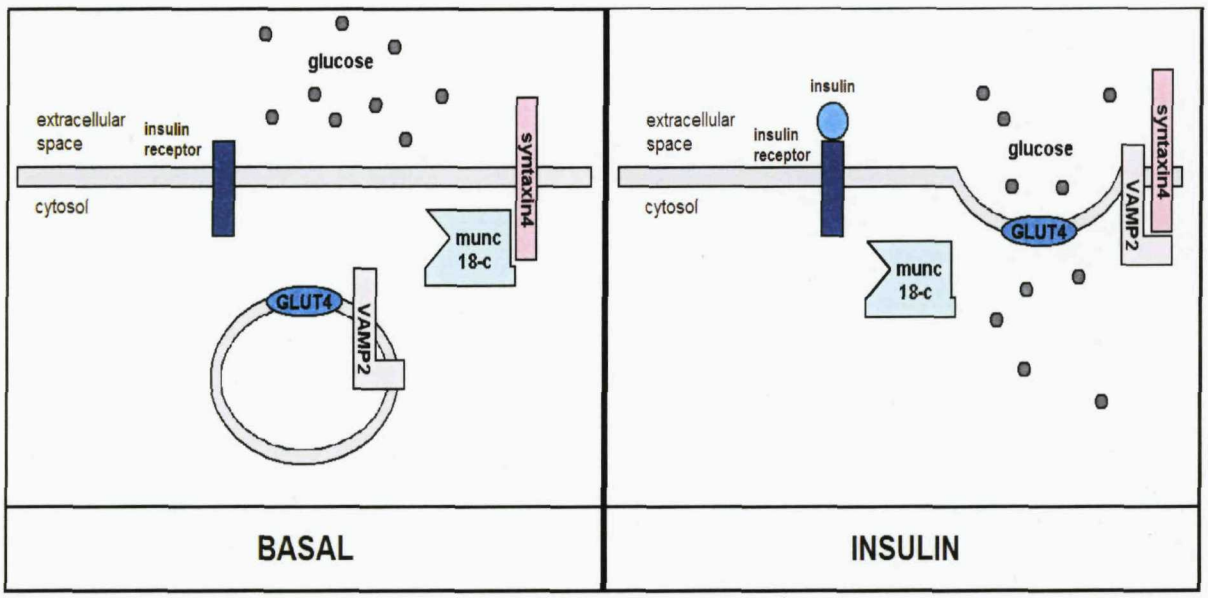

Figure 1.8. Hypothetical model for the action of insulin on munc18c and GLUT4 translocation to the plasma membrane.

In the absence of insulin, munc18c clamps onto syntaxin4, preventing VAMP2 binding. Insulin triggers the un-clamping of munc18c. This allows VAMP2 to bind to syntaxin-4, thereby promoting GLUT4 vesicle fusion to the plasma membrane.

1.5.4.2. The SM family of proteins

SM proteins are cytosolic proteins of ~600–700 residues that directly or indirectly bind to SNAREs. The entire sequence of SM proteins are homologous to each other, with a high degree of evolutionary conservation from yeast to humans. Only 7 SM protein isoforms have been found in vertebrates, namely munc18a, -b and -c, Sly1, Vps45, Vps33a, and Vps33b. Most commonly, SM proteins interact with SNAREs via a direct interaction with the syntaxins. However, despite conserved sequence and structural homology, finding a common mode of binding and mechanism of action for them has proved problematic. Results suggest that the N-terminus of SM proteins (the N-terminal 100-150 residues) is essential for their binding to SNAREs, whilst the role of the remaining protein sequence is as yet unknown [Dulubova et al. 2003, Traffic 2006; 7: 1–12].

So far, there have been three diverse modes of SM:SNARE interaction identified. Neuronal Sec1 (nSec1) binds to the closed conformation of syntaxin, making extensive contacts with both the SNARE motif and the H_{abc} domain [Misura et al. 2000]. In contrast, Sec1p in yeast only binds to the syntaxin ortholog Sso1p when it is part of an already assembled SNARE complex [Carr et al. 1999]. A third mode of interaction in which many SM proteins bind to the extreme N terminus of the t-SNAREs has also been elucidated [Bracher & Weissenhorn 2002, Dulubova et al. 2003, Dulubova et al. 2002,Yamaguchi et al. 2002]. The exact function of the SM proteins is also still ambiguous. There is much evidence to suggest that the SM proteins perform an inhibitory role on vesicle fusion, by clamping over the corresponding t-SNAREs and/or locking them in the "closed" conformation. However, there is also evidence that the SM proteins play an important positive role. In synaptic vesicle exocytosis and yeast vacuole fusion, the SM proteins appear to play a more significant role than the corresponding SNARE proteins. [Banta et al. 1990, Verhage et al. 2000, Ungermann and Wickner W 1998, Schoch et al. 2001, Washbourne et al. 2002]. Indeed, in vivo evidence suggests that SM proteins can play both negative and positive roles [Carr & Novick 2000, Gallwitz & Jahn 2003, Rizo & Südhof 2002].

1.5.4.3. Experimental evidence for munc18c's role in GLUT4 vesicle trafficking

Much work has been done to investigate the role of munc18c in insulin-mediated GLUT4 trafficking. Although much evidence points towards it playing an inhibitory role, there is also evidence to suggest that munc18c is crucial for the docking and/or fusion of the GLUT4 protein at the plasma membrane in response to insulin. Over-expression of munc18c in 3T3-L1 adipocytes was shown to inhibit insulin-stimulated GLUT4 translocation to the plasma membrane[Tamori 1998, Thurmond et. al. 1998] and microinjection of antibodies directed against munc18c stimulated GLUT4 translocation to the plasma membrane in these cells. [Macaulay et. al. 2002] It was also shown that insulin stimulation disrupts the association between munc18c and syntaxin4 [Thurmond et. al. 1998]. The most convincing evidence so far comes from experiments using munc18c$^{(-/-)}$ adipocytes [Kanda et. al. 2005]. Kanda et al. showed that ablation of munc18c in adipocytes did not affect insulin-stimulated GLUT4 trafficking to the cell periphery, but did enhance the externalisation of GLUT4. This suggests that munc18c does not play a role in the movement of GLUT4 vesicles into close proximity with the plasma membrane, but does play a role in either the docking or fusion with the plasma membrane. Some work, however, has given conflicting evidence for the role of munc18c in GLUT4 vesicle exocytosis. The introduction of a peptide fragment that inhibits the binding of munc18c to syntaxin4 was shown to inhibit the integration of GLUT4 into the plasma membrane [Thurmond et. al. 2000]. This suggests that the interaction between these two proteins is necessary for, and not inhibitory to, GLUT4 vesicle exocytosis. It could be that in the basal state, munc18c interacts with syntaxin4 and inhibits GLUT4 vesicle exocytosis by maintaining syntaxin4 in an inactive "closed" conformation. Upon insulin stimulation, munc18c may undergo a conformational change that allows syntaxin4 to adopt an "open" conformation to allow it to bind VAMP2. These conflicting results highlight the complexity of the processes involved in GLUT4 vesicle exocytosis, and the need for additional research in this area.

1.5.6. The Role of the Cytoskeleton in GLUT4 Vesicle Exocytosis

1.5.6.1. Overview

It is generally recognised that the cytoskeleton plays important roles in the retention of, and trafficking of, membrane-bound organelles to specific locations within the cell. The GLUT4 vesicle is a highly regulated and dynamic organelle. In the basal state, GLUT4 protein slowly yet continually cycles between the plasma membrane and intracellular storage vesicles. Upon insulin stimulation, there is a rapid and dramatic reorganisation of the cytoskeleton that results in the substantial increase in targeted exocytosis of GLUT4 vesicles and a decrease in GLUT4 endocytosis. Although it is well known that the cytoskeleton is responsible for this rapid reorganisation of GLUT4, the exact functional roles of the cytoskeleton, and the regulatory mechanisms behind them, remain unclear. Cytoskeleton-perturbing reagents such as nocodazole (for microtubules) and latrunuculin (for actin filaments) have been shown to disrupt the integrity of the GLUT4 storage compartment and to diminish insulin-stimulated GLUT4 translocation and glucose uptake [Watson et al. 2004]

1.5.6.2. Actin

The most abundant cytoskeletal protein in mammalian cells is monomeric globular actin (G actin). G actin is a globular monomer that polymerises into a fibrous form called F actin, in an ATP-dependent manner. The rate of polymerisation, as well as other properties and functions of the actin cytoskeleton, is regulated by various actin-binding proteins. These provide actin with the means to perform dynamic processes within the cell, which may be regulated by extracellular signals, including insulin. The role of actin filaments in GLUT4 vesicle trafficking has been examined by the use of actin depolymerising agents such as cytochalasin D and latrunculin A and B. Use of all these compounds was shown to inhibit insulin-induced glucose uptake and GLUT4

translocation [Watson et al. 2004]. Also, with the use of YFP-tagged actin and real-time imaging techniques, it was shown that insulin induces the dynamic remodelling of the actin cytoskeleton at both the cortical and perinuclear regions in 3T3-L1 adipocytes and that this correlated with an increase in GLUT4 translocation and glucose uptake [Kanzaki and Pessin 2001].As mentioned, actins highly dynamic and complex role in the cell can be modulated by its interaction with regulatory proteins. Two well known regulators are phosphoinositides and the Rho family of small GTP-binding proteins. Both of these can be modulated by insulin action through the PI3K and TC10 signalling pathways respectively, further implicating the actin cytoskeleton in insulin-stimulated GLUT4 translocation and glucose transport.

1.5.6.3. Microtubules

Microtubules are long, hollow cylinders composed of alternating α- and β-tubulin. They are polar structures, with a plus (+) end at the cell periphery and a minus (-) end attached to a centrosome at the perinuclear region. They are highly dynamic structures, continually polymerising and depolymerising. As with the actin cytoskeleton, accessory proteins play a crucial role in microtubule-based transport within the cell. Microtubules associate with motor proteins that function to transport cargo molecules and position organelles. There are two main classes of these motor proteins: Dyneins, which transport molecules to the (-) end of the microtubule (inward), and kinesins, which transport molecules to the (+) end of the microtubule (outward).

Inhibition of either of the microtubule proteins, dynein or kinesin, reduces insulin-stimulated GLUT4 translocation [Guilherme et. al. 2000, Emoto et. al.. 2001]. Experimental evidence to date has been inconclusive as to a role of the microtubule network in GLUT4 vesicle trafficking. It is widely agreed that microtubules and dynein motors are involved in the endocytosis of GLUT4 to perinuclear membranes, but it is unsure as to whether microtubules and kinesins play a role in the insulin stimulated outward trafficking of GLUT4 to the plasma membrane. A study using YFP-tagged GLUT4 and microtubules

of CFP-tagged tubulin in adipocytes showed that microtubules are involved in the long-range movement of GLUT4 both towards, and away from, the perinuclear region, and that the frequency of these movements are increased in response to insulin. In addition to this, they showed that the increase of velocity of these movements in response to insulin was not dependent on PI3K, as determined by the use of the PI3K inhibitor wortmanin. To further investigate the role of the microtubules and PI3K in GLUT4 vesicle trafficking, they used a GLUT4 construct with an exofacial Myc-tag and an intracellular GFP tag. This showed that the movement of GLUT4 to the plasma membrane along the microtubules was not dependent on the PI3K pathway, but that the insertion of GLUT4 protein into the plasma membrane (resulting in the detection of the Myc tag on unpermeabilised cells) was dependent on PI3K. This would explain why the presence of wortmanin nearly completely disrupts insulin stimulated glucose transport, despite their findings that it has no affect on microtubule movement of GLUT4 to the cell periphery. In contrast, other studies have shown that disruption or stabilisation of the microtubule network has no significant effect on insulin-stimulated GLUT4 translocation, and suggests that the microtubules role in GLUT4 trafficking is one of correct recycling of the vesicle to the perinuclear region [Molero JC et. al. 2001, Shigematsu et. al. 2002]. More research needs to be done to decipher the exact roles of both actin and microtubules in the complex trafficking mechanisms of GLUT4.

1.6. Novel proteins in insulin signalling

1.6.1. 80K-H

1.6.1.1. Overview

Recent work in our laboratory using a yeast-2-hybrid screen found a novel interactor of PKCζ. This was a 398 amino acid protein corresponding to the C-terminal section of a protein called 80K-H. Another yeast-two-hybrid screen, this time using munc18c as bait,

identified both PKCζ and 80K-H to be novel interactors with munc18c. It was hypothesised that 80K-H could be the missing link between the signalling cascade (PKCζ) and the vesicle trafficking machinery (munc18c). 80K-H was hence chosen for further investigation, partly due to its poor characterisation to date, but also because the bovine version of 80K-H, VASAP60, has been shown to be involved in vesicle transport [Brule et al. 2000].

The interaction between PKCζ and 80K-H was confirmed *in vitro* using GST pull-down techniques, which also showed that the region of 80K-H responsible for binding was located between residues 302-378. Co-immunoprecipitation studies showed that insulin stimulation increases the interaction between PKCζ and 80K-H 3-5 fold. Co-immunoprecipitation studies also showed that an 80K-H construct interacts with munc18c and that this interaction is too increased by insulin stimulation. Overexpression of 80K-H fragments was shown to greatly enhance glucose transport and GLUT4 vesicle trafficking to the plasma membrane in both the basal and insulin stimulated states. It is hence possible that interactions between PKCζ, munc18c and 80K-H play a role in GLUT4 vesicle trafficking and glucose transport.

1.6.1.2. 80K-H Structure

80K-H is a 528 amino acid protein of approximately 59 kDa. Sequence similarity and theoretical secondary structure analyses predict at least 6 structural domains or motifs: an N-terminal signal sequence for translocation across the ER membrane, a low-density lipoprotein class A domain, 2 putative Ca^{2+} binding EF hands, a glutamic acid–rich segment, a region with low homology to the mannose 6-phosphate receptor, and a C-terminal His-Asp-Glu-Leu (HDEL) ER retrieval signal. This protein was originally identified as a phosphorylation substrate for a crude PKC extract and has numerous PKC phosphorylation motifs throughout its sequence, though it has yet to be determined which PKC (if any) it is a physiological substrate for. Although discovered in 1989, there has been little research conducted on this protein, and work so far has shown 80K-H to have

numerous and diverse roles. These include a cellular receptor for advanced glycation endproducts (AGEs) [Li et. al. 1996], a vacuolar system-associated protein [Brule S et. al. 2000], the noncatalytic β-subunit of glucosidase II (an endoplasmic reticulum-resident enzyme involved in carbohydrate processing and quality control of newly synthesised glycoproteins) and a Ca^{2+} sensor for an epithelial Ca^{2+} channel. The research in our laboratory, and the involvement of this protein in carbohydrate processing and membrane trafficking events make this protein an ideal target for further investigation into a possible role in GLUT4 vesicle trafficking.

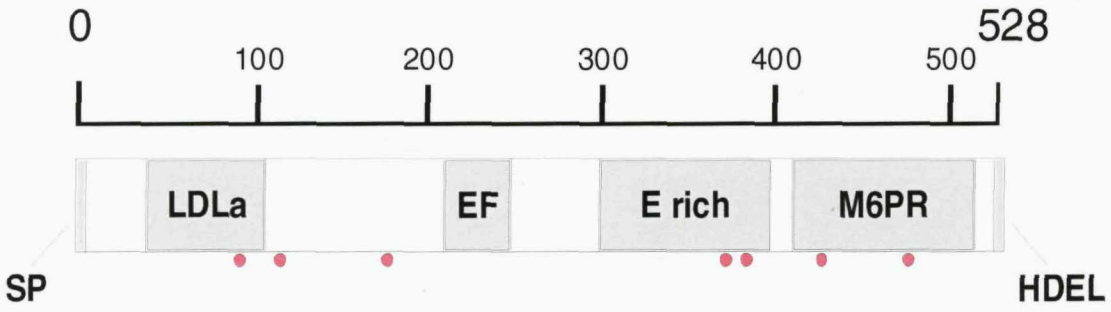

Figure 1.9. Structure of 80K-H

Diagram showing putative structural domains of the 80K-H protein. The full length protein consists of 528 amino acids, with an N-terminal signal peptide domain (SP), a low density lipoprotein receptor domain A (LDLa), two EF-hand calcium binding domains (EF), a glutamic acid rich stretch (E rich), a mannose-6-phosphate receptor domain (M6PR) and an endoplasmic reticulum targeting sequence *(HDEL.) Putative PKC phosphorylation substrate motifs are shown as pink circles.*
Information regarding the structure of 80K-H was from the Prosite website which is a database of protein domains, families and functional sites: www.expasy.ch/prosite/

1.6.1.3. Role in carbohydrate processing: Advanced Glycation Endproduct Receptor

Advanced glycation endproducts (AGEs) are derivatives of non-enzymatic reactions between sugars and protein or lipids. They accumulate in diabetics due to the increased carbohydrate and lipid substrate availability as well as oxidative conditions favouring the glycation process, and in the case of associated renal failure, reduced kidney clearance. AGEs are responsible for a large number of pathogenic effects associated with diabetic complications including nephropathy, neuropathy, disruption of renal function and atherosclerosis. AGEs exert these detrimental effects via two mechanisms. The first is by forming cross links with extracellular proteins thereby permanently altering the cells structure. The second is via an interaction with cell surface AGE receptors. Binding of AGEs to these receptors alters the cells function by activating signalling cascades and transcriptional events. This not only leads to cell activation and dysregulated tissue remodelling, but also the removal of the irreversibly glycated molecules, thereby protecting the tissues from further damage. A protein of ~90 kDa was shown to act as an AGE receptor and was later identified as the 80K-H protein [Li et al. 1996, Yang et al. 1991]. The details of the roles of 80K-H as an AGE receptor remain unknown. The critical role that AGEs play in the pathogenesis of diseased states associated with diabetes, coupled with the recent discovery of its interaction with PKCζ and munc18c and involvement in GLUT4 vesicle exocytosis makes 80K-H an exciting candidate for further investigation.

1.6.1.4. Fibroblast Growth Factor Receptor Signalling

Several studies have suggested a role for 80K-H in fibroblast growth factor (FGF) signalling. FGF signalling bears many similarities with and is often interchangeable with, insulin signalling. The signal transduction pathways following activation of FGF receptors are thought to be primarily mediated by the tyrosine phosphorylation of key substrates, as is the case with other receptor tyrosine kinases. Several groups have

demonstrated that 80K-H is phosphorylated by FGF in a number of different cell types [Goh et al. 1996, Kanai et al. 1997, Coughlin et al 1988.]

1.6.1.5. β subunit of ER glucosidase II

It was recently discovered that 80K-H is the non-catalytic β-subunit of glucosidase II. Glucosidase II is an ER resident enzyme involved in the processing and quality control of glycoproteins within the ER. The α-subunit is responsible for deglycosylation of the glycoproteins, which initiates and assists in the correct folding and oligomerization of them in the ER. Glucosidase II is composed of two non-covalently attached subunits, α and β. The α-subunit is the catalytic subunit of the enzyme, whilst the β-subunit (80K-H) performs an as yet unidentified role in Glucosidase II function. Mutations in the 80K-H gene have been shown to be a cause of autosomal dominant polycystic liver disease [Drenth et al. 2003, Li A. et al 2003, Drenth et al. 2004 a. and b.]

1.6.2. Kifap3

A yeast-2-hybrid screen recently conducted in our laboratory, using munc18c as bait, discovered a protein called Kifap3 to be a novel interactor. Very little research has been performed on this protein, but it has been found to associate with KIF3A/3B, a member of the kinesin superfamily [Yamazaki H et. al. 1996]. As mentioned previously, the kinesin superfamily of proteins are motor proteins that transport molecules anterograde (towards the cell periphery) along microtubules. Kinesins possess a highly homologous motor domain which converts energy from ATP hydrolysis into the mechanical energy needed to move the motor along the microtubule [Manning and Snyder 2000]. Apart from the conserved motor domain, kinesins are a diverse family of proteins with vast functional specificity. It is thought that the functional potential of the kinesins is enhanced by regulatory subunits called kinesin-associated proteins (KAPs). These proteins interact with the variable non-motor domains of the kinesins and are speculated to play a role in cargo selectivity and

binding. It is possible that Kifap3 somehow plays a role in microtubule-dependent GLUT4 vesicle trafficking, through it's interactions with munc18c, and is hence an attractive candidate for further investigation.

1.7. This thesis

The prevalence of obesity, diabetes and other insulin-associated diseases has reached epidemic proportions and with numbers of these set to continue rising into the foreseeable future, research into these pathophysiological conditions is even more essential than ever. With so many gaps in our knowledge of insulin signalling and its effects on the cell, investigating the molecular machinery of insulin action is a necessity. With GLUT4 vesicle docking at the plasma membrane being the "finale" of insulin mediated glucose transport, the GLUT4 vesicle trafficking machinery has been the focus of intense study for some time. Much has been learnt of the GLUT4 storage compartment, the insulin signalling pathways to the GLUT4 vesicles, the trafficking machinery and the processes involved in the final docking and fusing of the GLUT4 vesicle at the plasma membrane. However, there are still large gaps in our knowledge that need to be filled in order to develop new strategies for preventing, treating and curing diseases such as diabetes.

The recent findings in our laboratories of the role of 80K-H in GLUT4 vesicle trafficking is an exciting one. As mentioned, for many years people have researched the insulin signalling pathways and the GLUT4 vesicle trafficking machinery. However, no link between the two had been discovered. 80K-H is that missing link and provides an attractive candidate for further research and possible therapeutic intervention. 80K-H is an Advanced Glycation Endproduct Receptor. The main cause of diabetic complications is the production of Advanced Glycation Endproducts from the persistently increased blood sugar levels. This additional link between 80K-H and diabetes further supports the notion that 80K-H is crucial to GLUT4 vesicle docking. This thesis aims to further elucidate the roles of proteins involved in insulin mediated GLUT4 vesicle trafficking, with particular emphasis on 80K-H, PKCζ and munc18c.

MATERIALS AND METHODS

2. MATERIALS AND METHODS

2.1. MATERIALS

Chemicals were from Sigma Chemical Company (Poole, Dorset, UK) unless stated otherwise.

2.2. MICROBIOLOGICAL TECHNIQUES

2.2.1. Materials

BL21 (DE3) *E.coli* were from Novagen (Nottingham, UK), JM109 *E.coli* were from Promega (Southampton, UK), pcDNA3 and pcDNA4 vectors were from Invitrogen (USA,) pGex-5X-1 vector was from Amersham (Bucks, UK).

2.2.2. Sterilisation

All media, stock solutions, pipette tips and micro-fuge tubes were sterilised by autoclaving at 120°C and 15 lbs/inch^2 for 20 minutes. Labile stock solutions such as antibiotics (ampicillin 100 μg/ml, kanamycin 30 μg/ml) and IPTG (1M), which cannot be autoclaved, were filter sterilised using 0.20 μm Millipore disposable filters. All work was carried out under sterile conditions.

2.2.3. Cloning vectors

Vector	Properties	Size (kb)
pGex-5X-1	Amp^r, laq l^q, Ptac promoter, N-terminal Glutathione S-transferase tag	4.9
pcDNA3-myc	Amp^r, T7 promoter, CMV promoter, N-terminal c-myc tag	5.1
pcDNA4-HisMax3	Amp^r, T7 promoter, CMV promoter, N-terminal polyhistidine tag and Xpress™ epitope	5.3
ECFP -N2/ EYFP-N2	Kan^r, CMV IE promoter, C-terminal ECFP or EYFP tag	4.7

Table 2.1. Vectors used in this study.

Amp^r = gene encoding resistance to ampicillin. Kan^r = gene encoding resistance to kanamycin. laq l^q = lac operator gene. Ptac = tac promoter gene. CMV promoter = cytomegalovirus promoter. CMV IE promoter = cytomegalovirus immediate early promoter. ECFP = enhanced cyan fluorescent protein. EYFP = enhanced yellow fluorescent protein.

2.2.4. Media

All bacterial cultures were grown in Luria Broth (LB) which contains 10 g/l tryptone, 5 g/l yeast extract and 5 g/l NaCl. Once autoclaved and cooled to 50°C, this was supplemented with the appropriate antibiotic for selection of the microbes containing the relevant plasmid. Ampicillin was added to a final concentration of 100 μg/ml. Bacterial colonies were grown on plates of LB solidified by the addition of 1.5% w/v agar with antibiotic.

2.2.5. Strain storage

Short term storage of bacterial strains were maintained as streaks on LB-agar plates supplemented with the appropriate antibiotic. These may be stored at 4°C for approximately 2 weeks. Long term storage of bacterial strains was achieved by adding 700 µl of mid-log phase LB culture to 300 µl sterile glycerol in sterile micro-fuge tubes. These can then be stored at -80°C for up to two years.

2.2.6. Transformation of competent *E.coli* with plasmid DNA

All bacterial strains were transformed with plasmid DNA by heat shock, using the supplier's protocol.

2.2.6.1. Heat shock of JM109 cells

1-5 µl of plasmid DNA (typically 1-50 ng) was added to 50 µl of competent cells, mixed and incubated on ice for 20 minutes. These transformation reactions were heat shocked at 42°C for 45 seconds, then incubated on ice for a further 2 minutes. 500 µl of cold LB (without addition of antibiotic) was added to the cells before incubation at 37°C and 200 r.p.m. for one hour. Cells were then pelletted by pulse spin, resuspended in 50 µl of LB and plated on LB-agar plates containing the appropriate antibiotic. These plates were incubated at 37°C for 16-24 hours.

2.2.6.2. Heat shock of BL21 cells

1-5 µl of plasmid DNA (typically1-50 ng) was added to 20 µl of competent cells, mixed and incubated on ice for 5 minutes. These transformation reactions were heat shocked at

42°C for 30 seconds, then incubated on ice for a further 2 minutes. 80 µl of cold SOC media (without addition of antibiotic) was added to the cells before incubation at 37°C and 200 r.p.m. for one hour. Cells were then pelletted by pulse spin, resuspended in 50 µl of LB and plated on LB-agar plates containing the appropriate antibiotic. These plates were incubated at 37°C for 16-24 hours.

2.3. MOLECULAR BIOLOGY

2.3.1. Materials

All enzymes and corresponding buffers, dNTPs were from Promega (Southampton, UK.) Primers were from Invitrogen (USA.)

2.3.2. Amplification of DNA and production of truncation/deletion constructs by PCR

A standard protocol was used for all PCRs, using the constituents shown in table 2.2. Reagents were placed in a 0.5 ml microcentrifuge tube, with the *Pfu* DNA polymerase being added last and immediately before the cycling commenced. The 50 µl reaction mixture was mixed and spun in a bench top centrifuge in order to collect all reaction volume at the bottom of the tube. PCR reactions were then carried out using a Hybaid Omn-E thermocycler (Hybaid Ltd, Middlesex, UK) with the temperature cycles shown in section 3.

Reagent	Volume (µl)
Template DNA	1 (10-200 ng)
50 µM Primer 1	1
50 µM Primer 2	1
dH_2O	38
DMSO	1
10 x *Pfu* polymerase enzyme buffer	5
10 mM dNTP	2.5
Pfu DNA polymerase enzyme	0.5

Table 2.2. Reagents used for PCR

2.3.3. Ethanol Precipitation of DNA

The DNA produced from the PCR reaction must then be isolated in order to remove any remaining DNA polymerase and buffers, as these would inhibit the restriction enzymes required for subsequent cutting of the PCR products. The PCR product was added to 0.3 volumes of 1M sodium acetate and 2½ volumes of 100% v/v ethanol before vigorous mixing. This was then left on ice for at least 15 minutes before being spun at 12000 rpm at 4 °C for 15 minutes to collect the DNA. The supernatant was removed and the pellet of DNA washed with 100 µl of 70% v/v ethanol. This was spun again at the same settings as before, for 5 minutes. The supernatant was removed, the pellet of DNA air-dried for 5 minutes before being resuspended in 30-50 µl of EB.

2.3.4. *Eco*RI/*Xho*I digestion of DNA

The PCR products were then cut with *Eco*RI and *Xho*I in order to produce the correct "sticky" ends required for ligation into either the pcDNA4-HisMax-C, pGex5X-1 or pcDNA3-myc vectors. The same buffer is suitable for efficient digestion of DNA using these two enzymes, enabling complete digestion to be achieved in one step. 25 µl of DNA (typically 10-500 ng) was placed in a 0.5 ml microcentrifuge tube with 3 µl of buffer H, 10 units (1 µl) of *Eco*R1 and 10 units (1 µl) of *Xho*1. This was mixed then incubated at 37 °C for three hours. The required DNA was purified from other digest species by separation on a 1% w/v agarose gel followed by extraction of the DNA band of interest using a Qiagen DNA extraction kit, according to the manufacturers' instructions.

2.3.5. *Eco*RI/*Kpn*I digestion of DNA

The PCR products were then cut with *Eco*RI and *Kpn*I in order to produce the correct "sticky" ends required for ligation into the ECFP-N2 and EYFP-N2 vectors. Efficient digestion of DNA was not possible with these two enzymes when used in the same buffer, so each enzyme was used separately. 26 µl of DNA (typically 10-500 ng) was placed in a 0.5 ml microcentrifuge tube with 3 µl of buffer H and 10 units (1 µl) of *Eco*R1. This was mixed then incubated at 37 °C for three hours. The DNA was then separated from the buffer and enzyme by ethanol precipitation (see section 2.3.3. above.) This was then resuspended in 26 µl of EB with 3 µl of buffer J and 10 units (1 µl) of *Kpn*I. This was mixed then incubated at 37 °C for three hours. The required DNA was purified from other digest species by separation on a 1% w/v agarose gel followed by extraction of the DNA band of interest using a Qiagen DNA extraction kit, according to the manufacturers' instructions.

2.3.6. Ligation of DNA insert into vector

"Sticky" end ligation of the DNA insert (produced from the PCR reactions above) and either the pGex5X-1, pcDNA4-HisMax-C or pcDNA3-myc vectors was performed in a total volume of 10 µl. Included in this was 3 units (1 µl) of T4 DNA ligase, 1 µl of 10 x ligation buffer (300 mM Tris-HCl pH 7.8, 100 mM DTT, 5 mM ATP) and 100-200 ng of vector DNA. The molar ratio of insert: vector was between 3:1 and 9:1 in order to achieve efficient ligation. Ligation reaction was then incubated overnight at 4 °C. This was then incorporated into *E.coli* by heat-shock, as explained previously.

2.3.7. Amplification and purification of plasmid DNA

The above ligation reaction was incorporated into E.coli by heat-shock as explained previously. Single colonies were transferred into a 25 ml tube containing 5 ml of LB with the appropriate antibiotic and incubated at 37 °C with shaking (200 rpm) for 16-18 hours. Plasmid DNA was purified using a Qiagen spin miniprep kit, according to the manufacturer's instructions. Once purified, 5 µl of DNA was digested with appropriate restriction enzymes and buffer at 37 °C for 1 hour. The presence/quality of extracted DNA was then checked by running on a 1% (w/v) agarose gel containing 5 mg/litre ethidium bromide, alongside 2 µl of 1 kb ladder. DNA banding was visualised with a UV-transilluminator and the size of the DNA insert determined by comparison to the 1 kb ladder. Once the DNA had been checked to contain the correct sized plasmid and insert, a glycerol stock of the *E.coli* was made for storage as described previously.

2.3.8. Purification of plasmid DNA for tissue culture transfections

5 µl of glycerol stock was added to a 25 ml tube with 5 ml LB containing the appropriate antibiotic and shaken (200 rpm) at 37 °C for 8 hours. 80 µl of this was then transferred to a 200 ml flask containing 80 ml of LB and the appropriate antibiotic and grown with the same conditions for 16-18 hours. All of the overnight culture was then used for purification of the plasmid DNA using a Qiagen maxiprep kit, as per the manufacturer's instructions. The presence of the correct insert in the vector was checked as above. Spectrophotometry was used to determine the purity (A260/A280), with a ratio of 1.7-2.0 indicating pure DNA and concentration of DNA (At 260 nm, a 1 cm light path with an absorbance of 1 is equal to 50 µg/ml.)

2.4. PROKARYOTIC PROTEIN EXPRESSION AND PURIFICATION

2.4.1. Materials

IPTG was from Amersham Biosciences (Buckinghamshire, UK). BugBuster, rlysozyme, benzonase and glutathione-sepharose 4B beads were from Novagen (Nottingham, UK.) PBS tablets were from Oxoid (Hampshire, UK.)

2.4.2. GST-Protein expression and extraction

GST-tagged proteins were produced using the BL21 strain of *E.coli* containing a pGEX-5X-1 plasmid with an insert. 5 µl of glycerol stock was placed in a 25 ml tube containing 5 ml of LB and the appropriate antibiotic. This was incubated with shaking (200 rpm) at 37 °C for 16-18 hours. 1 ml of this overnight culture was then placed in a 50 ml tube with 10 ml of LB and appropriate antibiotic and grown under the same conditions for 1 hour.

Expression of the GST-tagged protein was induced by addition of IPTG to a final concentration of 0.1 mM and further incubation under the same conditions for 2½ hours. Cells were harvested by centrifugation at 3000 rpm for 5 minutes at 4°C, using a Sorvall Legend centrifuge. After harvesting, the supernatant was discarded and the cells lysed in 500 µl of BugBuster reagent with 0.5 KU rlysozyme and 12.5 units benzonase at room temperature for 30 minutes with constant agitation. Any remaining cell debris was removed by centrifugation at 12000 rpm for 10 minutes at 4°C. 100 µl of the resultant protein extract was used for analysis of protein expression and relative concentration, whilst the rest was stored at -20°C until needed.

2.4.3. Purification of GST-tagged proteins

The GST-tagged proteins were purified using glutathione-sepharose beads. 40 µl of beads were placed in a 1.5 ml microcentrifuge tube and washed with 1 ml PBS. 100 µl of the crude protein extract was added to the beads and left at room temperature with constant agitation for 1 hour. Beads were then spun down using a pulse spin on a benchtop centrifuge and washed in 3 x 1 ml PBS. The dry beads could then be stored at -20°C until being analysed for relative protein concentration.

2.4.4. Estimation of relative quantity of GST-tagged protein

40µl of PBS and 10 µl of 5X Laemmli sample buffer (312.5 mM Tris, 10% w/v SDS, 10% v/v glycerol, 0.01% w/v pyronin Y) containing DTT (19 µg/250 µl) was added to the beads then boiled for 3 minutes. Tubes were then vortexed and the beads spun down by pulse spin. 20 µl of the supernatant was then separated by SDS-page (for methods, see below.) Once separated, the proteins were stained using Coomassie brilliant blue stain.

2.5. TISSUE CULTURE

2.5.1. Materials

3T3-L1 fibroblasts, Cos-1 cells and CHO cells were purchased from the American Type Culture Company (Mananas, USA.) Tissue culture 25 cm^2 and 75 cm^2 flasks, and 6, 12, 24 and 96 well tissue culture plates were from Falcon (San Jose, USA.) 50 ml and 15 ml centrifuge tubes, 1 ml and 10 ml serological pipettes and cell scrapers were from Helena Biosciences (Sunderland, UK.) 0.22 μm filters were from Triple Red (Buckinghamshire, UK.) 20 ml syringes from Becton Dickinson (Bedford, USA). Nunc cryotubes, glutamine and fetal bovine serum (FBS) were from Gibco Life Technologies (Invitrogen, UK). Phosphate buffered saline (PBS) was from Oxoid (Hampshire, UK). GeneJuice transfection reagent was from Novagen (Nottingham, UK). Polyfect transfection reagent was from Qiagen (Surrey, UK). Transfection reagent for electroporation was from Amaxa Biosystems (Germany).

2.5.2. General cell culture conditions

All cell culture procedures were carried out under sterile conditions, in a Fasta Ultrasafe48 Type 2 tissue culture hood (Triple Red, Buckinghamshire, UK.) Cell growth media and solutions were filtered with 0.22 μm filters and any non-sterile solutions autoclaved (121°C, 15 lbs/$inch^2$, 20 minutes) prior to use.

3T3-L1 fibroblasts and Cos-1 cells were grown at 37°C with 5% CO_2, in a humidified incubator (NUAIRE™ DH AUTOFLOW CO_2 Air-jacketed incubator, Triple Red, Buckinghamshire, UK.) Cells were grown as monolayers in 75cm^2 cell culture flasks in Dulbeccos Modified Eagle Media (DMEM), 10% (v/v) Fetal Bovine Serum (FBS) and 2 mM glutamine. CHO cells were grown as above, but with Nutrient Mixture-12 HAM Media instead of DMEM. Each flask of cells was supplied with 10 mls of fresh,

prewarmed media every 48 hours. Cells were sub-cultured as required once cells had reached 60-90% confluency.

2.5.3. Sub-culturing of cells

When cells in the 75cm^2 flasks reached 60-90% confluency, the growth media was discarded, and the cells washed with serum-free media or PBS (serum inhibits trypsin, so must be removed prior to sub-culturing of cells.) The cells were detached from the flask by incubating the cells for 2-5 minutes with 5ml of Trypsin-EDTA. The trypsin was then neutralised by addition of 9 mls of pre-warmed growth media. Cell clusters were broken up by careful repeated expulsion through a Pasteur pipette. The cell suspension was then divided into 75 cm^2 flasks for further culture (1 in 10 sub-cultivation ratio) and/or multiwell plates with growth media as necessary.

2.5.4. Cryostorage and resuscitation of cells

For long term storage of cells, the media was removed from a 75 cm^2 flask of cells once they had reached 80-90% confluency. Cells were washed twice with 10 mls of PBS, then once with 2 mls of trypsin. Cells were then incubated at 37°C with 1 ml of trypsin for 2-5 minutes to detach cells them from the flask surface. 9 mls of prewarmed growth medium was added to the cells to terminate trypsinisation, then the suspension centrifuged for 5 mins at 1500 r.p.m. (Centurion 4000 series, Jepson Bolton, Hertfordshire, UK) to pellet the cells. Cells were resuspended in 10 mls of cryoprotectant medium (DMEM supplemented with 10% v/v DMSO and 20% v/v FBS). Cell suspension was pipetted into cryotubes, frozen at -20°C for1 hr, then -80°C overnight, before being transferred for storage in liquid Nitrogen.

For resuscitation of the cells, one vial was thawed for 1 min at room temperature, then 2-3 minutes at 37°C, before being transferred to a 75 cm^2 flask with 12 mls of pre-warmed growth medium.

2.5.5. Differentiation of 3T3-L1 fibroblasts into adipocytes

3T3-L1 fibroblasts were differentiated into adipocytes once they had been confluent for 2-5 days. Media was then replaced (day 0) with growth media containing 175nM insulin, 0.5mM 1-methyl-3-isobutylxanthine (IMIX) and 0.25µM dexamethazone. At 48 hour intervals (day 2 and day 4), this was then replaced with growth media containing 175nM insulin. After a further 24 hours (day 5) this was replaced with normal growth media, and changed every 48 hours until the cells were used. Cells were ready for use once fully differentiated (between day 8 and day 12).

2.5.6. Transfection of eukaryotic cells with plasmid DNA

2.5.6.1. Transient transfection of Cos-1 cells for GST pull-down assays

Cos-1 cells were sub-cultured onto 75 cm^2 flasks 24 hours preceding transfection so that the cells were 50-80% confluent for transfection. 7.5µg of plasmid DNA was made up to a volume of 227.5µl with serum-free media. In a separate tube, 22.5µl of GeneJuice transfection reagent was mixed with 750µl of serum-free media. Both tubes were left for 5 minutes at room temperature. The GeneJuice/media was then added to the DNA/media, mixed gently and left at room temperature for 15-20 minutes. Meanwhile, the cells were washed twice with 10 mls of serum free media. After 15-20 minutes, the GeneJuice/DNA mixture was applied drop wise onto the cells, and an additional 9 mls of complete media added before incubating at 37°C for 48 hours.

2.5.6.2. Transient transfection of CHO cells for co-immunoprecipitations

CHO cells were sub-cultured onto 75 cm^2 flasks 24 hours preceding transfection so that the cells were 50-80% confluent for transfection. 9.0 µg of plasmid DNA was made up to a volume of 600 µl with serum-free media. 60 µl of Polyfect was then added to the DNA/media, mixed gently and left at room temperature for 5-10 minutes. Meanwhile, the cells were washed twice with 10 mls of serum free media. After 5-10 minutes, the Polyfect/DNA mixture was applied drop wise onto the cells, and an additional 9.4 mls of complete media added before incubating at 37°C for 48 hours.

2.5.6.3. Transient transfection of CHO cells for glucose transport assays

CHO cells were sub-cultured onto 12-well plates 24 hours preceding transfection so that the cells were 50-80% confluent for transfection. A total of 1.0 µg of plasmid DNA was used per well. DNA for the wells of the controls consisted of 1.0 µg of GLUT4-pcDNA3-myc only whilst DNA for all other wells consisted of 0.1 µg of GLUT4-pcDNA3-myc and 0.9 µg of other DNA as appropriate. This was made up to a volume of 53 µl with serum-free media. 5.3 µl of Polyfect was then added to the DNA/media, mixed gently and left at room temperature for 5-10 minutes. Meanwhile, the cells were washed twice with 1 ml of serum free media. After 5-10 minutes, the Polyfect/DNA mixture was applied drop wise onto the cells, and an additional 1.0 mls of complete media added before incubating at 37°C for 48 hours.

2.5.6.4. Transient transfection of CHO cells for fluorescence microscopy

CHO cells were sub-cultured onto 2 cm^2 dishes 24 hours preceding transfection so that the cells were 50-80% confluent for transfection. A total of 1.5 μg of plasmid DNA was used per well, with ratios of DNA for double transfections varying depending on the constructs being used (see table 2.3 below). An additional 1.5 μg of empty pcDNA4-HisMax-C vector was added in order to get low enough expression of the fluorescent proteins for FCS data collection. The DNA was made up to a volume of 100 μl with serum-free media, 10 μl of Polyfect added to the DNA/media, then mixed gently and left at room temperature for 5-10 minutes. Meanwhile, the cells were washed twice with 1.5 ml of serum free media. After 5-10 minutes, the Polyfect/DNA mixture was applied drop wise onto the cells, and an additional 1.5 ml of complete media added before incubating at 37°C for 48 hours.

construct	%	construct	%
MFL	50	KH302	50
MFL	20	PKCζ	80
MFL	70	Syntaxin4	30
MFL	10	Kifap3	90
M295	50	KH302	50
M295	20	PKCζ	80
M295	70	Syntaxin4	30
M338	30	KH302	70
M338	20	PKCζ	80
M338	70	Syntaxin4	30

construct	%	construct	%
KHFL	70	PKCζ	30
KHFL	50	Syntaxin4	50
KH302	20	PKCζ	70
KH302	10	Syntaxin4	90
KH378	50	M295	50
KH378	20	PKCζ	80
KH378	50	Syntaxin4	50

Table 2.3. Ratios of DNA used for double transfection of CHO cells for fluorescence correlation spectroscopy.

CHO cells were transiently transfected using Polyfect transfection reagent and DNA in the ratios shown, 48 hours prior to FCS data collection.

2.5.6.5 Transient transfection of 3T3-L1 adipocytes for fluorescence microscopy

3T3-L1 fibroblasts were grown and differentiated on 75 cm^2 flasks as described above. Cells were transfected once they had reached day 5-10 of differentiation and 24 hours prior to data collection. A total of 5 µg of DNA was prepared into minifuge tubes as appropriate, with ratios of DNA for double transfections varying depending on the constructs being used (see table 2.3.) Cells were trypsinised as explained in section 2.5.3 and stored at 37 °C until needed. The amount of cell mortality and efficiency of transfection when using electroporation is highly dependant upon the number of cells used per transfection. Therefore, the cell density must be determined and a suitable number of cells used. For this the cell density was determined using a haemocytometer. 150 µl of mixed cell suspension was added to 50 µl of 0.4% w/v trypan blue (making a ¾ dilution of cells.) A small amount of this was then added to the haemocytometer plate and the number of cells contained within the triple-edged squares (4 x 4 single squares) were counted. In order to calculate the cell density, the following equation was used:

$$\text{Number of cells per ml} = \frac{\text{number of cells counted}}{\text{number of single squares}} \times 25 \times 10^4 \times \frac{1}{\text{dilution}}$$

$$= \frac{\text{number of cells counted}}{16} \times 33.3 \times 10^4$$

A total of 5 x 10^6 cells were required per transfection. The appropriate amount of cells for the required number of transfections was placed in a 15 ml centrifuge tube and centrifuged at 500 xg for 2 minutes. The supernatant was discarded so that no residual medium covered the cells. The cell pellet was then resuspended in room temperature Nucleofector™ Solution V (Amaxa, Germany) so that there was 100 µl per transfection. 100 µl of the Nucleofector™ Solution-cell mixture was mixed with the appropriate DNA, placed in an Amaxa certified cuvette. This was then placed in the cuvette holder of the

Amaxa machine and cells electroporated with Amaxa Programme T-20. 500 µl of medium was added immediately to the cells which were then plated out onto 24 well plates with collagen-coated cover-slips, with an additional 500 µl of medium. Cells were not serum starved prior to data collection, as they were unable to survive both electroporation and serum starving.

construct	%	construct	%
MFL	10	Kifap3	90
MFL	50	KHFL	50
MFL	10	KH302	90
M295	50	KH302	50

Table 2.4. Ratios of DNA used for double transfection of 3T3-L1 adipocytes for fluorescence correlation spectroscopy.

3T3-L1 ad ipocytes were transiently transfected using electroporation and DNA in the ratios shown, 24 hours prior to FCS data collection.

2.5.7. Stimulation of cells with insulin

For a number of different experiments, cells must firstly be stimulated with insulin. Prior to insulin stimulation, cells were starved of serum for at least 48 hours, as serum mimics many of the effects of insulin. Cells were washed 2-3 times in serum-free media, before incubation with serum-free media for >24 hours prior to use. When ready to use, cells were exposed to 10^{-7} M insulin for 10 mins whilst incubated at 37°C. Insulin stimulation was terminated by removal of the medium/insulin and addition of ice-cold PBS.

2.6. PROTEIN EXTRACTION FROM MAMMALIAN CELLS

Protein extraction was carried out at 4°C. Growth medium was discarded, and cells washed twice with 10 mls of ice-cold PBS. The cells were then scraped into 2 X 0.5-1.0 mls of lysis buffer (62.5 mM Tris, pH 7.4, 1% v/v NP-40, 1% v/v Sigma protease inhibitor cocktail) then taken through a 0.5 x 25 mm needle 6 times. This mixture was incubated for 10 mins to ensure cells had lysed completely, then spun at 12000 r.p.m. for 5 mins. The supernatant of the cell extract was then used for appropriate experimental procedures, or diluted with 5X Laemmli sample buffer (312.5 mM Tris, 10% w/v SDS, 10% v/v glycerol, 0.01% w/v pyronin Y) containing DTT (19 µg/250 µl) and boiled for 3 mins, prior to storage at -80°C if sample is required for SDS-PAGE and immunoblotting.

2.7. DETERMINATION OF PROTEIN CONCENTRATION

Prior to SDS PAGE and immunoblotting, the protein concentration of the cell extracts was determined using the BioRad DC assay (similar to the Lowry protein assay.) Protein standard solutions of 0.2, 0.4, 0.6, 0.8, 1.0 and 1.2 mg/ml were prepared in a 1% w/v SDS solution. Protein standards (5 µl) and cell extract (5 µl) were placed in triplicate in to a 96 well microtiter plate. The working reagent A' was prepared by adding 20 µl of reagent S to 1 ml of reagent A (an alkaline copper tartate solution.) 25 µl of this reagent A' was then added to each well, followed by 200 µl of reagent B (a dilute folin reagent). The plate was agitated to mix the reagents and the absorbances read at 630 nm in a 96 well plate reader (Dynatech) using Revelation software. The average readings for the protein standards were plotted on a graph of Absorbance against protein concentration (mg/ml) and the average absorbances of the cell extracts used to extrapolate their protein concentration from the graph.

2.8. SDS-PAGE

2.8.1. Materials

Ultra pure protogel (30% w/v) acrylamide was from National Diagnostics (USA.) ECL reagent and Hyperfilm MP were from Amersham International plc (UK).SeeBlue™ pre-stained standard 1 x molecular weight marker was from Invitrogen (USA.)

2.8.2. Protocol

SDS-PAGE was carried out using the BioRad Minigel apparatus system. Slab gels of 5 x 8 cm were prepared as follows. 10% v/v resolving gels were made from 3 ml acrylamide stock (30% w/v acrylamide, 0.8% w/v bis-acrylamide) 5 ml resolving buffer (0.3725 M Tris-HCl, 0.1% w/v SDS, pH 8.8) and 2 ml dH_2O. Polymerisation was started with the addition of 20 µl TEMED and 0.1% w/v ammonium persulphate and loaded into the glass plates. Immediately, a layer of isopropanol was added to the top of the gel to ensure the gel set with a flat top. Once the resolving gel had set (~15 mins) the isopropanol was washed off with dH_2O. The 4% v/v stacking gel was then prepared with 1 ml acrylamide (30% w/v acrylamide, 0.8% w/v bis-acrylamide), 3 ml stacking buffer (0.123 M Tris-HCl, 0.1% w/v SDS, pH 6.8) and 2 ml of dH_2O. This was polymerised with 7 µl of TEMED and 33 µl of ammonium persulphate, layered on top of the resolving gel layer and a 10 well comb inserted so as to leave ~1 cm of the stacking layer (from the bottom of the well to the start of the resolving gel.) Once set (~15 mins) the comb was removed, and the wells washed thoroughly with dH_2O.

The protein samples were boiled for 3 mins to fully dissolve the SDS and ensure proteins were completely denatured. Typically 20 µg of protein was loaded into each well, with one well containing 2.5 µl of SeeBlue™ molecular weight marker (Invitrogen), in order to assess the molecular weight of the protein bands. The proteins were then separated in

running buffer (25 mM Tris, 192 mM glycine, 0.1% w/v SDS) at 32 mA for approximately 40 mins.

2.9. IMMUNODETECTION

2.9.1. Materials

Protran nitrocellulose transfer membrane was from Schleider and Schuell (Germany.) 3MM paper was from Watman (UK.) Anti-GST, anti-HA-tag and anti-Myc-tag antibodies were from Cell Signalling Technology Inc (USA.) Anti-Xpress^{TM} antibody was from Invitrogen. Anti-Protein Kinase C ζ and goat-anti-mouse antibody were from Sigma. Goat-anti-rabbit antibody was from Santa Cruz (USA.) Anti-GFP Antibody was from SySy, Germany. ECL reagents and Hyperfilm MP were from Amersham Biosciences (Buckinghamshire, UK).

2.9.2 Protein transfer to nitrocellulose membrane

The transfer of proteins from the SDS-PAGE gels to nitrocellulose membranes was carried out using the Hoefer Semi-dry apparatus. The nitrocellulose membrane (1 sheet, 5.5x8.5 cm) and whatman 3MM paper (6 sheets, 5.5 x 8.5 cm) were pre-soaked in transfer buffer (25 mM Tris, 192 mM glycine, 20% v/v methanol) for 5 mins. A gel-membrane "sandwich" was subsequently prepared by sequentially layering 3 sheets of 3MM paper onto a glass plate, followed by the nitrocellulose membrane, the gel and a further 3 sheets of 3MM paper. This was then placed onto the Hoefer apparatus with addition of more transfer buffer. The protein was transferred onto the nitrocellulose membrane for 1 hr 40 mins-2 hrs at 72 mA.

2.9.3. Immunodetection

The nitrocellulose membranes were washed in appropriate blocking buffer at room temperature, immediately after completion of transfer. The membrane was then incubated with constant agitation at room temperature for 1 hr with 20 mls of appropriate blocking buffer. Membranes were then incubated with constant agitation with the appropriate dilution of primary antibody, at 4°C overnight. Membranes were then washed 3 times with 10 mls of appropriate washing buffer, before being incubated with the appropriate secondary antibody for 1½ hrs at room temperature. Membranes were then washed 3 times in wash buffer prior to detection of proteins. The proteins were detected using the ECL reagents and Hyperfilm MP by enhanced chemiluminescence.

	Anti-GST	Anti-HA	Anti-Xpress
Wash	1x5 min TBS-Tw (0.1%)	1x5 min TBS-Tw (0.1%)	1x5 min TBS-Tw (0.1%)
Block	5% milk in TBS-Tw (0.1%)	5% milk in TBS-Tw (0.1%)	5% milk in TBS-Tw (0.1%)
Wash	---	---	---
Primary antibody	1:1000 5% milk in TBS-Tw (0.1%)	1:1000 5% milk in TBS-Tw (0.1%)	1:5000 5% milk in TBS-Tw (0.1%)
Wash	3x5 min 5% milk in TBS-Tw (0.1%)	3x5 min 5% milk in TBS-Tw (0.1%)	3x3 min 5% milk in TBS-Tw (0.1%)
Secondary antibody	1:2000 GAM 5% milk in TBS-Tw (0.1%)	1:2000 GAM 5% milk in TBS-Tw (0.1%)	1:2000 GAM 5% milk in TBS-Tw (0.1%)
Wash	3x5 min TBS-Tw (0.1%)	3x5 min TBS-Tw (0.1%)	3x5 min TBS-Tw (0.1%)

Table 2.3. Reagents and conditions for Western blotting.

BSA = bovine serum albumin. GAM = goat-anti-mouse antibody. GAR = goat anti rabbit antibody. TBS = Tris buffered saline. TBS-Tw = Tris buffered saline with Tween20.

	Anti-Phospho-PKB substrate	**Anti-80K-H**	**Anti-PKCζ**
Wash	1x5 min TBS-Tw (0.1%)	1x5 min TBS-Tw (0.05%)	1x5 min TBS-Tw (0.05%)
Block	5% milk in TBS-Tw (0.1%)	5% milk in TBS-Tw (0.05%)	3% milk in TBS-Tw (0.05%)
Wash	3x5 min 5% BSA in TBS-Tw (0.1%)	---	---
Primary antibody	1:1000 5% BSA in TBS-Tw (0.1%)	1:200 5% milk in TBS-Tw (0.05%)	1:20000 3% milk in TBS-Tw (0.05%)
Wash	3x5 min 5% milk in TBS-Tw (0.1%)	3x5 min 5% milk in TBS-Tw (0.05%)	3x5 min 3% milk in TBS-Tw (0.05%)
Secondary antibody	1:2000 GAR 5% milk in TBS-Tw (0.1%)	1:2000 GAM 5% milk in TBS-Tw (0.05%)	1:2000 GAR 3% milk in TBS-Tw (0.05%)
Wash	3x5 min TBS-Tw (0.1%)	3x5 min TBS-Tw (0.05%)	3x5 min TBS-Tw (0.05%)

Table 2.3. Reagents and conditions for Western blotting.

BSA = bovine serum albumin. GAM = goat-anti-mouse antibody. GAR = goat anti rabbit antibody. TBS = Tris buffered saline. TBS-Tw = Tris buffered saline with Tween20.

	Anti-GFP
Wash	1x5 min TBS-Tw (0.1%)
Block	5% milk in TBS-Tw (0.1%)
Primary antibody	1:2000 5% milk in TBS-Tw (0.1%)
Wash	3x5 min 5% milk in TBS-Tw (0.1%)
Secondary antibody	1:2000 GAR 5% milk in TBS-Tw (0.1%)
Wash	3x5 min TBS-Tw (0.1%)

Table 2.3. Reagents and conditions for Western blotting.

BSA = bovine serum albumin. GAM = goat-anti-mouse antibody. GAR = goat anti rabbit antibody. TBS = Tris buffered saline. TBS-Tw = Tris buffered saline with Tween20.

2.10. PROTEIN: PROTEIN INTERACTION ASSAYS

2.10.1. GST pull-down assay

2.10.1.1. Overview

Analysis of protein: protein interactions *in vitro* were performed using a GST pull-down technique. GST (glutathione-S-transferase) is an enzyme family that catalyzes the addition of glutathione to endogenous substrates. The use of gene fusion systems in E.coli enables the inducible expression of genes or gene fragments as fusions with the GST moiety, which preserves its enzymatic activity. This allows for versatile expression, purification and detection of the fusion proteins. The fusion proteins can be purified using immobilized glutathione (e.g. glutathione immobilized on sepharose, such as glutathione Sepharose 4B). GST fusion proteins are captured by the affinity medium and impurities are removed by washing. The protein of interest may then be removed from the beads by either elution with reduced glutathione, cleavage of the protein of interest from the GST moiety, or through denaturing conditions. A GST pull down assay involves the production of bacterially expressed GST-fusion proteins which are immobilized on glutathione sepharose beads, then exposed to a cell extract overexpressing a second protein of interest. After washing, the proteins of interest may be removed from the beads and the presence of binding assessed by SDS-PAGE and western blotting (please see figure 2.1 below).

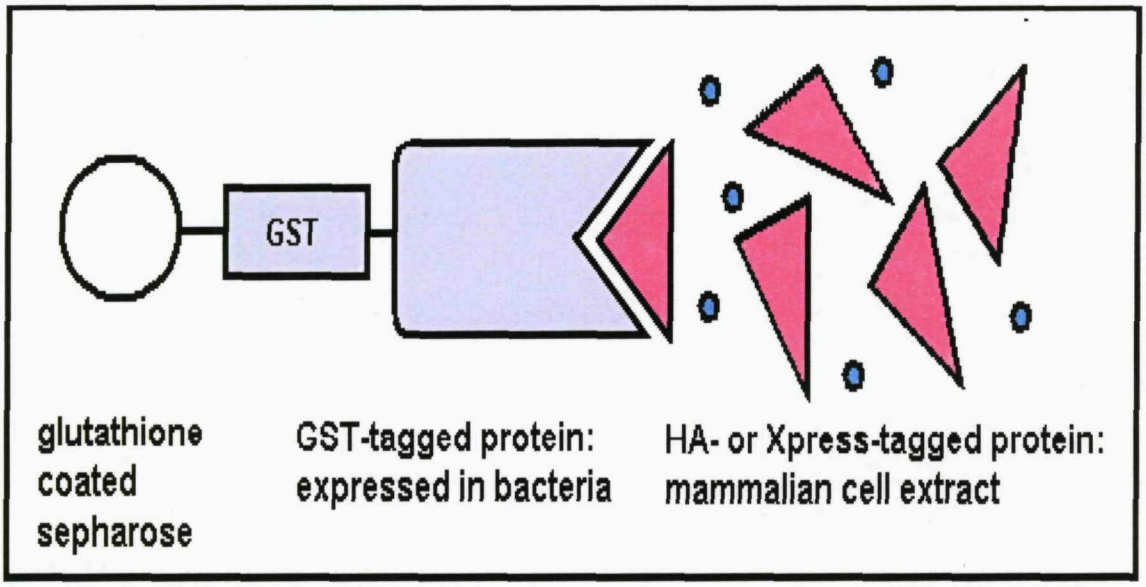

Figure 2.1. GST pull-down assay.

Diagram showing the principles of a GST pull-down assay.

2.10.1.2. Method

40 µl of glutathione-sepharose beads were placed in each 1.5 ml microcentrifuge tube. Beads were washed by the addition of 1 ml PBS, followed by a pulse spin and the removal of all liquid. Beads were then exposed to 100-500 µl of the appropriate crude *E.coli* protein extract (see above) at room temperature with constant agitation for 1 hour. Any remaining unbound protein was removed by washing the beads in 3 x 1 ml of PBS. 200-500 µl of Cos-1 cell extract (see above) overexpressing the appropriate protein, was then added to the dry beads and incubated at 4 °C with constant agitation for 3½ hours. Any remaining unbound protein was removed by washing the beads in 3 x 1 ml of PBS at 4 °C and samples stored at -80 °C, prior to analysis by SDS-PAGE and immunoblotting. All experiments were repeated on at least three separate occasions.

2.10.2. Immunoprecipitation

2.10.2.1. Overview

Detection of protein: protein interactions between two mammalian expressed proteins were carried out using co-immunoprecipitation. Antibodies directed against one protein antigen can be used to concentrate that specific antigen from a complex mixture such as a cell lysate. The antigen-antibody complex can be easily collected by capturing the complex onto a solid-phase matrix. Protein A and Protein G are bacterial proteins that have a high affinity for the Fc region of most mammalian immunoglobulins. These proteins are commonly used to coat Sepharose or agarose beads in order to immobilise the antibody-antigen complex. Because these proteins bind to the Fc region of the antibody, the antigen binding sites of the antibodies remain available for antigen binding. Once the protein of interest has been isolated, the sample can then be analysed for the presence of binding partners by western blotting.

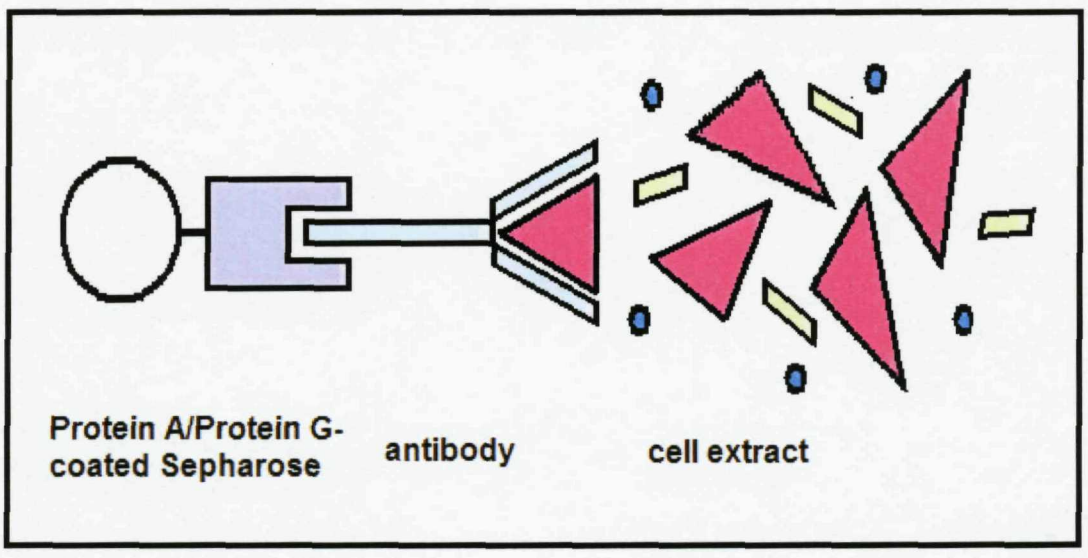

Figure 2.2. Immunoprecipitation.

Diagram showing the principles of an immunoprecipitation.

2.10.2.2. Method

20 µl of Protein A and 20 µl of Protein G-sepharose beads were placed in each 1.5 ml microcentrifuge tube. Beads were washed by the addition of 1 ml PBS, followed by a pulse spin and the removal of all liquid. The antibody was added to the beads as per the manufacturer's instructions. 200-500 µl of mammalian cell extract over-expressing the appropriate protein (see section 2.6.) was then added to the bead/antibody complex and incubated at 4 °C with constant agitation for 5 hours. Any remaining unbound protein was removed by washing the beads in 3 x 1 ml of PBS at 4 °C and samples stored at -80 °C, prior to analysis by SDS-PAGE and immunoblotting. All experiments were repeated on at least three separate occasions.

2.10.3. Fluorescence Correlation Spectroscopy

2.10.3.1. Overview

The development of sophisticated biochemical and cell-based assays has lead to an incredibly detailed understanding of the molecular interactions and processes within the cell. However, trying to analyse the complexity of cellular events with simplistic in vitro models has its obvious disadvantages. The cell is a highly dynamic and complex system, undergoing constant and subtle modifications. Although in vitro biochemical techniques allow a simple and reproducible way of studying individual components of the cell, they do not take into consideration factors such as subcellular localization, concentration, mobility or accessibility of the molecule of interest. For example, endogenous proteins may be able to interact *in vitro*, but they may never be in the correct locality at the correct time for an interaction to occur within a living cell. The development of live cell imaging and analysis has provided scientists with the tools to overcome such problems. Advances in the use of fluorescence probes and microscopy have enabled the detailed study of

specific activities within subcellular compartments. FCS is one particularly sophisticated technique that enables such analysis on a single-molecule scale. This technique uses confocal imaging to measure minute changes in fluorescence fluctuations over a given time. This enables the determination of parameters such as concentration, diffusion coefficients and binding characteristics of fluorescently labelled proteins. Above all, such characteristics can be determined from living cells.

2.10.3.2. Autocorrelation

Fluorescence correlation spectroscopy (FCS) uses confocal microscopy to observe fluorescently-tagged molecules moving through a small fixed observation volume. When a fluorescent molecule enters the observation volume, the fluorescence intensity will increase. When it leaves the observation volume the fluorescence intensity will decrease. These fluctuations in fluorescence are measured over time and can be used to determine various characteristics of the fluorescent molecules of interest, such as concentration or molecular speed.

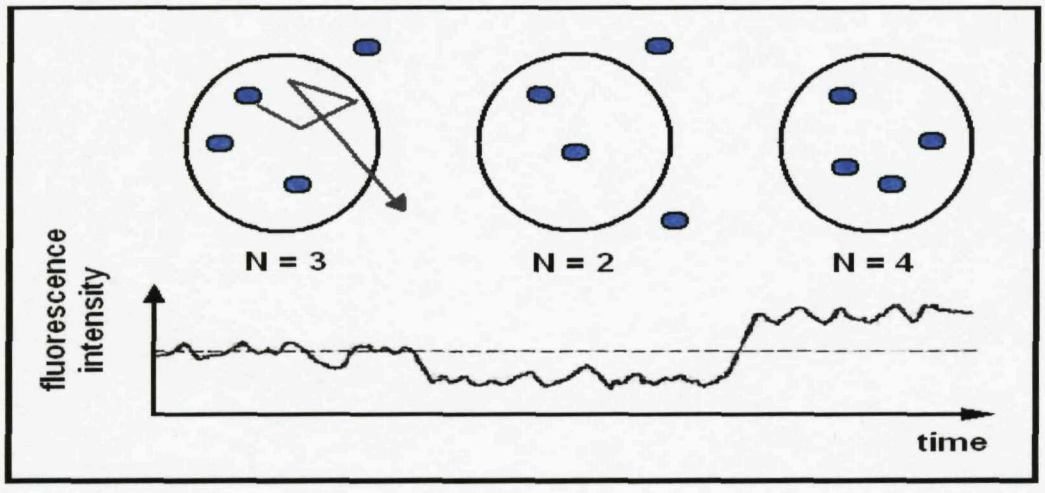

Figure 2.3. FCS: measuring changes in fluorescence intensity over time.

The fluorescence intensity within a small, fixed observation volume is measured over time. When a fluorescently-tagged molecule enters the observation volume, the fluorescence intensity increases. When a fluorescently-tagged molecule leaves the observation volume, the fluorescence intensity decreases.

The amplitude of each fluctuation provides information concerning the concentration of the molecule during the time it is in the observation volume (the greater the number of fluorescently tagged molecules in the observation volume, the greater the fluorescence intensity).The duration of each fluctuation provides information concerning the molecular motion (its diffusion coefficient or speed) through the observation volume (please refer to figure 2.3). This data is then *autocorrelated.* Autocorrelating the data removes any "non-randomness" that may be seen due to factors such as Brownian motion. The autocorrelation function $G(\tau)$ is a measure of the **self-similarity** of the fluorescence signal. When the autocorrelation curve is completely overlaying itself, it will have 100 % autocorrelation. The autocorrelation curve is then shifted along the time axis (the x-axis) by numerous lag times, τ, and the amount of autocorrelation measured.

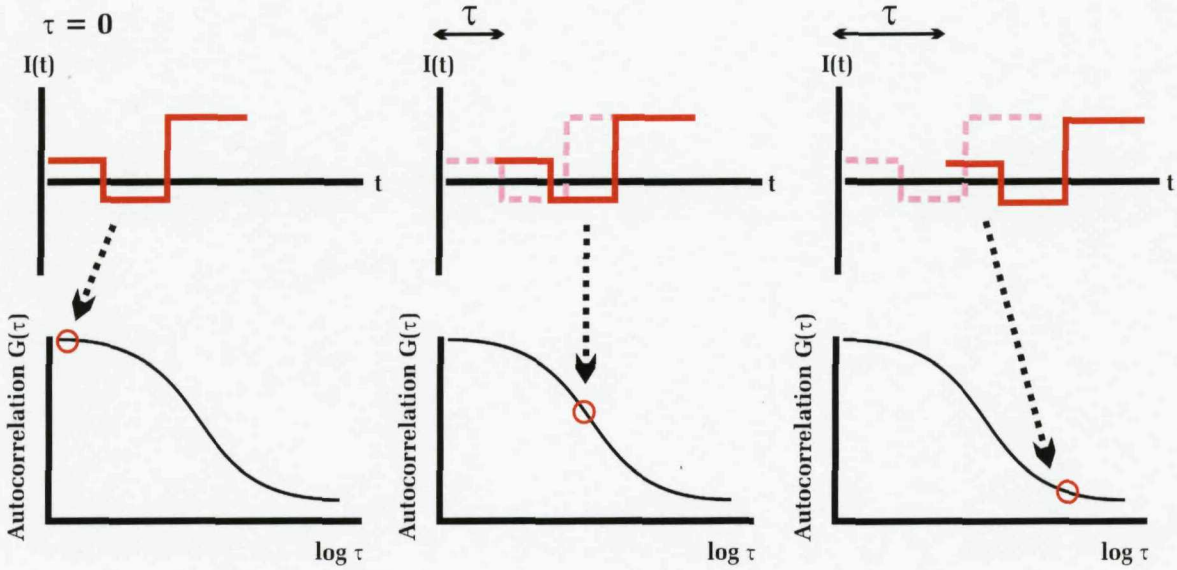

Figure 2.4. FCS: Autocorrelation.

The top graphs show fluorescence intensity, I(t), versus time, t. The fluorescence intensity graph is autocorrelated. This involves shifting the graph along the x-axis by a lag time (τ), and measuring the level of self-similarity. When the fluorescence intensity graph completely overlays itself, the autocorrelation, G(τ), will be 100%. This gradually decreases as τ is increased. The level of autocorrelation, G(τ), is plotted on the y-axis versus the log of the lag time (log τ).

The autocorrelation function is plotted on the y-axis versus the log of the lag time (log τ). Please refer to figure 2.4. At $\tau = 0$, the autocorrelation is inversely proportional to the number of molecules in the fixed volume. The time, τ, corresponding to 50% autocorrelation is the average time that the fluorescently-tagged molecule spends in the fixed volume. This value is called TauD1. Please refer to figure 2.5. Therefore, if the autocorrelation curve moves to the right hand side, the TauD1 value will be larger. This indicates that on average, the molecule is spending a greater amount of time in the fixed volume and is therefore moving more slowly. Hence, if the autocorrelation curve shifts to the left hand side, the TauD1 value is smaller, indicating that the molecule of interest is moving faster.

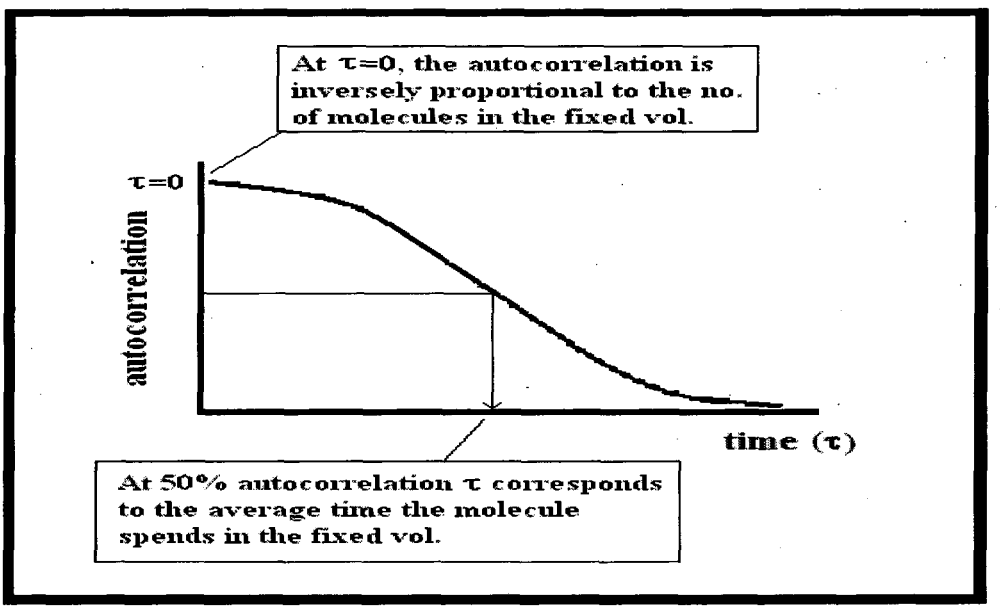

Figure 2.5. FCS: The autocorrelation curve.

The autocorrelation curve can be used to determine the average speed of a fluorescently-tagged molecule.

2.10.3.3. FCS Equipment and Methods

FCS and confocal microscopy were carried out with a Leica 63 × water immersion objective and Leica SP2 confocal laser scanning microscope (Leica, Germany). Samples were excited with a 514 nm Ar/Kr laser at low-average laser power. Cells were first washed twice with 1 ml of pre-warmed Krebs-Ringer buffer (10 mM Hepes, pH 7.4, 100 mM $CaCl_2$, 136 mM NaCl, 4.7 mM KCl and 1.25 mM $MgSO_4$). Cells were then incubated with 2 mls of the same buffer. A pre-bleaching illumination period of 160 s was used prior to data collection. Correlation curves of 600 s were collected from cells and traces analysed with the Leica FCS software. Experiments were performed at room temperature to reduce the mobility of the cells. When required, cells were stimulated with 100 nM insulin in Krebs-Ringer buffer for 20 minutes. FCS data was collected for the EYFP-tagged protein only. This data was collected from 6 individual cells both pre and post insulin stimulation. FCS data was fitted using a 3D Gaussian triplet calculation (Leica software) and the time corresponding to 50% autocorrelation calculated. This value is the diffusion coefficient of the EYFP-tagged construct, which is the average time that the EYFP molecules spend in the observation volume. A larger diffusion coefficient corresponds to a longer time spent in the observation volume and hence relates to a slower moving molecule. Knowing the average speed of the protein of interest *in vivo* provides valuable insight into its behaviour. For example, larger or more membrane bound complexes will move slower than smaller or less tethered ones. Mean and s.e.m. were calculated for pre-and post-insulin experiments. The presence of the over-expressed proteins was confirmed by detection of the fluorescence by microscopy and subsequent western blotting of the cell extract using the anti-GFP antibody (SySy, Germany) (Data not shown).

CLONING

3. CLONING

3.1. Overview

DNA was truncated and amplified using the polymerase chain reaction (PCR) method. PCR proceeds in three distinct stages (denaturing, annealing and elongation) each governed by temperature (see figure 3.1.) First the template DNA is denatured to separate the complimentary strands (95 °C for 2 minutes). Next the reaction mixture is cooled to a temperature that enables the oligonucleotide primer to hybridise to the single stranded template DNA (the choice of annealing temperature depends on the properties of the oligonucleotide primer and should last for > 45 seconds. The reaction is then heated to the optimal polymerisation temperature of the thermostable DNA polymerase (72 °C for 1-3 minutes). This allows the DNA polymerase to bind to and extend the primers, enabling the template DNA to be amplified (the length of time for the elongation step is dependant on the size of the DNA to be amplified). This three-step process is repeated, allowing a small concentration of DNA to be amplified to very high levels.

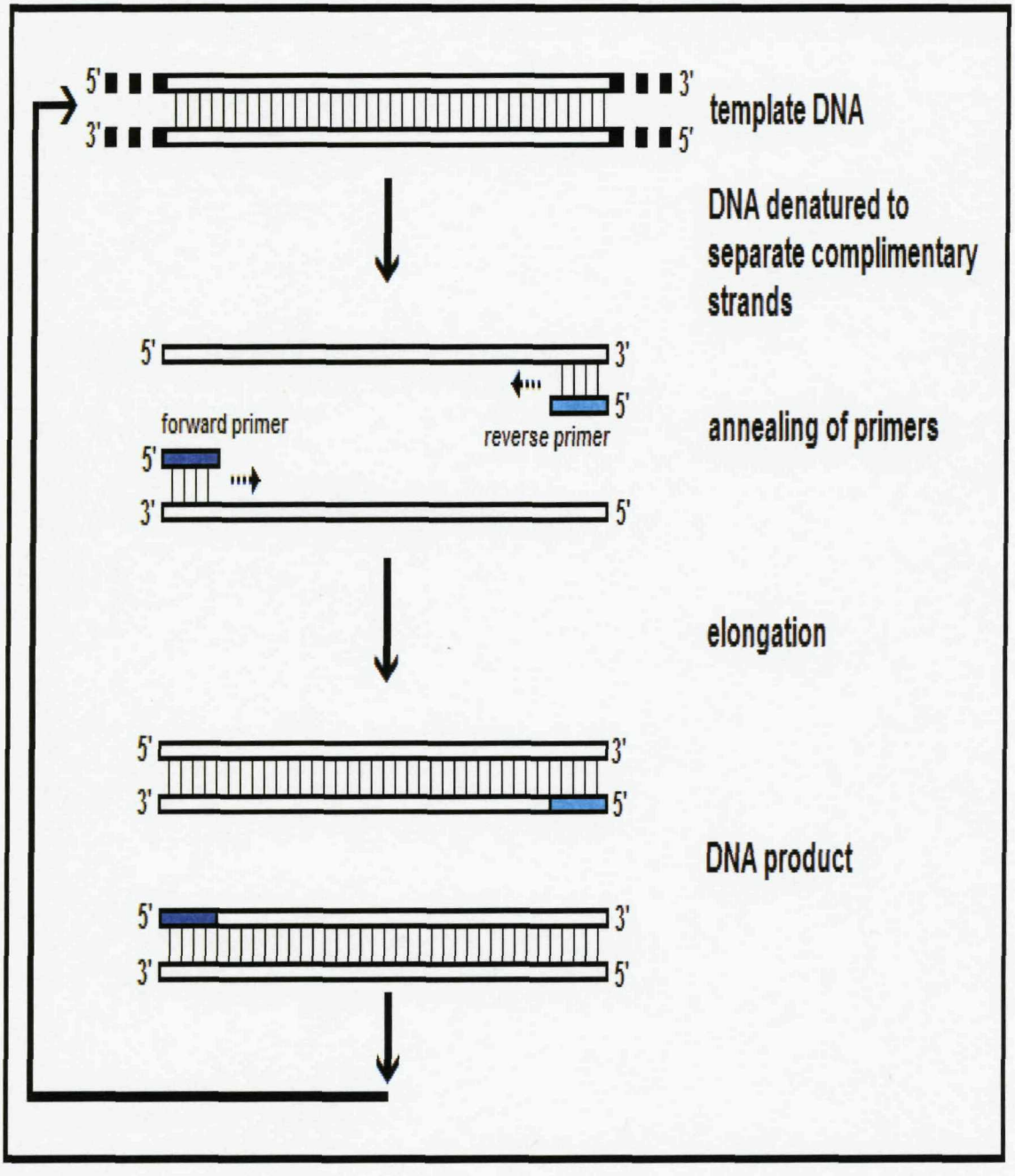

Figure 3.1. The Polymerise Chain Reaction

Figure representing the stages of PCR. Template DNA is denatured, primers bind and the resulting double-stranded DNA is extended by a DNA Polymerase.

The use of the PCR technique allows great scope for manipulation of DNA/proteins. By careful design of the primers, restriction sites (or other minor modifications e.g. mutations) can be introduced to the ends of the DNA. This enables restriction digest of the PCR products and ligation of the DNA into appropriate vectors. Synthetic oligonucleotide primers can be targeted to precise regions of the DNA sequence allowing the amplification of a specific section of DNA, for example truncations of the full length gene. When designing primers, the forward primer must be complementary to the 3'- end of the non-coding strand of target DNA (i.e. this makes the primer the same sequence as the coding strand of target DNA).The reverse primer must be complementary to the 3'- end of the coding strand of target DNA. Any modifications to the DNA (such as insertions of restriction sites) must remain in frame with the coding sequence of the target gene, so that they are coded for correctly. In addition to standard PCR, a PCR protocol called SOEing (Splicing by Overlap Extension) allows the introduction of deletions, insertions or point mutations into a DNA sequence. In this study a two-sided SOEing method was used to generate deletions in the DNA. In this method, four primers are used in three PCR reactions to generate the final deletion in the DNA (see figure 3.2.) In the first round of PCR, two separate PCR reactions are used to generate the two sequences of DNA either side of the region to be deleted. One of the internal primers is designed with a 5'- extension sequence complementary to the other primer sequence. The ends of the two PCR products will therefore be complementary and can be joined in a second round of PCR.

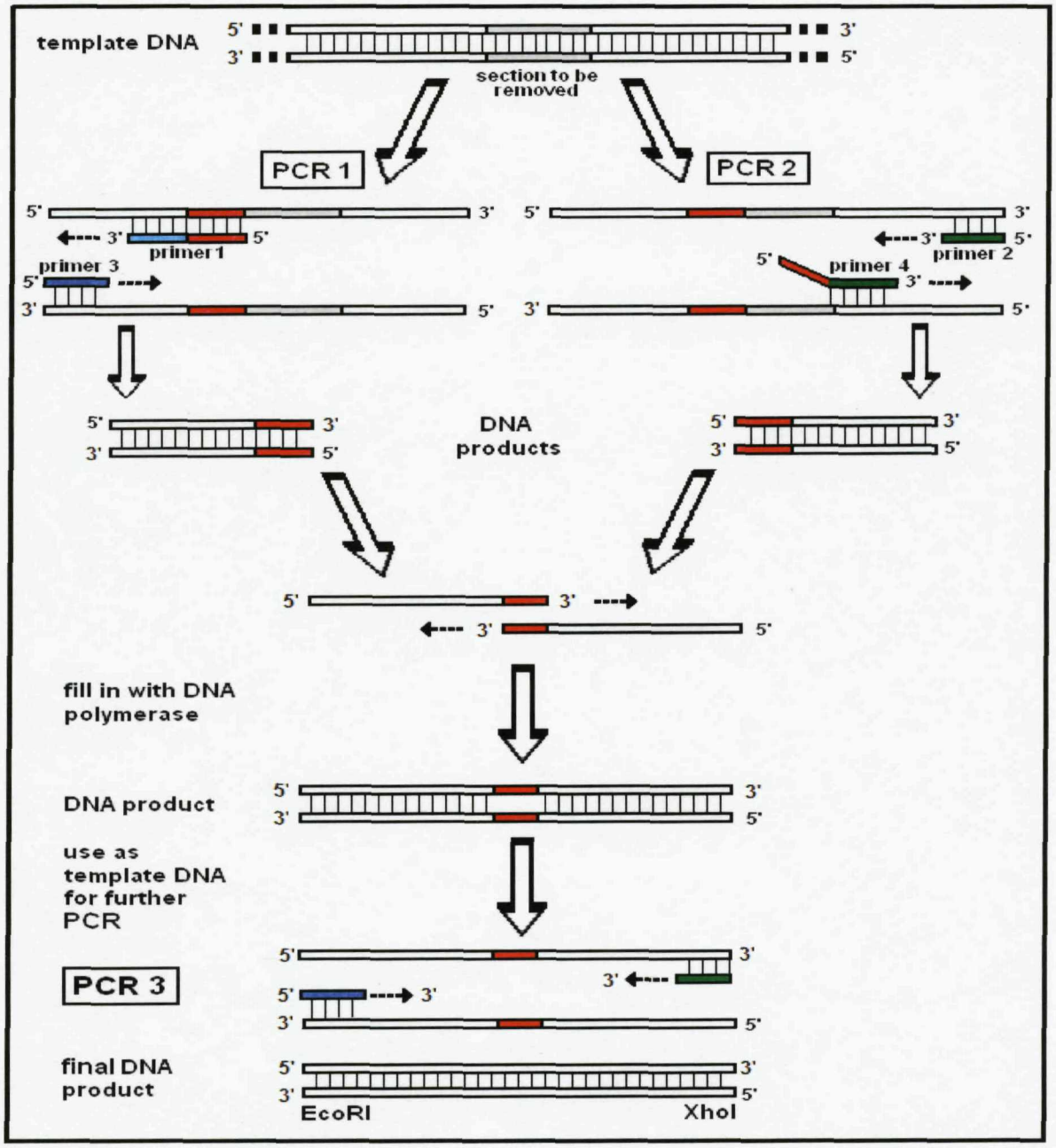

Figure 3.2. The two-sided SOEing method of PCR for the production of deletions in DNA

Figure representing the two-sided SOEing technique. Two separate PCR reactions are first used to amplify the two regions of DNA either side of the section to be deleted. These are then annealed; Pfu polymerase fills in the DNA strands. This is then amplified to give a DNA product that lacks the deleted region (as shown in red).

3.2. Cloning of 80K-H constructs

3.2.1. 80K-H constructs: Ligation into pcDNA4HisMax-C and pGex-5X-1 vectors

3.2.1.1. 80K-H truncation constructs

The KH302, KH378, KH460 and KH490 constructs, in both pGex5X-1 and pcDNA4-C vectors, were a kind present from Dr. Conrad Hodgkinson (see figure 3.3.).

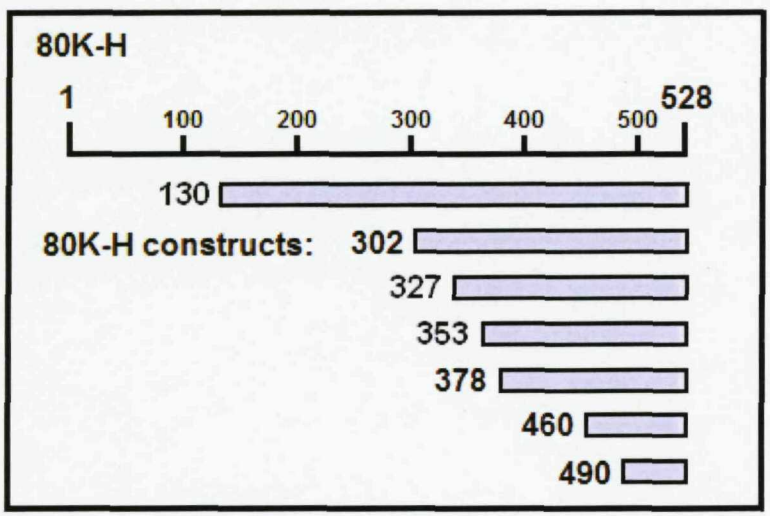

Figure 3.3. 80K-H truncation constructs

A further two 80K-H truncation constructs were made, with N-termini lying between KH302 and KH378, these being KH327 and KH353, using a standard PCR protocol (see figure 3.3.) KH302-pGex5X-1 was used as template DNA. The reverse primer was complementary to the C-terminal of the multiple cloning site of the pGex5X-1 vector. The forward primers were designed to be complementary to the required section of 80K-H, with the insertion of a 5' *Eco*RI restriction site to enable cloning into pGex5X-1 or pcDNA4HisMax-C (see figure 3.4.).

1081 tcagaagcgg aagctcaggc cctcctcagt ggggacacac agacagacgc cacctctttc
1141 tacgaccgcg tctgggccgc catcagggac aagtaccggt ccgaggcact gcccaccgac
1201 cttccagcac cttctgcccc tgacttgacg gagcccaagg aggagcagcc gccagtgccc

1261 tcgtcgccca cagaggagga ggaggaggag gaggaggagg aggaagaaga ggctgaagaa
KH327▼----------▼
1321 gaggaggagg **aggaggattc cgaggaggcc ccaccgccac tg**tcaccccc gcagccggcc
KH353▼----------▼
1381 agccctg**ctg aggaagacaa aatgccgccc tacgacgagc** agacgcaggc cttcatcgat

1441 gctgcccagg aggcccgcaa caagttcgag gaggccgagc ggtcgctgaa ggacatggag
1501 gagtccatca ggaacctgga gcaagagatt tcttttgact ttggccccaa cggggagttt
1561 gcttacctgt acagccagtg ctacgagctc accaccaacg aatacgtcta ccgcctctgc

Type in blue = sequence that was changed for *Eco*RI restriction site

Figure 3.4. 80K-H sequence and positioning of primers for KH327 and KH353

	Primer	Sequence	Tm(° C)
1	KH327 forward	5'- agg agg aat tcg agg agg ccc cac cgc cac tg -3'	66
2	KH353 forward	5'- ctg agg aat tca aaa tgc cgc cct acg acg ag -3'	61
3	pGex5X-1 reverse	5'- ccg gga gct gca tgt gtc aga gg -3'	57

Type in blue = *Eco*RI restriction site

Table 3.1. Primer Sequences for the production of KH327 and KH353

Reactions were set up as in section 2.3.2. K302-pGex5X-1 was used as template DNA. Primers 1 and 3 (see table 3.1) were used for the production of the KH327 construct and primers 2 and 3 (see table 3.1) were used for the production of the KH353 construct using the following PCR conditions (see table 3.2.).

	No. of cycles	KH 327 and KH353	
denaturing	1	95°C	2 min
amplification	25	95°C	45 sec
		58°C	45 sec
		72°C	90 sec
elongation	1	72°C	6 min

Table 3.2. PCR conditions used for the production of KH327 and KH353

The DNA product from these PCR reactions were then digested with the restriction enzymes *Eco*RI and *Xho*I, purified with a gel extraction kit (Qiagen) and ligated into the pcDNA4HisMax-C and pGex5X-1 vectors (see section 2.3.) Prior to gel extraction, the DNA bands were visualized on a gel against a 1 kb ladder to ensure they were of the correct size (see figure 3.4.).

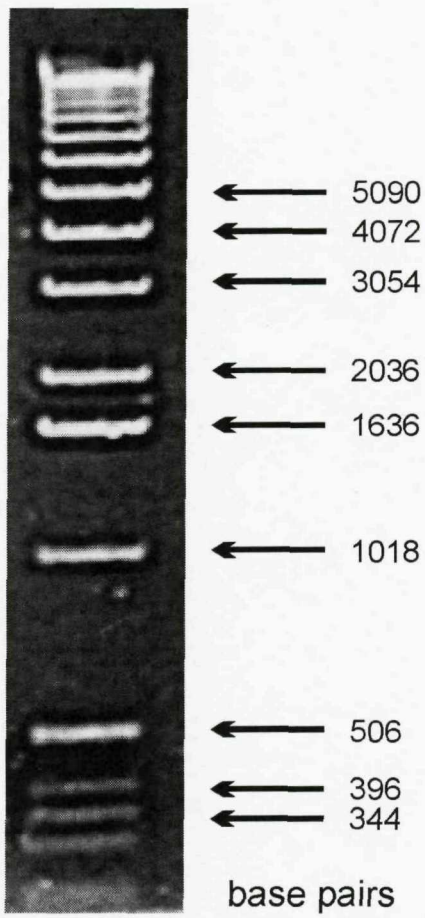

Figure 3.4. 1 kb DNA ladder

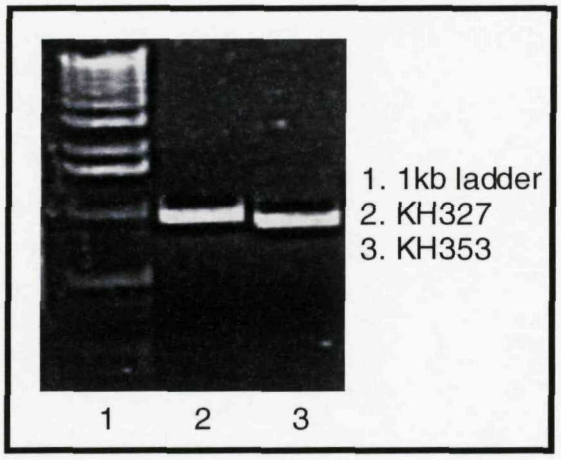

Figure 3.5. KH327 and KH353 DNA from PCR reactions

3.2.1.2. KH130

The 80K-H clone (Invitrogen) arrived in the pcDNA3-myc vector. Although this contains both *Eco*RI and *Xho*I restriction sites, they are not in frame with the *Eco*RI and *Xho*I restriction sites for the vectors I wished to use. Primers were designed (see table 3.3) so that the DNA could be cut with *Eco*RI and *Xho*I, ligated into the vectors of choice and remain in frame.

	Primer Name	Primer Sequence	Tm
1	KH130 forward	5'- ccc tg**g aat tc**a tgg ccg agg tca ccc gcg -3'	65
2	KH130 reverse	5'- g cgc cc**c tcg ag**c tag agc tcg tca tgg tcg -3'	66

Type in blue = *Eco*RI restriction site

Type in green = *Xho*I restriction site

Table 3.3. Primer Sequences for the production of KH130

The DNA product from this PCR reaction was then purified by ethanol precipitation, digested with the restriction enzymes *Eco*RI and *Xho*I, purified with a gel extraction kit (Qiagen) then ligated into the pcDNA4HisMax-C and pGex5X-1 vectors. Prior to gel extraction, the DNA bands were visualized on a gel against a 1 kb ladder to ensure they were of the correct size (see figure 3.5.).

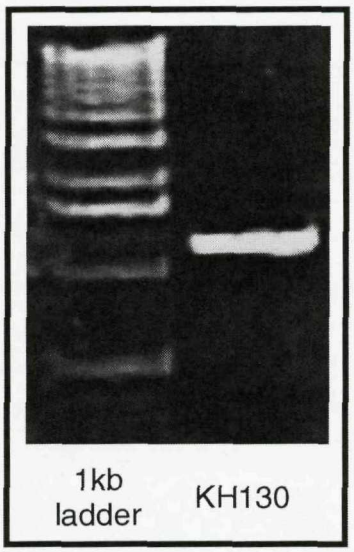

Figure 3.6. KH130 DNA from PCR reaction

3.2.1.3. 80K-H deletion constructs.

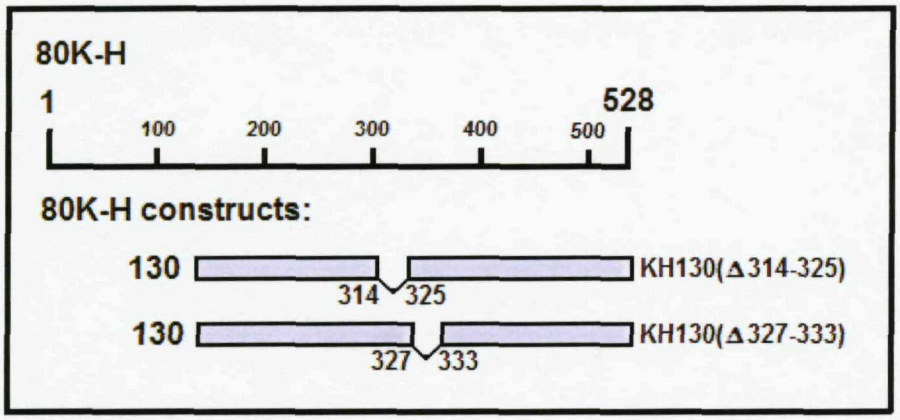

Figure 3.7. 80K-H deletion constructs

In order to produce the KH130 deletion constructs (see figure 3.6), lacking the glutamic-rich region, a two-sided SOEing method was used to produce two deletion mutants: one lacking the region corresponding to amino acids 314-225 and one lacking the region corresponding to amino acids 327-333 of the full length 80K-H. Using this method, four primers were used in three separate PCR reactions in order to generate each deletion construct (see tables 3.4 and 3.5.). In the first round of PCR, two separate PCR reactions were used to generate the two sequences of DNA either side of the glutamic-rich region. The forward internal primer was designed with a 5' extension sequence complementary to the reverse internal primer. The ends of the two PCR products were therefore complementary so could be annealed and extended with *Pfu* DNA Polymerase, before amplification with a second round of PCR.

	Primer Name	Primer Sequence	Tm
1	KH130(Δ314-325) forward	5'- gtg ccc tcg tcg ccc aca gct gaa gaa gag gag gag -3'	67
2	KH130(Δ314-325) reverse	5'- tgt ggg cga cga ggg cac tgg -3'	57
3	KH130(Δ327-333) forward	5'- gag gag gag gaa gaa gag gcc cca ccg cca ctg tca -3'	67
4	KH130(Δ327-333) reverse	5'- agc ctc ttc ttc ctc ctc ctc -3'	51
5	pGex5X-1 forward	5'- ggg ctg gca agc cac gtt tgg tg -3'	57
6	pGex5X-1 reverse	5'- ccg gga gct gca tgt gtc aga gg -3'	57

Table 3.4. Primer Sequences for the production of KH130(Δ314-325) and KH130(Δ327-333)

Reactions were set up as in section 2.3.2. KH130-pGex5X-1 was used as template DNA. Two primers were used for each reaction (1 with 6, 2 with 5, 3 with 6 and 4 with 5) to make the 4 products (A, B, C and D respectively). Product A was then mixed with product B and product C mixed with product D and the DNA extended with DNA polymerase. Each of the two DNA products from this were then used as template DNA for another round of PCR, each with primers 5 and 6.

		Primer numbers							
	No. of cycles	[1+6]		[2+5]		[3+6]		[4+5]	
denaturing	1	95°C	120 s	95°C	120 s	95°C	120 s	95°C	120 s
amplification	25	95°C	45 s	95°C	45 s	95°C	45 s	95°C	45 s
		57°C	45 s	57°C	45 s	52°C	45 s	57°C	45 s
		72°C	90 s	72°C	90 s	72°C	90 s	72°C	90 s
elongation	1	72°C	6 m	72°C	6 m	72°C	6 m	72°C	6 m
PCR products		A		B		C		D	

Table 3.5. PCR conditions used for the first round of PCR for the production of KH130(Δ314-325) and KH130(Δ327-333)

Products from the PCR reactions were visualized to be the correct size, then primers and enzymes removed from the DNA using a Qiagen PCR purification kit (as per the manufacturers instructions) before the second round of PCR with primers 5 and 6 (the forward and reverse pGex5X-1 primers).

	No. of cycles	[A+B] and [C+D]	
denaturing	1	95°C	120 sec
amplification	25	95°C	45 sec
		57°C	45 sec
		72°C	90 sec
elongation	1	72°C	6 min

Table 3.6. PCR conditions used for the second round of PCR for the production of KH130(Δ314-325) and KH130(Δ327-333)

The DNA products from these PCR reactions were then purified by ethanol precipitation, digested with the restriction enzymes *Eco*RI and *Xho*I, purified with a gel extraction kit (Qiagen) then ligated into the pcDNA4HisMax-C and pGex5X-1 vectors. Prior to gel extraction, the DNA bands were visualized on a gel against a 1 kb ladder to ensure they were of the correct size (see figure 3.7.).

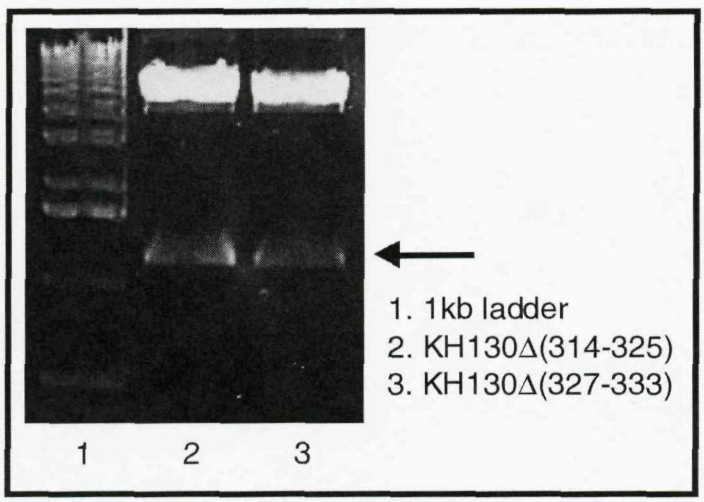

Figure 3.8. KH130Δ(314-325) and KH130Δ(327-333) DNA from PCR reactions

3.2.1.4. Full length 80K-H (KHFL)

The 80K-H clone (Invitrogen) arrived in the pCMV Sport 6.0 vector. The multiple cloning site of this vector contains none of the restriction sites required for insertion into the vectors used in this thesis (pGex5X-1 and pcDNA4HisMax-C) so the PCR primers were designed to insert the *Eco*RI and *Xho*I restriction sites 5'- and 3'- to the DNA sequence respectively in order to put the KHFL sequence in frame. Two rounds of PCR were used, as the presence of the restriction site in the primers before the 80K-H DNA had been liberated from the pCMV Sport 6.0 vector proved to be too destabilizing. For the first round of PCR, primers 1 and 2 (see table 3.7) were used to liberate and amplify the full length 80K-H from the pCMV Sport 6.0 vector. The primers and vector were removed with a PCR purification kit (Qiagen). The remaining DNA was then used as template for a second round of PCR with primers 3 and 4 (see table 3.7) to insert the required restriction sites into the DNA.

	Primer Name	Primer Sequence	Tm
1	80K-H FL forward	5'- atg ctg ctg ctg ctg cta ct -3'	49
2	KHFL reverse	5'- cat ctc gtc atg gtc ccc at -3'	49
3	KHFL + Eco forward	5'- gcc gc**g aat tc**a tgc tgc tgc tgc tgc tac t -3'	62
4	KHFL + Xho reverse	5'- ccg ct**c tcg ag**c atc tcg tca tgg tcc cca t -3'	63

Type in blue = *Eco*RI restriction site

Type in green = *Xho*I restriction site

Table 3.7. Primer Sequences for the production of KHFL with EcoRI and XhoI restriction sites

The DNA products from this PCR reaction were then purified by ethanol precipitation, digested with the restriction enzymes *Eco*RI and *Xho*I, purified with a gel extraction kit (Qiagen) then ligated into the pcDNA4HisMax-C and pGex5X-1 vectors. Prior to gel extraction, the DNA bands were visualized on a gel against a 1 kb ladder to ensure they were of the correct size (see figure 3.8.).

3.2.2. 80K-H constructs: Ligation into ECFP-N2 or EYFP-N2 vectors

Further PCR reactions were performed in order to insert the KHFL, KH302 and KH378 DNA into the ECFP-N2 and EYFP-N2 vectors. The appropriate 80K-H construct in the pcDNA4HisMax-C vector was used as a template. The cloning site of the ECFP-N2 and EYFP-N2 vectors contains an EcoRI restriction site in frame with the EcoRI restriction site of the pcDNA4HisMax-C vector. However, they do not contain an XhoI restriction site, so the PCR primers were designed to insert a *Kpn*I restriction site (which is in the correct orientation and frame in the ECFP-N2 and EYFP-N2 vectors) 3'- of the DNA sequence.

	Primer Name	Primer Sequence	Tm
1	pcDNA forward	5'- c gca aat ggg cgg tag gcg tg -3'	55
2	KHFL N2 reverse	5'- cgc ctg gta cct gag ctc gtc atg gtc gtc-3 '	63

Type in green = *Kpn*I restriction site

Table 3.8. Primer Sequences for the production of KHFL, KH302 and KH378 with EcoRI and KpnI restriction sites

	No. of cycles	KH 327 and KH353	
denaturing	1	95°C	2 min
amplification	3	95°C	45 sec
		40°C	1 min
		72°C	3 min 30 sec
amplification	30	95°C	45 sec
		55°C	1 min
		72°C	3 min 30 sec
elongation	1	72°C	6 min

Table 3.9. PCR conditions used for the production of KHFL for ligation into ECFP-N2 and EYFP-N2 vectors.

	No. of cycles	KH 327 and KH353	
denaturing	1	95°C	2 min
amplification	3	95°C	45 sec
		40°C	45 sec
		72°C	3 min
amplification	30	95°C	45 sec
		57°C	1 min
		72°C	3 min
elongation	1	72°C	6 min

Table 3.10. PCR conditions used for the production of KH302 and KH378 for ligation into ECFP-N2 and EYFP-N2 vectors.

The DNA product from these PCR reactions were then purified by ethanol precipitation, digested with the restriction enzyme *Kpn*I in Promega buffer J, ethanol precipitated again, digested with the restriction enzyme *Eco*RI, purified with a gel extraction kit (Qiagen) then ligated into the ECFP-N2 and EYFP-N2 vectors. Prior to gel extraction, the DNA bands were visualized on a gel against a 1 kb ladder to ensure they were of the correct size (see figure 3.8.).

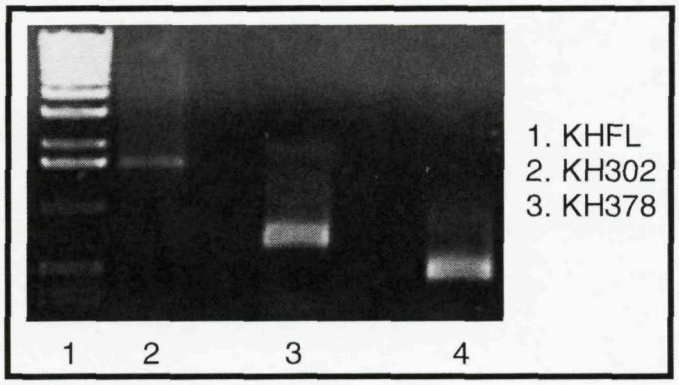

Figure 3.9. KHFL, KH302 and KH378 DNA from PCR reactions

3.3. Cloning of munc18c constructs

3.3.1. Munc18c constructs: Ligation into pGex-5X-1 and pcDNA4HisMax-C vectors

The MFL, M295, M338, M381 and M468 constructs, in both pGex5X-1 and pcDNA4HisMax-C vectors, were a kind present from Dr. Conrad Hodgkinson (see figure 3.9.).

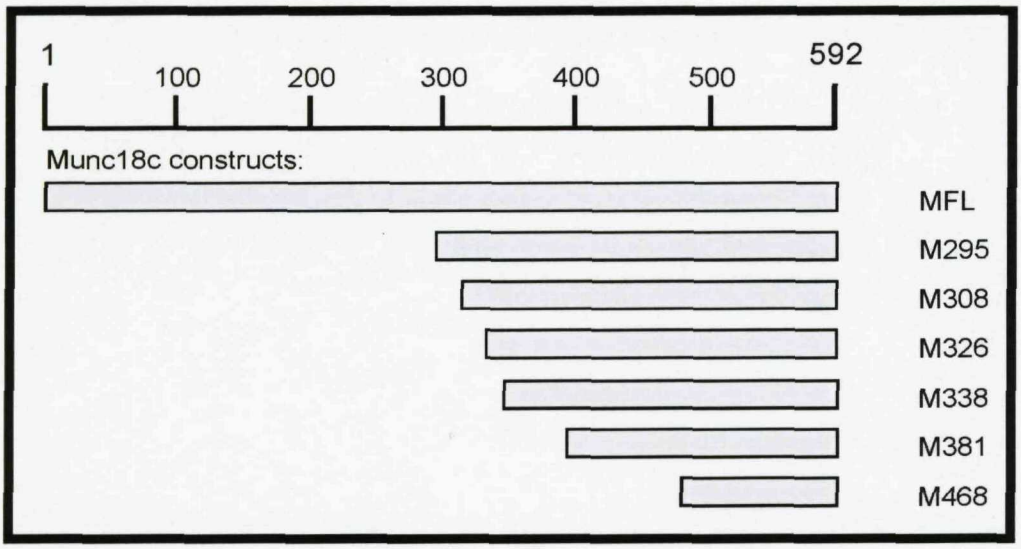

Figure 3.10. Munc18c truncation constructs

A further two munc18c truncation constructs were made, with N-termini lying between M295 and M338, these being M308 and M326 (see figure 3.9) using a standard PCR protocol. The reverse primer (see table 3.11) was complementary to the C-terminal of the multiple cloning site of the pGex5X-1 vector, including the XhoI restriction site. The forward primers (see table 3.11) were designed to be complementary to the required

section of munc18c, with the insertion of a 5' *Eco*RI restriction site to enable cloning into pGex5X-1 or pcDNA4HisMax-C.

```
901  gtcctgcatg aactgacctt tcaggcaatg gcatatgatc tactaccaat tgagaatgat
961  acatacaagt acaaaacaga tggaaaagag aaggaggcag ttcttgaaga agacgacgac
                                                    M308▼----------
1021 ctgtgggtgc gggttcgaca ccggcacatc gcggttgtgt tggaggaaat tccaaagctt
     ------------------------------------▼                M326▼----------
1081 atgaaggaaa tttcatcaac aaagaaagct acagagggga agacatcact tagcgctctt
     -------------------------▼
1141 acccagctga tgaaaaagat gccgcacttc cgaaagcaga tctcgaagca agtagtccat
1201 cttaacttag ctgaagactg catgaataag tttaagctga atattgagaa gctctgcaaa
```

Type in blue = sequence that was changed for *Eco*RI restriction site

Figure 3.10: Munc18c sequence and positioning of primers for M308 and M326

	Primer Name	Primer Sequence	Tm
1	M308 forward	5'- ttc cag aat tca tga agg aaa ttt cat caa ca -3'	52
2	M326 forward	5'- cat cag aat tcg ctc tta ccc agc tga tga aa -3'	57
3	pGex5X-1 reverse	5'- ccg gga gct gca tgt gtc aga gg -3'	57

Type in blue = *Eco*RI restriction site

Table 3.11. Primer Sequences for the production of M308 and M326

Reactions were set up as in "Methods." M308-pGex5X-1 was used as template DNA. Primers 1 and 3 were used for the production of the M308 construct and primers 2 and 3 were used for the production of the M326 construct using the PCR conditions listed below in table 3.12.

	No. of cycles	M308 and M326	
denaturing	1	95°C	2 min
amplification	25	95°C	45 sec
		52°C	45 sec
		72°C	1 min 30 sec
elongation	1	72°C	6 min

Table 3.12. PCR conditions used for the production of M308 and M326

The DNA products from these PCR reactions were then purified by ethanol precipitation, digested with the restriction enzymes *Eco*RI and *Xho*I, purified with a gel extraction kit (Qiagen) then ligated into the pcDNA4HisMax-C and pGex5X-1 vectors. Prior to gel extraction, the DNA bands were visualized on a gel against a 1 kb ladder to ensure they were of the correct size (see figure 3.11.).

Figure 3.12. M308 and M326 DNA from PCR reactions

3.3.2. Munc18c constructs: Ligation into ECFP-N2 or EYFP-N2 vectors

Further PCR reactions were performed in order to insert the MFL, M295 and M338 DNA into the ECFP-N2 and EYFP-N2 vectors. The appropriate munc18c construct in the pcDNA4HisMax-C vector were used as a template. The cloning site of the ECFP-N2 and EYFP-N2 vectors contains an *Eco*RI restriction site in frame with the *Eco*RI restriction site of the pcDNA4HisMax-C vector. However, they do not contain an *Xho*I restriction site, so the PCR primers were designed to insert a *Kpn*I restriction site (which is in the correct orientation and frame in the ECFP-N2 and EYFP-N2 vectors) 3'- of the DNA sequence (see table 3.13.)

	Primer Name	Primer Sequence	Tm
1	pcDNA forward	5'- c gca aat ggg cgg tag gcg tg -3'	55
2	MFL N2 reverse	5'- c cgt cgg tac cac tca tcc tta aag gaa act t-3'	58

Type in green = *Kpn*I restriction site

Table 3.13. Primer Sequences for the production of MFL, M295 and M338 with EcoRI and KpnI restriction sites

	No. of cycles	KH 327 and KH353	
denaturing	1	95°C	2 min
amplification	3	95°C	45 sec
		40°C	1 min
		72°C	3 min 30 sec
amplification	30	95°C	45 sec
		55°C	1 min
		72°C	3 min 30 sec
elongation	1	72°C	6 min

Table 3.14. PCR conditions used for the production of MFL, M295 and M338 DNA with EcoRI and KpnI restriction sites.

The DNA product from this PCR reaction was then purified by ethanol precipitation, digested with the restriction enzyme *Kpn*I in Promega buffer J, ethanol precipitated again, digested with the restriction enzyme *Eco*RI in Promega buffer H, purified with a gel extraction kit (Qiagen) then ligated into the ECFP-N2 and EYFP-N2 vectors. Prior to gel extraction, the DNA bands were visualized on a gel against a 1 kb ladder to ensure they were of the correct size (see figure 3.12.)

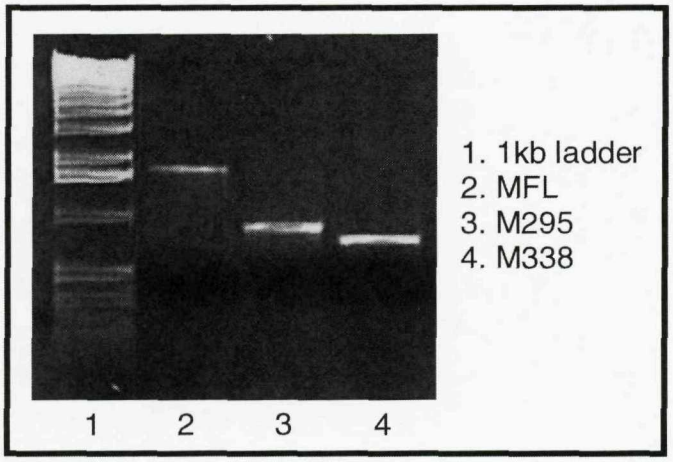

Figure 3.13. MFL, M295 and M338 DNA from PCR reactions

3.4. Sub-cloning of PKCζ

3.4.1. PKCζ: Ligation into ECFP-N2 or EYFP-N2 vectors

The full length PKCζ in pcDNA3-myc vector was a kind present from Dr. Conrad Hodgkinson.

PCR was performed in order to insert the PKCζ DNA into the ECFP-N2 and EYFP-N2 vectors. PKCζ in the pcDNA4HisMax -C vector was used as a template. The cloning site of the ECFP-N2 and EYFP-N2 vectors contains an *Eco*RI restriction site in frame with the *Eco*RI restriction site of the pcDNA4HisMax-C vector. However, they do not contain an *Xho*I restriction site, so the PCR primers were designed to insert a *Kpn*I restriction site (which is in the correct orientation and frame in the ECFP-N2 and EYFP-N2 vectors) 3'- of the DNA sequence (see table 3.15.).

	Primer Name	Primer Sequence	Tm
1	pcDNA forward	5'-c gca aat ggg cgg tag gcg tg-3'	55
2	PKCζ-N2 reverse	5'- g ccc tgg tac cac acc gac tcc tcg gtg gac-3 '	66

Type in green = *Kpn*I restriction site

Table 3.15. Primer Sequences for the production of KHFL with EcoRI and KpnI restriction sites

	No. of cycles	KH 327 and KH353	
denaturing	1	95°C	2 min
amplification	3	95°C	45 sec
		40°C	1 min
		72°C	3 min 30 sec
amplification	30	95°C	45 sec
		55°C	1 min
		72°C	3 min 30 sec

Table 3.16. PCR conditions used for the production of PKCζ DNA with EcoRI and KpnI restriction sites.

The DNA product from this PCR reaction (see table 3.16) was then purified by ethanol precipitation, digested with the restriction enzyme *Kpn*I in Promega buffer J, ethanol precipitated again, digested with the restriction enzyme *Eco*RI in Promega buffer H, purified with a gel extraction kit (Qiagen) then ligated into the ECFP-N2 and EYFP-N2 vectors. Prior to gel extraction, the DNA bands were visualized on a gel against a 1 kb ladder to ensure they were of the correct size (see figure 3.13.).

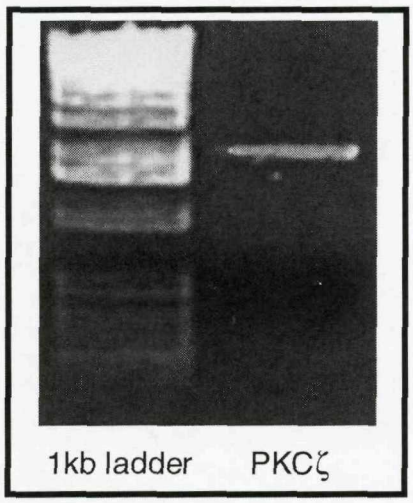

Figure 3.14. PKCζ DNA from PCR reaction

3.5. Cloning of Kifap3

3.5.1. Kifap3 constructs: Ligation into pcDNA4HisMax-C and pGex-5X-1 vectors

Full length Kifap3 clone was purchased from Invitrogen. The clone arrived in the pCMV Sport 6.0 vector. The multiple cloning site of this vector contains none of the restriction sites required for insertion into the vectors required (pGex5X-1 and pcDNA4HisMax-C) so the PCR primers were designed to insert the *Eco*RI and *Xho*I restriction sites 3'- and 5'- to the DNA sequence respectively (see table 3.17.)

	Primer Name	Primer Sequence	Tm
1	Kifap3 forward	5'- g ccg ctg **aat tc**a tgc aag ggg agg acg cca gat -3'	64
2	Kifap3 reverse	5'- gg aaa cag at**c tcg ag**t caa gat cca tag cca tag ta -3'	59

Type in blue = *Eco*RI restriction site

Type in green = *Xho*I restriction site

Table 3.17. Primer Sequences for the production of Kifap3

The DNA product from this PCR reaction was then purified by ethanol precipitation, digested with the restriction enzymes *Eco*RI and *Xho*I, purified with a gel extraction kit (Qiagen) then ligated into the pcDNA4HisMax-C and pGex5X-1 vectors. Prior to gel extraction, the DNA bands were visualized on a gel against a 1 kb ladder to ensure they were of the correct size (see figure 3.14.).

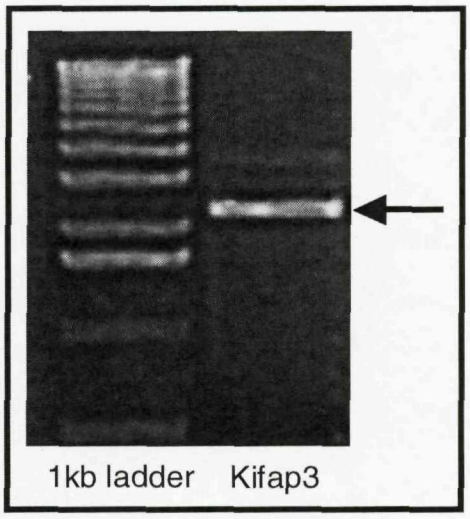

Figure 3.15. Full length Kifap3 DNA from PCR reaction

A series of C-terminal truncation constructs were then made using a standard PCR protocol. The reverse primer was complementary to the C-terminal of the multiple cloning site of the pGex5X-1 vector, including the *Xho*I restriction site. The forward primers were designed to be complementary to the required section of Kifap3, with the insertion of a 5'- *Eco*RI restriction site to enable cloning into pGex5X-1 or pcDNA4HisMax-C.

	Primer Name	Primer Sequence	Tm
1	Kif 160	5'- cc tgc agg aat tcc gaa atc ctg ata act tg -3'	57
2	Kif 240	5'- ggc aag aat tcc tct caa aga aga aga aa -3'	52
3	Kif 320	5'- ttg agg aat tca ttt tag ttg tgt cat tc -3'	49
4	Kif 400	5'- g aca acg aat tcc aaa tag caa tgt gtg tt -3'	52
5	Kif 480	5'- ga agt ttg aat tcc cat tgc tga tga aaa tg -3'	53
6	Kif 560	5'- c cag gtg aat tcg aag atg atc ttg ttt ta -3'	52
7	Kif 640	5'- t atc tcg aat tcc taa tgc atg ata aga at -3'	50
8	Kif 700	5'- a gac ctg aat tcc tct aca act cag atg ga -3'	55
9	pGex5X-1 reverse	5'- ccg gga gct gca tgt gtc aga gg -3'	57

Type in blue = *Eco*RI restriction site

Table 3.18. Primer Sequences for the production of Kifap3 truncation constructs

541 acagctgttg tactatctac agaaccgccg tgattcattg tcaggaaaag agaaaaaaga
601 aaaatcaagc aagcctaaag atccacctcc ttttgaagga atggagattg atgaagttgc
661 taacattaat gacatggatg aatatattga gttattatat gaagatattc ctgacaaagt

Kif160▼----------▼

721 tcggggttct gctttgatcc tgcagcttgc tcgaaatcct gataacttgg aagaactact
781 attgaatgaa actgcccttg gtgcattagc aagggtcctg agagaagact ggaagcaaag
841 tgtcgagtta gctacaaaca taatttacat ctttttttgt ttctccagct tttctcaatt
901 tcatggactt attactcact ataaaattgg agctctgtgt atgaatatta ttgatcatga

Kif240▼----------▼

961 gttaaaaaga catgagcttt ggcaagaaga actctcaaag aagaagaaag ctgttgatga
1021 agaccctgaa aaccaaacct tgagaaagga ttatgaaaaa acctttaaaa agtaccaggg

1081 gcttgtggta aaacaggaac agctattacg agttgctctt tatttgcttc tgaatcttgc

Kif320▼----------▼

1201 agcccttgat cgggacaatt ttgagctgct aattttagtt gtgtcattct tgaagaaact
1261 cagcattttt atggagaata aaaatgatat ggtggaaatg gatattgttg aaaaactggt
1321 gaaaatgata ccttgtgagc atgaagacct gctgaatatc accctccgac ttttactaaa
1381 cctatccttt gacacaggac tgaggaataa gatggtacaa gttggactgc ttcccaagct

Kif400▼----------▼

1441 cactgcactc ctaggcaatg acaactacaa acaaatagca atgtgtgttc tttaccacat
1501 aagcatggat gaccgcttta aatcaatgtt tgcatacact gactgtatac cacagttaat
1561 gaagatgctg tttgaatgtt cagatgaacg aattgacttg gaactcattt ctttctgcat
1621 taatcttgct gctaacaaaa gaaatgtaca gcttatctgt gaaggaaatg ggctgaagat

Kif480▼----------▼

1681 gctcatgaag agggctctga agtttaagga tccattgctg atgaaaatga ttagaaacat
1741 ttctcagcat gatggaccaa ctaaaaatct gtttattgat tatgttgggg accttgcagc
1801 ccagatctct aatgatgaag aagaggagtt tgtgattgaa tgtttgggaa ctcttgcaaa
1861 cttgaccatt ccagacttag actgggaatt ggttcttaaa gaatataagt tggttccata

Kif 560▼----------▼

1921 cctcaaggat aaactaaaac caggtgctgc agaagatgat cttgttttag aagtggttat
1981 aatgattgga actgtatcca tggatgactc ttgtgctgca ttgctagcca aatctggcat
2041 aatccctgca ctcattgaat tgctaaatgc tcaacaagaa gatgatgaat ttgtgtgtca
2101 gataatttat gtcttctacc agatggtttt ccaccaagcc acaagagacg tcataatcaa

Kif 640▼----------▼

2161 ggaaacacag gctccagcat atctcataga cctaatgcat gataagaata atgaaatccg

2221 aaaggtctgt gataatacat tagatattat agcggaatat gatgaagaat gggctaagaa

2281 aattcagagt gaaaagtttc gctggcataa ctctcagtgg ctggagatgg tagagagtcg

2341 tcagatggat gagagtgagc agtacttgta tggtgatgat cgaattgagc catacattca

Kif 700▼----------▼

2401 tgaaggagat attctcgaa**a gacctgacct tttctacaac tcagatgga**t taattgcctc

2461 tgaaggagcc ataagtcccg atttcttcaa tgattaccac cttcaaaatg gagatgttgt

2521 tgggcagcat tcatttcctg gcagccttgg aatggatggc tttggccaac cagttggcat

2581 tcttggacgc cctgccacag catatggatt ccgccctgat gaaccttact actatggcta

2641 tggatcttga taaagtatct gtttccatgt gtaatctcag cttagaagaa atctgtgtgg

2701 gttgggttaa ttttggatct ttgcctaata atgcatgttg atgttattgt gggtctgtgt

2761 ttgtttttat ttttatatgt tgttagctgc agattaaccc cagcccctct gtcttctgtt

2821 aagtacagtt gatactgaca ttgttcactc atcaaaccac atcttgatgc taagtaacat

2881 ttcccatgag cctcaaaact gaatgctgaa aagctactag actggaaaac aaacactgca

2941 ttatgtatgt taagtgacta atttaatttc aattaaaaag cgtaaagtga aaatgaa

Type in blue = sequence to be changed for *Eco*RI restriction site (gaattc)

Figure 3.16 Kifap3 sequence and position of primers for production of truncated Kifap3 constructs

Reactions were set up as in section 2.3.2. KifapFL-pGex5X-1 was used as template DNA. Primers 1 and 6 were used for the production of the Kif160 construct, primers 2 and 6 for Kif300, primers 3 and 6 for Kif380, primers 4 and 6 for Kif460 and primers 5 and 6 for the Kif540 construct using the PCR conditions listed in table 3.19.

	No. of cycles	M308 and M326	
denaturing	1	95°C	2 min
amplification	25	95°C	45 sec
		55°C	45 sec
		72°C	3 min
elongation	1	72°C	6 min

Table 3.19. PCR conditions used for the production of full length and truncated Kifap3 constructs

The DNA products from these PCR reactions were then purified by ethanol precipitation, digested with the restriction enzymes *Eco*RI and *Xho*I, purified with a gel extraction kit (Qiagen) then ligated into the pcDNA4HisMax-C and pGex5X-1 vectors. Prior to gel extraction, the DNA bands were visualized on a gel against a 1 kb ladder to ensure they were of the correct size (see figure 3.16.)

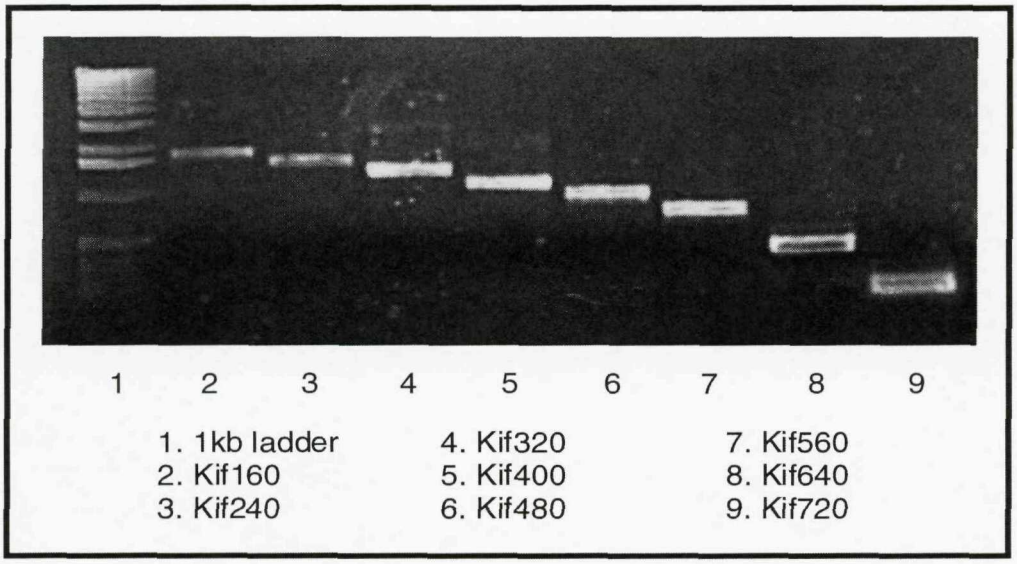

Figure 3.17. Kif160, Kif240, Kif329, Kif400, Kif480, Kif560, Kif640 and Kif720 DNA from PCR reactions

3.5.2. Kifap3 constructs: Ligation into ECFP-N2 or EYFP-N2 vectors

PCR was performed in order to insert the full length Kifap3 DNA into the ECFP-N2 and EYFP-N2 vectors. Kifap3 in the pcDNA4HisMax-C vector was used as a template. The cloning site of the ECFP-N2 and EYFP-N2 vectors contains an *Eco*RI restriction site in frame with the *Eco*RI restriction site of the pcDNA4-C vector. However, they do not contain an *Xho*I restriction site, so the PCR primers were designed to insert a *Kpn*I restriction site (which is in the correct orientation and frame in the ECFP-N2 and EYFP-N2 vectors) 3'- of the DNA sequence.

	Primer Name	Primer Sequence	Tm
1	pcDNA forward	5'-c gca aat ggg cgg tag gcg tg-3'	55
2	reverse	5'- g cgg tgg tac caa gat cca tag cca tag ta -3 '	58

Type in green = *Kpn*I restriction site

Table 3.20. Primer Sequences for the production of KHFL with EcoRI and KpnI restriction sites

	No. of cycles		
denaturing	1	95°C	2 min
amplification	3	95°C	45 sec
		45°C	1 min
		72°C	3 min 30 sec
amplification	50	95°C	45 sec
		57°C	1 min
		72°C	3 min 30 sec

Table 3.21. PCR conditions used for the production of PKCζDNA with EcoRI and KpnI restriction sites.

RESULTS

4.1. Investigations into 80K-H, munc18c and PKCζ interactions

4.1. Investigations into 80K-H, munc18c and PKCζ interactions

4.1.1. Introduction

PKCζ (Protein Kinase C zeta) is a 67 kDa serine/threonine kinase belonging to the atypical PKC subfamily. Atypical PKCs are known to mediate signalling responses either by phosphorylating targets or by binding other proteins [Moscat and Diaz-Meco 2000]. They can be activated by insulin and various mitogens through the activation of Phosphoinositide 3-kinase (PI3K) and various studies have shown a clear role for PKCζ and its close relative PKCι/λ in insulin-stimulated glucose transport [Farese 2002, Bandyopadhyay et. al. 2004, Bandyopadhyay et.al 2002].However, the lack of discovery of relevant substrates that could be involved in glucose transport for phosphorylation by the atypical PKCs increases the prospect that their role in the enhancement of glucose transport is structural rather than catalytic. Discovering and studying interactors of the atypical PKCs that may play a role in insulin stimulated glucose transport is therefore of much interest. Our lab conducted a yeast two-hybrid screen of a brain cDNA library to identify interactors of PKCζ. One protein identified through this yeast two-hybrid screen was a 398 amino acid protein corresponding to the C-terminal section of a protein called 80K-H. This was chosen for further investigation, partly due to its poor characterisation to date, but mainly because the bovine version of 80K-H, VASAP60, has been shown to be involved in vesicle transport [Brule 2000].

Munc18c is another protein shown to play an important role in insulin and GLUT4 regulated glucose transport. Munc18c has been shown to negatively regulate GLUT4 vesicle docking/fusion with the plasma membrane by inhibiting the interaction between the v-SNARE, VAMP2, and the t-SNARE, syntaxin4. Insulin is proposed to regulate vesicle docking by decreasing the interaction between munc18c and syntaxin4, thus enabling VAMP2 to bind and the GLUT4 vesicle to dock at the plasma membrane

[Macaulay et al. 2002 and 2003, Spurlin et al. 2003, Kanda et al. 2005, Thurmond et al. 1998]. The use of another yeast two-hybrid screen in our laboratory, this time using munc18c as bait, showed both PKCζ and 80K-H to interact with munc18c.This, because of munc18c and PKCζ's well known involvement in insulin-stimulated glucose transport, and because of the results from both yeast-two-hybrid screens, makes further study of 80K-H, PKCζ and munc18c interactions suitably attractive.

Further to the yeast-two-hybrid screens, GST pull down assays showed that the region of 80K-H responsible for the interaction with PKCζ was between residues 302 and 378. It was also shown that endogenous 80K-H and PKCζ interact *in vivo* in two insulin responsive cell lines (L6 myoblasts and 3T3-L1 adipocytes) using co-immunoprecipitation and that this interaction increased when the cells were stimulated with insulin. Over-expression of an 80K-H construct lacking 302 amino acids at the N-terminus (KH302) that can associate with PKCζ and munc18c, increased basal and insulin-stimulated levels of both glucose transport and plasma membrane myc-tagged GLUT4 in these CHO cells. However, use of an 80K-H construct lacking 378 amino acids at the N-terminus (KH378) that had the PKCζ interaction site removed and interacts more strongly with munc18c, significantly increased basal and insulin stimulated responses over and above that found when over-expressing the KH302 construct. It was also found that 80K-H constructs were predominantly localized to the plasma membrane of CHO cells, placing it in the correct subcellular localization to interact with PKCζ and munc18c. In the published papers it was hypothesized that 80K-H together with PKCζ complexed with munc18c when cells were exposed to insulin (see Figure 4.1). This released the clamping action of munc18c that is seen in the basal state. In summary, previous work conducted in this laboratory identified a physiological interaction between 80K-H, PKCζ and munc18c that is insulin regulated and that 80K-H may be a missing link between the insulin signalling cascade (PKCζ) and the vesicle trafficking machinery (munc18c) of the GLUT4 vesicle.

Although the previous work in our laboratory using GST pull-down assays and co-immunoprecipitations showed that some sort of interaction occurs between PKCζ and 80K-H, PKCζ and munc18c and 80K-H and munc18c, the exact mechanics of these interactions are as yet unknown. The three proteins may join together in a triplex formation or join as a series of duplexes. This chapter aims to further characterize the interactions between these three proteins so that future work may elucidate their roles in GLUT4 vesicle trafficking. It is important to note that the protein identified by yeast-two-hybrid screens corresponded to 80K-H minus the N-terminal 130 amino acids. It could be that this is another splice variant of the 598 amino acid of the 80K-H version. The interaction studies conducted using KH302 therefore needs to be repeated with both the protein identified through yeast-two-hybrid screens (KH130) and the full length 80K-H protein. In addition, this study aims to further define the previously identified interaction sites of 80K-H and munc18c for PKCζ. Such results may enable the production of munc18c and 80K-H deletion mutants (i.e.: the full length protein minus the PKCζ interaction site) for use in future experiments to investigate the role of these proteins and their interaction with PKCζ in GLUT4 vesicle trafficking.

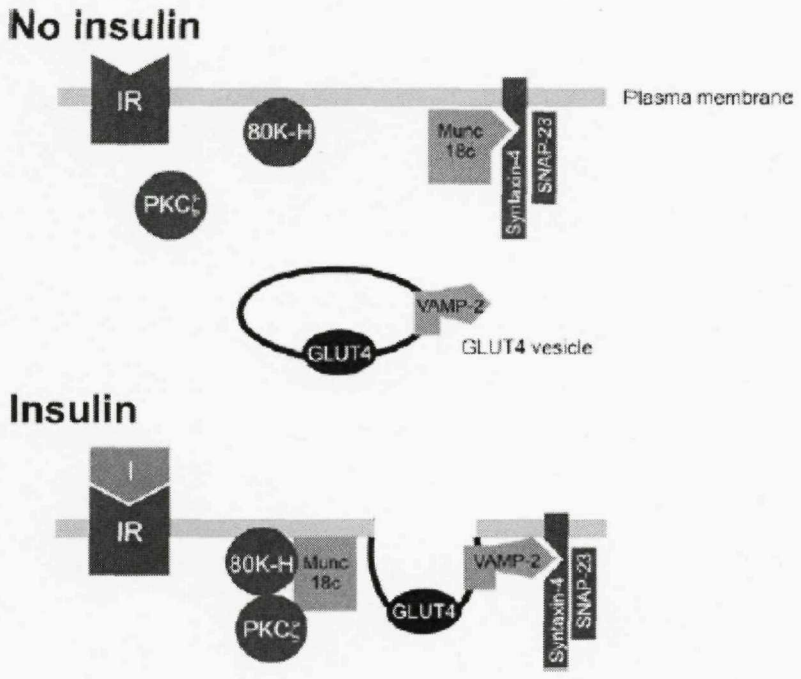

Figure 4.1.1. Hypothetical model of 80K-H, PKCζ and munc18c's role in GLUT4 vesicle trafficking.

The model shows how the complex formation may decrease the clamping action of munc18c, thereby allowing VAMP-2 to bind syntaxin4 and deliver GLUT4 to the plasma membrane. Displaced munc18c may also be involved in fusing the GLUT4 vesicle to the plasma membrane. Although PKCζ, 80K-H and munc18c are shown to bind each other, the precise interactions that result in the complex formation require elucidation. Other accessory proteins are omitted for simplicity [Diagram and legend taken from Hodgkinson, C.P et al (2005)].

4.1.2. Results

4.1.2.1. The use of 80K-H mutants

4.1.2.1.1. Determination of the domains of 80K-H that interact with munc18c

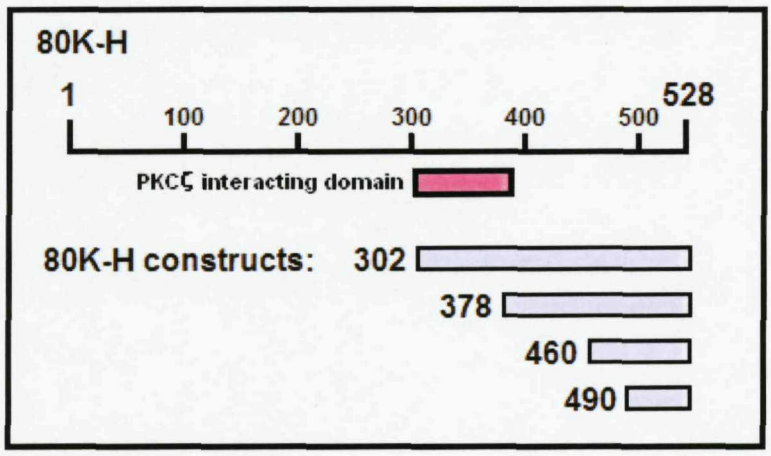

Figure 4.1.2: KH398 truncation constructs.

Figure showing the series of truncation constructs of 80K-H used as GST fusions in a GST pull-down assay and the region of 80K-H previously shown to be critical for binding to PKCζ.

Previous work in our laboratory, using a GST pull down technique, showed that the region of 80K-H between residues 302-378 was necessary for its binding to PKCζ. I used the same GST-tagged 80K-H constructs to determine which area of 80K-H was required for binding to munc18c. In addition, to further validate and characterize the interaction between 80K-H and munc18c as seen in the yeast-2-hybrid screen, GST pull-down assays were performed. For this, purified GST-tagged 80K-H truncation constructs (see Figure 4.1.2) were coupled to glutathione beads and incubated with extracts of Cos-1 cells that had been transiently transfected with Xpress-tagged full length munc18c. Complexes were washed to remove non-specific binding, separated by SDS-PAGE and

immunoblotted with anti-Xpress antibody to assess the co-precipitation of munc18c with the 80K-H constructs. As shown in Figure 4.1.3.A, munc18c associated with KH302, but showed little or no binding to KH378, KH460 and KH490. Munc18c was not precipitated when extracts were incubated with only GST coupled to glutathione beads (lane 1 figure 4.1.3.A) indicating that the association between munc18c and KH302 was specific. Quantities of the GST fusion proteins were checked by western blotting using an anti-GST antibody and shown to be comparative. This shows that differences in amounts of precipitated munc18c for each 80K-H construct is not due to relative amounts of the GST-tagged 80K-H proteins. This result indicates that the region of 80K-H that is responsible for binding PKCζ is also responsible for its binding to munc18c.

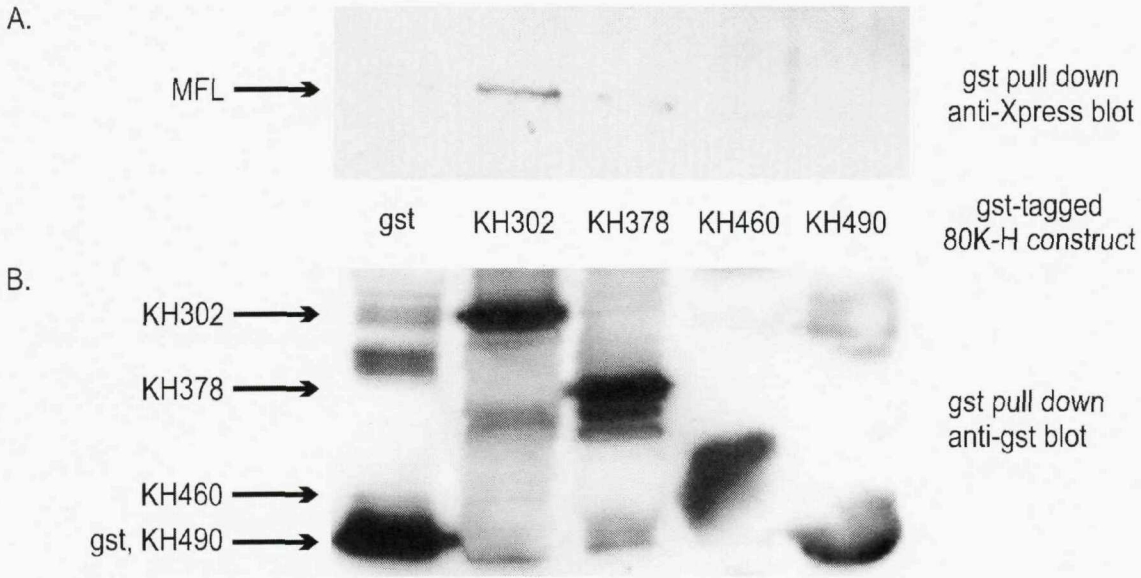

Figure 4.1.3: Determination of the region of 80K-H that is responsible for binding to munc18c.

Cos-1 cells were transiently transfected with munc18c expressed as an Xpress fusion. 80K-H constructs were bacterially expressed as GST fusion proteins and coupled to glutathione sepharose beads. GST bound to glutathione beads was used as a control (GST). Cos-1 cell extracts were incubated with the glutathione bead complexes, then washed to remove non-specific binding. Proteins were separated by SDS-PAGE, transferred to a nitrocellulose membrane, and probed for Xpress to detect co precipitated munc18c.

4.1.2.1.2. Does the presence of PKCζ affect the binding of 80K-H to munc18c?

To further define the binding characteristics of munc18c, PKCζ and 80K-H, another GST pull-down assay was performed with all three of the proteins present. For this, purified GST-tagged full length munc18c (MFL) was coupled to glutathione beads and incubated with extracts of Cos-1 cells that had been transiently transfected with Xpress-tagged KH302. Added to this was either an extract of untransfected Cos-1 cells (-PKCζ control) or an extract of Cos-1 cells that had been transiently transfected with PKCζ (+PKCζ). Complexes were washed to remove non-specific binding, separated by SDS-PAGE and immunoblotted with anti-Xpress antibody to assess the co-precipitation of KH302. As is shown in figure 4.1.4.A, KH302 associated with MFL (lanes 3 and 4, figure 4.4.A). There was no difference seen in the association between KH302 and MFL when PKCζ was added (figure 4.1.4 lanes 2 and 4) compared to controls (figure 4.1.4 lanes 1 and 3). KH302 was not precipitated when extracts were incubated with only GST coupled to glutathione beads (lanes 1 and 2, figure 4.1.4.A) indicating that the association between KH302 and MFL was specific. Quantities of the GST fusion proteins were checked by western blotting using an anti-GST antibody and shown to be comparative (figure 4.1.4.B, lanes 1-4). This shows that differences in amounts of precipitated KH302 are not due to relative amounts of the GST-tagged MFL protein. Quantities of the PKCζ protein were checked by western blotting of 10% of the cell extract (figure 4.4.D) which clearly shows the large increase in PKCζ expression when cells were transfected with PKCζ plasmid DNA (lanes 2 and 4) compared to untransfected cell (lanes 1 and 3). These results show that PKCζ does not compete with 80K-H for the binding of munc18c.

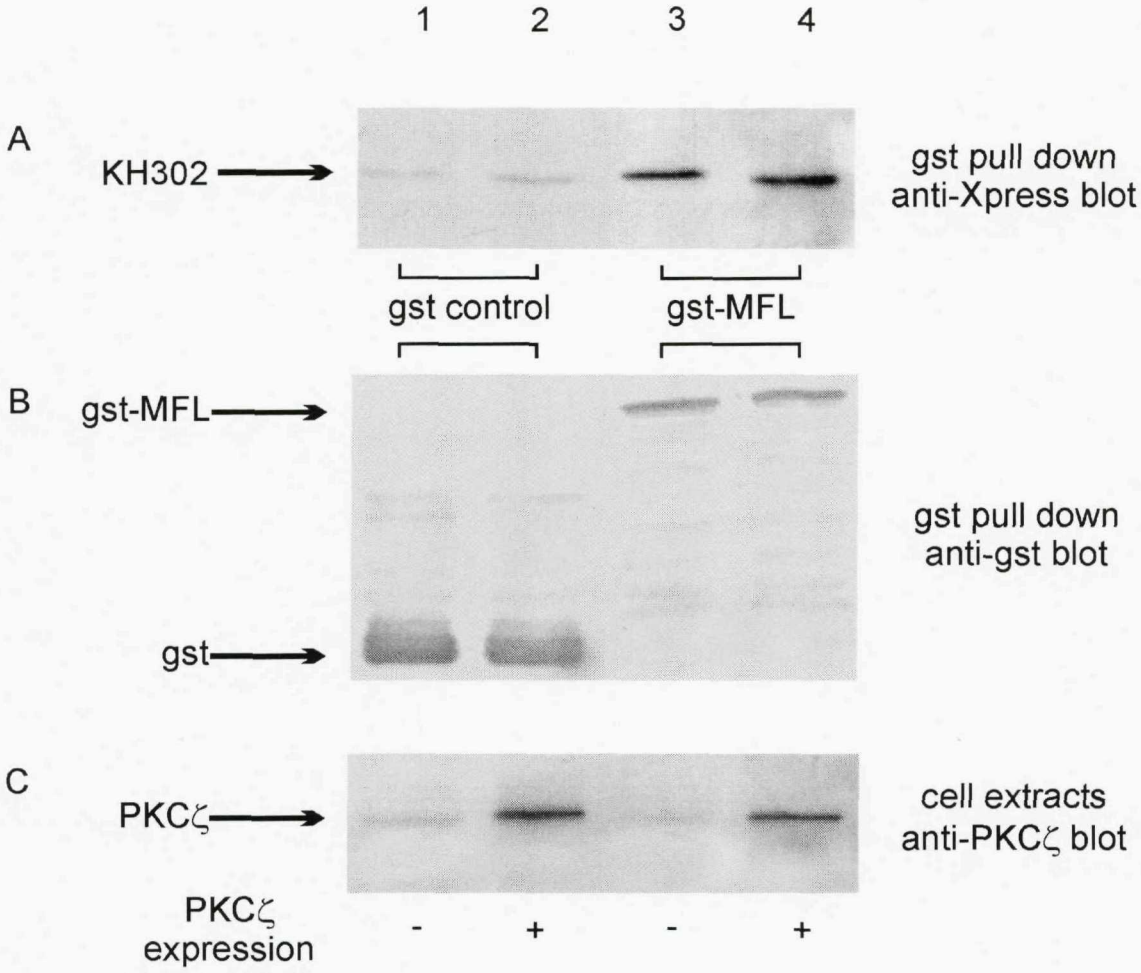

Figure 4.1.4: Determination of the affect of PKCζ on the interaction between 80K-H and munc18c.

Cos-1 cells were transiently transfected with Xpress-tagged KH302 or PKCζ. Full length munc18c (MFL) was bacterially expressed as a GST fusion protein and coupled to glutathione sepharose beads. GST bound to glutathione beads was used as a control (GST). Extracts of Cos-1 cells over expressing Xpress-tagged KH302 was incubated with the glutathione bead complexes with the addition of an extract of either untransfected Cos-1 cells or Cos-1 cells over expressing PKCζ. Beads were then washed to remove non-specific binding. Proteins were separated by SDS-PAGE, transferred to a nitrocellulose membrane and probed for either Xpress to detect for precipitated KH302 (Figure 4.4.A), GST to detect for amounts of the GST or GST-tagged MFL (figure 4.4B), or PKCζ (figure 4.4.C).

4.1.2.1.3. Further definition of the binding of PKCζ to 80K-H

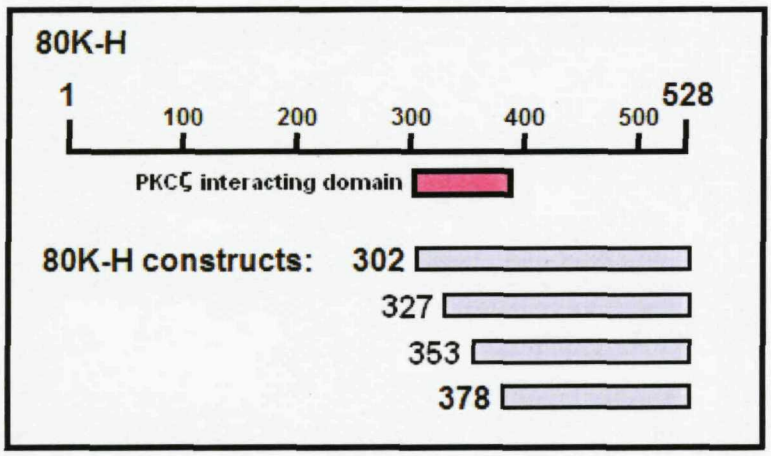

Figure 4.1.5. 80K-H truncation constructs.

Figure showing the series of truncation constructs of 80K-H used as GST fusions in a GST pull-down assay and the region of 80K-H previously shown to be critical for binding to PKCζ.

To further define the interaction between 80K-H and PKCζ, GST pull-down assays were performed using KH302, KH378 and a further two truncation constructs of 80K-H lying in between this region, KH327 and KH378. For this, purified GST-tagged 80K-H truncation constructs (see Figure 4.1.5) were coupled to glutathione beads and incubated with extracts of Cos-1 cells that had been transiently transfected with HA-tagged PKCζ. Complexes were washed to remove non-specific binding, separated by SDS-PAGE and immunoblotted with anti-HA antibody to assess the co-precipitation of PKCζ with the 80K-H constructs. As shown in Figure 4.1.6, PKCζ associated with KH302, but showed little or no binding to KH327, KH353 and KH378. PKCζ was not precipitated when extracts were incubated with only GST coupled to glutathione beads (lane 1 figure 4.6) indicating that the association between PKCζ and KH302 was specific. Quantities of the GST fusion proteins were checked by western blotting using an anti-GST antibody and

shown to be comparative. This shows that differences in amounts of precipitated PKCζ for each 80K-H construct is not due to relative amounts of the GST-tagged 80K-H proteins. This result indicates that the region of 80K-H that is predominantly responsible for binding PKCζ lies between residues 302-327.

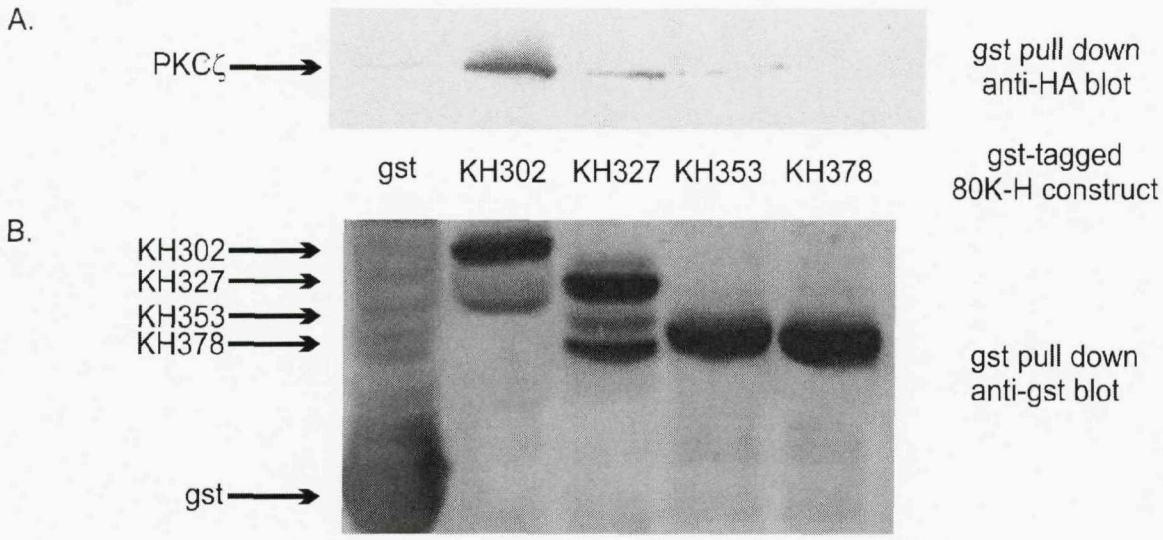

Figure 4.1.6: Determination of the region of 80K-H that is responsible for binding toPKCζ

Cos-1 cells were transiently transfected with PKCζ expressed as an HA fusion. 80K-H constructs were bacterially expressed as GST fusion proteins and coupled to glutathione sepharose beads. GST bound to glutathione beads was used as a control (GST). Cos-1 cell extracts were incubated with the glutathione bead complexes, then washed to remove non-specific binding. Proteins were separated by SDS-PAGE, transferred to a nitrocellulose membrane, and probed for either HA to detect for precipitated PKCζ (Figure 4.6.A) or GST to detect for amounts of the GST or GST-tagged 80K-H construct proteins (Figure 4.6.B).

4.1.2.1.4. Further definition of the binding of munc18c to 80K-H

To further define the interaction between 80K-H and munc18c, GST pull-down assays were performed using the same 80K-H truncation constructs that were used in the above section (section 4.1.2.3), namely KH302, KH327, KH353 and KH378. For this, purified GST-tagged 80K-H truncation constructs (see Figure 4.1.5) were coupled to glutathione beads and incubated with extracts of Cos-1 cells that had been transiently transfected with Xpress-tagged full length munc18c (MFL). Complexes were washed to remove non-specific binding, separated by SDS-PAGE and immunoblotted with anti-Xpress antibody to assess the co-precipitation of munc18c with the 80K-H constructs. As shown in Figure 4.7 A, munc18c was precipitated when extracts were incubated with GST-tagged KHFL, KH302, KH327, KH353 and KH378 but was not precipitated when extracts were incubated with only GST coupled to glutathione beads (lane 1 figure 4.7 A) indicating that the association between the 80K-H constructs and MFL was specific. Quantities of the GST fusion proteins were checked by western blotting using an anti-GST antibody. Amounts of all of the truncated 80K-H constructs were shown to be comparative. However, the levels of the full length 80K-H protein (KHFL) were considerably lower. This had proved to be the case despite continued attempts to increase the levels of this protein relative to the other constructs. The low levels of gst-tagged full length 80K-H protein probably explains the lower amounts of binding seen between full length munc18c and KHFL compared to KH302. Although these experiments clearly show that 80K-H binds to munc18c in vitro, it is unclear exactly what part of the 80K-H protein is essential for binding to munc18c. It appears that most binding is lost between residues 302 and 327 of 80K-H. However, all the 80K-H constructs support some binding to munc18c indicating that the N-terminal 378 residues of 80K-H do show some affinity for munc18c.

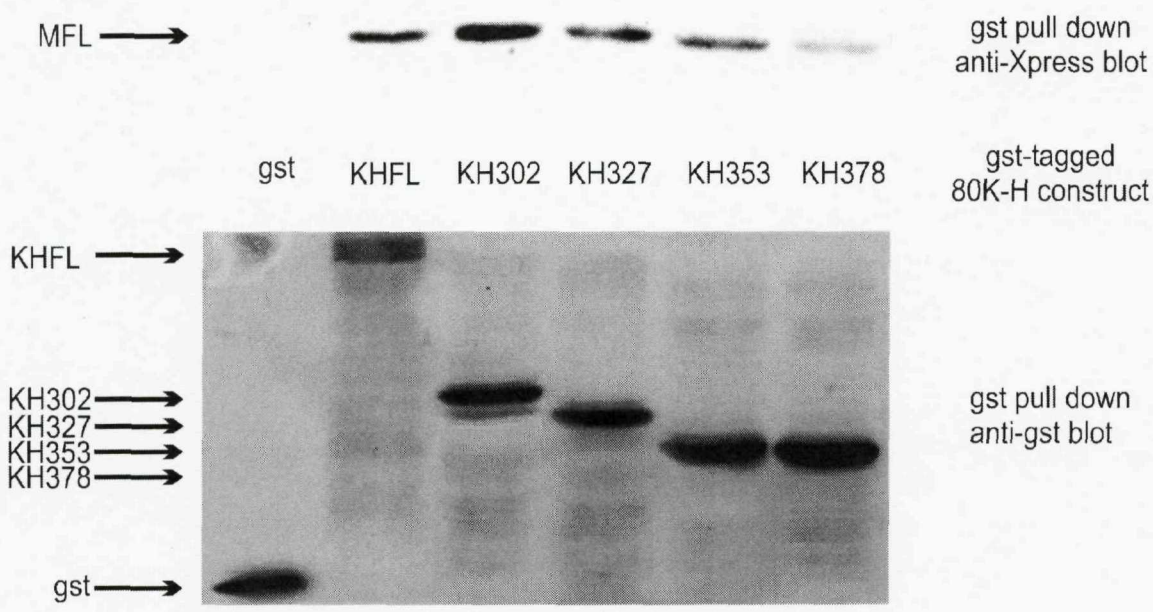

Figure 4.1.7: Determination of the region of 80K-H that is responsible for binding to munc18c.

Cos-1 cells were transiently transfected with full length munc18c expressed as an Xpress fusion (MFL.) 80K-H constructs were bacterially expressed as GST fusion proteins and coupled to glutathione sepharose beads. GST bound to glutathione beads was used as a control (GST). Cos-1 cell extracts were incubated with the glutathione bead complexes, then washed to remove non-specific binding. Proteins were separated by SDS-PAGE, transferred to a nitrocellulose membrane, and probed for either Xpress to detect precipitated MFL (Figure 4.1.7.A) or GST to detect for amounts of the GST or GST-tagged 80K-H construct proteins (Figure 4.1.7.B).

4.1.2.1.5. Investigation into the role of the glutamic acid stretch of 80K-H

The region of 80K-H that the GST pull-down assays showed to be crucial for binding to munc18c and PKCζ encompassed residues 302-353. This area contains an unusual glutamic-rich region with glutamic acid residues stretching from residue 314 to 335. A BLAST search of the region encompassing residues 302-378 of 80K-H showed it to have no homology to other proteins, and there is no information regarding a possible role for long glutamic acid stretches. This made this particular region of 80K-H an interesting candidate for further investigation. To further investigate the role of these glutamic acid residues in binding to munc18c and PKCζ, a two-sided SOEing method of PCR was employed to create deletion mutants, one lacking residues 314-325 and one lacking residues 327-333.

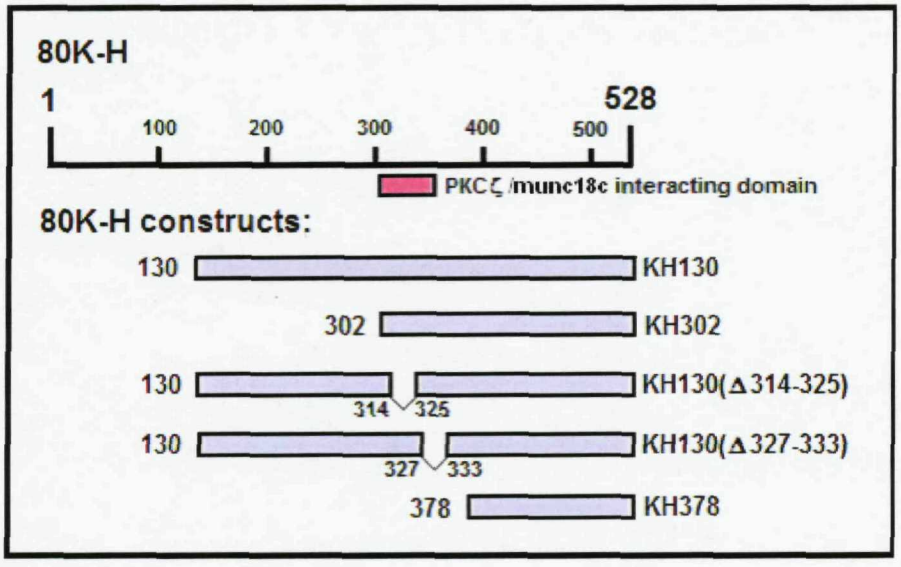

Figure 4.1.8: 80K-H deletion and truncation constructs.

Figure showing the series of truncation and deletion constructs of 80K-H used as GST fusions in a GST pull-down assay and the region of 80K-H previously shown to be critical for binding to PKCζ and munc18c.

I firstly wanted to investigate the role that this region of 80K-H played in binding to munc18c. For this, purified GST-tagged 80K-H truncation constructs (see Figure 4.1.8) were coupled to glutathione beads and incubated with extracts of Cos-1 cells that had been transiently transfected with Xpress-tagged full-length munc18c. Complexes were washed to remove non-specific binding, separated by SDS-PAGE and immunoblotted with anti-Xpress antibody to assess the co-precipitation of munc18c with the 80K-H constructs. As shown in Figure 4.1.9, munc18c associated with KH130, KH302, KH130(Δ314-325) and KH130(Δ327-333) but showed little or no binding to KH378. Munc18c was not precipitated when extracts were incubated with only GST coupled to glutathione beads (lane 1, figure 4.1.9) indicating that the association between munc18c and the 80K-H constructs was specific. Quantities of the GST fusion proteins were checked by western blotting using an anti-GST antibody and shown to be similar. This shows that differences in amounts of precipitated munc18c for each 80K-H construct was not due to relative amounts of the GST-tagged 80K-H proteins. This indicates that although these two areas of glutamic acid residues lie in a crucial area for binding to munc18c, they are not themselves required for binding.

Figure 4.1.9: Determination of the region of 80K-H that is responsible for binding munc18c.

Cos-1 cells were transiently transfected with munc18c expressed as an Xpress fusion. 80K-H constructs were bacterially expressed as GST fusion proteins and coupled to glutathione sepharose beads. GST bound to glutathione beads was used as a control (GST). Cos-1 cell extracts were incubated with the glutathione bead complexes, then washed to remove non-specific binding. Proteins were separated by SDS-PAGE, transferred to a nitrocellulose membrane, and probed for Xpress to detect co precipitated munc18c.

I then wanted to investigate the role that this region of 80K-H played in binding to PKCζ. For this, purified GST-tagged 80K-H truncation constructs (see Figure 4.1.8) were coupled to glutathione beads and incubated with extracts of Cos-1 cells that had been transiently transfected with HA-tagged full-length PKCζ. Complexes were washed to remove non-specific binding, separated by SDS-PAGE and immunoblotted with anti-HA antibody to assess the co-precipitation of PKCζ with the 80K-H constructs. As shown in Figure 4.1.10, PKCζ associated with KH130, KH302, KH130(Δ314-325) and KH130(Δ327-333) but showed little or no binding to KH378. PKCζ was not precipitated when extracts were incubated with only GST coupled to glutathione beads (lane 1 figure

4.1.10) indicating that the association between PKCζ and the 80K-H constructs was specific. Quantities of the GST fusion proteins were checked by western blotting using an anti-GST antibody and shown to be similar. This shows that differences in amounts of precipitated PKCζ for each 80K-H construct was not due to relative amounts of the GST-tagged 80K-H proteins. This indicates that although these two areas of glutamic acid residues lie in a crucial area for binding to PKCζ, they are not themselves required for binding.

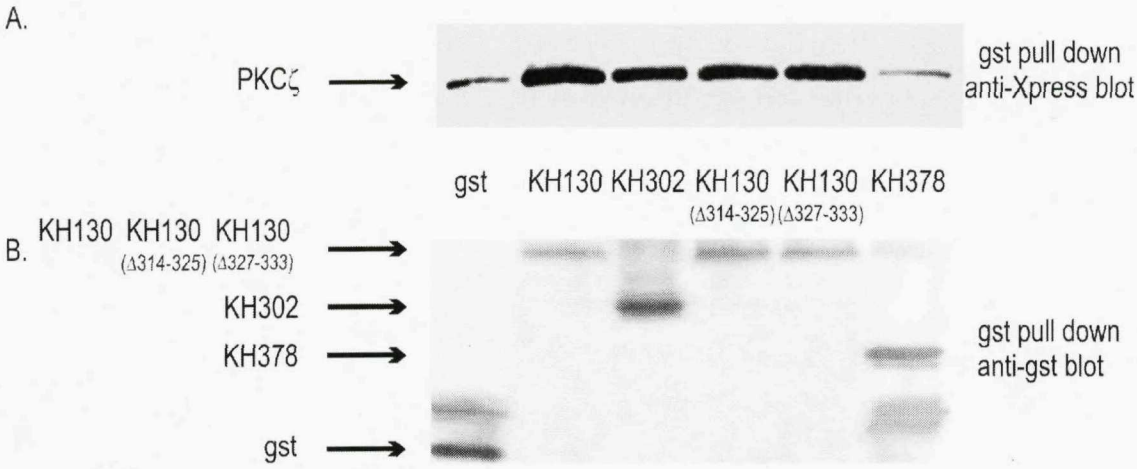

Figure 4.1.10: Determination of the region of 80K-H that is responsible for binding PKCζ

Cos-1 cells were transiently transfected with PKCζ expressed as an HA fusion. 80K-H constructs were bacterially expressed as GST fusion proteins and coupled to glutathione sepharose beads. GST bound to glutathione beads was used as a control (GST). Cos-1 cell extracts were incubated with the glutathione bead complexes, then washed to remove non-specific binding. Proteins were separated by SDS-PAGE, transferred to a nitrocellulose membrane, and probed for HA to detect co precipitated PKCζ.

4.1.2.2. The use of munc18c mutants

4.1.2.2.1. Determination of the domains of munc18c that interact with 80K-H

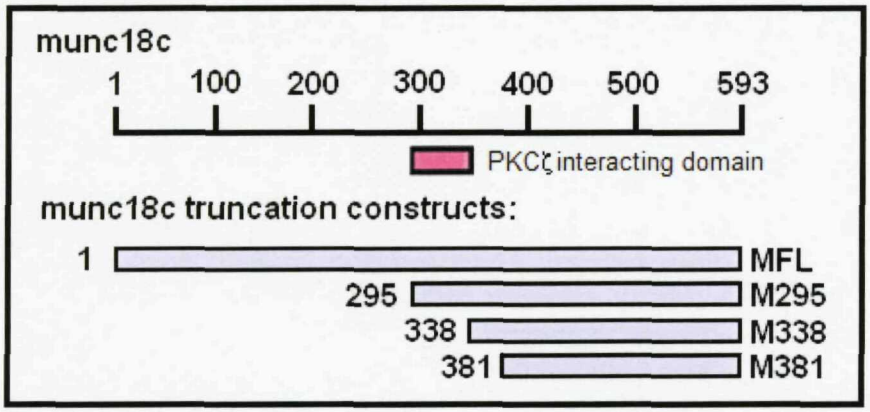

Figure 4.1.11: Munc18c truncation constructs. *Figure showing the series of truncation constructs of munc18c used as GST fusions in a GST pull-down assay and the region of munc18c previously shown to be critical for binding to PKCζ.*

To further validate and characterize the interaction between 80K-H and munc18c as seen in the yeast-2-hybrid screen, GST pull-down assays were performed. For this, purified GST-tagged munc18c truncation constructs (see Figure 4.1.11) were coupled to glutathione beads and incubated with extracts of Cos-1 cells that had been transiently transfected with Xpress-tagged KH302. Complexes were washed to remove non-specific binding, separated by SDS-PAGE and immunoblotted with anti-Xpress antibody to assess the co-precipitation of KH302 with the munc18c constructs. As shown in Figure 4.1.12, KH302 interacted with full length munc18c (MFL), M295, M338, M381 and M468. KH302 was not precipitated when extracts were incubated with only GST coupled to glutathione beads (lane 1 fig 4.1.12) indicating that the association between KH302 and munc18c was specific. Quantities of the GST fusion proteins were checked

by western blotting using an anti-GST antibody and shown to be similar. This shows that differences in amounts of precipitated KH302 for each munc18c construct is not due to relative amounts of the GST-tagged munc18c proteins. This result indicates that the region of munc18c that is responsible for binding to 80K-H lies in the C-terminus of munc18c (residues 381-593).

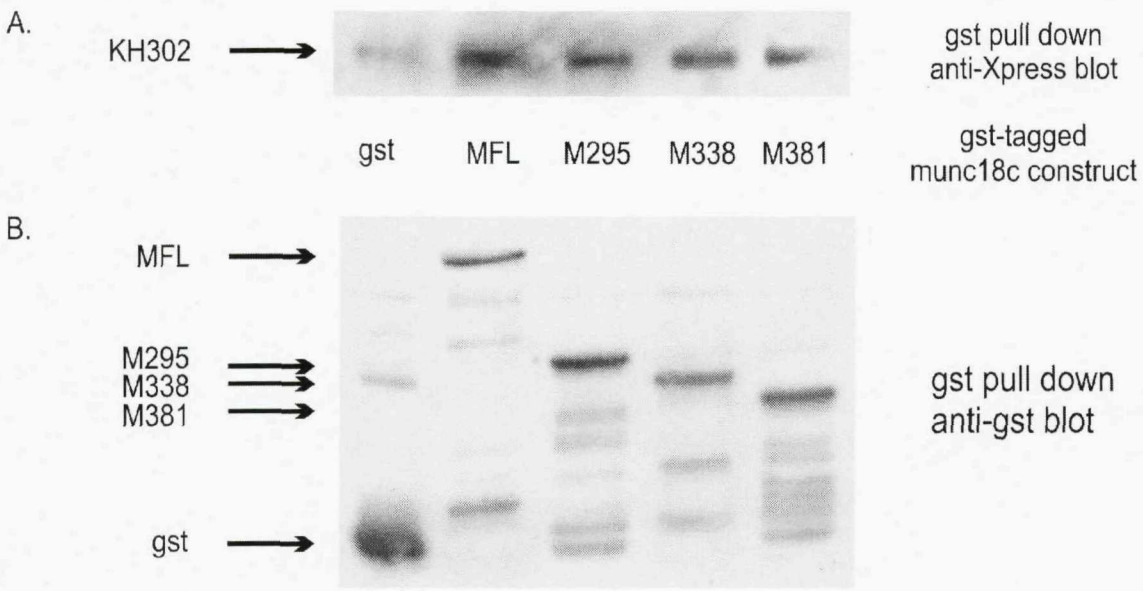

Figure 4.1.12: Determination of the region of munc18c that is responsible for binding to 80K-H.

Cos-1 cells were transiently transfected with KH302 expressed as an Xpress fusion. Munc18c constructs were bacterially expressed as GST fusion proteins and coupled to glutathione sepharose beads. GST bound to glutathione beads was used as a control (GST). Cos-1 cell extracts were incubated with the glutathione bead complexes, then washed to remove non-specific binding. Proteins were separated by SDS-PAGE, transferred to a nitrocellulose membrane, and probed for Xpress to detect co precipitated KH302 or GST to detect GST-tagged munc18c constructs.

4.1.2.2.2. Further definition of the binding of PKCζ to munc18c

To further define the interaction between munc18c and PKCζ, GST pull-down assays were performed using full length munc18c (MFL), the truncation constructs M295 and M338 and a further two truncation constructs of munc18c lying in between this region (M308 and M326) For this, purified GST-tagged munc18c truncation constructs (see Fig 4.1.13) were coupled to glutathione beads and incubated with extracts of Cos-1 cells that had been transiently transfected with HA-tagged PKCζ. Complexes were washed to remove non-specific binding, separated by SDS-PAGE and immunoblotted with anti-HA antibody to assess the co-precipitation of PKCζ with the munc18c constructs. As shown in Figure 4.1.14, PKCζ associated strongly with MFL and M295. Binding of PKCζ gradually decreased over M308, M326 and M338, with little or no binding to M338. PKCζ was not precipitated when extracts were incubated with only GST coupled to glutathione beads (lane 1 figure 4.13) indicating that the association between PKCζ and the munc18c constructs was specific. Quantities of the GST fusion proteins were checked by western blotting using an anti-GST antibody and shown to be comparative. This shows that differences in amounts of precipitated PKCζ for each munc18c construct is not due to relative amounts of the GST-tagged proteins. This result indicates that the regions of munc18c responsible for binding to PKCζ are spread out between residues 295-338.

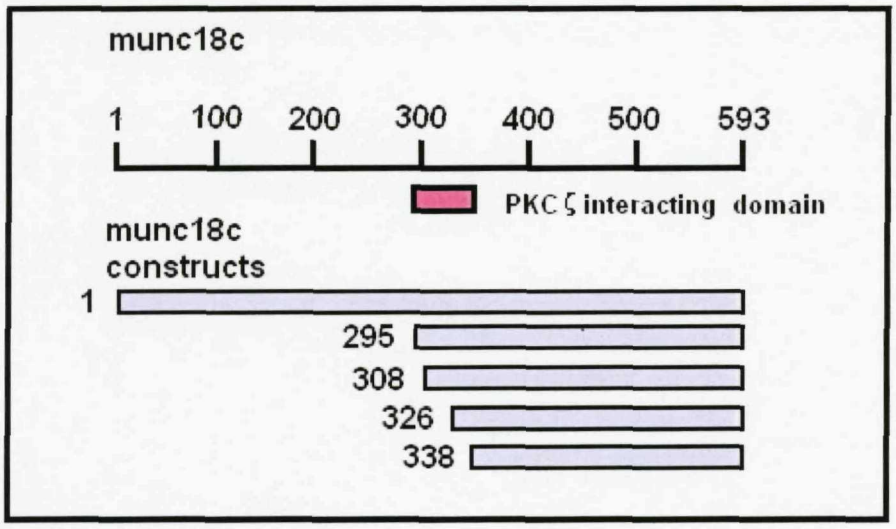

Figure 4.1.13: Munc18c truncation constructs.

Figure showing the series of truncation constructs of munc18c used as GST fusions in a GST pull-down assay and the region of munc18c previously shown to be critical for binding to PKCζ.

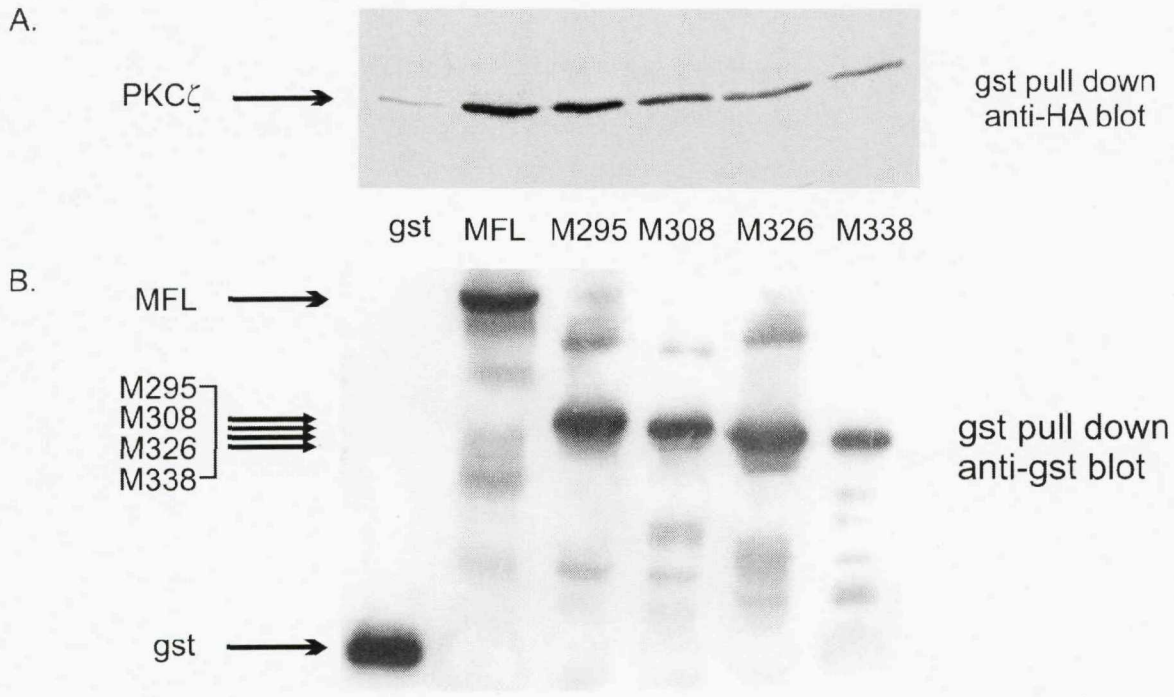

Figure 4.1.14: Determination of the region of munc18c that is responsible for binding to PKCζ

Cos-1 cells were transiently transfected with PKCζ expressed as an HA fusion. Munc18c constructs were bacterially expressed as GST fusion proteins and coupled to glutathione sepharose beads. GST bound to glutathione beads was used as a control (GST). Cos-1 cell extracts were incubated with the glutathione bead complexes, then washed to remove non-specific binding. Proteins were separated by SDS-PAGE, transferred to a nitrocellulose membrane, and probed for HA to detect co-precipitated PKCζ or GST to detect the GST-tagged munc18c constructs.

4.1.3. Discussion

One of the most fundamental of insulin's actions is to regulate glucose homeostasis. It does this by inducing a rapid increase in glucose uptake in muscle and fat cells by stimulating the translocation of the GLUT4 glucose transporter from intracellular vesicle stores to the cell surface. Insulin binding to its receptor activates a signalling cascade, ultimately leading to the targeting of the GLUT4 containing vesicles to specific docking sites at the plasma membrane. PKCζ has been clearly shown to be a kinase activated by this signalling pathway that is required for the translocation of the GLUT4 vesicles [Kanzaki et al. 2004, Sajan et al. 2006, Bandyopadhyay et al. 1999 and 2002, Hodgkinson et al. 2005, Liu et al. 2006]. PKCs often exert their effects by binding to and/or delivering proteins to their targets, rather than merely playing a role in catalytic phosphorylations. Few relevant substrates have been found for PKCζ, which supports the hypothesis that it's role in GLUT4 vesicle trafficking is structural rather than catalytic. More research needs to be undertaken to understand the role of this protein in insulin mediated glucose transport.

GLUT4 vesicle trafficking is similar to that seen in synaptic vesicles. The GLUT4 vesicle contains the v-SNARE VAMP2 which binds to its cognate t-SNARE receptor Syntaxin4 in the plasma membrane. [Chang, L. et al. (2004), Grusovin, J. and Macaulay, S.L. (2003), Kanda, H. et al. (2005), Rudich, A. and Klip, A. (2003)] .Insulin regulates VAMP2:Syntaxin4 binding by virtue of accessory proteins, the most important of which is munc18c. In the basal state, munc18c binds to syntaxin4 with high affinity, acting as a clamp over syntaxin4. This prevents VAMP2 from binding to syntaxin4 and hence inhibits GLUT4 vesicle docking at the plasma membrane [Chang et al. 2004, Kanda et al. 2005, Thurmond et al. 1998, Tamori et al. 1998]. Insulin stimulation has been proposed to decrease the binding of munc18c to syntaxin4, thus enabling the GLUT4 vesicle to dock at the plasma membrane via an interaction between VAMP2 and syntaxin4 [Tellam et al. 1997]. However, despite considerable research into the exact function of munc18c in insulin regulated GLUT4 vesicle trafficking, its precise role has remained elusive. In addition, there have been few binding partners found for this vesicle trafficking protein, further perplexing its role in insulin mediated glucose transport.

The discovery in our laboratory of 80K-H as a putative binding partner for both munc18c and PKCζ was an important and exciting one, providing a link between the insulin signalling pathway and the vesicle trafficking machinery. The previous work undertaken in our laboratory showed that *in vitro* and *in vivo* interactions occur between munc18c and PKCζ, munc18c and 80K-H and PKCζ and 80K-H. A key finding of these investigations was that insulin increased the association between these proteins. 80K-H truncation constructs were found to predominantly localize to the plasma membrane of CHO cells, placing it in the correct subcellular localization to interact with PKCζ and munc18c and were found to increase glucose transport when over expressed in CHO cells in the basal state. It was also shown that the region of 80K-H responsible for binding to PKCζ lay between residues 302-378 and that the region of munc18c responsible for binding to PKCζ lay between residues 295-338. Research previously undertaken in our laboratory led to the hypothesis that 80K-H together with PKCζ complexes with munc18c when cells are exposed to insulin (see Figure 4.1.1). This releases the clamping action of munc18c that is seen in the basal state.

The work undertaken in this chapter of my thesis aimed to further characterise the interactions between munc18c with PKCζ, munc18c with 80K-H and PKCζ with 80K-H. This was done with a view to further defining the role of these three proteins and their interactions with each other in insulin mediated GLUT4 vesicle trafficking and glucose transport.

The key results from this chapter are as follows: (A) The region of 80K-H (between residues 302-378) previously shown to be responsible for binding to PKCζ, is also responsible for binding to munc18c. (B) It was also shown that the presence of PKCζ did not inhibit the interaction between munc18c and 80K-H, *in vitro*. (C) The long stretch of glutamic acid residues within 80K-H is not responsible for its binding to munc18c or PKCζ. (D) I showed that the region of munc18c responsible for binding to PKCζ lies between residues 295-338, but (E) I was unable to define the interaction site for PKCζ on munc18c any further. (F) I also showed that it is the C-terminal section of munc18c (amino acids 381-593) that is responsible for its binding to 80K-H.

I have shown that the region of 80K-H previously shown to be responsible for an interaction with PKCζ is also required for an interaction to occur with munc18c. A GST pull down assay using GST-tagged 80K-H constructs showed that the region of 80K-H encompassing amino acids 302-378 was essential for binding to munc18c. I then went on to further define this interaction site by making two more 80K-H truncation constructs with N-termini lying between residues 302-378. These two constructs, KH327 and KH353, were then used in GST pull down assays to check for interactions with both munc18c and PKCζ. These experiments further defined the region of 80K-H responsible for binding to PKCζ to lie between residues 302-327. There was a sudden loss of binding to PKCζ once residues past amino acid 302 were removed. It could be that this region of 25 amino acids is solely responsible for binding to PKCζ. However, it could also be that this region (between residues 302 and 327) is one of many regions along the whole 80K-H protein that is necessary and required for binding to PKCζ and once binding from this region is lost, the other regions of 80K-H are also unable to bind. (i.e. KH302 is the smallest N-terminal truncation construct that will still facilitate binding to PKCζ). Future work should include the production of a full length 80K-H construct that is unable to interact with PKCζ (i.e. KHFL$\Delta_{302\text{-}327}$: full length 80K-H with residues 302-327 removed). This construct could be made using the two sided SOEing method employed earlier in this chapter and the construct could be used to further validate the role for the interaction between 80K-H and PKCζ. Although the KH378 construct does fulfil this role, the production of a KHFL$\Delta_{302\text{-}327}$ would produce results with a more convincing argument.

The two further 80K-H truncation constructs that were made (KH327 and KH353) did not produce a more definitive result regarding the binding of 80K-H to munc18c. As was seen before, munc18c bound strongly to KH302 but did not bind to KH378, suggesting that the region of 80K-H between residues 302-378 is responsible for binding to munc18c. However, further dissection of this stretch of amino acids produced a gradual loss of binding to munc18c rather than the sudden loss of binding seen with PKCζ. This

would suggest that the residues responsible for binding to munc18c are more widespread than those responsible for binding to PKCζ. It could be that within the stretch of amino acids from residues 302-378 lay numerous "domains" that bind to munc18c in a cumulative fashion. For example, regions 302-327, 327-353 and 353-378 of 80K-H may all form contacts with munc18c and the more of these regions that are able to bind, the stronger the interaction. Hence deleting amino acids 302-327 would reduce the interaction with munc18c, but some binding would still occur via the 327-353 and 353-378 regions. Further truncation of 80K-H to amino acid 353 would reduce the interaction further, but still enable some binding to munc18c via amino acids 353-378. It is not until all of these munc18c binding "domains" are lost by truncation of 80K-H to amino acid 378 that complete loss of binding is seen.

The use of munc18c truncation constructs and GST pull down assays showed that it is the C-terminal section of munc18c (amino acids 381-593) that is responsible for binding to 80K-H. All of the munc18c truncation constructs used (MFL, M295, M308, M326, M338 and M381) showed binding to 80K-H. This shows that the region of munc18c responsible for binding to 80K-H is different to that responsible for binding to PKCζ, as previous work in our laboratory had shown amino acids 295-338 of munc18c to be responsible for binding to PKCζ. Through the production of more truncation constructs and GST pull down assays, I further defined the region of munc18c that is responsible for binding PKCζ. The loss of binding of PKCζ to the munc18c truncation constructs occurs more gradually than that seen with PKCζ to the 80K-H truncation constructs. This would suggest that the residues responsible for binding to PKCζ are more widespread in munc18c than in 80K-H. The two further munc18c truncation constructs that were made did not produce a more definitive result regarding the binding of PKCζ to munc18c. As was seen before, PKCζ bound strongly to M295 but did not bind to M338, suggesting that the region of munc18c between residues 295-338 is responsible for binding to PKCζ. However, further dissection of this stretch of amino acids produced a gradual loss of binding to PKCζ, rather than a sudden loss of binding. This would suggest that the residues responsible for binding to PKCζ are more widespread in munc18c than those in

80K-H. It could be that within the stretch of amino acids from residues 295-338 lie numerous "domains" that bind to PKCζ in a cumulative fashion. For example, regions 295-308, 308-326 and 326-338 of munc18c may all form contacts with PKCζ and the more of these regions that are able to bind, the stronger the interaction. Hence deleting amino acids 295-308 would reduce the interaction with PKCζ, but some binding would still occur via the 308-326 and 326-338 regions. Further truncation of munc18c to amino acid 326 would reduce the interaction further, but still enable some binding to PKCζ via amino acids 326-338. It is not until all of these PKCζ binding "domains" are lost by truncation of munc18c to amino acid 338 that complete loss of binding is seen.

The addition of PKCζ did not cause any change in the association between munc18c and 80K-H. This suggests that the binding of PKCζ, munc18c and 80K-H is in a triplex formation rather than a series of duplexes. If the addition of PKCζ caused a decrease in binding between munc18c and 80K-H, it would suggest that PKCζ and 80K-H compete for munc18c binding. However, the addition of PKCζ had no effect on the interaction between munc18c and 80K-H, suggesting the formation of a non-competitive complex. This implies that all three proteins come together in one complex. This is quite surprising considering that the results also show that the small region of 80K-H responsible for binding to PKCζ is also responsible for binding to munc18c (residues 302-378). The fact that such a small stretch of amino acids is responsible for binding to two individual proteins suggests two possibilities for the binding between PKCζ, munc18c and 80K-H. One possibility is that the three proteins come together in a triplex formation with the protein in the middle preventing a direct interaction between the two proteins on the ends. The other possibility is that all PKCζ, munc18c and 80K-H associations are direct interactions, but that only two of them have a direct association at any one time (i.e. PKCζ with 80K-H, PKCζ with munc18c and 80K-H with munc18c). If the latter was true, binding between the three proteins would be competitive and the addition of PKCζ should reduce the interaction between munc18c and 80K-H in an in vitro assay such as the one performed. Work previously conducted in our laboratory, using co-immunoprecipitations in L6 myotubes and 3T3-L1 adipocytes showed a large insulin

stimulated increase in association between munc18c and 80K-H (with little association in the basal state.) They also showed an increase in association between PKCζ and 80K-H and between PKCζ and munc18c upon insulin stimulation. This supports the theory that these three proteins come together in a triplex formation.

It would be interesting to investigate 80K-H phosphorylation, the possibility that PKCζ is involved in the phosphorylation of 80K-H and that this phosphorylation enables binding to munc18c. This is a distinct possibility as 80K-H was shown to be robustly phosphorylated by PKCζ immunoprecipitates [Hodgkinson et. al. 2005]. It is highly possible that PKCζ, although not directly responsible for phosphorylating 80K-H, could be closely involved, perhaps through interaction or phosphorylation of other proteins. This would depend on PKCζ acting through its well-known ability to exert its effects through binding other proteins [Hodgkinson et. al. 2002, Moscat and Diaz-Meco 2000]. The phosphorylation of 80K-H is something else that is investigated later on in this thesis (see chapter 4.6).

Within the region of 80K-H found to be responsible for binding to both PKCζ and munc18c is a long stretch of glutamic acid residues (residues 314-335). By use of a PCR method called two-sided SOEing, I produced two deletion constructs of 80K-H. Both of these were deletion constructs of the GST-tagged KH130 construct used previously, one lacking residues 314-325 and one lacking residues 327-333. GST pull down assays using these constructs showed that deletion of either one of these glutamic acid stretches caused no effect to the binding of 80K-H to either PKCζ or munc18c. The GST pull down assays I performed previously implied that the region of 80K-H responsible for binding to munc18c lay between amino acids 302-378 and those responsible for binding to PKCζ lay between amino acids 302-327. The use of the deletion constructs implied that the regions of 80K-H encompassing amino acids 314-325 and 327-333 were not responsible for binding to either munc18c or PKCζ. There are a couple of explanations for these results. It is possible that the long stretch of glutamic acid residues is indeed responsible for 80K-H's binding to munc18c or PKCζ, but that loss of binding is not seen unless the entire stretch of glutamic acid residues is deleted. This was something that was prepared for by designing three deletion mutants: the two that are discussed in this chapter, each

lacking one of the stretches of glutamic acids and also one lacking the entire stretch of glutamic acids from amino acid 314-333. However, problems with both the cloning and expression of this construct prevented gaining any experimental data from it. Truncation of amino acids 1-327 of 80K-H prevented its binding to PKCζ. However, truncation of amino acids 1-302, or deletion of amino acids 314-325 or 327-333 of 80K-H did not affect its binding to PKCζ. If the entire stretch of glutamic acid residues must be deleted in order for binding to PKCζ to be lost, then the KH327 80K-H construct (which still contains the second long stretch of glutamic acids) should still be able to bind. Because KH327 was unable to bind to PKCζ, the only logical explanation is that amino acids 302-314 of 80K-H contain the residues that are crucial for its binding to PKCζ. These experiments hence indicate that the region of 80K-H from amino acid 302 to 314 is critical for binding to PKCζ. Firstly an 80K-H construct lacking residues 302-314 should be made. If this proves to be a non-interacting mutant, then this should be used in overexpression studies in insulin-responsive cell lines to investigate the role of 80K-H and PKCζ interactions in insulin signalling. If GST pull down assays show that the 80K-H construct lacking residues 302-314 is still capable of binding to PKCζ, then a full length construct lacking residues 302-327 should be investigated.

The results are less clear-cut for 80K-H's binding to munc18c. The GST pull down assays with the truncation constructs of 80K-H implied that binding of munc18c was not entirely lost until the N-terminal 378 amino acids of 80K-H had been removed (see Figures 4.1.3 and 4.1.7). N-terminal truncations of 80K-H up to amino acids 302, 327 and 353 still supported some binding to munc18c, with a gradual loss of binding as more of the N-terminus was removed. It is not until the N-terminus has been truncated up to amino acid 378 of 80K-H that the binding to munc18c is nearly completely diminished. It could well be that 80K-H residues from amino acid 302-378 are part of a number of binding domains that support binding to munc18c and that these bind in a cumulative fashion. Removal of these residues will cause gradual loss of binding to munc18c. This could explain why there was still significant binding of munc18c to the 80K-H constructs lacking the two stretches of glutamic acid residues. It may be that removal of these stretches of glutamic acids is not enough to disrupt binding to munc18c as there is still

more than adequate "contacts" formed from the rest of the 80K-H residues from amino acid 302-378.

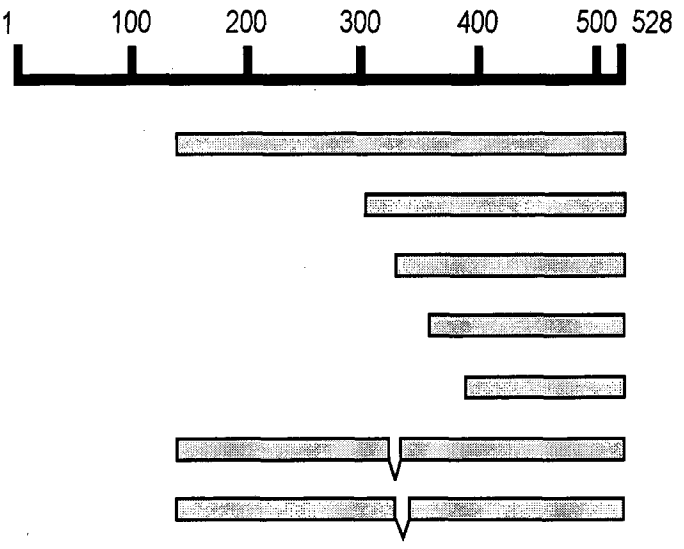

80K-H construct	binding to:	
	PKCζ	munc18c
KH130	✓	✓
KH302	✓	✓
KH327	✗	
KH353	✗	
KH378	✗	✗
KH130(Δ314-325)	✓	✓
KH130(Δ327-333)	✓	✓

Figure 4.1.15: Binding of the 80K-H constructs to PKCζ or munc18c:

Figure to show the structure of the 80K-H constructs (KH130, KH302, KH327, KH353, KH378, KH130(Δ314-325) and KH130(Δ327-333)) and whether binding to PKCz or munc18c was supported. KH130 and KH302 supported binding to PKCζ. There was then a sudden loss of binding, with KH327, KH353 and KH378 showing no binding. Both of the 80K-H deletion mutants, KH130(Δ314-325) and KH130(Δ327-333) bound to PKCζ. KH130 and KH302 supported binding to munc18c. There was then a gradual loss of binding as the 80K-H constructs were truncated further, with KH378 showing no binding to munc18c. Both of the 80K-H deletion mutants, KH130(Δ314-325) and KH130(Δ327-333) bound to munc18c.

If time had have permitted, it would have been interesting to carry out further investigations using the 80K-H deletion mutants already produced (KH130Δ314-325 and KH130Δ327-333) to ascertain the function of this region. The most obvious initial

experiment should be to investigate the effect of over-expressing these constructs on glucose transport, using the glucose transport assays described in Methods section 2.10.4. Various protein domain searches (e.g. Prosite) showed no other proteins to have such a long continuous stretch of glutamic acid residues and I have been unable to find any connotations as to its putative function. Proteins containing a long stretch of one amino acid (Homopolymeric Amino Acid-containing Proteins) are regularly found in nature but the function of such stretches remains largely unknown. Such a long stretch of glutamic acid residues is likely to be found on the surface of the protein, due to the hydrophilic nature of this amino acid. This adds to the likelihood of this region of 80K-H playing a role in interactions with other proteins or cellular structures. The long stretch of negative charge in 80K-H produced by this region of glutamic acid residues may well be involved in ionic interactions with an area of positive charge (e.g. in another protein with areas of many basic amino acids). However, neither PKCζ nor munc18c have any areas of high density of basic residues in their protein structure. Stretches of glutamic acid residues have also been found to serve as a site for proteolytic cleavage (most notably by PKA and meprin-β[Chestukhin et al. 1997]) raising the possibility that this section of 80K-H could be proteolytically cleaved. If this does occur, there has been no evidence of it in any of the experiments I have performed, with no sign of any fragment of suitable size with the anti-HA or anti-Xpress antibodies. Future work could include overexpression studies in mammalian cell lines to investigate the possibility of this region of 80K-H playing a role in its subcellular localization as well as the subcellular localization of munc18c and PKCζ. If time had been permitting, it may have been interesting to clone these 80K-H deletion constructs into fluorescently tagged vectors for use in *in vivo* subcellular localization studies using fluorescence microscopy. However, attachment of a poly-glutamic acid stretch to the C-terminus of yellow fluorescent protein was found to have no influence on its cellular location in a study investigating Homopolymeric Amino Acid-containing Proteins [Oma et al. 2004]. This suggests that stretches of glutamic acid residues do not play a role in a protein's subcellular location and should be considered before embarking on any future work with the 80K-H deletion constructs that I have made in this study.

In conclusion, the results from this chapter have further defined the interaction sites of munc18c, 80K-H and PKCζ for each other. Amino acids 302-327 of 80K-H are responsible for its association with PKCζ whilst amino acids 302-378 are required for its binding to munc18c. Removal of either one of the two long glutamic acid stretches in 80K-H did not disrupt its association with either PKCζ or munc18c. The C-terminal of munc18c is responsible for its interaction with 80K-H, whilst amino acids 295-338 of munc18c are required for an interaction to occur with PKCζ. Finally, the results suggest that insulin stimulation causes munc18c, 80K-H and PKCζ come together in a triplex formation, rather than a series of duplexes.

4.2. Using FCS to investigate 80K-H, PKCζ and munc18c interactions and their role in GLUT4 vesicle trafficking

4.2. Using FCS to investigate 80K-H, PKCζ and munc18c interactions and their role in GLUT4 vesicle trafficking

4.2.1. Introduction

The cell is a highly dynamic and complex system, undergoing constant and subtle modifications. Trying to analyse the complexity of such a system using only simple in vitro models has its clear disadvantages. Although *in vitro* techniques allow a simple and reproducible way of studying individual components of the cell, they do not take into consideration factors such as subcellular localization, concentration, mobility or accessibility of the molecule of interest. For example, endogenous proteins may be able to interact *in vitro*, but they may never be in the correct locality at the correct time for an interaction to occur within a living cell. The development of live cell imaging and analysis has provided scientists with the tools to overcome such problems. Advances in the use of fluorescence probes and microscopy have enabled the detailed study of specific activities within subcellular compartments.

Fluorescence Correlation Spectroscopy (FCS) is one particularly sophisticated technique that enables such analysis on a single-molecule scale. This technique uses confocal imaging to measure minute changes in fluorescence fluctuations over a given time [Petra Schwille and Elke Haustein Fluorescence Correlation Spectroscopy : An Introduction to its Concepts and Applications, Krichevsky O and Bonnet G 2002, Levin and Carson 2004, Vukojevic et al. 2005, Lippincott-Schwartz et al 2005, Haustein and Schwille 2003]. This enables the determination of parameters such as concentration, diffusion coefficients and binding characteristics [Larson et al. 2003, Kuroki et al. 2007] of the fluorescently labelled proteins. Above all, such characteristics can be determined for proteins within their native cellular environment. Live cell imaging and FCS were therefore ideal ways to study the proteins of interest to add to our previous knowledge of their role in GLUT4 vesicle translocation.

As has been described previously, GLUT4 vesicle exocytosis is similar to that seen in synaptic vesicles. The GLUT4 vesicle contains the v-SNARE, VAMP2, which binds to the t-SNAREs syntaxin4 and SNAP23 at the plasma membrane. It is this interaction which enables the GLUT4 vesicle to dock and fuse with the plasma membrane. Insulin is able to affect the interaction between these proteins (and hence affect the ability of the GLUT4 vesicle to dock/fuse with the plasma membrane) by virtue of accessory proteins. One of the most important of these is munc18c. In the basal state, munc18c is bound to syntaxin4 and prevents it interacting with VAMP2. *In vitro* assays indicate that insulin action either releases syntaxin4 from munc18c, or weakens the interaction between the two proteins. This then enables an interaction to occur between syntaxin4 and VAMP2, thus facilitating GLUT4 vesicle docking and fusion at the plasma membrane. However, the exact mechanism of munc18c's role in GLUT4 vesicle docking in vivo has remained uncharacterised. Insulin action somehow enables an interaction to occur. Insulin also activates a signalling cascade which leads to the activation of kinases such as PKB and PKCζ. Although there is much evidence for these two kinases playing an important positive role in GLUT4 vesicle translocation, their mechanism in this process still remains elusive. Until recently, no link had been found between the insulin signalling pathway and the vesicle trafficking machinery. Work in our laboratory identified a protein called 80K-H, which linked the insulin signalling kinase PKCζ to the vesicle trafficking protein munc18c. GST pull-down assays showed that a truncation construct of 80K-H (corresponding to amino acids 302-528 of the full length protein) interacted with munc18c and PKCζ when over-expressed in CHO cells. Interactions between PKCζ and munc18c were also seen. Co-immunoprecipitation studies also showed that the endogenous full length proteins also interacted in 3T3-L1 adipocytes and L6 myotubules. A series of GST pull-down assays with various truncation constructs of 80K-H and munc18c identified areas of these proteins crucial for binding to the other two proteins.

Appropriate truncation constructs were used as interacting and non-interacting mutants for further studies and for this thesis (please refer to tables 4.2.1, 4.2.2 and 4.2.3).

	KH302	KH378
PKCζ	√	x

Table 4.2.1: Binding between PKCζ and the two 80K-H constructs, KH302 and KH378

	MFL	M295	M338
PKCζ	√	√	x

Table 4.2.2: Binding between PKCζ and the three munc18c constructs, MFL, M295 and M338.

	MFL	M295	M338
KH302	√	√	√
KH378	x	x	x

Table 4.2.3: Binding between the two 80K-H constructs, KH302 and KH378 and the three munc18c constructs, MFL, M295 and M338.

Tables 4.2.1-3: Binding characteristics of 80K-H, PKCζ and munc18c constructs

GST pull-down assays were used previously to determine the binding characteristics of the 80K-H, PKCζ and munc18c constructs. (√) indicates that an interaction occurs between the two constructs, whereas (x) indicates that they do not interact.

Previous work in our laboratory using the KH302 and KH378 constructs also showed that 80K-H played a role in insulin-mediated glucose transport. Over-expression of KH302 in CHO cells mimicked the action of insulin on glucose transport, with basal and insulin stimulated glucose transport levels far exceeding those for control cells. An even greater effect was seen when KH378 was used.

In this study, the FCS data was used to calculate the diffusion coefficients (TauD1 values) for the EYFP-tagged proteins. This value is the average time that the EYFP molecules spend in the observation volume. Therefore a larger diffusion coefficient corresponds to a longer time spent in the observation volume and hence relates to a slower moving molecule. Smaller diffusion coefficients correspond to less time spent in the observation volume and hence indicate a faster moving molecule. Knowing the average speed of the protein of interest *in vivo* provides valuable insight into its behaviour. For example, larger or more membrane bound complexes will move slower than smaller or less tethered ones. In this section, 80K-H and its interactions with PKCζ and munc18c were investigated using fluorescence correlation spectroscopy (FCS). The full length munc18c, 80K-H and PKCζ proteins, as well as the 80K-H truncations KH302 and KH378 and the munc18c truncations M295 and M338, were cloned into the ECFP-N2 and EYFP-N2 vectors (see sections 3.2.2 and 3.3.2 respectively). Either single or double transfections of the various combinations were performed (see section 2.5.6.4) and FCS data collected for the EYFP-tagged protein only.

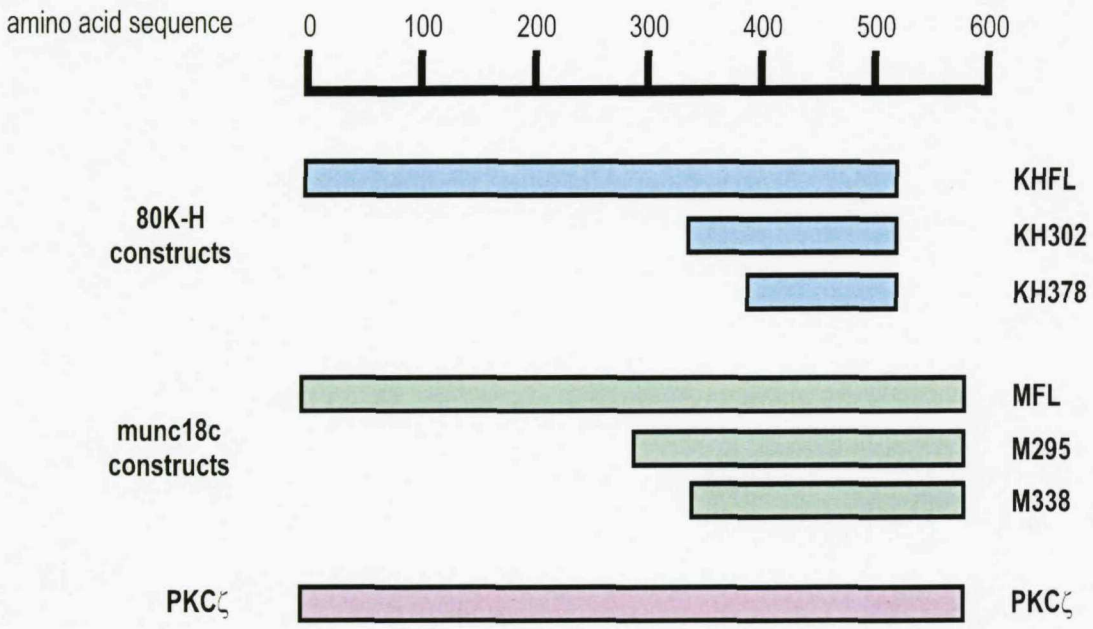

Figure 4.2.1: 80K-H, munc18c and PKCζ constructs used in this study.

Three 80K-H constructs were used: the full length protein of 528 amino acids (KHFL) and the two truncated constructs KH302 and KH378 which lacked the N-terminal 302 and 378 amino acids respectively. Three munc18c constructs were used: the full length protein of 592 amino acids (MFL) and the two truncated constructs M295 and M338 which lacked the N-terminal 295 and 338 amino acids respectively. Only the full length PKCζ construct of 592 amino acids was used.

The data presented show that PKCζ:80K-H:munc18c complex formation is critically dependant upon 80K-H and illustrates the crucial importance of 80K-H to glucose transport via GLUT4.

4.2.2. Results

4.2.2.1 80K-H

I first investigated whether the diffusion coefficient of 80K-H was affected by insulin stimulation. For this, both the 80K-H truncation construct, KH302 and the full length protein (KHFL) were used, as KHFL did not co-express with PKCζ or any of the munc18c constructs in these cells. As mentioned previously, KH302 binds both PKCζ and munc18c and mimics the effect of insulin on glucose transport (Hodgkinson et al., 2005a). Insulin had no effect on the average diffusion coefficient when KHFL was expressed alone (816 ± μs 58 μs pre insulin stimulation vs. 649 ± 153 μs post insulin stimulation; mean ± s.e.m.) Insulin also had no effect on the average diffusion coefficient of KH302 when it was expressed alone (1349 ± 138 μs pre insulin vs. 1205 ± 102 μs post insulin; mean ± s.e.m.) (Figure 4.2.2, Table 4.2.4).

I then examined whether the co-expression of munc18c or PKCζ had an effect on the diffusion coefficient of KH302. CHO cells were transfected with EYFP-tagged KH302 and either the ECFP-tagged munc18c truncation construct, M295 or ECFP-tagged full length PKCζ. The munc18c construct has previously been shown to function as the full length protein by binding 80K-H and PKCζ and inhibiting glucose transport (Hodgkinson et al. 2005a and 2005b). In the basal state, the presence of M295 had no effect on the diffusion coefficient of the EYFP-tagged KH302 (1349 ± 138 μs when KH302 was expressed alone, compared to 1125 ± 5 μs when M295 was co-expressed, Figure 4.2.2, Table 4.2.4.) However, in the insulin stimulated state, the presence of M295 caused KH302 to spend significantly less time in the observation volume (diffusion coefficient of 1205 ± 102 μs when KH302 was expressed alone, compared to 510 ± 89 μs when M295 was co-expressed, Figure 4.2.2, Table 4.2.4) indicating that the speed of KH302 was increased by the presence of M295 upon insulin stimulation.

In the basal state, the presence of ECFP-tagged PKCζ caused a significant decrease in the diffusion coefficient of the EYFP-tagged KH302 (356 ± 18 μs when PKCζ was co-

expressed, compared to 1205 ± 102 μs when KH302 was expressed alone, Figure 4.2.2, Table 4.2.4). However, the diffusion coefficient for KH302 increased upon insulin stimulation (from 356 ± 18 μs to 803 ± 18 μs) showing that insulin caused KH302 to slow down when PKCζ was present (Figure 4.2.2, Table 4.2.4).

Construct(s) overexpressed		Diffusion coefficient (μs) Mean ± s.e.m.	
EYFP	ECFP	- insulin	+ insulin
KH302	-	1349 ± 138	1205 ± 102
KH302	M295	1122 ± 5	510 ± 89
KH302	PKCζ	356 ± 18	803 ± 18

Table 4.2.4: Diffusion coefficients for KH302

CHO cells were transiently transfected with EYFP-tagged KH302 (control) or EYFP-tagged KH302 plus ECFP-tagged M295 or PKCζ. Cells were serum starved for 24 hours prior to data collection. Where appropriate, cells were stimulated with 10^{-7} M insulin for 20 minutes. FCS data was collected for the EYFP-tagged protein only and are shown as the mean ± s.e.m. from 3 individual experiments, each using 6 separate cells.

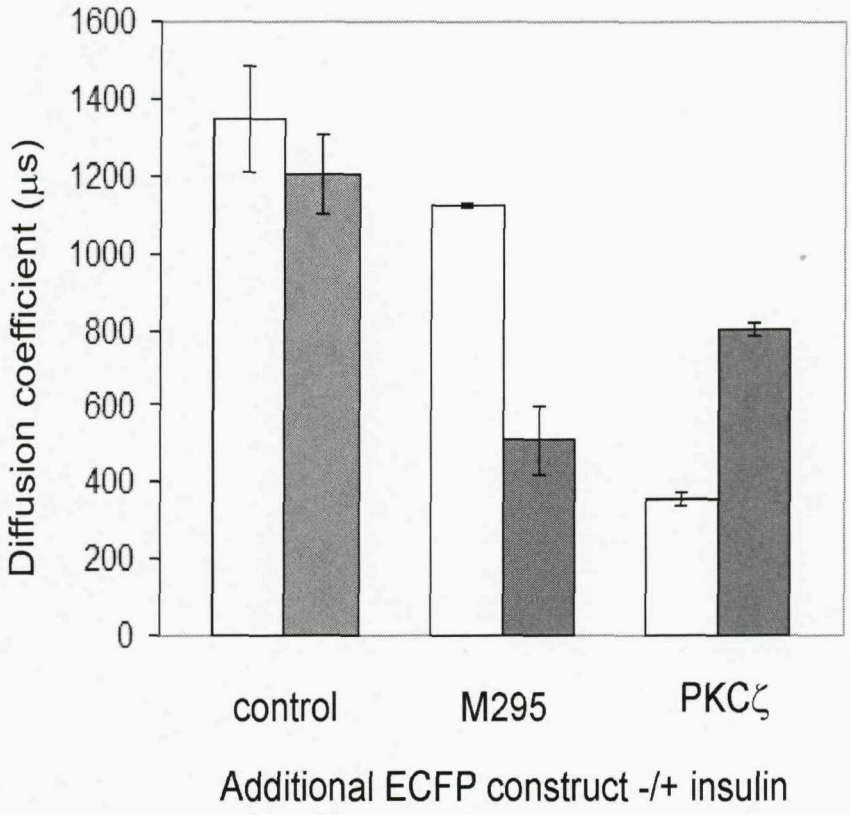

Figure 4.2.2: Diffusion coefficients for KH302

CHO cells were transiently transfected with EYFP-tagged KH302 (control) or EYFP-tagged KH302 plus ECFP-tagged M295 or PKCζ. Cells were serum starved for 24 hours prior to data collection. Where appropriate, cells were stimulated with 10^{-7} M insulin for 20 minutes. FCS data was collected for the EYFP-tagged protein only and are shown as the mean ± s.e.m. from 3 individual experiments, each using 6 separate cells.

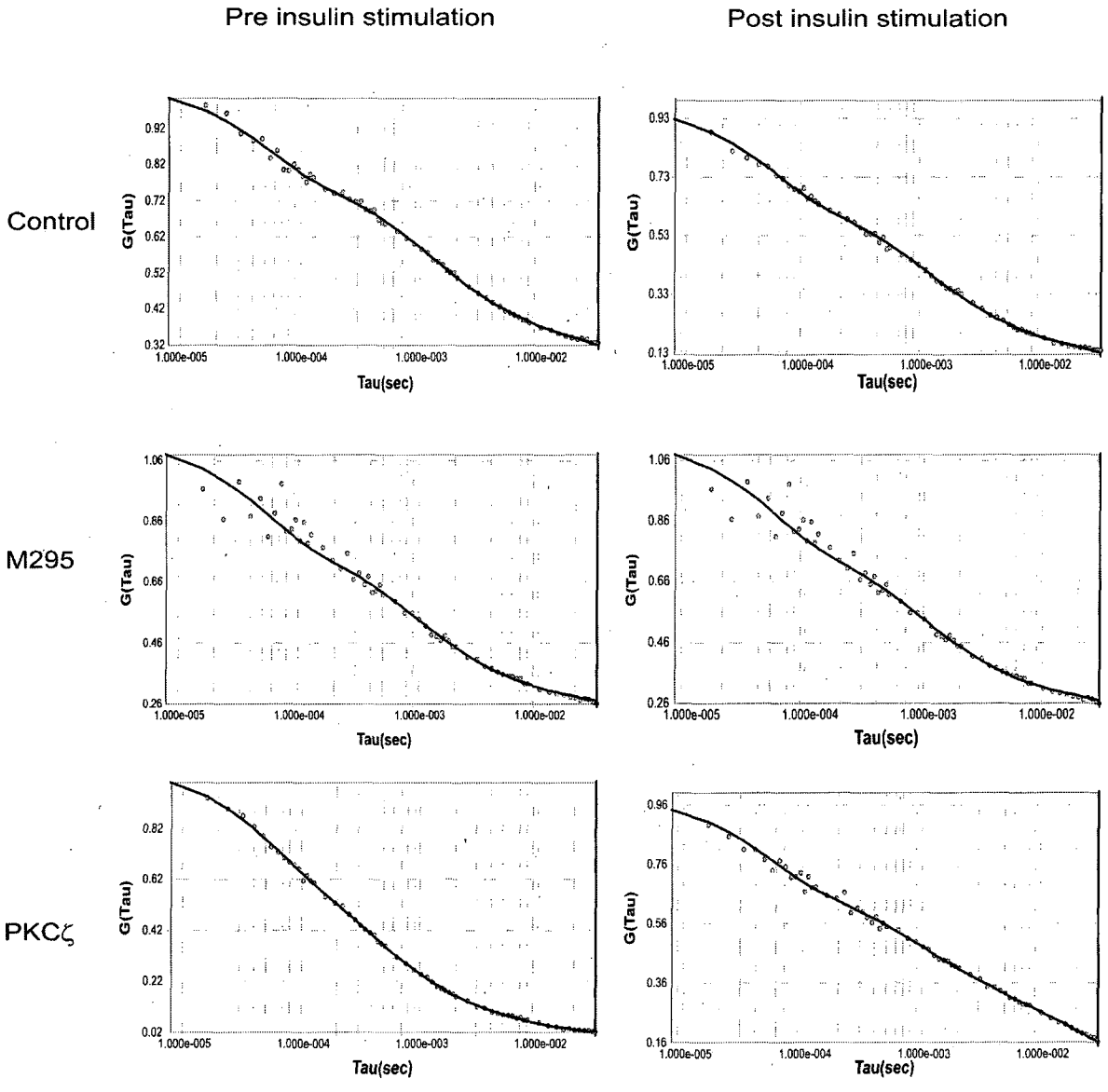

Figure 4.2.3: Example FCS traces for EYFP-tagged KH302

CHO cells were transiently transfected with EYFP-tagged KH302 (control) or EYFP-tagged KH302 plus ECFP-tagged M295 or PKCζ. Cells were serum starved for 24 hours prior to data collection. Where appropriate, cells were stimulated with 10^{-7} M insulin for 20 minutes. FCS data was collected for the EYFP-tagged protein only.

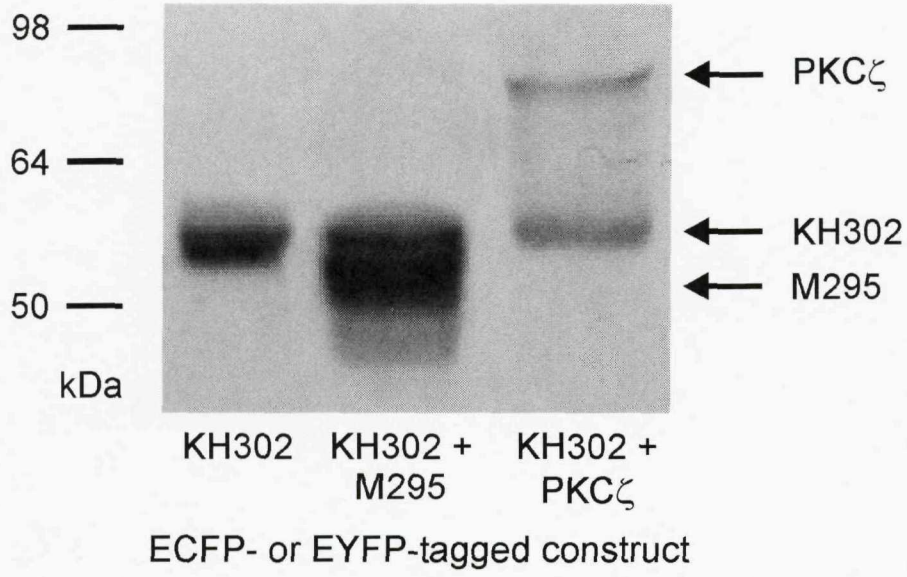

Figure 4.2.4: Western blot showing expression of EYFP-tagged KH302 with/without the co-expression of ECFP-tagged M295 or PKCζ

CHO cells were transiently transfected with EYFP-tagged KH302 (control) or EYFP-tagged KH302 plus ECFP-tagged M295 or PKCζ. Cells extracts were prepared using Tris-SDS buffer. Proteins were separated by SDS-PAGE, transferred to a nitrocellulose membrane then probed with anti-GFP primary antibody (SySy, Germany) to detect the ECFP/EYFP-tagged proteins.

It was then investigated to see whether these changes in diffusion coefficient of 80K-H were directly linked to the ability of 80K-H to bind to PKCζ. Therefore, the experiments were repeated using a non-interacting mutant of 80K-H, KH378. KH378 has previously been shown by co-immunoprecipitation [Hodgkinson et al., 2005a] and GST pull-down assays (see section 4.1 of this thesis) to be able to bind to munc18c, but is unable to bind PKCζ. The average diffusion coefficient for EYFP-tagged KH378 prior to insulin treatment was

514 ± 24 μs and 604 ± 65 μs after insulin stimulation (Figure 4.2.5, Table 4.2.5). This showed that although KH378 had a faster diffusion coefficient than KH302, insulin had no effect on its diffusion coefficient when no other additional proteins were over-expressed.

It was then investigated to see if the co-expression of munc18c or PKCζ had an effect on the diffusion coefficient of KH378. CHO cells were transfected with EYFP-tagged KH378 and ECFP-tagged M295 or PKCζ. In both the basal and insulin stimulated states, the presence of PKCζ had no effect on the diffusion coefficient of the EYFP-tagged KH378 (514 ± 24 μs for pre-insulin and 604 ± 65 μs for post-insulin stimulation when KH378 was expressed alone, compared to 446 ± 56 μs for pre-insulin and 471 ± 77 μs for post-insulin stimulation when PKCζ was co-expressed. Figure 4.2.5, Table 4.2.5).This indicates that the diffusion coefficient of KH378 was not affected by the presence of PKCζ before or after insulin stimulation.

As seen with the co-expression of PKCζ and KH378, the co-expression of M295 with KH378 caused no change in the KH378 diffusion coefficient in response to insulin stimulation. However, both the pre- and post-insulin diffusion coefficients were greater when M295 was co-expressed than when KH378 was expressed alone (935 ± 59 pre-insulin and 902 ± 55 post-insulin, when KH378 and M295 were over expressed. Figure 4.2.5, Table 4.2.5).

Construct(s) overexpressed		Diffusion coefficient (μs) Mean ± SEM	
EYFP	ECFP	- insulin	+ insulin
KH378	-	514 ± 24	604 ± 65
KH378	M295	935 ± 59	902 ± 55
KH378	PKCζ	446 ± 56	471 ± 77

Table 4.2.5: Diffusion coefficients for KH378

CHO cells were transiently transfected with EYFP-tagged KH378 (control) or EYFP-tagged KH378 plus ECFP-tagged M295 or PKCζ. Cells were serum starved for 24 hours prior to data collection. Where appropriate, cells were stimulated with 10^{-7} M insulin for 20 minutes. FCS data was collected for the EYFP-tagged protein only and are shown as the mean ± s.e.m. from 3 individual experiments, each using 6 separate cells.

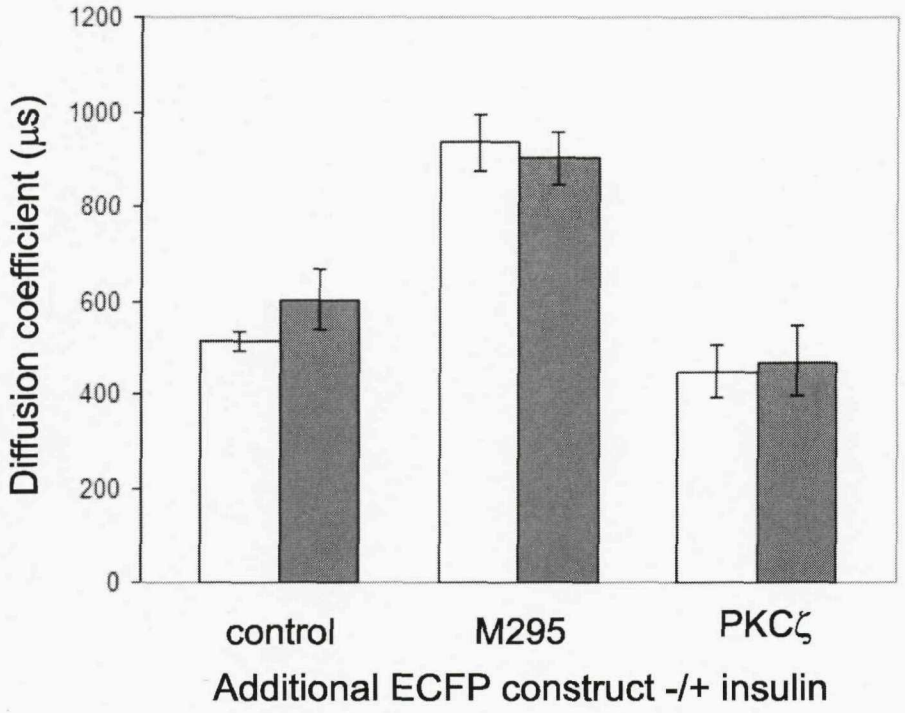

Figure 4.2.5: Diffusion coefficients for KH378

CHO cells were transiently transfected with EYFP-tagged KH378 (control) or EYFP-tagged KH378 plus ECFP-tagged M295 or PKCζ. Cells were serum starved for 24 hours prior to data collection. Where appropriate, cells were stimulated with 10^{-7} M insulin for 20 minutes. FCS data was collected for the EYFP-tagged protein only and are shown as the mean ± s.e.m. from 3 individual experiments, each using 6 separate cells.

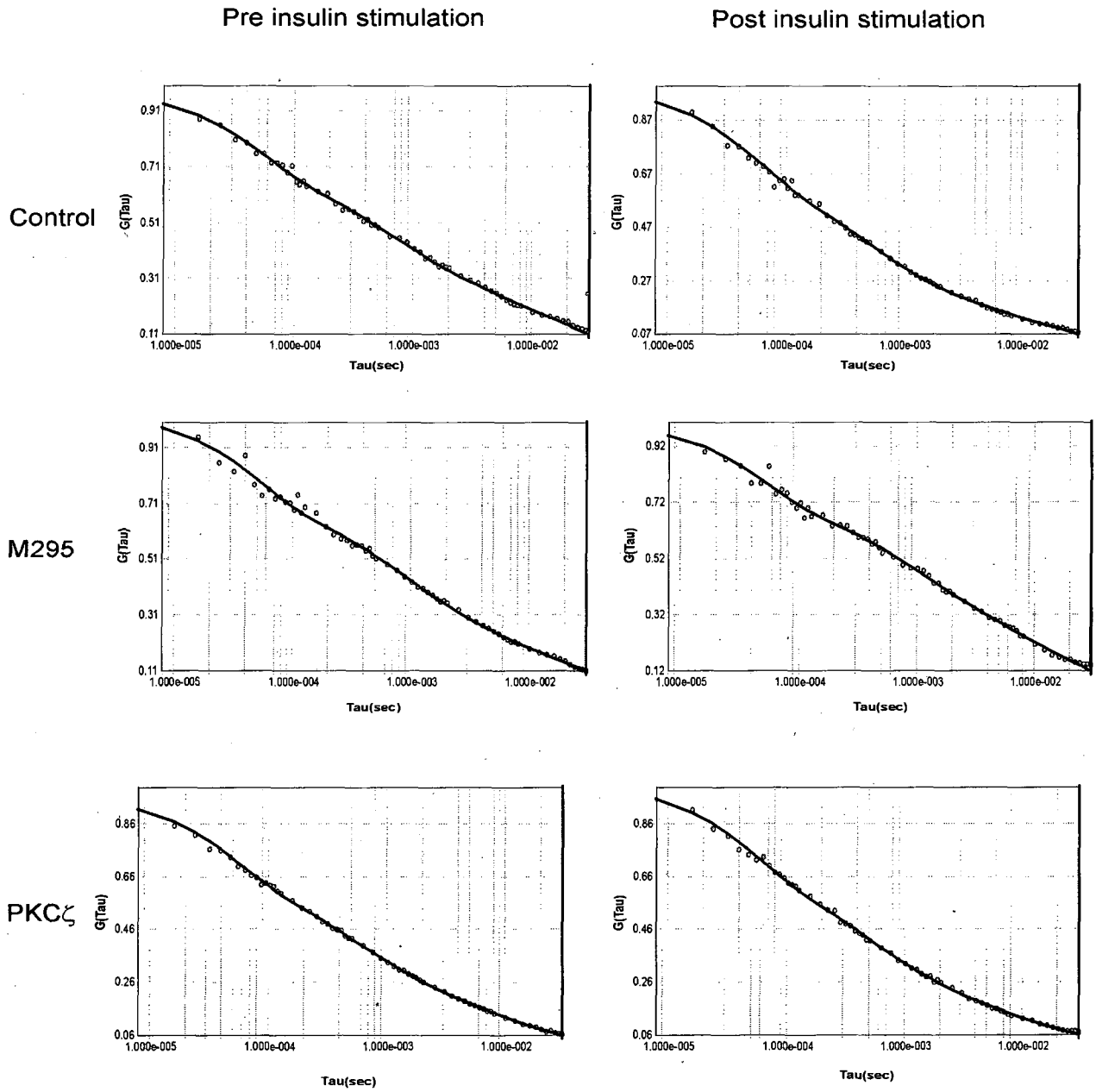

Figure 4.2.6: Example FCS traces for EYFP-tagged KH378

CHO cells were transiently transfected with EYFP-tagged KH378 (control) or EYFP-tagged KH378 plus ECFP-tagged M295 or PKCζ. Cells were serum starved for 24 hours prior to data collection. Where appropriate, cells were stimulated with 10^{-7} M insulin for 20 minutes. FCS data was collected for the EYFP-tagged protein only.

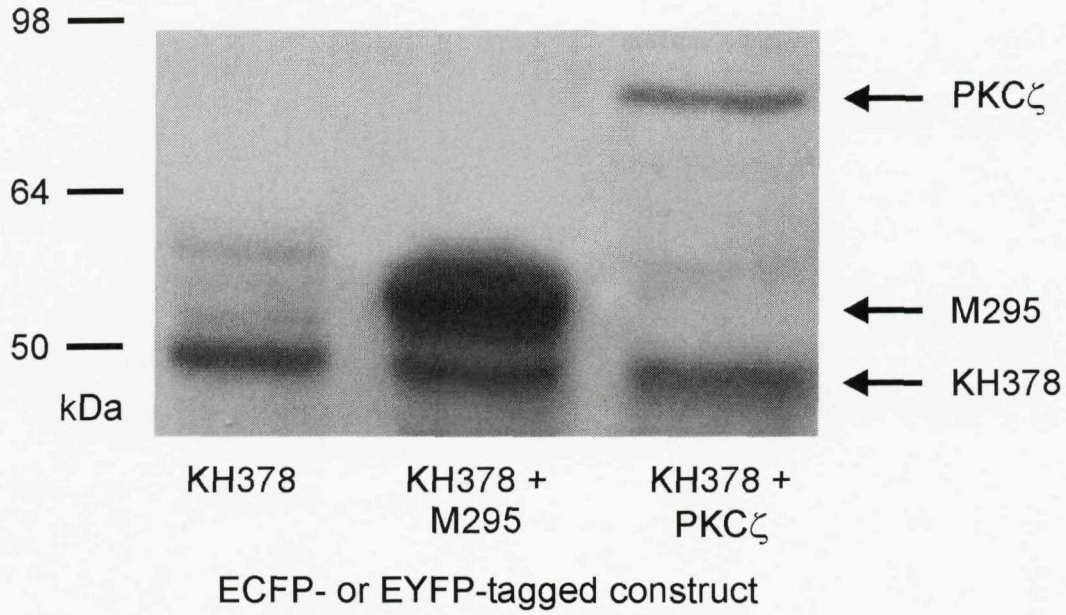

Figure 4.2.7: Western blot showing expression of EYFP-tagged KH378 with/without the co-expression of ECFP-tagged M295 or PKCζ

CHO cells were transiently transfected with EYFP-tagged KH378 (control) or EYFP-tagged KH378 plus ECFP-tagged M295 or PKCζ. Cells extracts were prepared using Tris-SDS buffer. Proteins were separated by SDS-PAGE, transferred to a nitrocellulose membrane then probed with anti-GFP primary antibody (SySy, Germany) to detect the ECFP/EYFP-tagged proteins.

4.2.2.2 Munc18c

The diffusion coefficient of munc18c was then investigated and whether this was affected by insulin stimulation or the presence of PKCζ or 80K-H. Three different EYFP-tagged munc18c constructs were used: full length munc18c (MFL), and two truncations M295 (binds to 80K-H and PKCζ) and M338 (binds to 80K-H but does not bind PKCζ).

The diffusion coefficient of full length munc18c when expressed alone as an EYFP fusion protein prior to insulin stimulation was 485 ± 36 μs compared to 611 ± 37 μs after insulin stimulation (mean ± s.e.m.). This increase was not statistically significant indicating that insulin had no effect on the diffusion coefficient of munc18c when no additional proteins where co-expressed (Figure 4.2.8, Table 4.2.6).

I next wanted to explore whether co-expression of 80K-H or PKCζ had any effect on the diffusion coefficient of full length munc18c. For this, CHO cells were transfected with EYFP-tagged munc18c (MFL) and the ECFP-tagged 80K-H truncation construct (KH302) or PKCζ. In the basal state, the presence of KH302 caused MFL to spend a far greater time in the observation volume (with a diffusion coefficient of 879 ± 32 μs) indicating that the presence of 80K-H was causing munc18c to slow down in the basal state. Insulin stimulation caused the diffusion coefficient of MFL to decrease to 497 ± 50 μs, indicating a faster complex (Figure 4.2.8, Table 4.2.6). However, co-expression of ECFP-tagged PKCζ had no statistically relevant effect on the diffusion co-efficient of MFL.

Construct(s) overexpressed		Diffusion coefficient (μs) Mean ± s.e.m.	
EYFP	ECFP	- insulin	+ insulin
MFL	-	485 ± 36	611 ± 37
MFL	KH302	879 ± 32	497 ± 50
MFL	PKCζ	654 ± 44	501 ± 39

Table 4.2.6: Diffusion coefficients for MFL

Cho cells were transiently transfected with EYFP-tagged MFL (control) or EYFP-tagged MFL plus ECFP-tagged KH302 or PKCζ. Cells were serum starved for 24 hours prior to data collection. Where appropriate, cells were stimulated with 10^{-7} M insulin for 20 minutes. FCS data was collected for the EYFP-tagged protein only and are shown as the mean ± s.e.m. from 3 individual experiments, each using 6 separate cells.

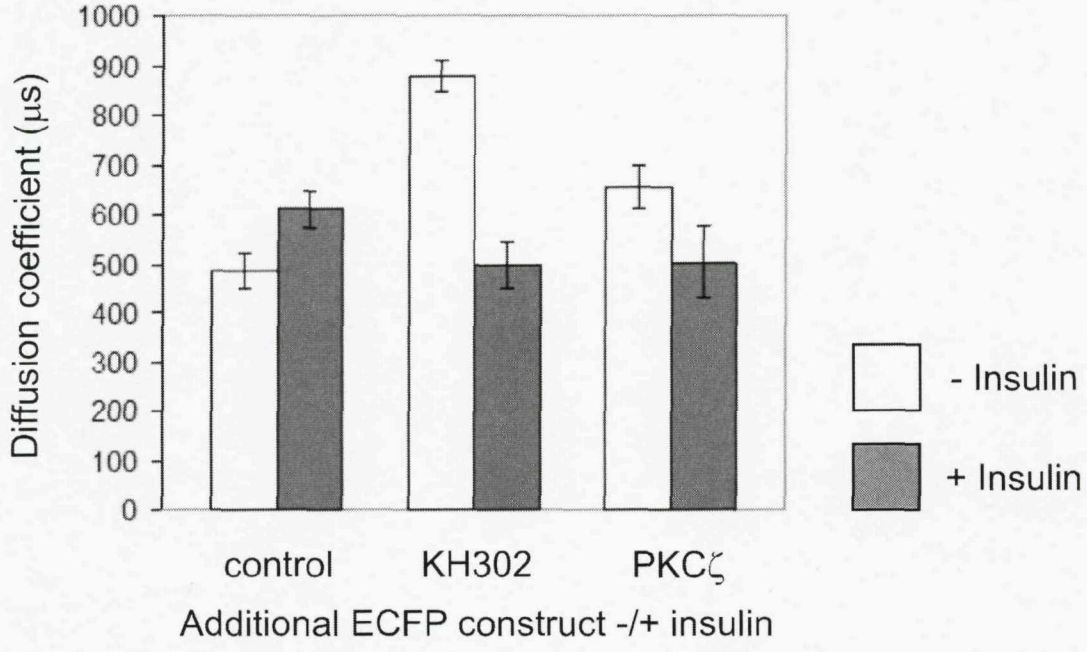

Figure 4.2.8: Diffusion coefficients for MFL

CHO cells were transiently transfected with EYFP-tagged MFL (control) or EYFP-tagged MFL plus ECFP-tagged KH302 or PKCζ. Cells were serum starved for 24 hours prior to data collection. Where appropriate, cells were stimulated with 10^{-7} M insulin for 20 minutes. FCS data was collected for the EYFP-tagged protein only and are shown as the mean ± s.e.m. from 3 individual experiments, each using 6 separate cells.

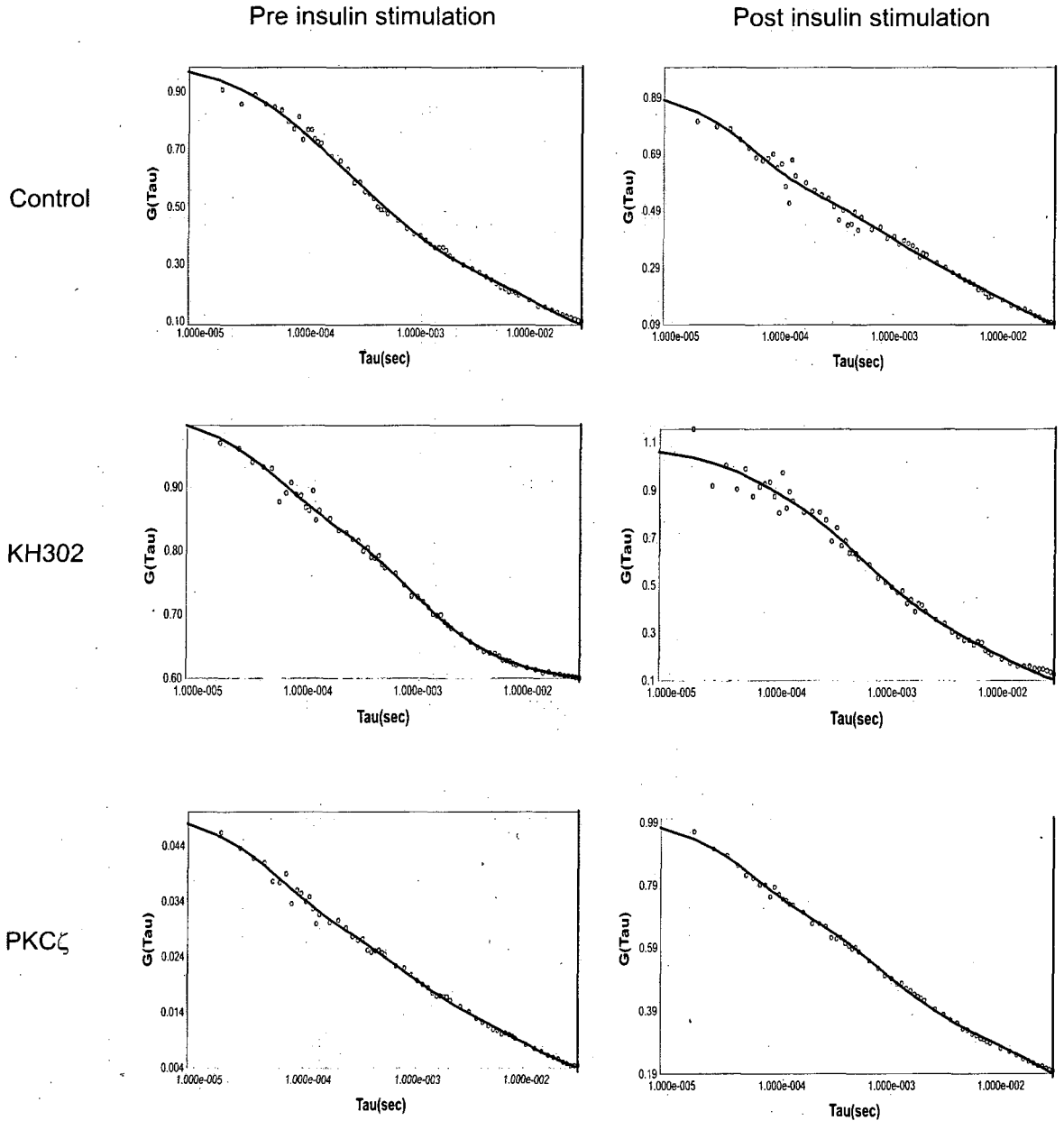

Figure 4.2.9: Example FCS traces for EYFP-tagged MFL

Cho cells were transiently transfected with EYFP-tagged MFL (control) or EYFP-tagged MFL plus ECFP-tagged KH302 or PKCζ. Cells were serum starved for 24 hours prior to data collection. Where appropriate, cells were stimulated with 10^{-7} M insulin for 20 minutes. FCS data was collected for the EYFP-tagged protein only.

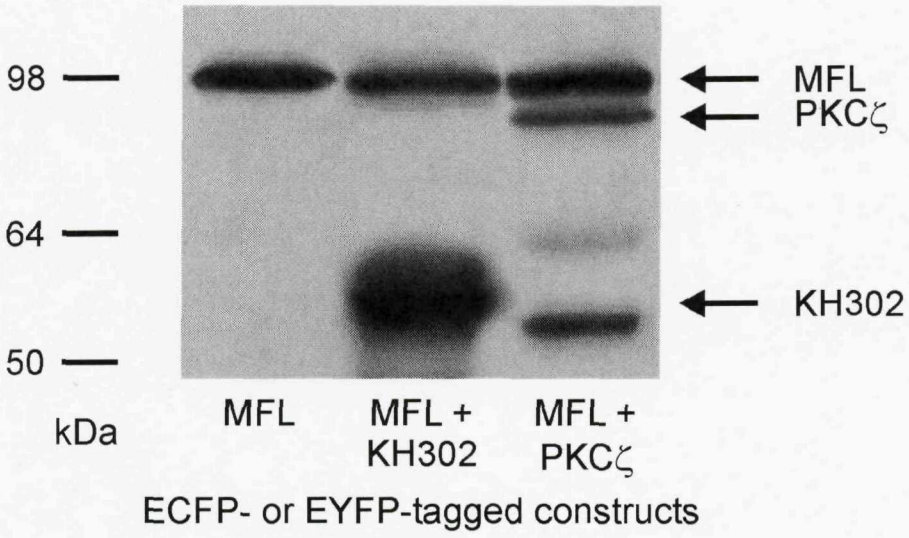

Figure 4.2.10: Western blot showing expression of EYFP-tagged MFL with/without the co-expression of ECFP-tagged KH302 or PKCζ

CHO cells were transiently transfected with EYFP-tagged MFL (control) or EYFP-tagged MFL plus ECFP-tagged KH302 or PKCζ. Cells extracts were prepared using Tris-SDS buffer. Proteins were separated by SDS-PAGE, transferred to a nitrocellulose membrane then probed with anti-GFP primary antibody (SySy, Germany) to detect the ECFP/EYFP-tagged proteins.

The study was extended by investigating the munc18c truncation construct M295. This truncated construct acts in a similar fashion to full length munc18c and binds to both PKCζ and 80K-H (Hodgkinson et al., 2005a). Firstly, M295 was expressed alone as an EYFP fusion protein. The average diffusion coefficient prior to insulin stimulation was 576 ± 61 μs and 500 ± 35 μs after insulin stimulation, showing that insulin no effect on the diffusion coefficient of M295 when no additional proteins were over-expressed (Figure 4.2.11, Table 4.2.7).

CHO cells were transfected with EYFP-tagged M295 and the ECFP-tagged 80K-H construct, KH302 or PKCζ. In the basal state, the presence of KH302 caused M295 to spend a far greater time in the observation volume (with a diffusion coefficient of 1003 ± 79 μs) indicating that the presence of 80K-H is causing M295 to slow down. Insulin stimulation caused the diffusion coefficient of M295 to decrease to 513 ± 72 μs indicating that M295 had sped up. Co-expression of ECFP-tagged PKCζ with the EYFP-tagged M295 did not affect the diffusion coefficient of M295 (Figure 4.2.11, Table 4.2.7).

Construct(s) overexpressed		Diffusion coefficient (μs) Mean ± s.e.m.	
EYFP	ECFP	- insulin	+ insulin
M295	-	576 ± 61	500 ± 35
M295	KH302	1003 ± 79	513 ± 72
M295	PKCζ	629 ± 51	552 ± 22

Table 4.2.7: Diffusion coefficients for M295

CHO cells were transiently transfected with EYFP-tagged M295 (control) or EYFP-tagged M295 plus ECFP-tagged KH302 or PKCζ. Cells were serum starved for 24 hours prior to data collection. Where appropriate, cells were stimulated with 10^{-7} M insulin for 20 minutes. FCS data was collected for the EYFP-tagged protein only and are shown as the mean ± s.e.m. from 3 individual experiments, each using 6 separate cells.

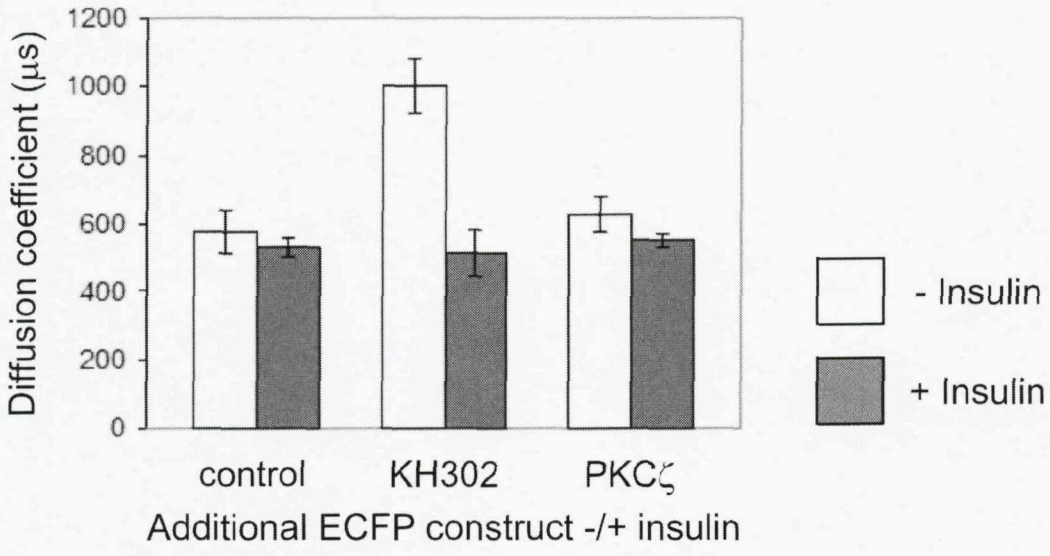

Figure 4.2.11: Diffusion coefficients for M295

CHO cells were transiently transfected with EYFP-tagged M295 (control) or EYFP-tagged M295 plus ECFP-tagged KH302 or PKCζ. Cells were serum starved for 24 hours prior to data collection. Where appropriate, cells were stimulated with 10^{-7} M insulin for 20 minutes. FCS data was collected for the EYFP-tagged protein only and are shown as the mean ± s.e.m. from 3 individual experiments, each using 6 separate cells.

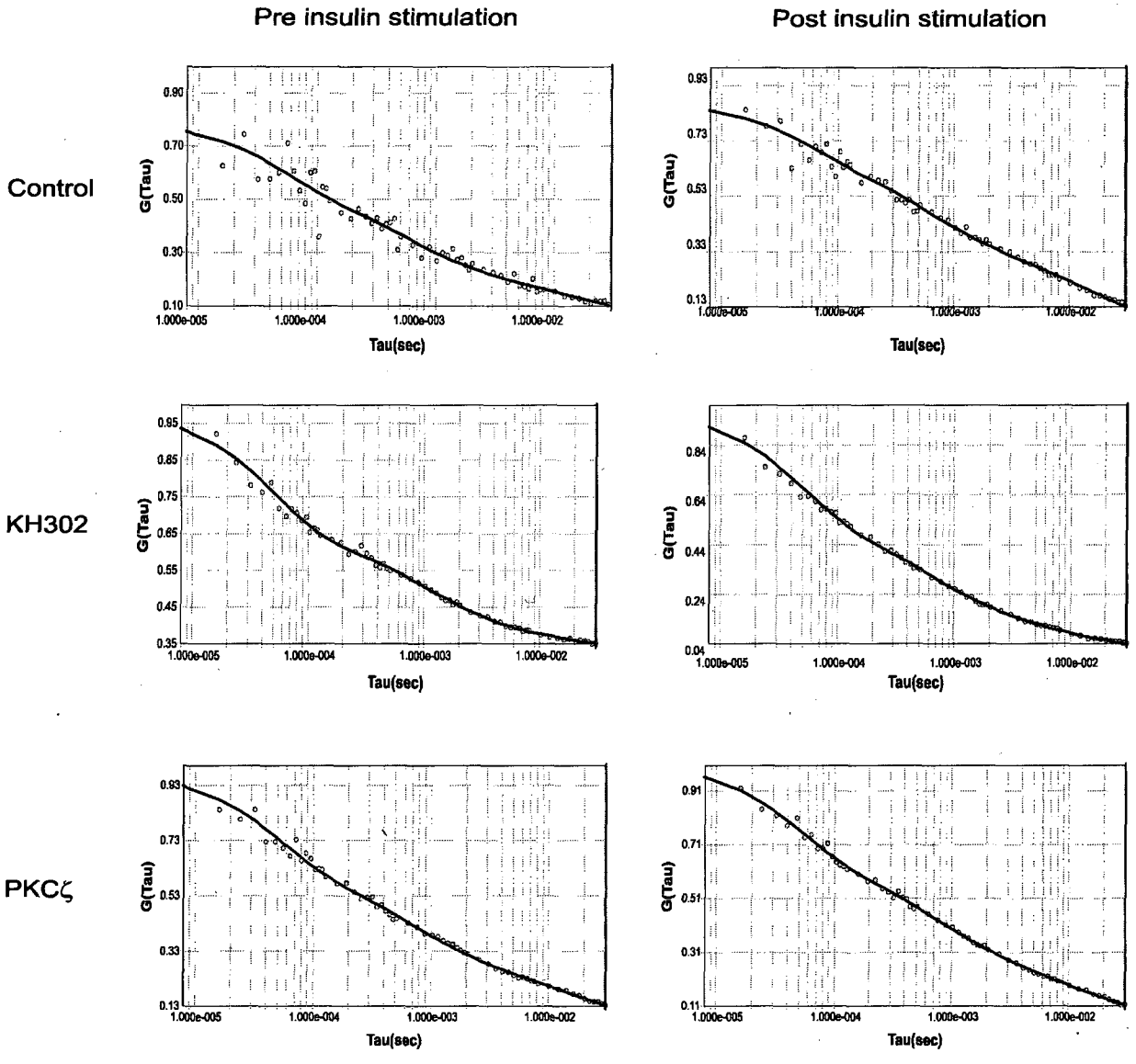

Figure 4.2.12: Example FCS traces for EYFP-tagged M295

CHO cells were transiently transfected with EYFP-tagged M295 (control) or EYFP-tagged M295 plus ECFP-tagged KH302 or PKCζ. Cells were serum starved for 24 hours prior to data collection. Where appropriate, cells were stimulated with 10^{-7} M insulin for 20 minutes. FCS data was collected for the EYFP-tagged protein only.

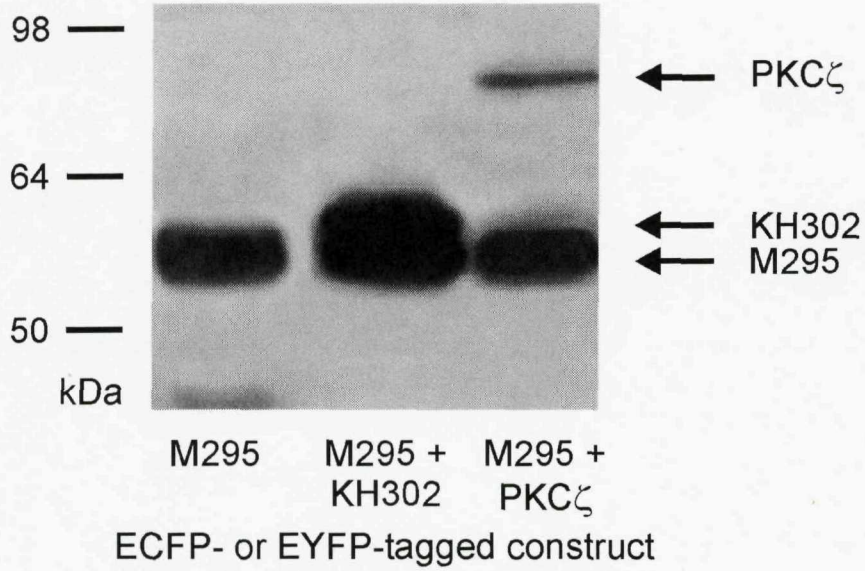

Figure 4.2.13: Western blot showing expression of EYFP-tagged M295 with/without the co-expression of ECFP-tagged KH302 or PKCζ

CHO cells were transiently transfected with EYFP-tagged M295 (control) or EYFP-tagged MFL plus ECFP-tagged KH302 or PKCζ. Cells extracts were prepared using Tris-SDS buffer. Proteins were separated by SDS-PAGE, transferred to a nitrocellulose membrane then probed with anti-GFP primary antibody (SySy, Germany) to detect the ECFP/EYFP-tagged proteins.

The above experiments were repeated using the munc18c truncation construct M338, which has previously been shown to be unable to interact with PKCζ (Hodgkinson et al., 2005a). Insulin had no effect on the diffusion co-efficient when the EYFP-tagged M338 construct was expressed alone or in combination with ECFP-tagged KH302 or PKCζ. Co-expression had did not alter the diffusion co-efficient of M338 (Figure 4.2.14, Table 4.2.8).

Construct(s) overexpressed		Diffusion coefficient (μs) Mean ± s.e.m.	
EYFP	ECFP	- insulin	+ insulin
M338	-	716 ± 170	865 ± 15
M338	KH302	882 ± 86	903 ± 49
M338	PKCζ	677 ± 64	559 ± 39

Table 4.2.8. Diffusion coefficients for M338

CHO cells were transiently transfected with EYFP-tagged M338 (control) or EYFP-tagged M338 plus ECFP-tagged KH302 or PKCζ. Cells were serum starved for 24 hours prior to data collection. Where appropriate, cells were stimulated with 10^{-7} M insulin for 20 minutes. FCS data was collected for the EYFP-tagged protein only and are shown as the mean ± s.e.m. from 3 individual experiments, each using 6 separate cells.

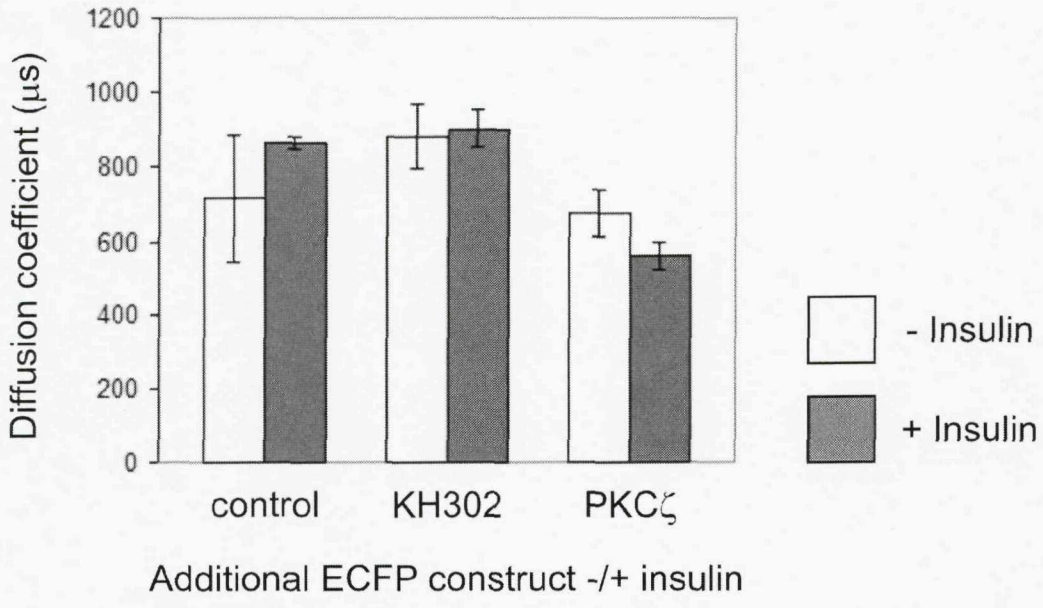

Figure 4.2.14: Diffusion coefficients for M338

CHO cells were transiently transfected with EYFP-tagged M338 (control) or EYFP-tagged M338 plus ECFP-tagged KH302 or PKCζ. Cells were serum starved for 24 hours prior to data collection. Where appropriate, cells were stimulated with 10^{-7} M insulin for 20 minutes. FCS data was collected for the EYFP-tagged protein only and are shown as the mean ± s.e.m. from 3 individual experiments, each using 6 separate cells.

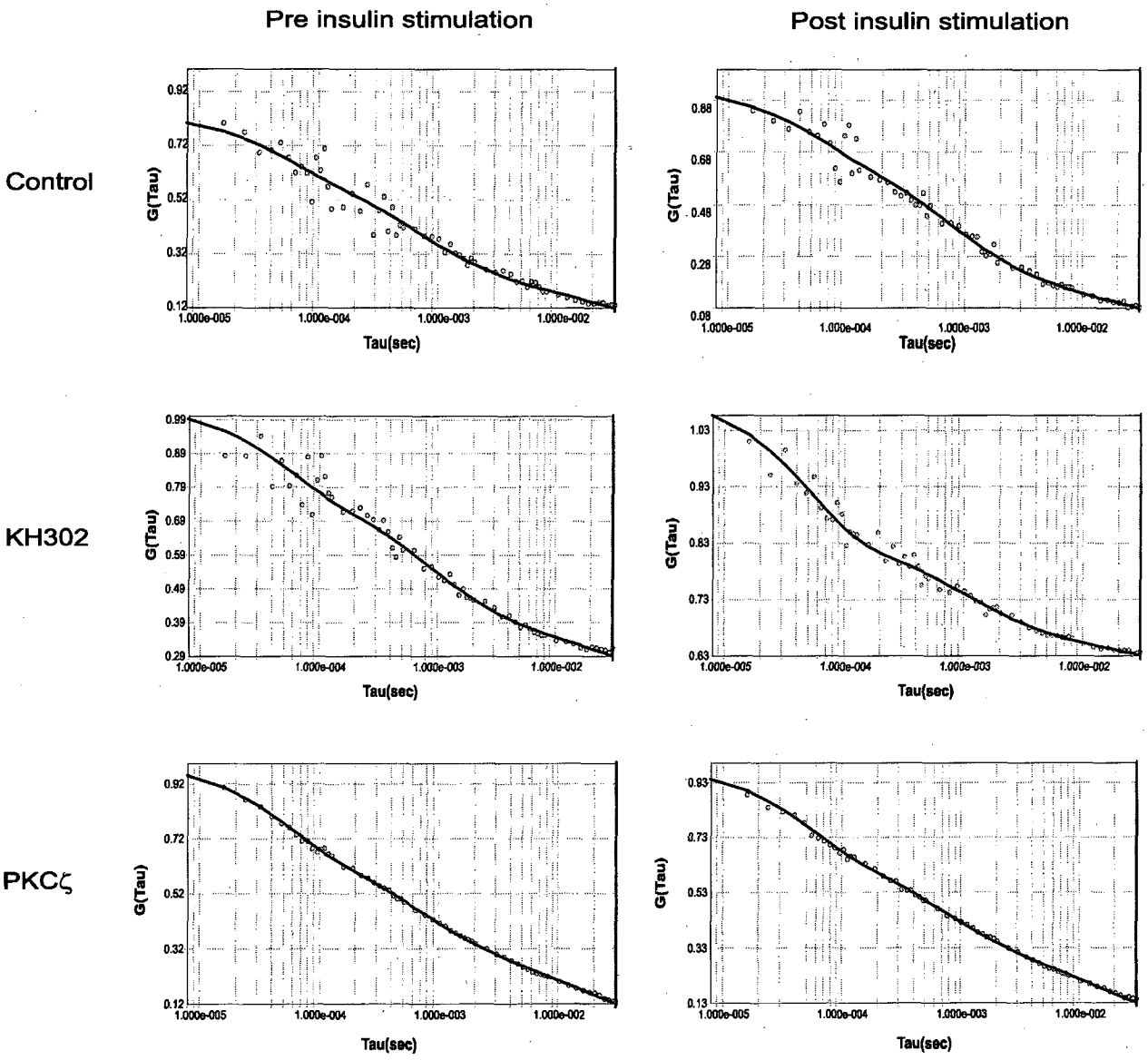

Figure 4.2.15: Example FCS traces for EYFP-tagged M338

CHO cells were transiently transfected with EYFP-tagged M338 (control) or EYFP-tagged M338 plus ECFP-tagged KH302 or PKCζ. Cells were serum starved for 24 hours prior to data collection. Where appropriate, cells were stimulated with 10^{-7} M insulin for 20 minutes. FCS data was collected for the EYFP-tagged protein only.

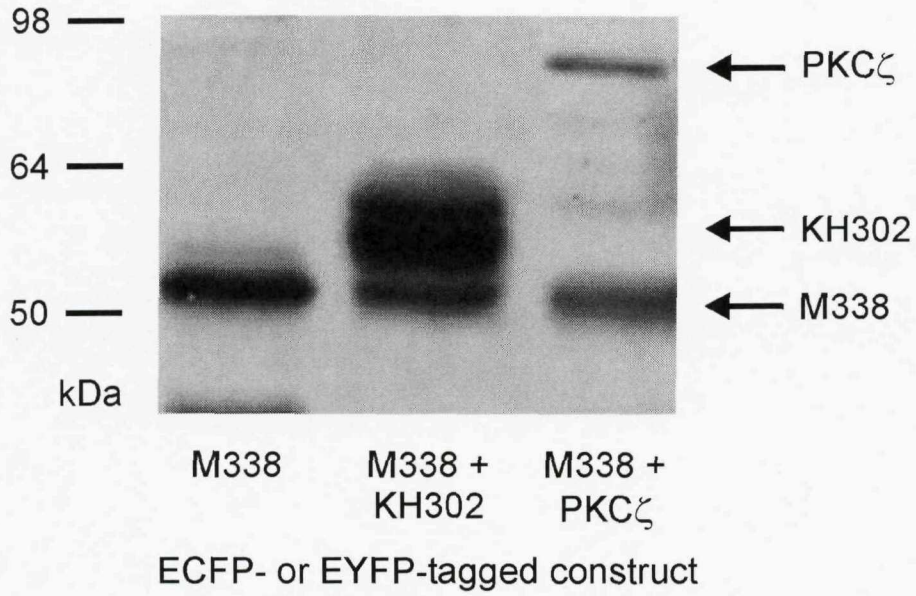

Figure 4.2.16: Western blot showing expression of EYFP-tagged M338 with/without the co-expression of ECFP-tagged KH302 or PKCζ

CHO cells were transiently transfected with EYFP-tagged M338 (control) or EYFP-tagged M338 plus ECFP-tagged KH302 or PKCζ. Cells extracts were prepared using Tris-SDS buffer. Proteins were separated by SDS-PAGE, transferred to a nitrocellulose membrane then probed with anti-GFP primary antibody (SySy, Germany) to detect the ECFP/EYFP-tagged proteins.

4.2.3. Discussion

4.2.3.1. Overview

One of the most fundamental of insulin's actions is to regulate glucose homeostasis. Insulin causes this by inducing a rapid increase in glucose uptake in muscle and fat cells, primarily by stimulating the translocation of the GLUT4 glucose transporter from intracellular vesicle stores to the cell surface. Insulin binds to its receptor which activates numerous signalling cascades, ultimately leading to the targeting of the GLUT4 containing vesicles to specific docking sites at the plasma membrane. PKCζ has been postulated to be one kinase activated by these signalling pathways that is required for the translocation of the GLUT4 vesicles [Bandyopadhyay et al., 1999; Kanzaki et al., 2004; Sajan et al., 2006; Tsuru et al., 2002, Zhou et al., 2004].

GLUT4 vesicle trafficking is similar to that seen in synaptic vesicles. The GLUT4 vesicle contains the v-SNARE VAMP2 which binds to its cognate t-SNARE receptor Syntaxin4 in the plasma membrane [Chang et al., 2004; Kanda et al., 2005; Kawanishi et al., 2000; Rudich and Klip, 2003]. Insulin regulates VAMP2:Syntaxin4 binding by virtue of accessory proteins, the most important of which is munc18c. In the basal state, munc18c binds to syntaxin4 with high affinity, acting as a clamp over syntaxin4. This prevents VAMP2 from binding to syntaxin4 and hence inhibits GLUT4 vesicle docking at the plasma membrane [Chang et al., 2004; Kanda et al., 2005; Tamori et al., 1998; Thurmond et al., 1998]. Insulin stimulation decreases the binding of munc18c to syntaxin4, thus enabling the GLUT4 vesicle to dock at the plasma membrane via an interaction between VAMP2 and syntaxin4 [Tellam et al., 1997]. How the clamping mechanism of munc18c is alleviated by insulin is as yet unknown. Although much research has been done on both the insulin signalling pathways and the GLUT4 vesicle trafficking machinery, it was only recently that 80K-H was proposed to link the two together via PKCζ and munc18c [Hodgkinson et al., 2005a]. 80K-H is involved in glucose regulation [Li et al., 1996; Thornalley, 1998] and is closely related to VASAP-60, a protein known to be involved in vesicle trafficking [Brule, 2000].

Our previous studies showed that insulin triggered the formation of a PKCζ:80K-H: munc18c complex in vitro. Previous results showed that over expression of KH302 mimicked the effect of insulin, causing a substantial increase in glucose transport in both the basal and insulin stimulated states. The effect seen was far greater when KH378 was over expressed.

Although it was known that these proteins interacted *in vitro*, the exact nature or role of these protein:protein interactions *in vivo* remained unknown. To continue and extend the previous work conducted in our laboratories, fluorescence correlation spectroscopy (FCS) was employed in living cells to elucidate the mechanics of the GLUT4 vesicle trafficking apparatus and to further define the roles of munc18c, PKCζ and 80K-H in this process. The use of FCS with the interacting and non-interacting constructs, along with the results from previous investigations, has enabled the piecing together of a hypothetical model for the insulin-mediated translocation and docking of GLUT4 to the plasma membrane.

The use of the fluorescently-tagged vectors and fluorescence microscopy has enabled the study of the proteins of interest *in vivo* in living cells. This provides insight into the exact nature of the proteins in their natural cellular environment. Fluorescence correlation spectroscopy (FCS) is a highly sophisticated technique. Although it is rapidly growing in popularity, there are few reports of it being employed for studies in living cells. An offshoot of FCS is Fluorescence cross correlation spectroscopy (FCCS). This employs the use of two spectrally distinct fluorescent tags to label two different species. The autocorrelation of each separate fluorescently-tagged particle is determined as per usual, but the fluorescence fluctuations of each tag are also correlated *with each other.* If the differently labelled particles are bound to each other, then they will move through the observation volume in a similar way, with identical fluctuations in fluorescence. This synchronization of the fluorescence fluctuations in the two colour channels gives a positive cross correlation reading, thus implying that the two species are bound to each other. If there is no binding of the two particles, then the fluctuations of the fluorescence of the two colours will be different and there will be no cross correlation. During the experiments performed in this thesis, we were unable to gain any data from the blue

channel (i.e. from the cfp-tagged proteins). This meant that data collection was only possible from one protein at a time (the yfp-tagged protein) making collection of cross correlation data impossible. Although this was highly disappointing, I was able to work around this problem and gain enough information from the data gathered in order to make significant conclusions. Despite not using the cfp-tagged proteins for FCS data collection, the blue fluorescent tag on these proteins gave the advantage of quick and easy verification of their expression. In addition, because all of the constructs were cloned into both the cfp- and yfp-tagged vectors, it was possible to compensate for the lack of cross correlation data by comparing yfp data for double transfections. Instead of measuring from both the blue and yellow channels at the same time to produce cross correlation data, the yfp diffusion coefficients for double transfections were compared. For example, cells were firstly transfected with yfp-tagged munc18c and cfp-tagged 80K-H, then transfected with yfp-tagged 80K-H and cfp-tagged munc18c. The diffusion coefficients for the yfp-tagged proteins were then compared. Performing the experiments in this way enabled comparison of the diffusion coefficients for the two proteins when expressed together, and allowing identification of any cross correlation.

4.2.3.2. 80K-H and munc18c are bound in both the basal and insulin-stimulated states

When the 80K-H construct KH302 was expressed alone, insulin had no effect on its speed. When the munc18c construct M295 was co-expressed, the basal speed of KH302 was unchanged to that seen when expressed alone. However, the action of insulin caused a substantial decrease in the KH302 diffusion coefficient. This shows that munc18c and insulin action causes 80K-H to speed up. There are two main possible explanations for this. One is that munc18c binds to 80K-H in the basal state and that insulin causes the release of 80K-H from munc18c, hence causing the increased speed of 80K-H. Another is that the addition of munc18c disrupts some sort of 80K-H tether or complex, thus freeing 80K-H and increasing its speed, but only when the cells are stimulated with insulin. The

data from the FCS experiments performed here, alongside the GST pull-down assays and co-immunoprecipitations performed previously, imply that the latter is the true explanation. Firstly, the speed of KH302 when M295 was co-expressed was identical to the speed of M295 when KH302 was co-expressed, both before and after insulin stimulation. This cross correlation of speeds of the 80K-H and munc18c constructs strongly suggests that they are bound in vivo in both the basal and insulin stimulated state. This is in accordance with the previous work in our laboratory. The previous work used co-immunoprecipitation experiments with endogenous proteins from CHO cells, 3T3-L1 adipocytes and L6 myotubes. These all showed an interaction between 80K-H and munc18c in the basal state which dramatically increased when the cells were first stimulated with insulin [Hodgkinson et al. 2005]. This cross-correlation of speeds and the co-immunoprecipitation studies rule out the possibility that insulin causes the release of munc18c from 80K-H. This, combined with the results showing that the speed of 80K-H increases in response to insulin when munc18c is also present suggests that 80K-H and munc18c are bound in both the basal and insulin stimulated states and that insulin enables munc18c to free 80K-H from some sort of slow moving tether. It is worth noting that addition of KH302 increases the diffusion co-efficient of M295 and full length munc18c, which further supports this hypothesis. These results suggest that in the basal state, munc18c and 80K-H are present in a slow-moving, large complex, the other components acting as a tether. However, when the cells are stimulated with insulin, munc18c and 80K-H dissociate together from this large tethering complex. This establishes a key interaction between 80K-H and munc18c that is crucial for an insulin-regulated event in living cells.

The FCS data strongly suggests that munc18c and 80K-H are bound in both the basal and insulin stimulated states, whereas the co-immunoprecipitations showed that there was little interaction between the two proteins prior to insulin stimulation. The most likely explanation for this is that the interaction between the two proteins is weak in the basal state and that insulin increases the strength of this association. It is possible that the Kd value for the munc18c:80K-H interaction in the basal state is below the threshold for detection by co-immunoprecipitations (typically ~1μM) and that the Kd value increases

dramatically upon insulin stimulation allowing its recognition in the co-immunoprecipitation experiments. Even if binding does occur, if the strength of the interaction is weak enough, the washes performed in an in vitro experiment such as co-immunoprecipitations could be enough to disrupt such an interaction, therefore washing off the bound protein. This would therefore make it appear that insulin causes an increase in association between munc18c and 80K-H with the in vitro experiments performed. In vivo experimental techniques such as FCS however, are sensitive enough to detect binding between two proteins no matter how low the Kd value. The increase in association between munc18c and 80K-H seen in these experiments in response to insulin will be discussed in more detail later.

4.2.3.3. PKCζ releases 80K-H from its tether in response to insulin

One obvious question is how munc18c and 80K-H dissociate from this large tether in response to insulin. As stated above, when KH302 was expressed alone, insulin had no effect on its speed. When PKCζ was co-expressed with KH302, insulin caused an increase in diffusion co-efficient of KH302 (meaning that KH302 had slowed down). This suggests that insulin stimulation causes the formation of an 80K-H: PKCζ complex. This is in accordance with the previous co-immunoprecipitation studies in our laboratory. The previous work used co-immunoprecipitation experiments with endogenous proteins from CHO cells, 3T3-L1 adipocytes and L6 myotubules which all showed little/no association between 80K-H and PKCζ in the basal state, but significant association between the proteins when the cells were first stimulated with insulin [Hodgkinson et al. 2005]. The increase in diffusion coefficient for 80K-H in response to insulin was not seen when KH378, an 80K-H construct unable to bind PKCζ was used, which further proves that it was the interaction between 80K-H and PKCζ that was causing this effect.

It is intriguing that co-expression of PKCζ with KH302 reduced the diffusion co-efficient of KH302 substantially in the basal state compared to when KH302 was expressed alone. It is unlikely that PKCζ was just substituting itself for the large tethering

complex described above, as it was previously shown *in vitro* that there was no association between endogenous PKCζ and 80K-H in the basal state [Hodgkinson et al. 2005a]. When PKCζ is over-expressed, it is constitutively active [Hodgkinson et al. 20002]. It is unknown from this data whether it was active PKCζ that was dissociating 80K-H from its tether per se or whether proteins bound to active PKCζ were responsible. Insulin increased the diffusion coefficient of KH302 when PKCζ was co-expressed (showing that KH302 was moving more slowly). Seeing as PKCζ is constitutively active, this shows that it is not just PKCζ activity that is responsible for the changes seen in 80K-H speeds upon insulin stimulation. Insulin stimulation of some other protein (i.e. munc18c) must be required.

When these experiments were repeated using KH378, an 80K-H construct unable to bind PKCζ, insulin failed to increase its speed when M295 was co-expressed. This means that an interaction between PKCζ and 80K-H is required in order for munc18c to release 80K-H from its tether in response to insulin.

4.2.3.4. PKCζ does not directly interact with munc18c

The co-expression of PKCζ had little effect on the speed of either M295 or munc18c full length protein *in vivo*, despite the ability of these proteins to co-precipitate with each other *in vitro* (as shown by GST pull down assays in Section 4.1.3.2 of this thesis and by co-immunoprecipitations previously conducted in our laboratory [Hodgkinson et al. 2005b]). However, expression of PKCζ did have an effect on the speed of the 80K-H constructs. This suggests that the interaction between munc18c and PKCζ is not a direct one, but instead occurs via a bridging protein. One obvious candidate for this bridge is 80K-H. The co-expression of PKCζ had a far greater impact on the speed of KH302 than it did on the munc18c constructs, which suggests that PKCζ has a greater bearing on 80K-H than it does on munc18c. This suggests that PKCζ only interacts with munc18c via an interaction with 80K-H rather than through a direct interaction. This implies that PKCζ, 80K-H and munc18c come together in a triplex formation, in a PKCζ:80K-H:munc18c

orientation. This is in accordance with previous findings in our laboratory [Hodgkinson et al. 2005 a and b], as well as the previous findings in this thesis (See Section 4.1.2.2. and Section 4.1.4). The GST pull-down assays performed in the above mentioned sections showed that the addition of PKCζ had no effect on the interaction between munc18c and 80K-H. They suggested that the three proteins come together in a non-competitive complex with the protein in the middle preventing a direct interaction between the two proteins at either end. The results from the FCS experiments performed in this section of my thesis support and develop the conclusions made from the GST pull-down assays. In accordance with the GST pull-down assays, the FCS data implies that 80K-H, PKCζ and munc18c come together in a triplex formation in response to insulin, with 80K-H preventing a direct interaction from occurring between PKCζ and munc18c. The interaction between PKCζ and munc18c would have been revealed by the GST pull-down assays despite the interaction not being a direct one.

4.2.3.5. The changes bought about by insulin stimulation are critically dependent on the interaction between PKCζ and 80K-H

Previous work in our laboratory using co-immunoprecipitations showed that the 80K-H construct, KH378, did interact with munc18c [Hodgkinson et al. (2005) unpublished data]. However, work conducted as part of this thesis using GST pull-down assays, showed there to be no interaction between KH378 and munc18c (Section 4.1.2.1., Figure 4.1.3.). The FCS data obtained in this section of my thesis agrees with the co-immunoprecipitation results and suggests that KH378 is indeed capable of binding to munc18c. As is shown in Figure 4.2.5, the diffusion coefficients for KH378 are not affected by insulin or the presence of PKCζ (further implying that KH378 is unable to bind to PKCζ). However, when the munc18c construct M295 was co-expressed with KH378, the diffusion coefficient for KH378 was dramatically increased. This would suggest that munc18c has an affect/binds to KH378. Unfortunately, I do not have data for EYFP-tagged M295 when ECFP-tagged

KH378 was co-expressed, meaning that I cannot compare the speeds of these two proteins when each other are co-expressed. However, the speed of KH378 when M295 was co-expressed was 935 ± 59 μs. This is analogous to that of M295 when co-expressed with the similar 80K-H construct, KH302, which is able to bind to M295 (1003 ± 79 μs). Although this is not an ideal comparison, it does further imply that KH378 is capable of binding to munc18c. The only data that implies that these two proteins do not interact are the GST pull-down assays undertaken in this thesis.

There are a couple of explanations for the discrepancies between the FCS and co-immunoprecipitaion data and the results obtained from the GST pull-down assays. The GST pull-down assays show that most binding to munc18c is lost between residues 353-378 of 80K-H (see section 4.1.2.1.4, figure 4.1.7). It is possible that the binding of 80K-H to munc18c is dependent upon 2 areas of 80K-H; one is between residues 302-353 (as 353 is where binding to munc18c seems to cease,) the other is due to post-translational modifications of the N-terminus of 80K-H past residue 353. This would mean that when KH378 is expressed in mammalian cells, although there are not the contacts with the 302-353 region, there are still the contacts with the modified 353-onwards region (as there would be the correct mammalian-produced post-translational modifications of the 80K-H molecule in place). However, when 80K-H is expressed in bacteria, truncating it down to residue 378 would mean that there is not the post-translational modifications of the 353-onwards region AND there is no 302-353 binding region. This would mean that the bacterially produced KH378 protein cannot bind with munc18c, despite mammalian KH378 actually being able to bind and would explain the GST pull-down assay results contradicting the results from mammalian cells. Another possibility is that the GST tag somehow interferes with the binding of KH378 to munc18c, but that the Xpress tag used in the co-immunoprecipitations and the ECFP and EYFP tags used in the FCS experiments don't. The Xpress tag is only a mere 1.1 kDa, so it is conceivable that this would not interrupt binding when the larger GST moiety (32 kDa) does. However, the GST tag is a similar size to the ECFP/EYFP tags (32 kDa Vs ~25 kDa respectively) and I would think it unlikely that the GST tag can interrupt binding when the ECFP/EYFP tags do not. This, combined with the fact that the GST tag did not interrupt binding between

munc18c and the 80K-H construct KH302, would lead me to predict that the first explanation for the discrepancies in the results is more likely.

In conclusion, the data for the 80K-H construct KH378 demonstrates the importance of PKCζ in the changes brought about by insulin stimulation. As shown previously in Section 4.1.2.3 (Figure 4.1.6), KH302 interacts with PKCζ, but KH378 is unable to bind. The FCS results for the two 80K-H truncation constructs, KH302 and KH378, were very different, despite the minimal difference in size and protein sequence. Insulin had a dramatic effect on the speed of KH302 when it was co-expressed with munc18c or PKCζ. However, insulin had no effect on the speed of KH378 in any of the experiments performed. This demonstrates that the changes insulin induces on 80K-H are not merely due to munc18c, but are critically dependent on the interaction between PKCζ and 80K-H.

4.2.3.6. Conclusions: a model for the role of 80K-H, munc18c and PKCζ in insulin mediated GLUT4 vesicle trafficking

The results from this chapter of my thesis, along with results from the other chapters and work previously conducted in our laboratory has enabled the formation of a model for the role of 80K-H, munc18c and PKCζ in the mechanics of insulin mediated GLUT4 vesicle trafficking. Firstly, the cross correlation of the diffusion coefficients for munc18c and 80K-H when the other is co-expressed suggest that munc18c and 80K-H are bound in both the basal and insulin stimulated states and that insulin somehow causes an increase in the strength of this association. The FCS data suggests that the 80K-H:munc18c complex is "tethered" at the membrane by some other slow moving complex. Although possibilities for what this tether may be are not discussed here, they are investigated later in this thesis. The FCS data, in particular that for the 80K-H constructs, suggest that the changes induced by insulin are critically dependent upon PKCζ and that it is PKCζ that releases 80K-H from this slow moving tether in response to insulin.

Un-stimulated Cells

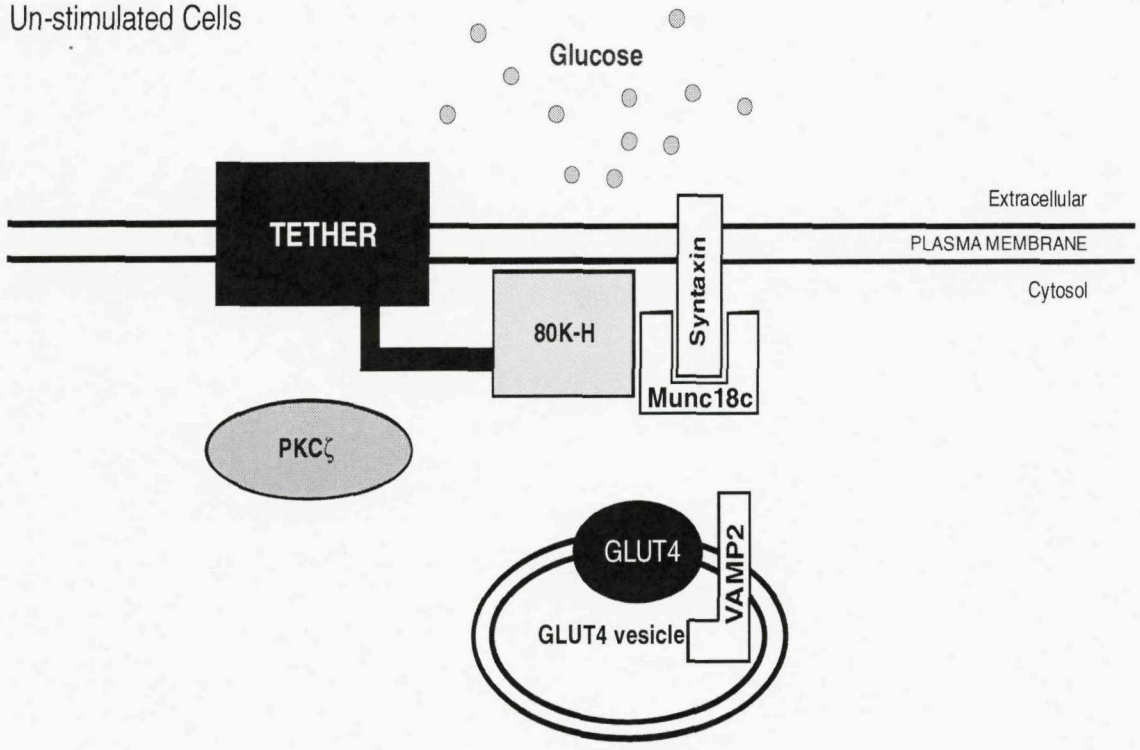

Insulin stimulated cells

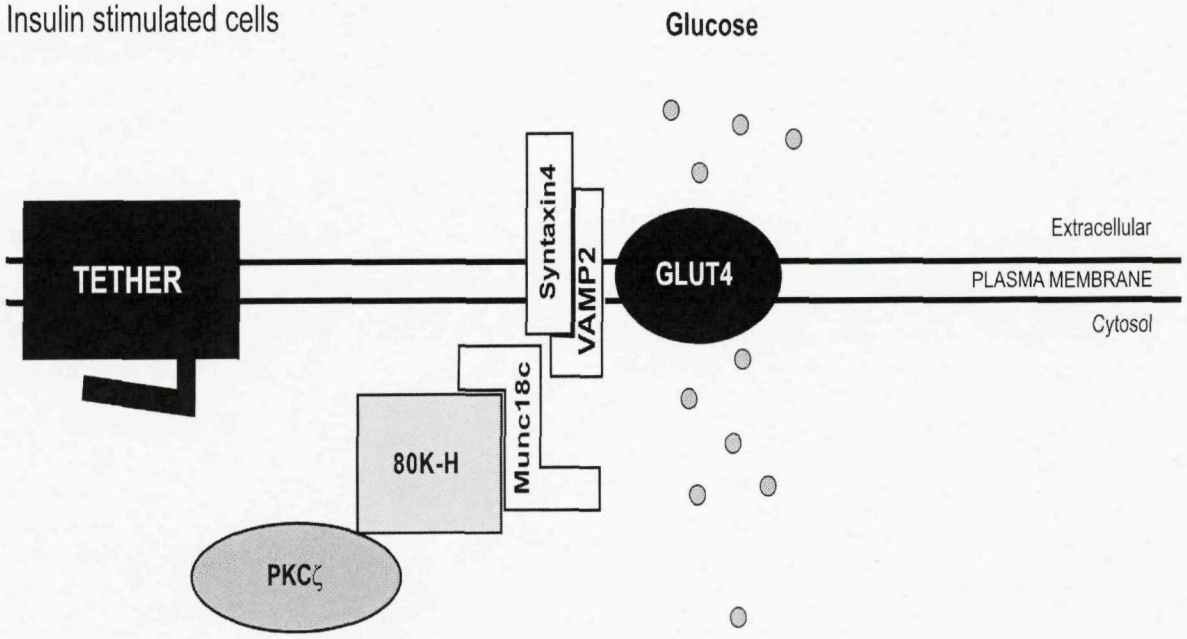

Figure 4.2.17: Proposed model for the role of 80K-H, munc18c and PKCζ in insulin mediated GLUT4 trafficking

In the basal state, PKCζ is inactive in the cytosol. 80K-H is bound to munc18c and is tethered at the membrane by an unknown protein complex. 80K-H positions munc18c onto syntaxin4, so that syntaxin4 is blocked and unable to bind VAMP2 in the GLUT4 vesicle. The GLUT4 vesicle is therefore unable to bind at the plasma membrane meaning that glucose cannot enter the cell.

Insulin stimulation activates PKCζ which is then able to bind 80K-H. PKCζ releases 80K-H from its membrane tether, which in turn increases the binding between 80K-H and munc18c. This releases the clamping action of munc18c on syntaxin4, enabling the VAMP2 protein in the GLUT4 vesicle to bind syntaxin4. The GLUT4 vesicle is then able to dock and fuse at the plasma membrane and glucose can enter the cell through the GLUT4 protein.

This model is consistent with the previous findings in our laboratory on the effect of 80K-H on glucose transport. These showed that expression of KH302 increased glucose transport and expression of KH378 further increased it. The speeds of KH378 when expressed alone were far faster than that of KH302. This would suggest that the region of 80K-H that lies between KH302 and KH378 is responsible for attaching it to its membrane tether. This is also the region of 80K-H required for binding to PKCζ (as has been shown in our laboratory's previous studies [Hodgkinson et al., 2005a] and this thesis, which further supports the hypothesis that insulin activation of PKCζ releases 80K-H from the membrane tether. Previous work in our laboratory showed that PKCζ did not directly phosphorylate 80K-H, ruling out the possibility that PKCζ phosphorylation of 80K-H (between residues 302-378) causes it to be released from its membrane tether. Other possibilities are a.) PKCζ binding to 80K-H disrupts the interaction between 80K-H and its membrane tether, b.) PKCζ phosphorylates the membrane tether in order to release it from 80K-H, or c.) Another protein associated with PKCζ is responsible for 80K-H's release. Interesting future experiments would be to investigate other interactors of PKCζ identified by the yeast-two-hybrid screen previously conducted in our laboratory. It would also be highly beneficial to conduct a yeast-two-hybrid screen on 80K-H and to see if any proteins are identified as interactors of both 80K-H and PKCζ.

Putting this information together suggests that the region of 80K-H responsible for interacting with PKCζ is also required for binding 80K-H to its large membrane tether, which has an inhibitory effect on glucose transport. Either removal of this tethering section of 80K-H (as occurs with expression of KH378) or insulin and PKCζ action, releases 80K-H from the tether and enables it to enhance glucose transport through GLUT4.

In conclusion I have formulated a hypothesis that explains how insulin affects 80K-H, munc18c and PKCζ interactions in order to induce GLUT4 vesicle trafficking and glucose transport. In the basal state, munc18c is clamped to syntaxin4. This means that

syntaxin4 is unable to bind to the VAMP2 protein of the GLUT4 vesicle, thereby preventing GLUT4 insertion into the plasma membrane. 80K-H is tethered at the membrane by a scaffolding complex and is also bound to munc18c. 80K-H and its tether are responsible for positioning munc18c in the correct orientation to prevent VAMP2 binding syntaxin4. PKCζ is inactive and is bound to neither munc18c nor 80K-H. Insulin causes the activation of PKCζ, which is then able to bind to 80K-H and release it from its membrane tether. Insulin action also increases the strength of association between 80K-H and munc18c. These insulin-induced changes in binding of 80K-H mean that it is free to move in the plane of the plasma membrane, enabling it to alleviate the clamping mechanism of munc18c on syntaxin4. This leaves syntaxin4 free to bind to VAMP2 so that the GLUT4 vesicle can dock and fuse with the membrane, allowing glucose to enter the cell.

4.3 Interactions between munc18c and syntaxin4

4.3 Interactions between munc18c and syntaxin4

4.3.1. Introduction

As has been described previously, GLUT4 vesicle exocytosis is similar to that seen in synaptic vesicles. The GLUT4 vesicle contains the v-SNARE, VAMP2, which binds to the t-SNAREs syntaxin4 and SNAP23 at the plasma membrane. It is this interaction which enables the GLUT4 vesicle to dock and fuse with the plasma membrane. Insulin is able to affect the interaction between these proteins and hence affect the ability of the GLUT4 vesicle to dock/fuse with the plasma membrane, by virtue of accessory proteins. One of the most important of these is munc18c. In the basal state, munc18c is bound to syntaxin4 and prevents it interacting with VAMP2. Insulin action relieves this inhibition, thus allowing an interaction to occur between syntaxin4 and VAMP2 and enabling the GLUT4 vesicle to dock and fuse with the plasma membrane.

It was at first believed that munc18c merely prevented an interaction from occurring between syntaxin4 and VAMP2. Various *in vitro* and *in vivo* studies showed that munc18c inhibited GLUT4 vesicle docking and/or fusion at the plasma membrane, apparently by preventing syntaxin4 from binding to VAMP2 [Macaulay et al. 2002, Thurmond et al. 1998, Tamori et al. 1998]. These observations led to the following hypothesis: In the absence of insulin, munc18c binds to syntaxin4 and holds it in its closed conformation, thus inhibiting GLUT4 vesicle docking/fusion at the plasma membrane. Upon insulin stimulation, munc18c dissociates from syntaxin4, allowing it to adopt the open conformation and enabling syntaxin4/VAMP2 interaction and GLUT4 vesicle docking/fusion [Tamori et al. 1998, Thurmond et. al. 1998, Macaulay et. al. 2002, Kanda et. al. 2005]

Although the above model is an attractive and well characterised one, it is almost certainly an over-simplistic depiction of the role of munc18c in insulin-mediated GLUT4 vesicle trafficking. Firstly, there is no evidence to support the theory that munc18c is

released from syntaxin4 in response to insulin. It is merely the most simple (and hence most popular) model for GLUT4 vesicle trafficking. Secondly, as more research has been done on munc18c and its interactions with syntaxin4, it appears that it plays a far more significant and positive role in GLUT4 vesicle docking and fusion than was first thought. Evidence suggests that although munc18c:syntaxin 4 interaction is not required for the insulin-stimulated trafficking to and association with the cell surface, the interaction between munc18c and syntaxin4 is required for the integration of the GLUT4 storage vesicles into the plasma membrane [Thurmond et al. 2000]. Various animal models have supported this theory. For example, heterozygous munc18c knockout mice (Munc18c$^{-/+}$) show significantly decreased insulin sensitivity in insulin tolerance tests and reduced insulin stimulated GLUT4 translocation compared to wild-type mice [Oh et al. 2005]. It is possible that munc18c positively regulates GLUT4 vesicle trafficking by accelerating the formation of the SNARE complex [Latham et al. 2006], which has found to be the case for other members of the SM family of proteins [Scott et al. 2004].

However, the role of munc18c in GLUT4 vesicle trafficking has remained elusive, despite extensive research on the project. Investigating the function of munc18c in GLUT4 vesicle exocytosis and dissecting its interactions with syntaxin4 has therefore been of much interest. This study utilized fluorescence correlation spectroscopy (FCS) and GST pull-down assays to investigate munc18c:syntaxin4 interactions. The results indicate that munc18c does not merely dissociate from syntaxin4 in response to insulin. Rather the results suggest that insulin triggers the repositioning of munc18c on syntaxin4 via an additional binding site, thus allowing VAMP2:syntaxin4 interaction and GLUT4 vesicle docking at the plasma membrane.

4.3.2. Results

4.3.2.1. Interactions between munc18c and syntaxin4 in vitro

I first wanted to investigate to see which section of the protein sequence is responsible for the interactions between munc18c and syntaxin4. For this, GST pull-down assays were performed. I was unable to express syntaxin4 sufficiently for detection by Western blotting in any of the mammalian cell lines used (3T3-L1 adipocytes, L6 myotubes, CHO or Cos-1 cells) so had to rely on bacterial expression of the GST-tagged syntaxin4 and mammalian expression of the munc18c constructs used previously. For this, purified GST-tagged syntaxin4 was coupled to glutathione beads and incubated with extracts of Cos-1 cells that had been transiently transfected with Xpress-tagged full length munc18c (MFL), or one of the munc18c truncation constructs M295, M308, M326 or M338. Complexes were washed to remove non-specific binding, separated by SDS-PAGE and immunoblotted with anti-Xpress antibody to assess the co-precipitation of munc18c with the syntaxin4 protein. As shown in figure 4.3.1.A (lanes 6-10) syntaxin4 associated with full length munc18c, but showed little or no binding to M295, M308, M326 or M338. None of the munc18c constructs were precipitated when extracts were incubated with only GST coupled to glutathione beads (lanes 1-5 figure 4.3.1.A) indicating that the association between munc18c and syntaxin4 was specific. Quantities of the GST protein (lanes 1-5 figure 4.3.1.B) or GST-tagged syntaxin4 proteins (lanes 6-10 figure 4.3.1.B) were checked by western blotting using an anti-GST antibody and shown to be comparative. Quantities of the Xpress-tagged munc18c constructs were checked by western blotting using an anti-Xpress antibody and shown to be comparative (figure 4.3.1). This shows that differences in amounts of precipitated munc18c constructs are not due to relative amounts of the GST proteins or Xpress-tagged proteins. This result indicates that the region of munc18c that is responsible for binding syntaxin4 lies between residues 1-295.

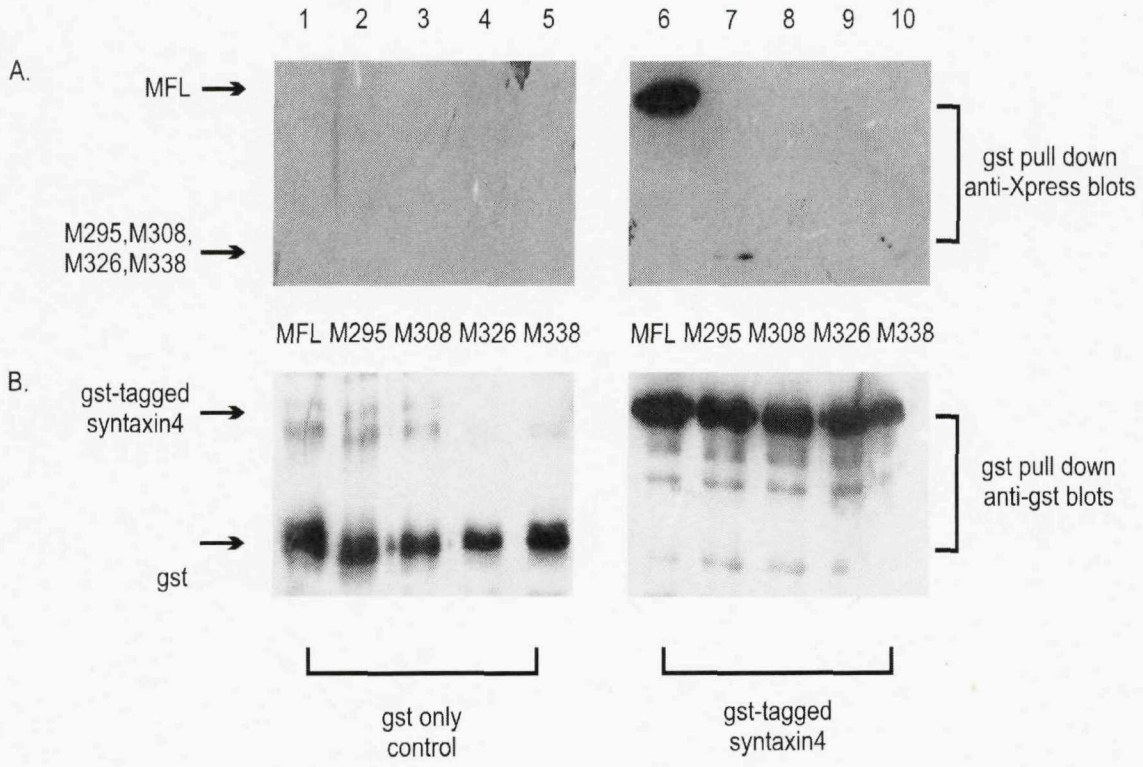
1 2 3 4 5
6 7 8 9 10
A.
MFL
M295,M308,
M326,M338
gst pull down
anti-Xpress blots
MFL M295 M308 M326 M338
MFL M295 M308 M326 M338
B.
gst-tagged
syntaxin4
gst
gst pull down
anti-gst blots
gst only
control
gst-tagged
syntaxin4

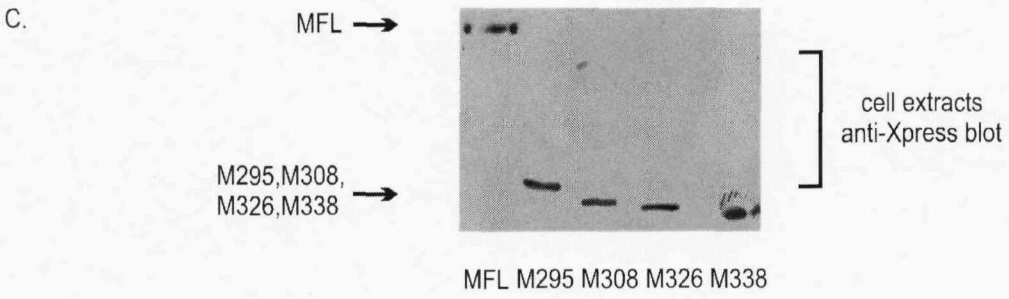
C.
MFL
M295,M308,
M326,M338
cell extracts
anti-Xpress blot
MFL M295 M308 M326 M338

Figure 4.3.1: Determination of the region of munc18c that is responsible for binding to syntaxin4

Cos-1 cells were transiently transfected with either full length munc18c (MFL) or one of the munc18c truncation constructs M295, M308, M326 or M338 expressed as an Xpress fusion. Syntaxin4 was bacterially expressed as a GST fusion protein and coupled to glutathione sepharose beads. GST bound to glutathione beads was used as a control (GST). Cos-1 cell extracts were incubated with the glutathione bead complexes, then washed to remove non-specific binding. Proteins were separated by SDS-PAGE, transferred to a nitrocellulose membrane, and probed for either Xpress to detect for the precipitated munc18c constructs (Figure 4.3.1.A) or GST to detect for amounts of the GST or GST-tagged syntaxin4 proteins (Figure 4.3.1.B).

4.3.2.2. Interactions between munc18c and syntaxin4 in vivo, as ascertained by FCS

As mentioned previously, despite continued efforts, there were great difficulties in expressing syntaxin4 in mammalian cell lines and I was unable to get expression levels high enough for detection on Western blots. However, when syntaxin4 was transfected into cells in the ECFP-N2 or EYFP-N2 vectors, expression levels obtained were high enough for detection of the fluorescence by the microscope. For the following in vivo experiments, detection of the cyan or yellow fluorescence was used to check for the expression of the ECFP-tagged syntaxin4 protein.

I first wanted to investigate the diffusion coefficient of munc18c, and whether this was affected by insulin stimulation or the presence of syntaxin4. For this, CHO cells were transfected with EYFP-tagged munc18c (MFL). The diffusion coefficient of full length munc18c when expressed alone as an EYFP fusion protein prior to insulin stimulation was 485 ± 36 μs compared to 611 ± 37 μs after insulin stimulation (mean ± s.e.m.). (Table 4.3.1). This is, in itself a novel finding as it suggests that munc18c isn't merely released from syntaxin4 into the cytosol upon insulin stimulation (as such a diffusion coefficient is too large to be that of a cytosolic protein).

It was next investigated as to whether co-expression of syntaxin4 had any effect on the diffusion coefficient of full length munc18c. For this, CHO cells were transfected with EYFP-tagged munc18c (MFL) and ECFP-tagged syntaxin4. When syntaxin4 was co-expressed, the diffusion coefficients for munc18c were increased to 672 ± 45 μs prior to insulin and 797 ± 49 μs post insulin stimulation (Table 4.3.1, figure 4.3.2). The co-expression of syntaxin4 caused munc18c to move slower in both the basal and insulin stimulated states and there was little change in the diffusion co-efficient of munc18c upon insulin stimulation, which is again suggestive of munc18c remaining bound to syntaxin4 in the insulin stimulated state.

An ideal way to confirm that syntaxin4 remains bound to munc18c in both the basal and insulin stimulated states would have been to perform fluorescence cross correlation spectroscopy analysis. This involves simultaneously measuring and analysing both of the fluorescently tagged proteins. As described previously in Section 4.2, this analysis was unable to be performed, for reasons not fully understood and data was not able to be collected for the ECFP-tagged proteins. To overcome this problem, EYFP-tagged munc18c was co-expressed with ECFP-tagged syntaxin4 or EYFP-tagged syntaxin4 was co-expressed with ECFP-tagged munc18c and the data collected for the EYFP-tagged protein only. This was performed both pre and post insulin stimulation. When ECFP-tagged munc18c was co-expressed, the diffusion coefficients for syntaxin4 were 661 ± 48 μs pre insulin and 789 ± 88 μs post insulin stimulation. The diffusion coefficient for syntaxin4 when munc18c was co-expressed was identical to the diffusion coefficient of munc18c when syntaxin4 was co-expressed. This was the case both pre and post insulin stimulation (Table 4.3.1 and figure 4.3.2).

Construct(s) over-expressed		Diffusion coefficient (μs), Mean ± SEM	
EYFP	ECFP	- insulin	+ insulin
MFL	-	485 ± 36	611 ± 37
MFL	Syntaxin4	672 ± 45	797 ± 49
Syntaxin4	MFL	661 ± 48	789 ± 88

Table 4.3.1: Diffusion coefficients for full length munc18c (MFL) and syntaxin4

CHO cells were transiently transfected with EYFP-tagged MFL only, EYFP-tagged MFL plus ECFP-tagged syntaxin4 or EYFP-tagged syntaxin4 plus ECFP-tagged MFL. Cells were serum starved for 24 hours prior to data collection. Where appropriate, cells were stimulated with 10^{-7} M insulin for 20 minutes. FCS data was collected for the EYFP-tagged protein only and are shown as the mean ± s.e.m. from 3 individual experiments, each using 6 separate cells.

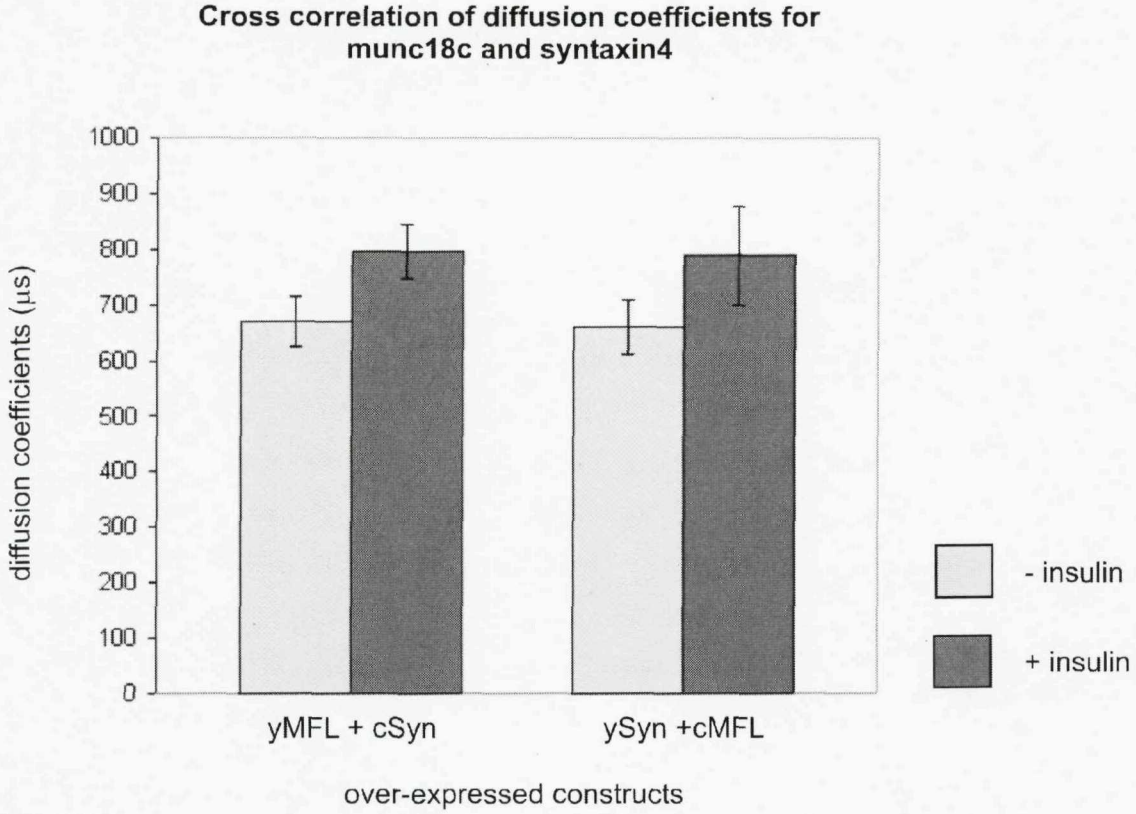

Figure 4.3.2: Diffusion coefficients for full length munc18c (MFL) and syntaxin4

CHO cells were transiently transfected with EYFP-tagged full length munc18c (MFL) plus ECFP-tagged syntaxin4 or EYFP-tagged syntaxin4 plus ECFP-tagged full length munc18c (MFL). Cells were serum starved for 24 hours prior to data collection. Where appropriate, cells were stimulated with 10^{-7} M insulin for 20 minutes. FCS data was collected for the EYFP-tagged protein only and are shown as the mean ± s.e.m. from 3 individual experiments, each using 6 separate cells.

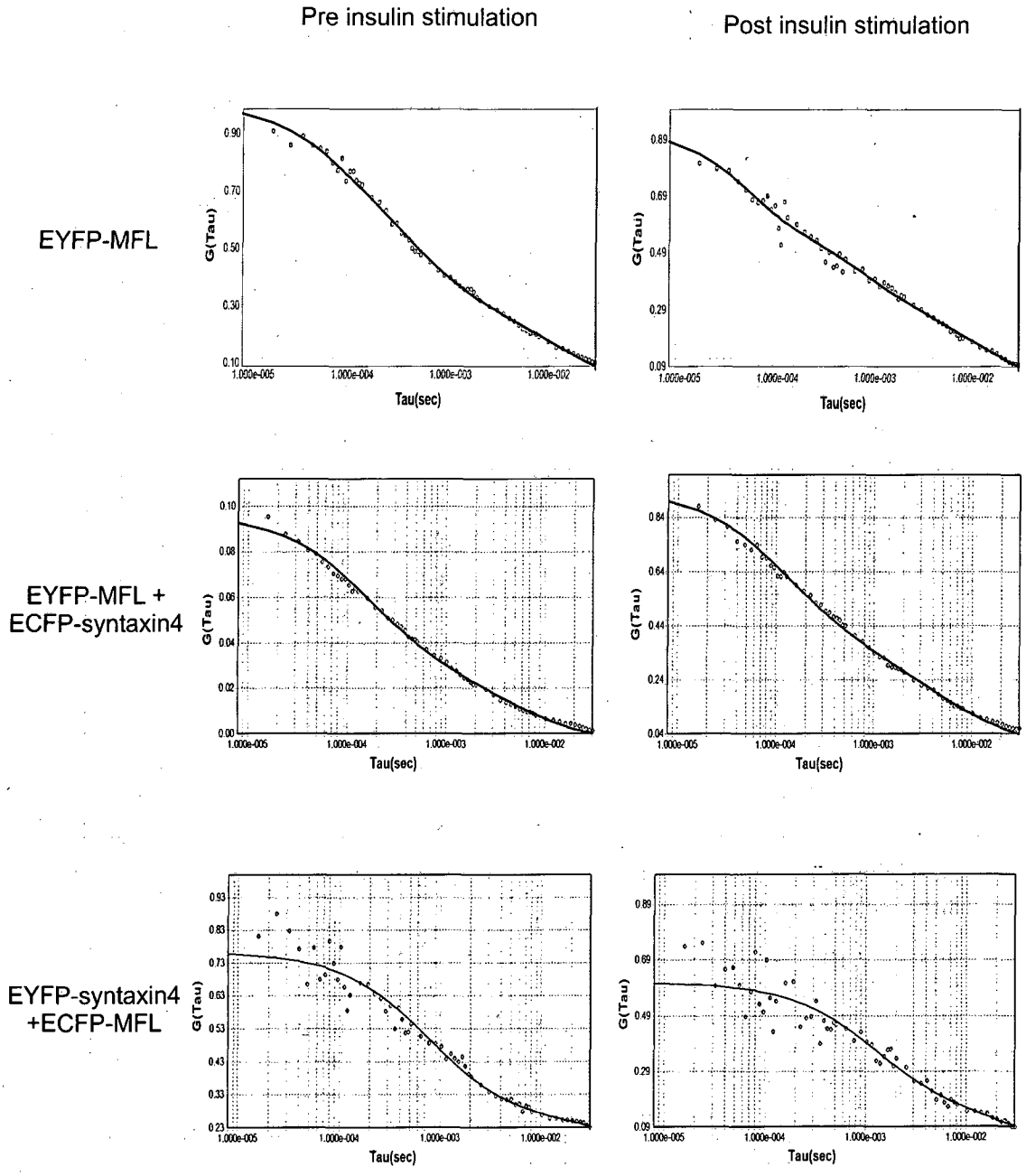

Figure 4.3.3: Example FCS traces for MFL and syntaxin4

CHO cells were transiently transfected with EYFP-tagged MFL only or EYFP-tagged MFL plus ECFP-tagged syntaxin4 or EYFP-tagged syntaxin4 plus ECFP-tagged MFL. Cells were serum starved for 24 hours prior to data collection. Where appropriate, cells were stimulated with 10^{-7} M insulin for 20 minutes. FCS data was collected for the EYFP-tagged protein only.

In order to further define the binding of munc18c to syntaxin4, the truncation construct of munc18c, M295, which lacks the N-terminal 295 amino acids, was employed. The GST pull-down assays shown above in this chapter indicate that this construct is unable to bind to syntaxin4 when expressed in the non insulin responsive Cos-1 cell line (see figure 4.3.1). Firstly, CHO cells were transfected with EYFP-tagged M295 alone. The diffusion coefficient for M295 was 576 ± 61 μs prior to insulin and 500 ± 35 μs post insulin stimulation. EYFP-tagged M295 was then co-expressed with full length ECFP-tagged syntaxin4. When syntaxin4 was co-expressed, the diffusion co-efficients for M295 were 619 ± 34 μs pre-insulin and 821 ± 37 μs post-insulin stimulation (Table 4.3.2 and Figure 4.3.3). The co-expression of syntaxin4 with M295 had no effect on the speed of M295 in the basal state, but caused it to slow upon insulin stimulation, indicating binding. This suggests that munc18c has two binding sites for syntaxin4: One that lies between residues 1-295, (as has been shown previously in this chapter of the thesis and in other published work [Grusovin et al. 2000]) and one that lies between residues 295-592 which only binds to syntaxin4 in response to insulin stimulation.

Construct(s) over-expressed		Diffusion coefficient (μs) Mean ± s.e.m.	
EYFP	ECFP	- insulin	+ insulin
MFL	-	485 ± 36	611 ± 37
MFL	Syntaxin4	672 ± 45	797 ± 49
M295	-	576 ± 61	500 ± 35
M295	Syntaxin4	619 ± 34	821 ± 37

Table 4.3.3: Diffusion coefficients for full length munc18c (MFL) and M295

CHO cells were transiently transfected with EYFP-tagged MFL or the munc18c truncation construct M295, with or without the co-expression of ECFP-tagged syntaxin4. Cells were serum starved for 24 hours prior to data collection. Where appropriate, cells were stimulated with 10^{-7} M insulin for 20 minutes. FCS data was collected for the EYFP-tagged protein only and are shown as the mean ± s.e.m. from 3 individual experiments, each using 6 separate cells.

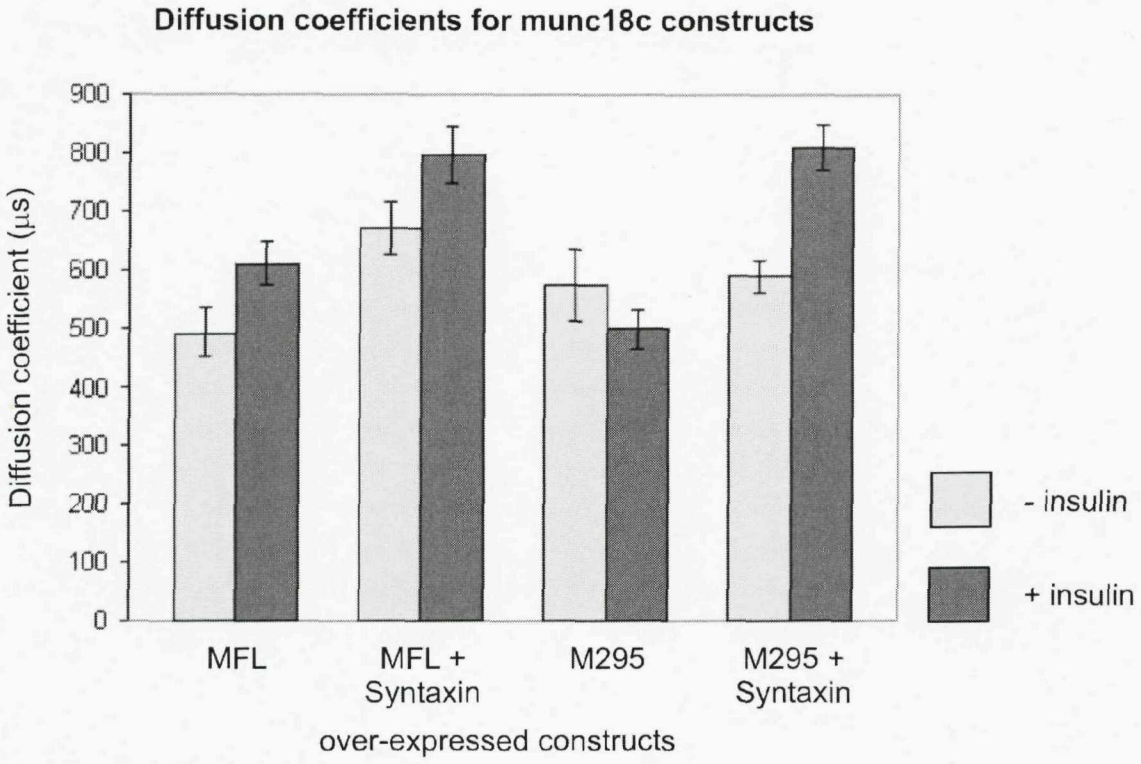

Figure 4.3.4: Diffusion co-efficients for full length munc18c (MFL) and M295

CHO cells were transiently transfected with EYFP-tagged full length munc18c (MFL) or the munc18c truncation construct M295, with or without the co-expression of ECFP-tagged syntaxin4. Cells were serum starved for 24 hours prior to data collection. Where appropriate, cells were stimulated with 10^{-7} M insulin for 20 minutes. FCS data was collected for the EYFP-tagged protein only and are shown as the mean ± s.e.m. from 3 individual experiments, each using 6 separate cells.

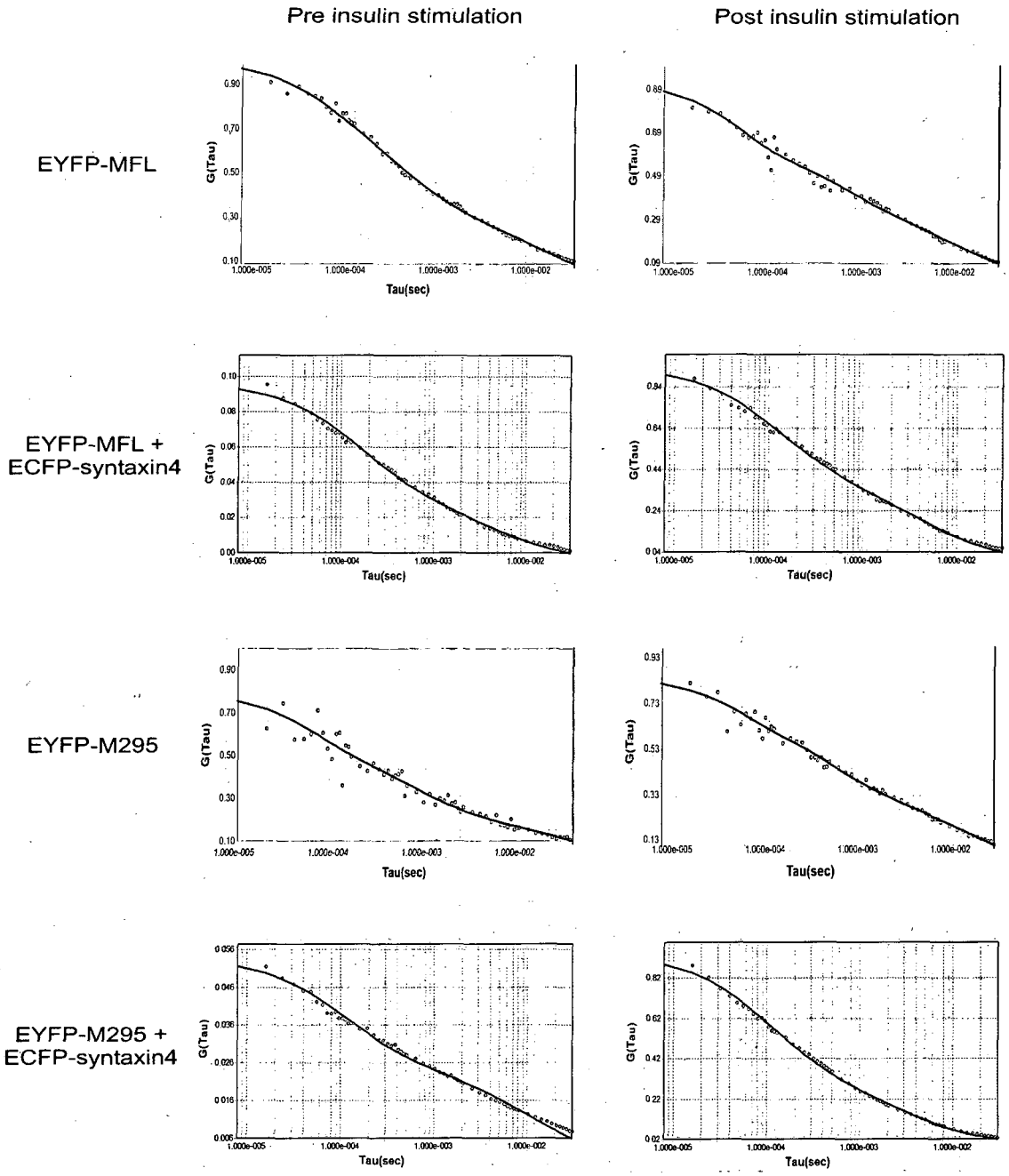

Figure 4.3.5: Example FCS traces for MFL, M295 and syntaxin4

CHO cells were transiently transfected with EYFP-tagged MFL only, EYFP-tagged MFL plus ECFP-tagged syntaxin4, EYFP-tagged M295 only or EYFP-tagged M295 plus ECFP-tagged syntaxin4. Cells were serum starved for 24 hours prior to data collection. Where appropriate, cells were stimulated with 10^{-7} M insulin for 20 minutes. FCS data was collected for the EYFP-tagged protein only.

4.3.3. Discussion

4.3.3.1. Overview

One of the most fundamental of insulin's actions is to regulate glucose homeostasis by inducing GLUT4 vesicle exocytosis. GLUT4 vesicle trafficking is similar to that seen in synaptic vesicles. The GLUT4 vesicle contains the v-SNARE VAMP2 which binds to its cognate t-SNARE receptor syntaxin4 in the plasma membrane [Kanda et al. 2005,Chang et al. 2004]. Insulin regulates VAMP2:Syntaxin4 binding by virtue of accessory proteins, the most important of which is munc18c. However, elucidation of the exact role of munc18c in GLUT4 vesicle trafficking has proved problematical. Munc18c has been shown to inhibit GLUT4 vesicle exocytosis [Macaulay et al. 2002, Thurmond et al. 1998] and yet to also be essential for this process [Oh et al. 2005, Thurmond et al. 2000]. In vitro assays have shown that in the basal state, munc18c binds to syntaxin4 with high affinity, acting as a clamp over syntaxin4. This prevents VAMP2 from binding to syntaxin4 and hence inhibits GLUT4 vesicle docking at the plasma membrane [Kanda et al. 2005, Thurmond et al. 1998, Tamori et al. 1998]. Insulin stimulation somehow relieves this inhibition, hence allowing an interaction to form between syntaxin4 and VAMP2 and allowing the GLUT4 vesicle to dock and fuse at the plasma membrane. Insulin stimulation was thought to either release munc18c from syntaxin4 [*J. Biol. Chem.* **273** 33876-33883], or to alter the interactions between the two proteins in such a way as to enable syntaxin4 to adopt an "open" conformation. Once syntaxin4 is in the "open" conformation it is then able to bind to VAMP2, thus enabling GLUT4 vesicle exocytosis [Jahn and Südhof 1999, James 2003]. Due to the complexities of the GLUT4 trafficking machinery, most research into the interactions between munc18c and syntaxin4 has been conducted in vitro. Hence the mechanistic detail of munc18c and syntaxin4 interactions in vivo has remained elusive.

Fluorescence correlation spectroscopy (FCS) was employed in living cells to elucidate the mechanics of the GLUT4 vesicle trafficking apparatus and to further define the roles of munc18c:syntaxin4 interactions in this process in vivo. The use of FCS with the

interacting and non-interacting constructs, along with previously published work from other laboratories, has enabled the piecing together of a hypothetical model for the insulin-mediated translocation and docking of GLUT4 to the plasma membrane. The two key findings of this section are: (A) Munc18c is bound to syntaxin4 in both the basal and insulin stimulated states, and (B) munc18c has two binding sites for syntaxin4.

4.3.3.2. Determination of the regions of munc18c that are responsible for binding to syntaxin4

Previously published data identified a region of munc18c between residues 1 and 139 as a minimal domain for its interaction with syntaxin 4 [Grusovin et al. 2000]. This implied that of all the munc18c constructs available, only the full length munc18c should be able to bind to syntaxin4 (meaning that M295 could be used as a non-interacting mutant). It was first required to check that this was indeed the case. A GST pull-down assay was hence employed to determine which of the N-terminal truncation constructs of munc18c were able to bind to syntaxin4 in the basal state. Full length munc18c (MFL) showed a strong interaction with syntaxin4, whilst the munc18c truncation constructs M295, M308, M326 and M338 showed little/no binding. This shows that in the unstimulated state, the binding region for syntaxin4 on munc18c lies within the N-terminal 295 amino acids of munc18c.

4.3.3.3. Munc18c is bound to syntaxin4 in the basal and insulin stimulated states

The fluorescence correlation spectroscopy data collected in this study shows that munc18c is not merely released into the cytosol upon insulin stimulation, but instead remains bound to syntaxin4. The diffusion coefficient for munc18c increased upon insulin stimulation, indicating that munc18c is moving slower upon stimulation with insulin (Table 4.3.1). This is, in itself a novel finding as it shows that munc18c isn't merely released from syntaxin4 into the cytosol upon insulin stimulation (as such a

diffusion coefficient is too large to be that of a cytosolic protein). When syntaxin4 was co-expressed with full length munc18c, the diffusion coefficients for munc18c were increased prior and post insulin stimulation (Table 4.3.1). The co-expression of syntaxin4 caused munc18c to move slower in both the basal and insulin stimulated states and there was little change in the diffusion coefficient of munc18c upon insulin stimulation, which is again suggestive of munc18c remaining bound to syntaxin4 in the insulin stimulated state. The FCS data for syntaxin4 when co-expressed with munc18c verifies this hypothesis. The speed of munc18c when syntaxin4 was co-expressed was identical to the speed of syntaxin4 when munc18c was co-expressed, both before and after insulin stimulation. This cross correlation of speeds strongly suggests that munc18c remains bound to syntaxin4 in vivo in both the basal and insulin stimulated state. These results suggest that munc18c is not only inhibitory to, but is also essential for GLUT4 vesicle docking at the plasma membrane. This is in accordance with findings from other laboratories [Macaulayet al. 2002, Thurmond et al. 1998 and 1999, Oh et al. 2005].

4.3.3.4. Munc18c has two binding sites for syntaxin4

If munc18c is not actually released by syntaxin4 in response to insulin, there must be some change on munc18c that allows syntaxin4 to bind to VAMP-2. This was then explained when the munc18c truncation construct M295 was used in FCS experiments. The FCS data using M295 suggested that munc18c has an additional binding site for syntaxin4. As explained above, the co-expression of syntaxin4 caused a decrease in speed of full length munc18c. However, this effect was not seen when the munc18c construct unable to bind to syntaxin4 in vitro, M295, was used in unstimulated cells. However, when the cells were stimulated with insulin, the co-expression of syntaxin4 caused M295 to slow down. This suggests that the munc18c construct M295 does bind to syntaxin4, but only when the cells are stimulated with insulin. This implies that munc18c has two binding sites for syntaxin4: One that lies between residues 1-295 (see section 4.3.2.1), and one that lies between residues 295-592, which only binds to syntaxin4 in response to insulin stimulation. Previous studies have shown the N-terminal section of munc18c to be

essential for binding to syntaxin4 but have also suggested that there may be another binding site on munc18c, similar to that seen with munc18a [Latham et al. 2006].

4.3.3.5. Insulin action on munc18c:syntaxin4 interactions; a new model

The data presented here show that munc18c is bound to syntaxin4 both prior to and post insulin stimulation and that munc18c has an additional binding site for syntaxin4 which only binds upon insulin stimulation.

As mentioned previously, there has been discrepancy as to the exact role of munc18c in GLUT4 vesicle exocytosis. The simplest model for the role of munc18c in this process (and hence the most frequently used) is that insulin causes the dissociation of munc18c from syntaxin4, which allows the binding of VAMP-2 to syntaxin4, thus enabling the docking and fusion of theGLUT4 vesicle at the plasma membrane. However, there is a great deal of recent evidence to suggest that this earliest model for munc18c function is overly simplistic.

In recent years it has become progressively more apparent that the mammalian munc18 proteins play a critical (and positive) role in vesicle exocytosis, including that of the insulin-stimulated GLUT4 vesicle exocytosis. However, the precise role and mechanism of their action in this process has remained controversial. On one hand, increased expression of munc18 isoforms in mammalian cells and their counterparts in lower organisms had an inhibitory effect on vesicle exocytosis [Schulze et al. 2004, Tamori et al. 1998, Thurmond et al. 1998]. These data have been interpreted as evidence for munc18c playing an inhibitory function in vesicle exocytosis and has led to the original model for munc18c's involvement in the process: The simplest model for the role of munc18c (and hence the most frequently used) is that insulin causes the dissociation of munc18c from syntaxin4, which allows the binding of VAMP-2 to syntaxin4, thus enabling the docking and fusion of the GLUT4 vesicle at the plasma membrane. However, there are other models that would fit this data and there is also much experimental evidence accumulating to suggest

that these proteins play an important positive role in vesicular trafficking. For example, genetic ablation of the *D. melanogaster* and *C. elegans* munc18 homologs (Rop and Unc18, respectively) results in a complete loss of exocytosis, suggesting that these proteins are necessary positive effectors of vesicular trafficking [Harrison et al. 1994, Hosono et al. 1992]. Consistent with this positive role in vesicle trafficking, expression of the temperature-sensitive munc18 yeast homolog Sly1p prevents endoplasmic-reticulum-derived transport vesicle fusion with Golgi membranes at the non-permissive temperature [VanRheenen et al. 1998, Cao et al. 1998]. This data is particularly supportive of munc18c playing an essential role in GLUT4 vesicle exocytosis considering that data represented in another journal article suggests that munc18c interacts with its cognate SNAREs in a manner that resembles the yeast proteins Sly1p and Sed5p rather than the mammalian neuronal proteins munc18a and syntaxin1a and plays an important positive role in the exocytosis process [Latham et al. 2006].

There is also evidence to suggest that although munc18c:syntaxin 4 interaction is not required for the insulin-stimulated trafficking to and association with the cell surface, the interaction between munc18c and syntaxin4 is required for the integration of the GLUT4 storage vesicles into the plasma membrane [Thurmond et al. 2000]. Additionally, the loss of munc18c (with munc18c$^{-/-}$ mice) leads to glucose intolerance, implicating the importance of this protein in insulin-mediated GLUT4 vesicle trafficking and diseased states such as glucose intolerance and diabetes [Oh et al. 2005].

All of the above mentioned data agrees with the findings from this chapter and has enabled the generation of the new model for munc18c's role in insulin mediated GLUT4 vesicle trafficking. In the basal state, munc18c is bound to syntaxin4 at the plasma membrane, via the N-terminal of munc18c. The interaction between these two proteins prevents an interaction from occurring between syntaxin4 and VAMP-2 and hence prevents GLUT4 vesicle exocytosis. Insulin stimulation causes a repositioning of munc18c on syntaxin4 via an additional binding site on munc18c. This allows syntaxin4 to adopt the open conformation, enabling GLUT4 vesicle docking at the plasma membrane via VAMP-2.

4.4. Interactions between 80K-H and Syntaxin4

4.4. Interactions between 80K-H and Syntaxin4

4.4.1. Introduction

In the basal state, munc18c is bound to syntaxin4 and prevents it interacting with VAMP2. Insulin action somehow enables an interaction to occur between syntaxin4 and VAMP2, which facilitates GLUT4 vesicle docking and fusion at the plasma membrane. Although the dependence of GLUT4 vesicle exocytosis on syntaxin4 is renowned [Spurlin et al. 2004, Yang C et al. 2001, Kawanishi et al. 2000, Tamori et al. 1998, Volchuk et al.1996, Tellam et al. 1997, Dulubova et al. 1999, Ishiki and Klip 2005], exactly how insulin enables an interaction between VAMP2 and syntaxin4 is as yet unknown.

As has been already been discussed, previous work in our laboratory identified a protein called 80K-H to interact with both munc18c and PKCζ in an insulin dependent fashion. Over-expression of an 80K-H truncation construct mimicked the effects of insulin on glucose transport, producing a dramatic increase in both basal and insulin stimulated glucose transport. Work in this thesis has enabled a putative model for the role of this protein in insulin regulated GLUT4 vesicle trafficking, as follows: In the basal state, munc18c is clamped to syntaxin4. This means that syntaxin4 is unable to bind to the VAMP2 protein of the GLUT4 vesicle, thereby preventing GLUT4 insertion into the plasma membrane. 80K-H is tethered at the membrane by a scaffolding complex and is also bound to munc18c. 80K-H and its tether are responsible for positioning munc18c in the correct orientation to prevent VAMP2 binding syntaxin4. PKCζ is inactive and is bound to neither munc18c nor 80K-H. Insulin causes the activation of PKCζ, which is then able to bind to 80K-H and release it from its membrane tether. Insulin action also increases the strength of association between 80K-H and munc18c. These insulin-induced changes in binding of 80K-H mean that it is free to move in the plane of the plasma membrane, enabling it to alleviate the clamping mechanism of munc18c on syntaxin4. This leaves syntaxin4 free to bind to VAMP2 so that the GLUT4 vesicle can dock and fuse with the membrane, allowing glucose to enter the cell.

Un-stimulated Cells

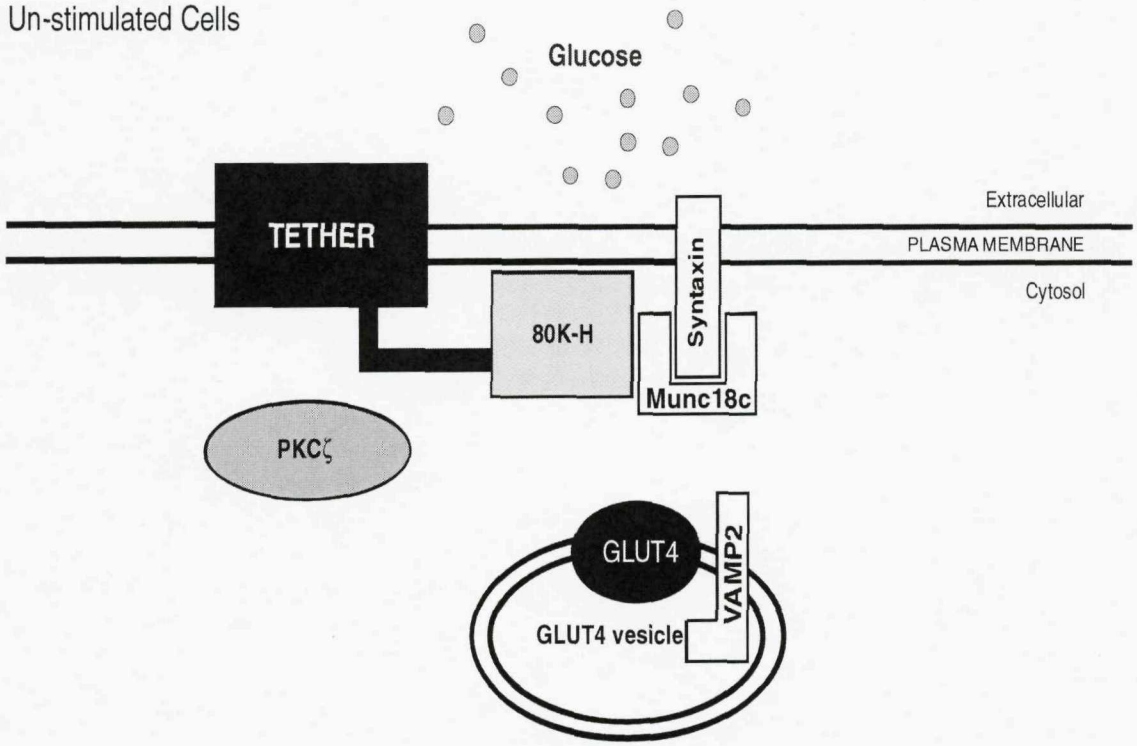

Insulin stimulated cells

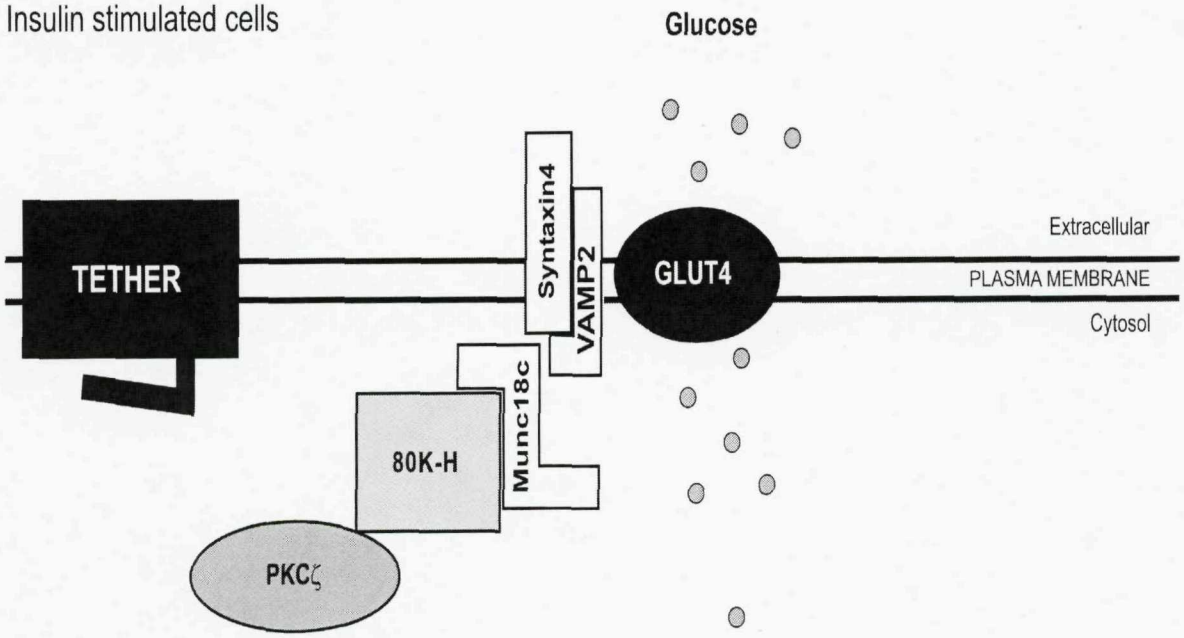

Figure 4.2.17: Proposed model for the role of 80K-H, munc18c and PKCζ in insulin mediated GLUT4 trafficking

In the basal state, PKCζ is inactive in the cytosol. 80K-H is bound to munc18c and is tethered at the membrane by an unknown protein complex. 80K-H positions munc18c onto syntaxin4, so that syntaxin4 is blocked and unable to bind VAMP2 in the GLUT4 vesicle. The GLUT4 vesicle is therefore unable to bind at the plasma membrane meaning that glucose cannot enter the cell.

Insulin stimulation activates PKCζ which is then able to bind 80K-H. PKCζ releases 80K-H from its membrane tether, which in turn increases the binding between 80K-H and munc18c. This releases the clamping action of munc18c on syntaxin4, enabling the VAMP2 protein in the GLUT4 vesicle to bind syntaxin4. The GLUT4 vesicle is then able to dock and fuse at the plasma membrane and glucose can enter the cell through the GLUT4 protein.

The experimental evidence linking 80K-H to munc18c and GLUT4 vesicle trafficking, alongside munc18c's well known close association with syntaxin4 encouraged me to investigate interactions between 80K-H and syntaxin4. Both GST pull-down assays and fluorescence correlation spectroscopy (FCS) were used to investigate the interactions between these two proteins. The results show that 80K-H and syntaxin4 do interact and that it is the C-terminal 150 amino acid residues of 80K-H that are responsible for this interaction.

4.4.2. Results

4.4.2.1. 80K-H and syntaxin4 interact with each other *in vitro*

Firstly, a simple GST pull-down assay was performed. I was unable to get high enough expression of syntaxin4 in mammalian cell lines for detection by Western blotting, so the bacterially expressed GST-tagged syntaxin4 was used and the 80K-H constructs were expressed in the mammalian cells. For this, purified GST-tagged full length syntaxin4 was coupled to glutathione sepharose beads and incubated with extracts of Cos-1 cells transiently transfected with ECFP-tagged full length 80K-H (KHFL) or the 80K-H truncation constructs KH302 or KH378. Complexes were washed to remove non-specific binding, separated by SDS-PAGE and immunoblotted with an anti-ECFP antibody to test for precipitation of the ECFP-tagged 80K-H constructs. As is shown in fig. 4.3.1 A lanes 4-6, syntaxin4 associated with all three of the 80K-H constructs, KHFL, KH302 and KH378. None/very little of the ECFP-tagged 80K-H constructs were precipitated when extracts were incubated with GST coupled to glutathione beads (Fig. 4.3.1 A lanes 1-3) indicating that the association between syntaxin4 and KH302 was specific. There was a little precipitation of KH302 and KH378 when incubated with GST coupled to glutathione beads (figure 4.3.1 A. lanes 1-3), which probably explains why there appears to be a greater association between these two 80K-H constructs and syntaxin4 than between the full length 80K-H construct and syntaxin4. Despite there being an

association between the GST-only control and KH302/KH378, there was clearly a far greater association when GST-syntaxin was coupled to glutathione beads (figure 4.3.1. A lanes 4-6).

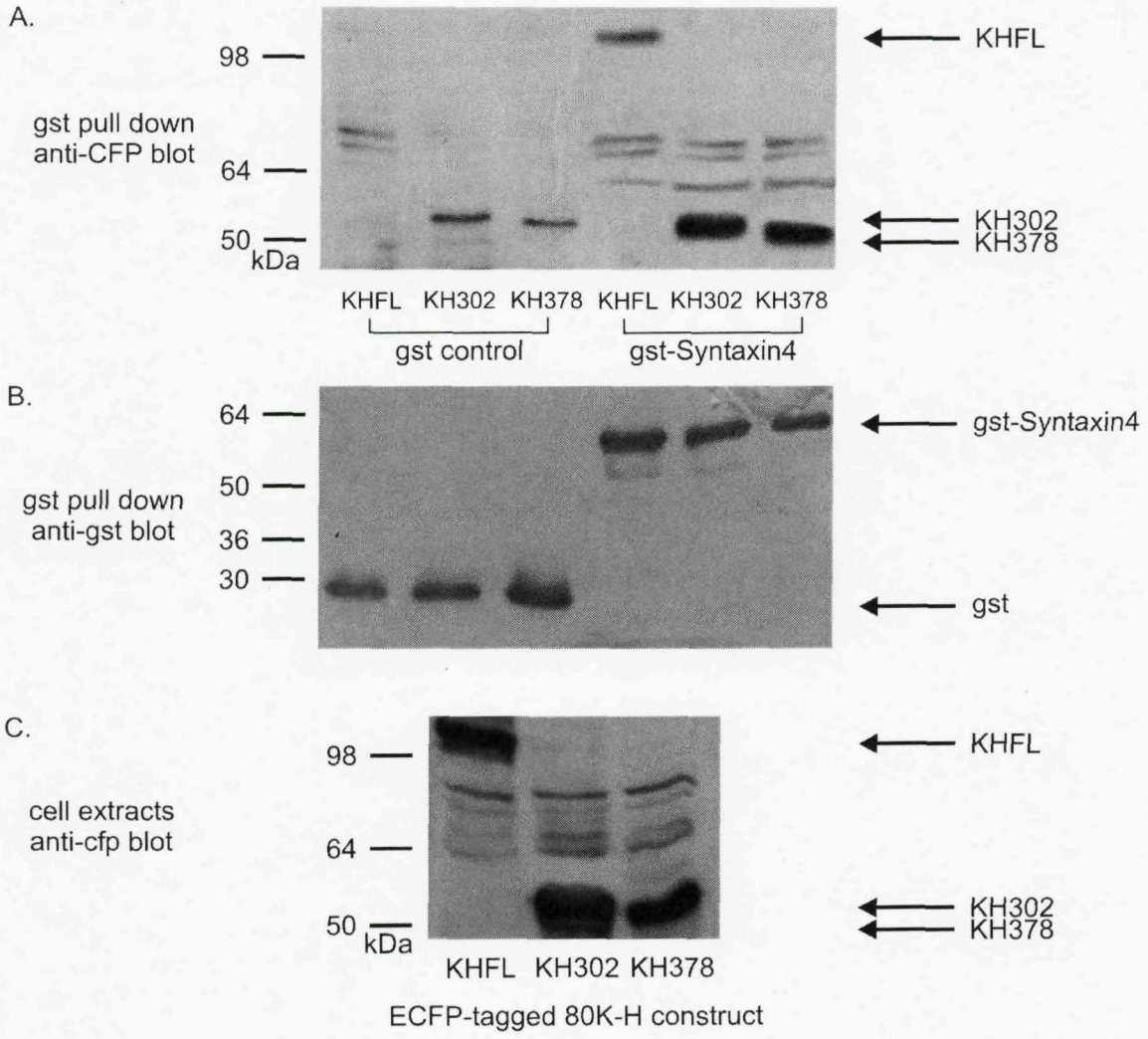

Figure 4.3.1: Determining whether 80K-H interacts with syntaxin4:

Cos-1 cells were transiently transfected with either the full length 80K-H construct, KHFL, or the 80K-H truncation constructs KH302 or KH378 expressed as ECFP fusions. Syntaxin4 was bacterially expressed as a GST fusion protein and coupled to glutathione sepharose beads. GST bound to glutathione beads was used as a control (GST). Cos-1 cell extracts were incubated with the glutathione bead complexes, then washed to remove non-specific binding. Proteins were separated by SDS-PAGE, transferred to a nitrocellulose membrane, and probed for ECFP to detect co precipitated 80K-H constructs.

4.4.2.2. Investigating 80K-H and syntaxin4 interactions in vivo using fluorescence correlation spectroscopy

I then wanted to see if the speed of 80K-H was affected by insulin or the presence of syntaxin4. Firstly, the 80K-H truncation construct KH302 was expressed alone as an EYFP fusion protein. When KH302 was expressed alone, the average diffusion coefficient prior to insulin stimulation was 1349 ± 138 μs and 1205 ± 102 μs after insulin stimulation (mean ± s.e.m.), showing that insulin had no effect on the speed of 80K-H when no other additional proteins were over-expressed. I next wanted to see if the presence of syntaxin4 had an effect on the speed of 80K-H. For this, CHO cells were transfected with EYFP-tagged KH302 and ECFP-tagged syntaxin4. When syntaxin4 was co-expressed, the diffusion coefficients for KH302 were reduced to 727 ± 51 μs in the basal state and 746 ± 81 μs in the insulin stimulated state. This shows that the presence of syntaxin4 significantly increases the speed of KH302, suggesting that syntaxin is somehow substituting a larger/slower 80K-H binding complex. However, there is little change in the speed of KH302 upon insulin stimulation, even when syntaxin4 was co-expressed, suggesting that 80K-H binds to syntaxin4 in both the basal and insulin-stimulated states.

Construct(s) overexpressed		Diffusion coefficient (μs) Mean ± s.e.m.	
EYFP	ECFP	- insulin	+ insulin
KH302	-	1349 ± 138	1205 ± 102
KH302	Syntaxin4	727 ± 51	746 ± 81

Table 4.3.1. Diffusion coefficients for KH302

CHO cells were transiently transfected with EYFP-tagged KH302 (control) or EYFP-tagged KH302 plus ECFP-tagged syntaxin4. Cells were serum starved for 24 hours prior to data collection. Where appropriate, cells were stimulated with 10^{-7} M insulin for 20 minutes. FCS data was collected for the EYFP-tagged protein only and are shown as the mean ± s.e.m. from 3 individual experiments, each using 6 separate cells.

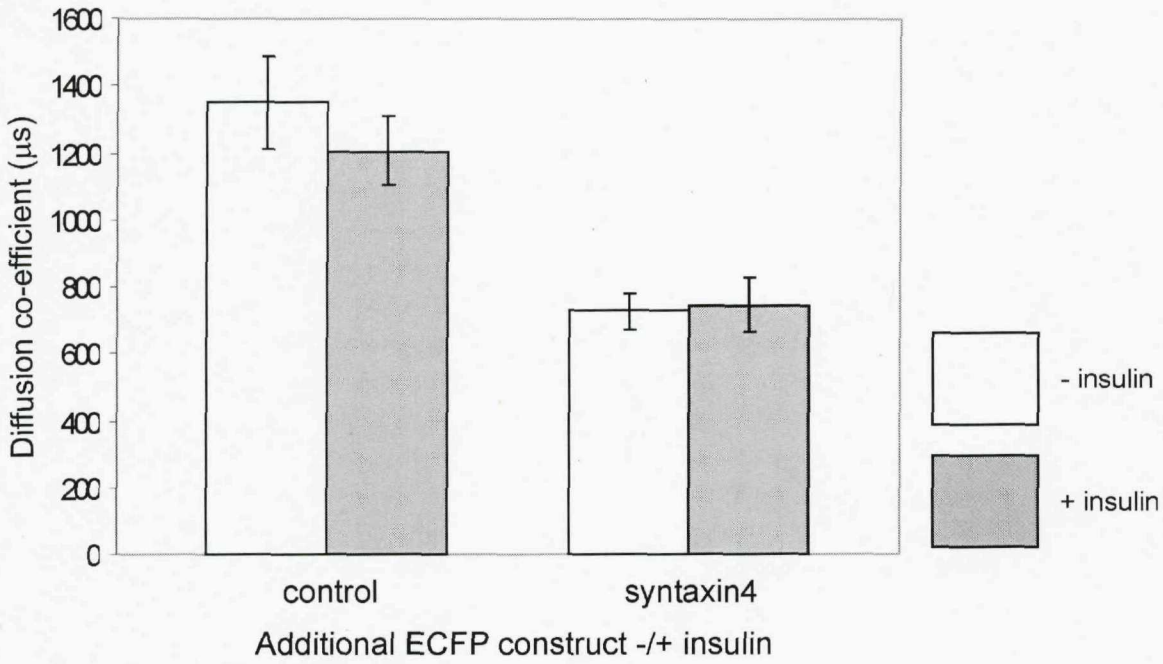

Figure 4.3.2. Diffusion coefficients for KH302

CHO cells were transiently transfected with EYFP-tagged KH302 (control) or EYFP-tagged KH302 plus ECFP-tagged syntaxin4. Cells were serum starved for 24 hours prior to data collection. Where appropriate, cells were stimulated with 10^{-7} M insulin for 20 minutes. FCS data was collected for the EYFP-tagged protein only and are shown as the mean ± s.e.m. from 3 individual experiments, each using 6 separate cells.

To analyze how the insulin signal may be delivered to munc18c to induce such a conformational change, experiments were conducted with 80K-H. Recent evidence suggests that 80K-H links insulin signalling to the machinery controlling GLUT4 exocytosis through an insulin triggered association with munc18c (Hodgkinson et al, 2005). For this, EYFP-tagged full length munc18c was expressed in the presence and absence of 80K-H. While insulin did not affect the mobility of EYFP-tagged full length munc18c when expressed alone, in the presence of 80K-H insulin induced a large increase in the mobility of the EYFP-tagged full length munc18c. These results indicate that 80K-H interacts with munc18c in intact living cells. How then does insulin trigger 80K-H to increase the speed of munc18c if, as shown above, munc18c remains associated with syntaxin4? One way that the mobility of munc18c can increase is if there is a decrease in the tethering of the syntaxin4 complex with other known interactors such as synip or tomosyn or other scaffolding proteins. In this model, insulin would break or reduce these interactions. However, we did not observe an increase in mobility of syntaxin4 when cells co-expressing munc18c and syntaxin4 were stimulated with insulin. This is likely because the availability of the other interactors was limiting and that most of the syntaxin4 was not tethered in the first place. Tyrosine phosphorylation of munc18c has been shown to promote VAMP-2 binding to syntaxin4 and this provides a further mechanism of delivering an insulin signal to munc18c [Oh and Thurmond 2006].

4.5 KIFAP3: a novel interactor of munc18c?

4.5 KIFAP3: a novel interactor of munc18c?

4.5.1. Introduction

4.5.1.1. Overview

A yeast-two-hybrid assay performed in our laboratory, using munc18c as bait, identified Kifap3 to be a novel interactor. Kifap3 is part of the KIF3 motor complex, which drives the transport of organelles along microtubules. Because of the experimental evidence already linking both microtubules [Olson et al. 2001, Fletcher et al. 2000] and munc18c [Macaulay et al. 2002, Grusovin and Macaulay 2003, Spurlin et al. 2003, Kanda et al. 2005] to a role in GLUT4 vesicle translocation, the function of Kifap3 in insulin-regulated GLUT4 trafficking was considered worthy of investigation.

4.5.1.2. Involvement of Microtubules and Kinesins in GLUT4 vesicle trafficking

The cytoskeleton plays important roles in the retention and trafficking of membrane-bound organelles to specific cellular locations. The GLUT4 vesicle is a highly regulated and dynamic organelle which requires stimulus-regulated movement around the cell. In the basal state, GLUT4 protein slowly yet continually cycles between the plasma membrane and intracellular storage vesicles. Upon insulin stimulation, there is a rapid and dramatic reorganisation of the cytoskeleton that results in the substantial increase in targeted exocytosis of GLUT4 vesicles and a decrease in GLUT4 endocytosis. Although it is well known that the cytoskeleton is responsible for this rapid reorganisation of GLUT4, the exact functional roles of the cytoskeleton, and the regulatory mechanisms behind them, remain unclear. Much research has been conducted in to the roles of both the actin cytoskeleton and microtubules in insulin regulated

GLUT4 vesicle trafficking, but many questions remain. In 3T3-L1 adipocytes and primary rat adipocytes it has been shown that pharmacological disruption of the microtubule network blocks insulin-dependent GLUT4 redistribution and to diminish insulin-stimulated GLUT4 translocation and glucose uptake [Watson et al. 2004, Karylowski et al. 2004, Fletcher et al. 2000, Emoto et al. 2001, Olson et al. 2001, Semiz et al. 2003, Lizinov et al. 2005]. However, none of the studies performed have been able to clearly distinguish exactly where or how the microtubules are playing a role. It remains poorly defined whether disruption of the microtubules causes a defect in the formation of the insulin signalling complex, in the trafficking of GLUT4 vesicles for fusion with the plasma membrane, or for some other, as yet unidentified reason.

4.5.1.3. Microtubules and Kinesins: An Overview

Microtubules are long, hollow cylinders composed of alternating α and β tubulin molecules. They form a straight, rigid, polarised pathway from the centrosome at the perinuclear region (the minus end) to the cell periphery (the positive end). Their main functions are to distribute various proteins to their proper destination after synthesis and to correctly position the organelles within the cell. They are also concerned in the generation of force in cilia and flagella and various aspects of mitotic spindle formation and function [Lakämper and Meyhöfer 2006, Fant et al. 2004]. Microtubules exist in equilibrium with a pool of monomeric tubulin in the cytoplasm. They are highly dynamic cellular structures and can be rapidly assembled or disassembled in response to various physiological stimuli. The specificity for microtubule transport around the cell comes from the Microtubule Associated Proteins (MAPs). Some of these are merely structural proteins that modify the properties of the microtubule, whilst the others (which are the more frequently documented) are motor proteins that play an integral part in the role of the microtubule. There are two classes of microtubule motor proteins that are associated with transporting cargo around the cell: the dynenins, which tend to move toward the minus end of the microtubule (inward, towards the nucleus) and the kinesins, which tend to move toward the positive end (outward, toward the plasma membrane). Kinesin motor

proteins are complexes composed of two identical heavy chains (each consisting of a motor domain, coiled-coil dimerization domain and tail [Yang JT et al. 1989]) plus several light chains. Each heavy chain forms a globular head that attaches to the microtubule in an ATP-dependant fashion, whilst the light chains form specific attachments to the cargo to be transported. Once the motor protein has attached to the microtubule, the ATPase activity of the motor protein is stimulated. The chemical energy released from this ATP hydrolysis is converted into mechanical energy for the movement of the motor protein along the microtubule. There is a vast array of different kinesin-family members. They are highly divergent and exhibit a high degree of functional and structural diversity but have a highly homologous motor domain.

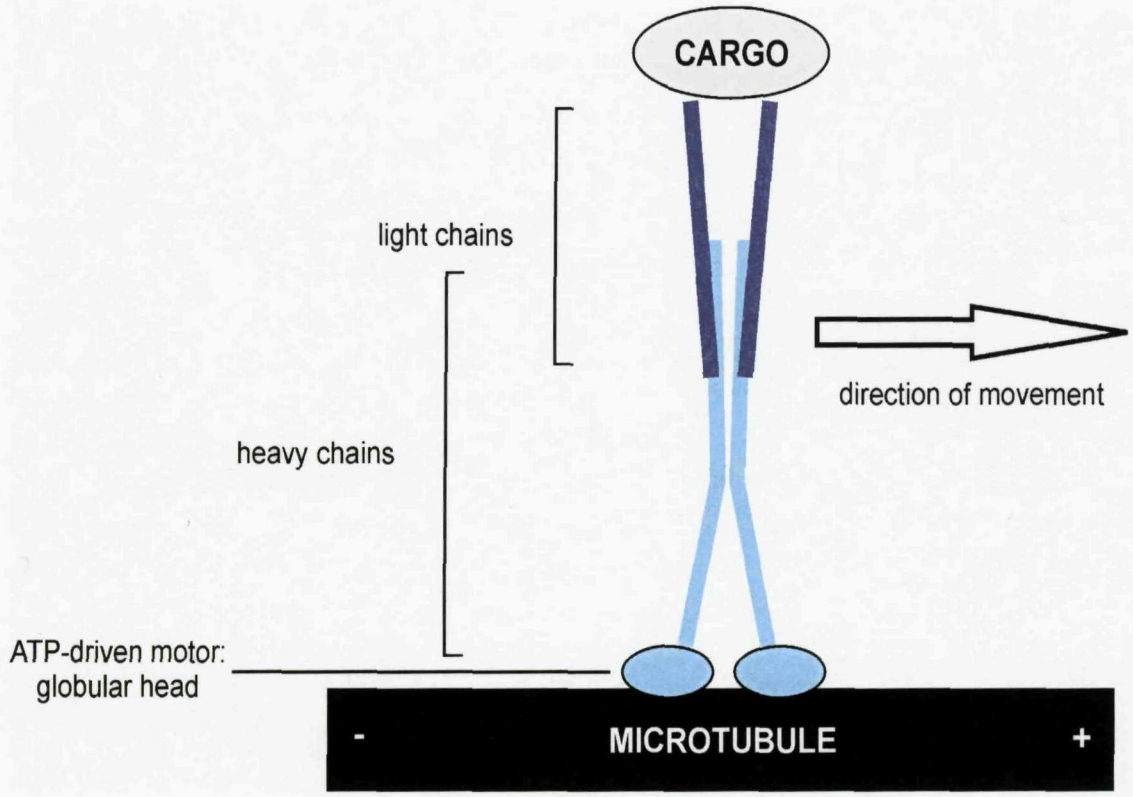

Figure 4.5.1: The kinesins: microtubule motor proteins.

The kinesin microtubule motor proteins are composed of two identical heavy chains and a number of light chains. The heavy chains consist of a tail, a coiled-coil dimerization domain and a globular head (the motor domain). This motor domain moves along the microtubule in an ATP-dependent fashion. The light chains are responsible for the specificity of the cargo binding.

Although the main role of the kinesin family of motor proteins appears to be in transporting organelles to their correct cellular location, they have also been found to play a role in a diverse range of cellular functions. Kinesins not only transport a wide variety of membranous vesicles and organelles, but are also responsible for the transport of proteins, nucleic acids (including mRNA) and chromosomes [Goldstein and Philp 1999, Titu and Gilbert 1999]. They have been shown to control the organization, movement and stability of

microtubules and are able to crosslink them via a number of binding sites (kinesins have even been shown to form bipolar complexes that can crosslink microtubules and slide them past one another in opposite directions) [Liao and Gundersen 1998, Goldstein and Philp 1999]. Some kinesins are able to affect the stability of microtubule complexes by binding and decreasing the depolymerisation of the microtubule [Wordeman 2005]. It is also possible that kinesin motor proteins possess more specialized functions such as involvement in signal transduction. Kinesins may sequester or tether signalling molecules to the microtubules until receiving the cellular signal to release them. Some kinesins may interact with kinases and may act to bring these kinases to the correct cellular location of their microtubule-bound substrate [Verhey and Rapoport 2001, Adio et al. 2006]. So how do the kinesins perform such a wide range of functions, especially considering their highly homologous motor domain? Although the specificity of kinesin cargo carrying is still not entirely understood, it is accepted that some specificity is due to proteins that constitutively interact with the kinesin protein, called kinesin associated proteins (KAPs). These are discussed below.

4.5.1.4. Kinesin Associated Proteins (KAPs)

Many of the details regarding the molecular movement of kinesins along the microtubules have been elucidated over the years. However, the way in which each distinct kinesin determines its functional specificity is still poorly understood. Some cargoes (e.g. mitochondria) may be moved by multiple types of kinesin, while some kinesins (e.g. kinesin-I) may have many different types of cargo [Goldstein and Philp 1999]. There are several levels at which the functional specificity of each kinesin-family member could be determined. For example, the subcellular localization and cellular environment in which the kinesin exists will determine the availability of both cargo and microtubule structures on which to operate. Structural characteristics inherent in each kinesin family member control important properties such as the oligomerization state of the kinesin complexes and motor directionality and speed. Additionally, proteins that interact with the variable non-motor domains of the kinesins have a large impact on the functional

possibilities of the kinesin motors. This is perhaps the most significant way that the kinesins confer their specificity for their cargo: via the kinesin interacting proteins. There are a number of different categories of these proteins with multiple functions, but perhaps the most important are the Kinesin Associated Proteins (KAPs), of which Kifap3 is a member. These have been found to be tightly associated with their motor protein partners and are believed to be constitutive components of the kinesin protein complex. These proteins are regulatory subunits and play an integral part in the function of the motor complex.

4.5.1.5. KIFAP3

As previously mentioned, a yeast-2-hybrid screen, using munc18c as bait, discovered a protein called Kifap3 to be a novel interactor. Kifap3 (also known as KAP3 and SMAP) is a kinesin associated protein (KAP) (see above), which has been shown to interact with the KIF3 kinesin family member. The KIF3 motor is one of the most abundantly and ubiquitously expressed kinesin protein family members. It is abundantly expressed in nerve tissue and ubiquitously expressed in other tissues in lower amounts. It has phylogenic diversity, being found in organisms ranging from the sea urchin (kinesin II; [Cole et al. 1993]), *Chlamydomonas reinhardtii* (FLA10; [Walther et al., 1994]), *Caenorhabditis elegans* (Cekinesin II; [Signor et al., 1999]), *Drosophila melanogaster* (KLP68D; [Pesavento et al., 1994]), *Xenopus laevis* (Xklp3; [Le Bot et al., 1998]) to higher organisms including mice [Yang Z et al. 1997] and humans [Whitehead et al. 1999].

The KIF3 motor is a complex formed of KIF3A [Aizawa et al.1992, Kondo et al., 1994], either KIF3B [Yamazaki et al., 1995] or KIF3C [Muresan et al. 1998, Yang and Goldstein, 1998] and the associated protein Kifap3 [Yamazaki et al. 1995 and 1996] in an equal ratio. KIF3A and KIF3B (or KIF3A and KIF3C) form a heterodimer that functions as a microtubule-based antereograde (plus end directed) motor for transport of membranous organelles [Yamazaki et. al. 1996]. Kifap3 interacts with the tail domain of this heterodimer. Kifap3 is an unusual kinesin associated protein, as at nearly 100 kDa, it is larger than its motor proteins, which are between 80-95 kDa.

There are two alternatively spliced variants of Kifap3, differing in the carboxy terminal regions, though the functional significance of these two splice variants is unknown. Secondary structure predictions indicate that the protein is almost entirely α-helical and contains a number of Armadillo repeats. The Armadillo motif is a tandemly repeated sequence of approximately 40 amino acid residues. Proteins containing Armadillo repeats have been found to be involved in a wide range of cellular functions in a number of different organisms. However, a function common to many is mediating important protein-protein interactions. The canonical Armadillo repeat consists of three helices, denoted H1, H2, and H3. The H2 and H3 helices pack against each other in an antiparallel fashion and are roughly perpendicular to the shorter H1 helix, with a sharp bend between helices H1 and H2. The neighbouring repeats in an Armadillo repeat protein stack together into a single domain with a continuous hydrophobic core, forming an elongated super-helix [Andrade et al. 2001].

As previously mentioned, because of the experimental evidence already linking both microtubules [Olson et al. 2001, Fletcher et al. 2000] and munc18c [Macaulay et al. 2002, Grusovin and Macaulay 2003, Spurlin et al. 2003, Kanda et al. 2005] to a role in GLUT4 vesicle translocation, the function of Kifap3 in insulin-regulated GLUT4 trafficking was considered worthy of investigation. This chapter aims to investigate the function of Kifap3 by examining its interactions with munc18c using a number of in vitro and in vivo assays.

4.5.2. Results

4.5.2.1 Confirmation of the interaction between Kifap3 and munc18c

To confirm the interaction between munc18c and Kifap3 as seen in the yeast-two-hybrid screen, Kifap3 was first cloned into the pGex5X-1 vector. Once expressed as a GST-tagged protein, a GST pull-down assay was performed. For this, purified GST-tagged

Kifap3 was coupled to glutathione beads and incubated with extracts of Cos-1 cells that had been transiently transfected with Xpress-tagged munc18c. Complexes were washed to remove non-specific binding, separated by SDS-PAGE and immunoblotted with anti-Xpress antibody to assess the co-precipitation of munc18c with Kifap3. As shown in Figure 4.5.2, munc18c did indeed associate with the full length Kifap3 protein (KifFL). Munc18c was not precipitated when extracts were incubated with only GST coupled to glutathione beads (lane 1 figure 4.5.2) indicating that the association between munc18c and Kifap3 is specific. Quantities of the GST fusion proteins were checked by western blotting using an anti-GST antibody and shown to be similar. This shows that differences in amounts of precipitated munc18c for the GST-tagged Kifap3 and GST only proteins is not due to relative amounts of protein.

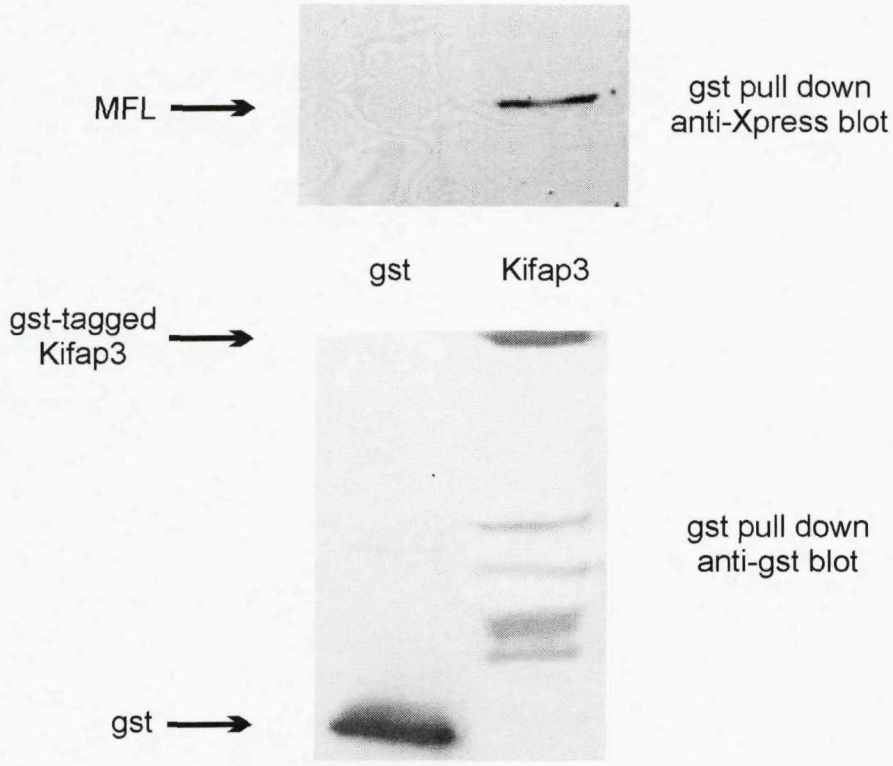

Figure 4.5.2: Confirmation of the interaction between munc18c and Kifap3.

Cos-1 cells were transiently transfected with full-length munc18c expressed as an Xpress fusion. Kifap3 was bacterially expressed as a GST fusion protein and coupled to glutathione sepharose beads. GST bound to glutathione beads was used as a control (GST). Cos-1 cell extracts were incubated with the glutathione bead complexes, and then washed to remove non-specific binding. Proteins were separated by SDS-PAGE, transferred to a nitrocellulose membrane, and probed for Xpress to detect co-precipitated munc18c

4.2.2.2. Determination of the regions of Kifap3 that interact with munc18c

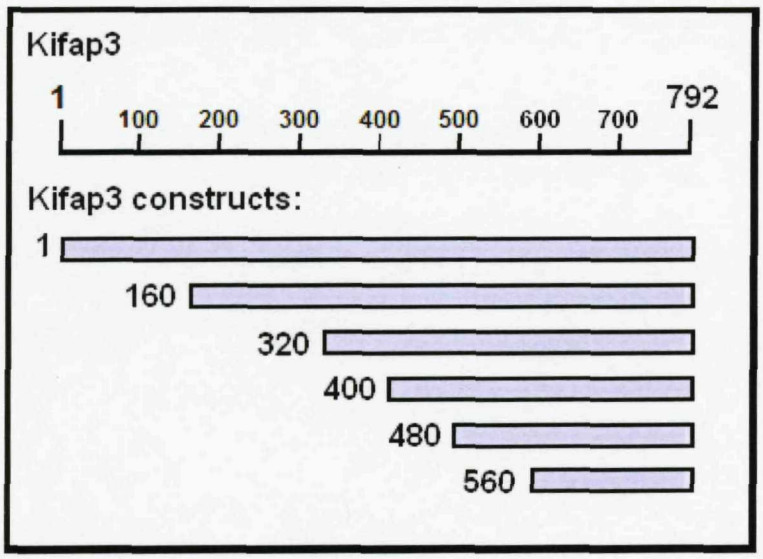

Figure 4.5.3: Kifap3 truncation constructs.

Figure showing the series of truncation constructs of Kifap3 used as GST fusions in a GST pull-down assay to determine the region responsible for binding to munc18c.

To further validate and characterize the interaction between Kifap3 and munc18c, GST pull-down assays were performed, with a series of N-terminal truncation constructs of Kifap3, namely Kif160, Kif320, Kif400, Kif480 and Kif560. Attempts were made to produce a number of other truncation constructs, with N-terminals starting at residues past 480, as well as C-terminal truncation constructs. However, despite continued attempts, bacterial expression of those constructs was not achieved. Purified GST-tagged Kifap3 truncation constructs (see Figure 4.5.3) were coupled to glutathione beads and incubated with extracts of Cos-1 cells that had been transiently transfected with Xpress-tagged munc18c. Complexes were washed to remove non-specific binding, separated by SDS-PAGE and immunoblotted with anti-Xpress antibody to assess the co-precipitation

of munc18c with the Kifap3 constructs. As shown in Figure 4.5.4, munc18c associated with the full length Kifap3 (KifFL) as well as the truncation constructs Kif160, Kif320, Kif400, Kif480 and Kif560. Munc18c was not precipitated when extracts were incubated with only GST coupled to glutathione beads (lane 1 figure 4.5.4) indicating that the association between munc18c and Kifap3 is specific. Quantities of the GST fusion proteins were checked by western blotting using an anti-GST antibody and shown to be similar. This shows that differences in amounts of precipitated munc18c for each Kifap3 construct is not due to relative amounts of the GST-tagged Kifap3 proteins. This result could indicate one of two possibilities: either there are numerous regions all along the protein structure of Kifap3 that enable it to bind to munc18c, or it could be that the region of Kifap3 responsible for its interaction with munc18c lies in the C-terminal 232 amino acids. Expression of the other N-terminal truncation constructs or the C-terminal truncation constructs would be required to test these possibilities.

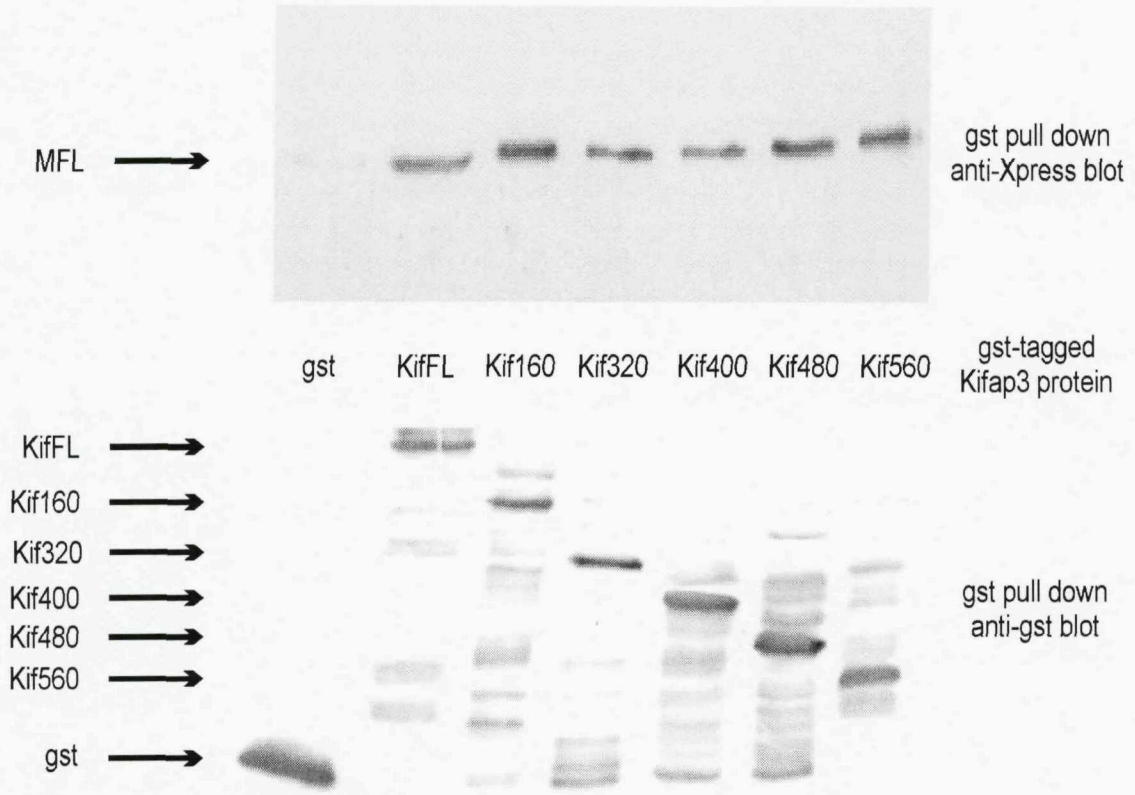

Figure 4.5.4: Determination of the region of Kifap3 that is responsible for binding to munc18c.

Cos-1 cells were transiently transfected with full-length munc18c expressed as an Xpress fusion. Kifap3 constructs were bacterially expressed as GST fusion proteins and coupled to glutathione sepharose beads. GST bound to glutathione beads was used as a control (GST). Cos-1 cell extracts were incubated with the glutathione bead complexes, and then washed to remove non-specific binding. Proteins were separated by SDS-PAGE, transferred to a nitrocellulose membrane, and probed for Xpress to detect co-precipitated munc18c.

4.2.2.3. Determination of the regions of munc18c that interact with Kifap3

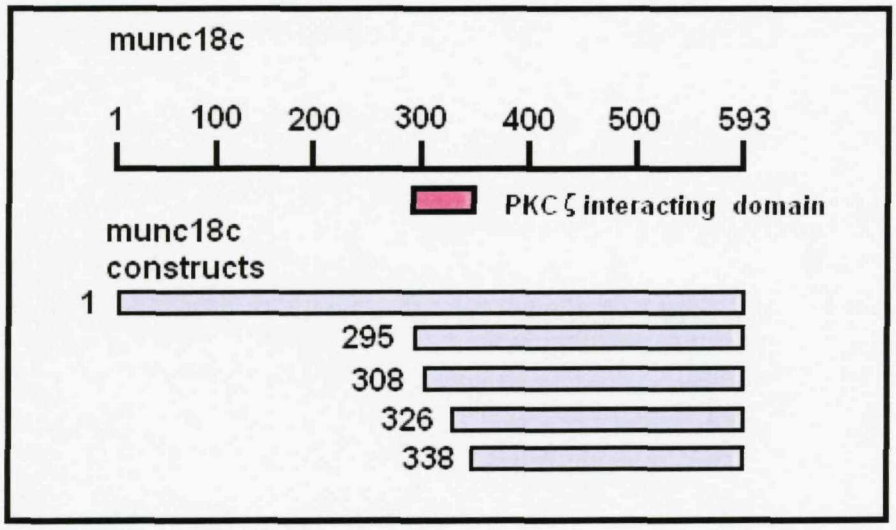

Figure 4.5.5: Munc18c truncation constructs.

Figure showing the series of truncation constructs of munc18c used as GST fusions in a GST pull-down assay to determine the region responsible for binding to Kifap3.

Despite continued efforts it was not possible to achieve enough mammalian cell expression of Kifap3 (or any of the truncation constructs) for visualisation on a Western blot. In order to further validate and characterize the interaction between Kifap3 and munc18c, GST pull-down assays were performed, this time using bacterially expressed GST-tagged Kifap3 and the Xpress-tagged munc18c truncation constructs used in previous chapters. For this, purified GST-tagged Kifap3 was coupled to glutathione beads and incubated with extracts of Cos-1 cells that had been transiently transfected with the Xpress-tagged munc18c truncation constructs (see figure 4.5.5). Complexes were washed to remove non-specific binding, separated by SDS-PAGE and immunoblotted with anti-Xpress antibody to assess the co-precipitation of the munc18c constructs with Kifap3. As

shown in Figure 4.5.6, Kifap3 associated with the full length munc18c (MFL) as well as the truncation constructs M295, M308, M326 and M338 (figure 4.5.6.A top panel, lanes 6-10.) None of the munc18c constructs were precipitated when extracts were incubated with only GST coupled to glutathione beads (figure 4.5.6.A top panel, lanes 1-5,) indicating that the association between Kifap3 and the munc18c constructs was specific. Quantities of the Xpress-tagged munc18c constructs were checked by western blotting using an anti-Xpress antibody and shown to be similar (figure 4.5.6.B, lanes 1-5). This shows that differences in amounts of precipitated munc18c are not due to relative amounts of the Xpress-tagged munc18c proteins. Quantities of the GST only control or GST-tagged Kifap3 protein were checked by western blotting using an anti-GST antibody and shown to be similar (figure 4.5.6.A bottom panel, lanes 1-10). This shows that differences in amounts of precipitated munc18c are not due to relative amounts of the GST proteins.

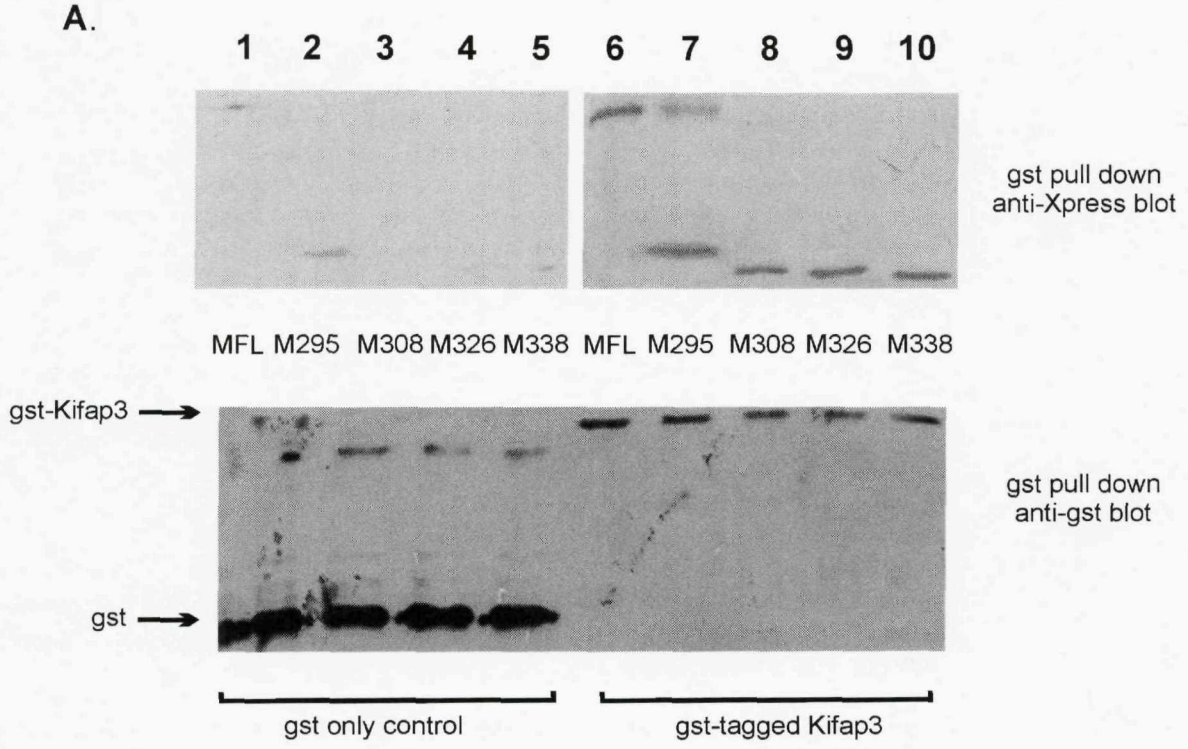

See next page for figure legend

Figure 4.5.6: Determination of the region of munc18c that is responsible for binding to Kifap3.

Cos-1 cells were transiently transfected with full-length munc18c (MFL) or one of the munc18c truncation constructs M295, M308, M326 or M338 expressed as Xpress fusion proteins. Full length Kifap3 was bacterially expressed as a GST fusion protein and coupled to glutathione sepharose beads. GST bound to glutathione beads was used as a control (GST). Cos-1 cell extracts were incubated with the glutathione bead complexes then washed to remove non-specific binding. Proteins were separated by SDS-PAGE, transferred to a nitrocellulose membrane, and probed for Xpress to detect the co-precipitated munc18c constructs.

(A.) GST only control (lanes 1-5) or GST-tagged Kifap3 (lanes 6-10) were used to pull down Xpress-tagged munc18c constructs MFL (lanes 1 and 6), M295 (lanes 2 and 7), M308 (lanes 3 and 8), M326 (lanes 4 and 9 or M338 (lanes 5 and 10). The top panel is an anti-Xpress blot to show the precipitated munc18c constructs. The bottom panel is an anti-GST blot to show the GST or GST-tagged Kifap3 proteins.

(B.) Cell extracts of Xpress-tagged munc18c constructs, MFL (lane 1), M295 (lane 2), M308 (lane 3), M326 (lane 4) or M338 (lane 5). Anti-Xpress blot shows 10% of the total cell extract used for the GST pull-down assays.

This result could indicate one of two possibilities: either there are numerous regions all along the protein structure of munc18c that enable it to bind to Kifap3, or it could be that the region of munc18c responsible for its interaction with Kifap3 lies in the C-terminal 254 amino acids (past residue 338). If time had have permitted, further C-terminal truncation constructs of munc18c could have been used to test these possibilities.

4.2.2.4. Interactions between munc18c and Kifap3 *in vivo*, as ascertained by FCS

As mentioned previously, despite continued efforts, there were great difficulties in expressing Kifap3 in mammalian cell lines and I was unable to get expression levels high enough for detection on Western blots. However, when Kifap3 was transfected into cells in the ECFP-N2 vector, expression levels obtained were high enough for detection of the fluorescence by the microscope. For the following in vivo experiments, detection of the cyan fluorescence was used to check for the expression of the ECFP-tagged Kifap3 protein. The expression levels of the fluorescent proteins are required to be low in order for data to be obtained using fluorescence correlation spectroscopy (if the fluorescence intensity of the protein of interest is too high, any small fluctuations in florescence intensity will be relatively too small to detect). This made FCS an ideal way to study the low expressing Kifap3 protein. All experiments described in this section were conducted as in Section 4.2.2, and data is presented as diffusion co-efficients in μs.

I firstly wanted to investigate whether the presence of Kifap3 had any bearing on munc18c. Firstly, it was investigated to see whether the diffusion coefficient of munc18c was affected by insulin stimulation. For this, full length munc18c was expressed in 3T3-L1 adipocytes as an EYFP-tagged fusion protein (MFL). Insulin had no effect on the average diffusion coefficient when MFL was expressed alone (480 ± μs 37 μs pre insulin stimulation vs. 649 ± 85 μs post insulin stimulation; mean ± s.e.m.) (Figure 4.5.7, Table 4.5.1.)

It was then examined to see whether the co-expression of Kifap3 had an effect on the diffusion coefficient of MFL. 3T3-L1 adipocytes were transfected with EYFP-tagged MFL and ECFP-tagged Kifap3. In both the basal and insulin stimulated states, the presence of Kifap3 dramatically increased the diffusion coefficient of the EYFP-tagged MFL. In the basal state, the diffusion coefficient for MFL increased from 480 ± 37 μs when MFL was expressed alone, compared to 1148 ± 135 μs when Kifap3 was co-expressed. In the insulin stimulated state, the diffusion coefficient for MFL increased from 649 ± 85 μs when MFL was expressed alone, compared to 1231 ± 225 μs when Kifap3 was co-expressed. Figure 4.5.7, Table 5.5.1).

Construct(s) overexpressed		Diffusion coefficient (μs) Mean ± s.e.m.	
EYFP	ECFP	- insulin	+ insulin
MFL	-	480 ± 37	649 ± 85
MFL	Kifap3	1148 ± 135	1231 ± 225

Table 5.5.1: Diffusion coefficients for MFL

3T3-L1 adipocyte cells were transiently transfected with EYFP-tagged MFL (control) or EYFP-tagged MFL plus ECFP-tagged Kifap3. Where appropriate, cells were stimulated with 10^{-7} M insulin for 20 minutes. FCS data was collected for the EYFP-tagged protein only and are shown as the mean ± s.e.m. each using 6 separate cells.

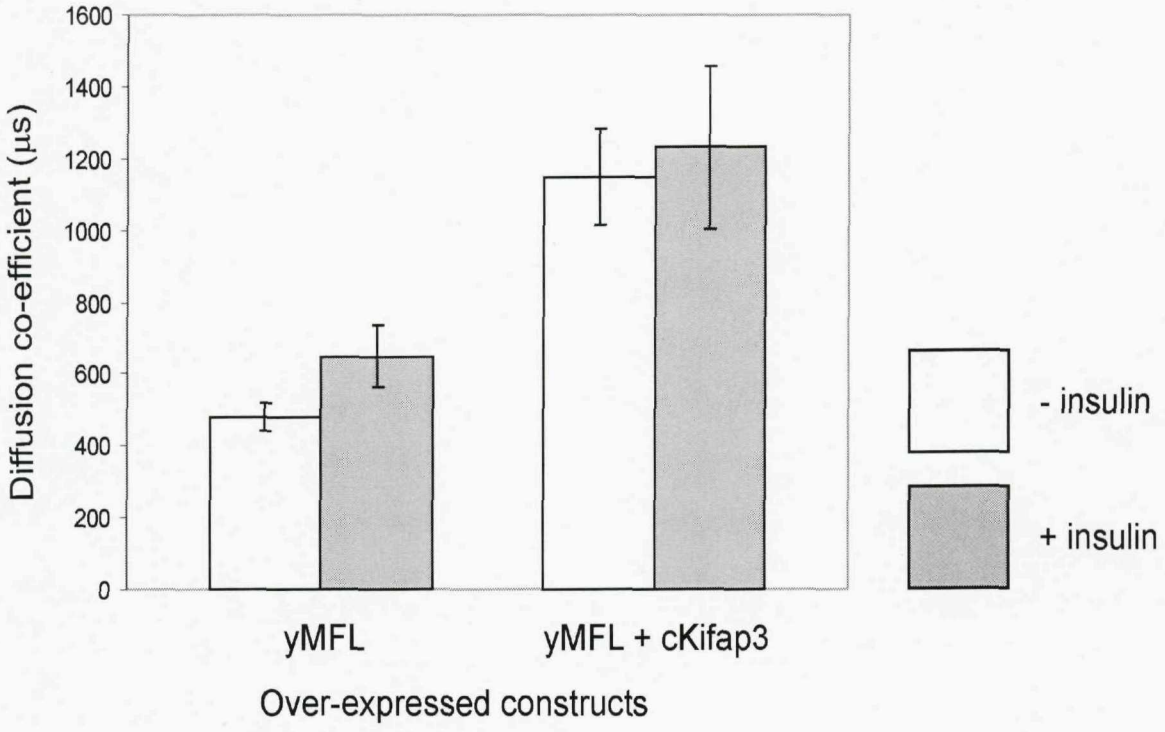

Figure 4.5.7: Diffusion coefficients for MFL

3T3-L1 adipocyte cells were transiently transfected with EYFP-tagged MFL or EYFP-tagged MFL plus ECFP-tagged Kifap3. Where appropriate, cells were stimulated with 10^{-7} M insulin for 20 minutes. FCS data was collected for the EYFP-tagged protein only and are shown as the mean ± s.e.m. each using 6 separate cells.

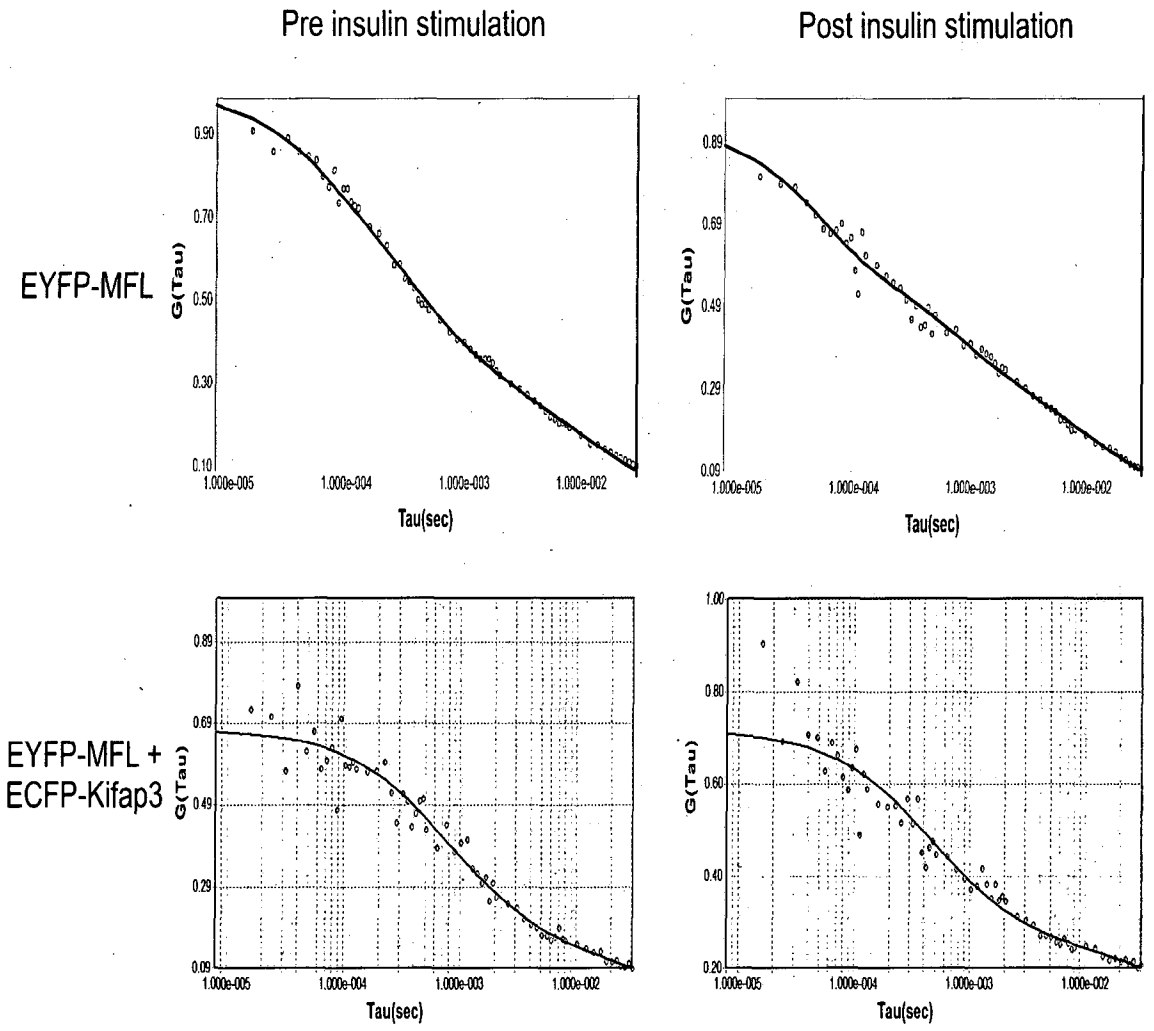

Figure 4.5.8. Example FCS traces for EYFP-tagged MFL

3T3-L1 adipocyte cells were transiently transfected with EYFP-tagged MFL (control) or EYFP-tagged MFL plus ECFP-tagged Kifap3. Cells were serum starved for 24 hours prior to data collection. Where appropriate, cells were stimulated with 10^{-7} M insulin for 20 minutes. FCS data was collected for the EYFP-tagged protein only.

4.2.3. Discussion

By use of GST pull down assays, I have shown that munc18c forms a novel interaction with a protein called Kifap3. All of the series of truncation constructs of Kifap3 bound to munc18c. This could suggest one of two possibilities, either the C-terminal section of Kifap3 (residues 560-792) is solely responsible for binding to munc18c and residues 1-560 are not involved in binding, or it could be that various sections along the Kifap3 structure are responsible for and sufficient for its binding to munc18c. Kifap3 has no homology to any known proteins and is composed mostly of tandem armadillo repeats [Yamazaki et. al. 1996]. Armadillo repeat proteins contain tandem arrays of multiple imperfect repeats which are believed to mediate protein:protein interactions. Each repeat often has multiple binding partners and functions [Peifer et al. 1994]. It may therefore be possible that one or more of the Armadillo repeats at the C-terminal end of the Kifap3 structure is responsible/sufficient for adequate binding to munc18c. Future work needs to include the production of C-terminal truncations of Kifap3 and N-terminal truncation constructs with the N-terminus past residue 560. Attempts were made to produce such constructs, but various problems with both the cloning and/or the bacterial expression of such constructs prevented any additional insight into the interactions between munc18c and Kifap3 from being obtained. If time had been permitting, greater efforts could have been made to produce additional Kifap3 constructs. These could then have been used in more GST pull-down assays with a view to finding a small region of the structure that is critical for its binding to munc18c. This would enable the production of a non-interacting mutant, so that the role of the Kifap3:munc18c interaction could be studied further.

By use of GST pull-down assays, I attempted to define the interaction site on munc18c for Kifap3. All of the series of truncation constructs of munc18c bound to Kifap3. This could suggest one of two possibilities, either the C-terminal section of munc18c (residues 338-592) is solely responsible for binding to Kifap3 and residues 1-338 are not involved, or it could be that various sections along the munc18c structure are responsible for and sufficient for its binding to Kifap3. As mentioned above, future work needs to include the production of C-terminal truncations of munc18c with a view to finding a small region of

the structure that is critical for its binding to Kifap3. This would enable the production of a non-interacting mutant, so that the role of the Kifap3:munc18c interaction could be studied in mammalian cells using over-expression studies.

Fluorescence correlation spectroscopy was used as a way to test the validity of the munc18c:Kifap3 interaction in vivo. The results obtained support the hypothesis of an interaction occurring between these two proteins. The co-expression of Kifap3 dramatically increased the diffusion co-efficient of munc18c in both the basal and insulin stimulated states, suggesting that they interact both pre and post insulin stimulation. Binding of munc18c to Kifap3 would indeed cause a large increase in diffusion co-efficient of munc18c. Kifap3 is a large globular protein of ~100 kDa which is intrinsically bound to the KIF3 motor, which is itself nearly 200 kDa in size [Yamazaki et al. 1996]. The large size of this protein complex, as well as its attachment to the cellular network of microtubules would be sufficient to cause such an increase of diffusion co-efficient for munc18c.

Much work has been published on the role of the cytoskeleton on insulin-mediated GLUT4 vesicle trafficking. There has however been disputing evidence with regard to the exact role of the microtubules in insulin-mediated GLUT4 vesicle trafficking. Although the cytoskeletal network is important for insulin-induced glucose uptake, several studies have assessed the effects of microtubule disruption on glucose transport with divergent results. There are some (though few) reports that suggest that disruption of the microtubule network has little or no effect to glucose transport [Ai et al. 2003, Molero et al. 2001]. However, the vast majority of experimental evidence shows that microtubules do indeed perform an essential role in the GLUT4 vesicle trafficking required for insulin-mediated glucose transport. Most evidence suggests that both the actin [Kanzaki and Pessin 2001, Liu L.Z. et al. 2006, Liu, X.J. 2007, Omata et al. 2000] and microtubule [Semiz et al. 2003, Eyster et al. 2006, Fletcher et al. 2000, Liu, L.B., 2003, Huang et al. 2005] networks are involved in this process.

The increase in GLUT4 vesicle exocytosis in response to insulin and the possible involvement of microtubules in this process could arise from a variety of regulated steps.

These include the fusion of GLUT4 vesicles with the plasma membrane, stimulation of the rate of movement of vesicles to the plasma membrane, increased fission from an endosomal precursor, or a combination of these processes. Until recently, few studies have been able to distinguish the exact role of microtubules, but have just shown that pharmalogical disruption of the microtubule network (with agents such as nocodazole or colchicine) inhibits insulin-mediated GLUT4 vesicle exocytosis and glucose transport.

It is worth speculating that it is the KIF3 motor and Kifap3 that are responsible for delivering the GLUT4 vesicle to munc18c (and the other membrane trafficking proteins) at the plasma membrane and that this is why the results from this thesis show an interaction between Kifap3 and munc18c. However, this explanation seems unlikely. Firstly, the FCS data from this thesis does not suggest that there is an increase in association between Kifap3 and munc18c upon stimulation with insulin. Secondly, recent evidence suggests that the microtubule network is responsible for the organization of the insulin signalling complex and the movement of the GLUT4 vesicles in the basal state, but not for the rearrangement of the GLUT4 vesicles in response to insulin [Eyster et al. 2006, Huang et al. 2005, Shigematsu et al. 2002]. The work from these papers also shows that this microtubule-dependent distribution and correct positioning of the GLUT4 vesicles in the perinuclear region is required for insulin stimulated GLUT4 translocation and glucose transport. Dispersion of the GLUT4 vesicles from the perinuclear region allows them to engage with insulin sensitive actin filaments for translocation to the plasma membrane (in a PI3K-dependant manner). Work has also shown that KIF3 siRNA does not inhibit insulin-mediated GLUT4 translocation to the plasma membrane after disruption of the microtubules by nocodazole [Huang et al. 2005]. These pieces of evidence, coupled with the FCS data from this thesis, rule out the possibility that the KIF3 motor and Kifap3 are responsible for insulin-mediated delivery of GLUT4 to munc18c at the plasma membrane.

Assessing the evidence from this thesis and the published data, the most plausible role for Kifap3 and the KIF3 motor with regards to insulin action would seem to be to deliver munc18c to its correct localisation at the plasma membrane. Research from various

laboratories (and section 4.3 of this thesis) show that munc18c does not merely inhibit GLUT4 vesicle docking, but actually plays an intrinsic role in the docking and fusion of the GLUT4 vesicle at the plasma membrane in response to insulin. As has been discussed in section 4.3.1., evidence suggests that although munc18c:syntaxin4 interaction is not required for the insulin-stimulated trafficking to and association with the cell surface, the interaction between munc18c and syntaxin4 is required for the integration of the GLUT4 storage vesicles into the plasma membrane [Thurmond et al. 2000, Oh et al. 2005, Latham et al. 2006]. It is hence possible that some of the decrease in glucose transport seen when microtubule networks are disrupted is due to the improper localization of munc18c. Although siRNA directed against the KIF3 motor did not cause a decrease in the translocation of GLUT4 vesicles in response to insulin [Huang et al. 2005], the effect of KIF3 siRNA on glucose transport, GLUT4 vesicle docking or insertion into the plasma membrane were not investigated. Additionally, earlier work from the same laboratory has shown that inhibition of KIF3 function using microinjection of a KIF3 antibody does inhibit GLUT4 vesicle exocytosis [Imamura 2003]. Such investigations would be an ideal extension to the work carried out in this thesis.

Future work should include immunohistochemistry of adipocytes using antibodies for Kifap3 and munc18c in order to determine the subcellular location of both proteins. Obtaining a Kifap3 antibody would enable the study of the endogenously expressed protein, rather than having to rely on over-expression of the tagged Kifap3 protein. Knockdown methods such as siRNA could then be employed in order to study the function of this protein. Another alternative to the problems encountered with expression of this protein would be to produce a cell line stably expressing Kifap3. Unfortunately, time restraints prevented the production of a stable cell line during the course of this thesis.

Experiments to be performed in order to test the hypothesis that Kifap3 functions to deliver munc18c to its correct cellular location should include the production of non-interacting mutants of Kifap3 and/or munc18c. The subcellular location of munc18c could be assessed by the use of fluorescently tagged vectors and microscopy, or by the

use of immunohistochemistry. This could be performed with both the full length proteins and a non-interacting mutant, in order to see if disruption of munc18c:Kifap3 interactions affect the subcellular location of munc18c. Glucose transport assays could then also determine the effect of this interaction on insulin mediated glucose transport.

Because of the associations between 80K-H and PKCζ with munc18c previously discussed in this thesis, it may be interesting to study interactions between both 80K-H and PKCζ with Kifap3 using techniques similar to the ones mentioned above. It would be particularly interesting to study potential interactions between PKCζ and Kifap3, considering the work of Imamura et al. on PKCλ [Imamura et al. 2003]. The work performed in this research article investigated PKCλ (an atypical PKC isotype, with much structural and functional similarity to PKCζ: see section 1.5.2.2.4.2. of this thesis), Rab4 (a small GTPase involved in regulation of membrane transport: see section 1.5.2.4. of this thesis) and KIF3. The work showed that insulin can stimulate both Rab4 and KIF3 activities through a PKCλ dependent signalling mechanism and that activated (GTP-bound) Rab4 can associate with KIF3. They propose a model in which insulin leads to activation of Rab4 within GLUT4 vesicles, thereby enabling recognition of the GLUT4 vesicle by the motor protein KIF3. PI3-kinase-dependent activation of PKCλ facilitates this process and may promote the activation of KIF3 with respect to its microtubule binding and motility functions. As mentioned, PKCλ is closely related to PKCζ and there is evidence to suggest that the two proteins can function interchangeably [Bandyopadhyay et al. 1999, Idris et al. 2001, Moscat and Diaz-Meco 2000, Ohno and Nishizuka 2002]. This, together with the evidence from this thesis of both munc18c's association with Kifap3 and PKCζ's association with munc18c and role in GLUT4 vesicle trafficking strongly suggest a role for Kifap3 in this process. The cellular roles of Kifap3 and its interactions with proteins of the GLUT4 vesicle trafficking machinery hence warrant further investigation.

4.6. 80K-H: insulin-dependent PKB phosphorylation?

4.6. 80K-H: insulin-dependent PKB phosphorylation?

4.6.1. Introduction

The phosphorylation state of proteins within signalling pathways is the key regulator of their activity, and controls the progression of a signal down a pathway. The phosphorylation and dephosphorylation of proteins must therefore be exquisitely controlled in order to maintain normal functioning of the signalling pathways. As previously mentioned, two kinases that are fundamental to cellular control of the insulin signalling cascade are PKB (also known as Akt) and the atypical PKCs (PKCζ and PKCι/λ). PKB acts as a transducer of many functions initiated by growth factors' activation of PI3K. PKB has shown to be involved in a huge variety of cellular processes, particularly playing a substantial role in various aspects of metabolism [Whiteman, 2002]. Of specific interest is the evidence linking PKBβ to GLUT4 vesicle translocation and glucose transport [Katome et. al., 2003, Bae et. al 2003],though despite the great deal of experimental evidence for PKB's involvement in insulin signalling, it's physiological substrates and role in the signalling pathways involved are yet to be elucidated. The minimum consensus sequence for efficient phosphorylation by Akt/PKB is Arg-Xaa-Arg-Yaa-Zaa-Ser/Thr-Hyd, where Xaa is any amino acid, Yaa and Zaa are small amino acids other than glycine, and Hyd is a bulky hydrophobic residue [Alessi et. al., 1996]. Although protein database searches (such as Prosite) identify numerous proteins with such a consensus sequence, few have been shown to be substrates for PKB *in vitro*, yet alone *in vivo*. A motif scan of 80K-H (http://scansite.mit.edu/) identified a PKB phosphorylation motif at Ser24 (VKRPRGV**S**LTNHHFY). Due to the evidence linking PKB activity to insulin signalling and glucose transport and the possible involvement of 80K-H in GLUT4 vesicle translocation [Hodgkinson et. al., 2005], further investigation into the putative phosphorylation of 80K-H by PKB was considered important.

4.6.2. Results

The antibody I used for this study was a phospho-PKB substrate motif antibody (NEB). This antibody claims to recognize the phosphorylated PKB substrate motif regardless of the flanking protein sequence, so can be used to assess PKB-dependent phosphorylations. As shown in figure 4.17, the antibody was shown to work and showed Cos-1 cells to be insulin responsive, with a number of phosphorylations by PKB in response to insulin.

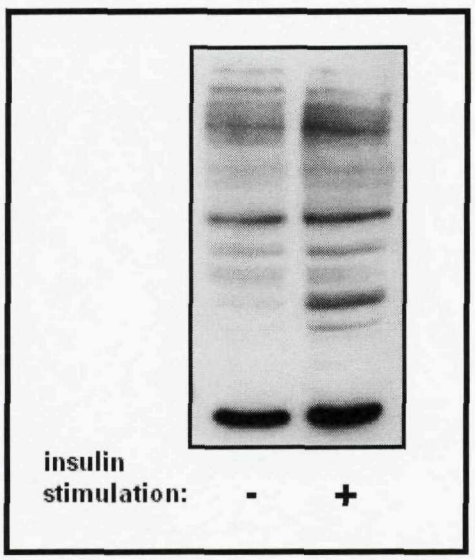

Figure 4.6.1: Insulin-responsive PKB phosphorylation

Cos-1 cells were either left unstimulated or stimulated with 10^{-7} M insulin for 10 minutes. Proteins were separated by SDS-PAGE, transferred to a nitrocellulose membrane, and probed for phospho-PKB substrate motifs to assess any increases in PKB phosphorylation after insulin stimulation.

Once the cells had been shown to be insulin responsive, a simple western blot was performed using extracts of Cos-1 cells. Cos-1 cells were either left untransfected, or transfected with full length 80K-H expressed as an Xpress fusion. Insulin was added to

one transfected and one untransfected flask of cells to a concentration of 10^{-7} M for 10 minutes at 37°C. Cell lysates were prepared and proteins separated by SDS-PAGE. The membranes were then immunoblotted with phospho-PKB substrate antibody to show any changes in phosphorylation of PKB substrate motifs, and Xpress antibody to show the expression of 80K-H in the transfected cells. Lanes 3 and 4 of Figure 4.18 show the expression of the Xpress-tagged 80K-H in Cos-1 cells. Lanes 5-8 show the presence of phosphorylated PKB-substrate motifs and show that there are none corresponding to the molecular weight of 80K-H, with or without insulin stimulation or 80K-H over-expression. This shows that 80K-H was likely not phosphorylated by PKB, even after insulin stimulation.

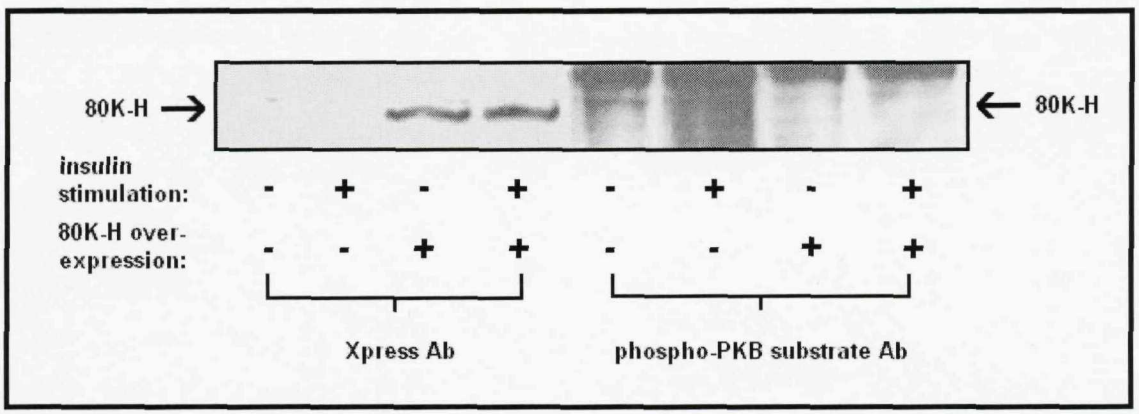

Figure 4.6.2: Investigation into putative 80K-H phosphorylation by PKB in Cos-1 cells

Cos-1 cells were left un-transfected, or transiently transfected with full-length 80K-H expressed as an Xpress fusion. For those required, cells were stimulated with 10^{-7} M insulin for 10 minutes. Proteins were separated by SDS-PAGE, transferred to a nitrocellulose membrane, and probed for both Xpress and phospho-PKB substrate motifs.

However, the above result did not categorically show that PKB was not phosphorylating 80K-H. In order to concentrate the amount of 80K-H and therefore increase the

sensitivity of detection in the protein samples for SDS-PAGE, immunoprecipitations were performed. For this, Cos-1 cells were transiently transfected with Xpress-tagged 80K-H and either left unstimulated, or stimulated with 10^{-7} M insulin for 10 minutes before production of a cell lysate. Anti-Xpress antibody was coupled to a mixture of Protein A-coated agarose and Protein G-coated agarose beads and incubated with the Cos-1 cell extracts. Complexes were washed to remove non-specific binding and separated by SDS-PAGE. Once transferred to a nitrocellulose membrane, proteins were immunoblotted with anti-Xpress antibody to assess the precipitation of the 80K-H and anti-phospho-PKB substrate to detect for the presence of phosphorylated PKB substrate motifs. As shown in Figure 4.19, 80K-H immunoprecipitated with the Xpress antibody (lanes 3 and 4). However, there was no phosphorylated PKB substrate motif corresponding to 80K-H, with or without insulin stimulation. This shows that 80K-H is not a substrate for PKB, before or after activation by insulin.

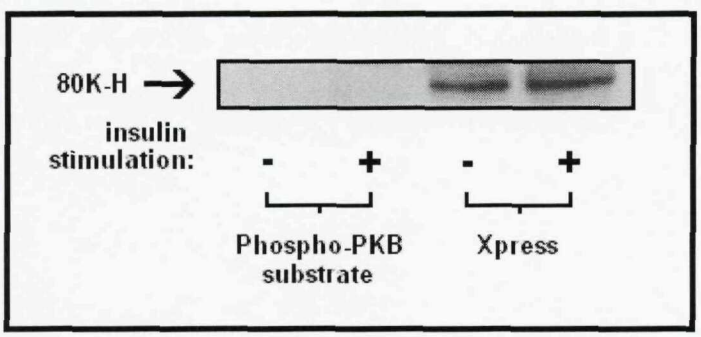

Figure 4.6.3: Investigation into putative 80K-H phosphorylation by PKB in Cos-1 cells

Cos-1 cells were transiently transfected with full-length 80K-H expressed as an Xpress fusion. For those required, cells were stimulated with 10^{-7} M insulin for 10 minutes. Anti-Xpress antibody was coupled to a mixture of Protein A-coated agarose and Protein G coated agarose beads. Cos-1 cell extracts were incubated with the Protein A/Protein G bead complexes, and then washed to remove non-specific binding. Proteins were separated by SDS-PAGE, transferred to a nitrocellulose membrane, and probed for both Xpress and phospho-PKB substrate.

I next wanted to ensure that the above results weren't cell-specific and wanted to check for PKB phosphorylation of 80K-H in a more canonical insulin-sensitive cell line. For this, I performed an immunoprecipitation of endogenous 80K-H in 3T3-L1 adipocytes. 3T3-L1 cells were differentiated into adipocytes (as described in methods). Cells were either left unstimulated, or were stimulated with 10^{-7} M insulin for 10 minutes before production of a cell lysate. Anti-80K-H antibody was coupled to a mixture of Protein A-coated agarose and Protein G-coated agarose beads and incubated with the 3T3-L1 adipocyte cell extracts. Complexes were washed to remove non-specific binding and separated by SDS-PAGE. Once transferred to a nitrocellulose membrane, proteins were immunoblotted with anti-80K-H antibody to assess the precipitation of the 80K-H and anti-phospho-PKB substrate to detect for the presence of phosphorylated PKB substrate motifs. As shown in Figure 4.20, 80K-H immunoprecipitated with the 80K-H antibody (lanes 3 and 4). However, there was no phosphorylated PKB substrate motif corresponding to 80K-H, with or without insulin stimulation. This shows that 80K-H is not a substrate for PKB, before or after activation by insulin, even in highly insulin-responsive cells.

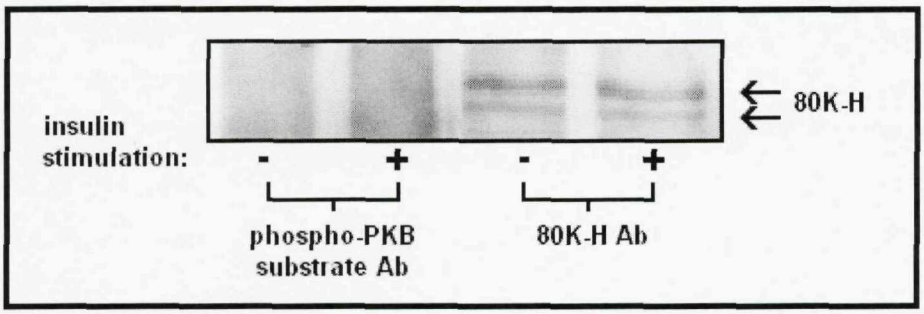

Figure 4.6.4: Investigation into putative 80K-H phosphorylation by PKB in 3T3-L1 adipocytes

Untransfected 3T3-L1 adipocyte cells were stimulated with 10^{-7} M insulin for 10 minutes. Anti-80K-H antibody was coupled to a mixture of Protein A-coated agarose and Protein G coated agarose beads. 3T3-L1 adipocyte cell extracts were incubated with the Protein A/Protein G bead complexes, and then washed to remove non-specific binding. Proteins were separated by SDS-PAGE, transferred to a nitrocellulose membrane, and probed for both 80K-H and phospho-PKB substrate.

4.6.3. Discussion

By use of western blotting and immunoprecipitation, I have shown that 80K-H is not a substrate for PKB, before or after insulin stimulation in both Cos-1 cells and 3T3-L1 adipocytes. These results suggest that although 80K-H does contain an R X R X X S/T PKB phosphorylation motif, it may not be accessible to PKB when the protein is in its folded state. Western blotting of both cell extract and immunoprecipitated 80K-H from Cos-1 cells showed no phosphorylated PKB substrate motif corresponding to 80K-H, before or after insulin stimulation. Although immunoprecipitation of 80K-H from 3T3-L1 adipocytes showed there to be no PKB phosphorylation of 80K-H, it may be possible that there was insufficient amounts of endogenous 80K-H for detection by western blotting. Ideally, the same immunoprecipitation should also be performed with over-expression of 80K-H, though this has, as yet, not been possible in our laboratory. This apparent negative result may also have been caused by an issue with the sensitivity/specificity of the phospho-PKB substrate antibody. Although it has been shown to detect numerous phosphorylated PKB substrate motifs, it is unlikely to detect all phospho-PKB substrates with the same degree of affinity and may therefore not adequately detect the particular motif of interest in the 80K-H protein. Ways to overcome this problem would be to either have an antibody made to the PKB substrate motif on 80K-H, or to extend the experiments already conducted using the antibodies that are already available. Such experiments should include the production of a full length 80K-H construct with the mutation of the serine in the PKB substrate motif to an amino acid such as alanine. A phosphate-incorporation assay could then be performed using cells over-expressing wildtype or mutant 80K-H pre- and post-insulin stimulation to see if such a mutation causes a decrease in phosphorylation. This experiment could then be furthered by repetition after PKB depletion or inhibition. Many PKB inhibitors are commercially available and our laboratory already has a working protocol for the depletion of the three isoforms of PKB using antisense, making this a logical experimental progression if time had have permitted.

SUMMARY AND FUTURE WORK

5. Summary and future work

Insulin is the key anabolic hormone and is responsible for a vast array of cellular and physiological processes, the most important of these being the maintenance of glucose homeostasis. Insulin causes activation of numerous signalling cascades which result in the selective targeting of the GLUT4 vesicle to specific areas of the plasma membrane, thus allowing glucose to enter the cell from the circulation. Although much is known of proteins in the signalling pathways (for example PKCζ) and of the vesicle trafficking machinery (for example syntaxin4, VAMP2 and munc18c), it was only recently that a protein called 80K-H was identified as the missing link between these two aspects of GLUT4 vesicle translocation. To this end, a variety of in vitro and in vivo techniques were employed to determine the roles of these proteins in GLUT4 vesicle exocytosis and ascertain how the signalling pathways couple to the vesicle trafficking machinery. The results show that 80K-H plays an integral part in the process of GLUT4 vesicle exocytosis. It suggests that, in the basal state, munc18c is bound to syntaxin4 via the N-terminal 295 amino acids of munc18c. 80K-H is bound to munc18c whilst also tethered at the plasma membrane by some other large complex. Insulin stimulation activates PKCζ, which then moves to the plasma membrane. PKCζ releases 80K-H from its membrane tether. This allows a repositioning of munc18c on syntaxin4, via an additional binding site found between residues 295-592 of munc18c. This repositioning of munc18c on syntaxin4 allows an interaction to occur between syntaxin4 and VAMP2, thus lowing the GLUT4 vesicle to dock and fuse at the membrane.

Although in vitro techniques such as GST pull down assays and co-immunoprecipitations are valuable tools for studying protein:protein interactions, results from such experiments should be treated with some caution if there is no in vivo data to support it. Binding of GST-tagged proteins may be affected not only by the GST-tag, but also because the protein is produced in bacteria rather than in the cells being studied. This means that there may be differences in the post-translational modifications of the protein, which may have an impact on its function, including its ability to bind other proteins. As well as the

makeup of the protein, the issue of subcellular localization is not addressed in any *in vitro* assay. Even if endogenous proteins can be made to interact *in vitro*, they may never be in the correct locality at the correct time within the cell for an interaction to occur. One of the best ways to overcome this problem is to use fluorescently-tagged proteins. These can then be used for live cell imaging and *in vivo* fluorescent techniques such as the FCS (fluorescence correlation spectroscopy) used in this thesis.

Another fluorescence microscopy technique which is an ideal method for studying protein:protein interactions, such as the ones studied here, is FRET (fluorescence resonance energy transfer). EYFP and ECFP function as a donor-acceptor pair for fluorescence resonance energy transfer (FRET), in which excitation of the donor (cyan) molecule leads to emission from the acceptor (yellow) molecule, provided that the proteins are close enough for energy transfer to occur. FRET can therefore be used to monitor direct protein-protein interactions between EYFP and ECFP fusion proteins in living or fixed cells and would have therefore been an ideal technique for use in this study. However, attempts to use this method were unsuccessful. This was most likely due to the ECFP and EYFP tags being too far apart on the proteins studied if/when binding occurred. Because of this, the FCS technique was employed.

It would have been highly beneficial to study the subcellular localization of the proteins of interest using the fluorescently tagged proteins. Attempts were made to do this with the confocal microscope, but were unfortunately unsuccessful. CHO cells have an intricate system of internal membranes which means that confocal pictures of them are poor and makes subcellular localization studies with them impossible. The best cells for studying the subcellular localization of insulin responsive proteins are muscle and fat cells, the most commonly used being L6 myotubes and 3T3-L1 adipocytes. However, our laboratory does not have the facilities to transfect such cells and I had little success developing such techniques, despite continued efforts. Future work must include further development of the electroporation technique that was tried for transfection of the L6 myotubes and 3T3-L1 adipocytes. This will enable experiments such as subcellular

localization studies to be performed on such cells and would be extremely beneficial to future work in the laboratory.

The results for munc18c and syntaxin4 are novel and exciting and warrant further investigation. The results from this thesis suggest that insulin causes a repositioning of munc18c, rather than causing its release from VAMP2. These results are supported by journals published since the completion of this PhD and the Biochemical Journal paper from this thesis (please see appendix) [D'Andrea-Merrins et al. 2007, Latham et al. 2007, Hu et al. 2007].

The available results suggest that the second (insulin stimulated) binding site lies between residues 295-592 of munc18c. Attempts were made to see if the munc18c construct, M295, did bind to syntaxin4 upon insulin stimulation, but these were unsuccessful. GST pull-down assays were performed, with GST-tagged syntaxin4 used to pull-down X-press tagged M295. However, these showed no binding of M295 to syntaxin4 prior to, or post insulin stimulation. This does not mean that the conclusions drawn from this thesis are incorrect, but emphasises the points made above regarding the use of in vitro assays. Seeing as the syntaxin4 was bacterially expressed, it was only the munc18c protein that was first stimulated with insulin before performing the pull-down assay. It is highly likely that insulin also has to act on the syntaxin4 protein in order for the repositioning of munc18c to occur. Future work should include attempting to express syntaxin4 in mammalian cell lines. Ideally 3T3-L1 adipocytes or L6 myotubes should be used to over-express syntaxin4 or various truncation constructs of munc18c. Unfortunately, there was little success with this during this thesis. These could then be used for a co-immunoprecipitation using cell extracts from basal and insulin stimulated cells. If this did confirm the presence of another binding site for syntaxin4 on munc18c, then attempts should be made to identify the precise location of it on munc18c. A deletion mutant of munc18c could then be made and used for a glucose transport assay. If GLUT4 vesicle exocytosis is indeed dependent on the repositioning of munc18c on syntaxin4 through this second binding site, then over-expressing such a mutant should cause a decrease in glucose transport.

Previous studies have shown the N-terminal section of munc18c to be essential for binding to syntaxin4 but have also suggested that there may be another binding site on munc18c, similar to that seen with munc18a [*Traffic* 7 1–12]. How could insulin cause this repositioning of munc18c on syntaxin4? The first obvious suggestion is 80K-H. The data show that 80K-H is bound to munc18c in both the basal and insulin stimulated states. It is possible that 80K-H, when "tethered" at the membrane in the basal state, is responsible for holding munc18c in position on syntaxin4. It is possible that it is the freeing of 80K-H from this tethering complex that allows munc18c to reposition on syntaxin4. This would mean that removal of the section of 80K-H responsible for its tethering would cause munc18c to reposition on syntaxin4 and enable GLUT4 vesicle exocytosis. This is in accordance with the other findings of this thesis and previous findings in our laboratory. The speeds of KH378 when expressed alone were far faster than that of KH302. This suggests that the region of 80K-H that lies between KH302 and KH378 is responsible for attaching it to its membrane tether. Previous studies in our laboratory on the effect of 80K-H on glucose transport showed KH378 to cause a far greater increase in glucose transport than KH302. This is also the region of 80K-H required for binding to PKCζ (as has been shown in our laboratory's previous studies (Hodgkinson et al., 2005a.) and this thesis, which further supports the hypothesis that insulin activation of PKCζ releases 80K-H from the membrane tether.

This model is consistent with the previous findings in our laboratory on the effect of 80K-H on glucose transport. These showed that expression of KH302 increased glucose transport and expression of KH378 further increased it. The speeds of KH378 when expressed alone were far faster than that of KH302. This would suggest that the region of 80K-H that lies between KH302 and KH378 is responsible for attaching it to its membrane tether. This is also the region of 80K-H required for binding to PKCζ (as has been shown in our laboratory's previous studies [Hodgkinson et al., 2005a] and this thesis, which further supports the hypothesis that insulin activation of PKCζ releases 80K-H from the membrane tether. Previous work in our laboratory showed that PKCζ did not directly phosphorylate 80K-H, ruling out the possibility that PKCζ phosphorylation of 80K-H (between residues 302-378) causes it to be released from its membrane tether. Other

possibilities are a.) PKCζ binding to 80K-H disrupts the interaction between 80K-H and its membrane tether, b.) PKCζ phosphorylates the membrane tether in order to release it from 80K-H, or c.) Another protein associated with PKCζ is responsible for 80K-H's release. Interesting future experiments would be to investigate other interactors of PKCζ identified by the yeast-two-hybrid screen previously conducted in our laboratory. It would also be highly beneficial to conduct a yeast-two-hybrid screen on 80K-H and to see if any proteins are identified as interactors of both 80K-H and PKCζ.
It is interesting that the 80K-H mutant KH378 causes a far greater increase on glucose transport than either full length 80K-H or KH302. Seeing as the region of 80K-H responsible for interacting with PKCζ is between residues 302 and 378 on 80K-H and that removal of this section causes 80K-H to increase glucose transport, it is possible to speculate that it is also this region of 80K-H that is responsible for binding it to the tether and that insulin-induced PKCζ activity causes the release from the tether, hence allowing glucose transport through GLUT4. It seems likely that KH378 is unable to bind to the tether, meaning that it is continually in the stimulated state. This explains the large increase in glucose transport in both the insulin stimulated and basal states when KH378 is over-expressed. The FCS data in this thesis for the 80K-H constructs shows KH378 to have a faster diffusion co-efficeient than KH302, which further supports this explanation.

The results from this thesis have further defined the interaction sites of munc18c, 80K-H and PKCζ for each other and suggest that insulin stimulation causes munc18c, 80K-H and PKCζ come together in a triplex formation in a PKCζ-munc18c-80K-H orientation. The use of in vitro assays, namely GST binding assays and immunoprecipitations, enabled the determination of the regions of each protein responsible for its binding to another. Binding and non-binding truncation mutants of the three proteins were then used for in vivo fluorescence correlation spectroscopy. The in vitro assays used in this thesis are valuable tools for studying the binding characteristics of proteins and give essential information for deciphering the role of such proteins in the cell. As mentioned above, issues such as subcellular location or post-translational modifications of the protein are not taken into consideration. In vitro methods, such as the ones used in this thesis, are however ideal ways to begin an investigation. They provide a platform from which to

develop the investigations with in vivo analysis such as the fluorescence correlation spectroscopy used here. The results obtained from the GST pull-down assays and immunoprecipitations were both verified and extended by the results from the FCS studies. The only discrepancy with the results from the in vitro and in vivo studies is that for the binding of the 80K-H truncation mutant, KH378, to munc18c. The GST pull-down assays performed in this thesis clearly show that KH378 does not bind to munc18c, whilst KH353 does. This suggests that amino acids 353-378 of 80K-H are responsible for its binding to munc18c. However, previous work in our laboratory using co-immunoprecipitations showed that the 80K-H construct, KH378, did interact with munc18c [Hodgkinson et al. (2005) unpublished data]. Additionally, the FCS data suggests that an interaction does indeed occur. As described in section 4.2.3.5. of this thesis, this suggests that post translational modification of 80K-H (most likely in the N-terminus of 80K-H past residue 353) is necessary for its binding to munc18c. Future work should investigate the post-translational modifications of 80K-H and such affects on it's binding to munc18c. The first obvious line of work should be to investigate phosphorylation of 80K-H. Phosphorylation incorporation assays should be performed on cells over-expressing the various 80K-H constructs both pre- and post-insulin stimulation.

The first implication that 80K-H plays a role in insulin mediated glucose transport and GLUT4 vesicle trafficking came when a yeast-two-hybrid screen conducted in our laboratory showed 80K-H to be a novel interactor of PKCζ. A brain cDNA library was used as bait and the protein identified as interacting with PKCζ was in fact the KH130 construct used in this thesis, not the full length protein (so the protein identified by the screen was the full length 80K-H protein minus the first 130 amino acids). It is possible that these are two different splice variants of 80K-H. It would therefore be worth investigating possible splice variants of the 80K-H protein and what differences they have in structure, function and location. The easiest initial investigation would be to purchase monoclonal antibodies, one to the full length 80K-H protein and one to the truncated form. Western blotting of extracts from cell types such as L6 myotubules and 3T3-L1 adipocytes using these antibodies would indicate the expression levels in muscle

and fat respectively. Immunohistochemistry and confocal microscopy of various cell types (both pre- and post-insulin stimulation) would then provide information of the subcellular location of the different variants of 80K-H and their movements (if any) in response to insulin. This may provide further valuable insight as to the roles of 80K-H.

Investigations conducted on the protein Kifap3 are few and far between and no work before has linked Kifap3 to munc18c, insulin signalling or GLUT4 vesicle trafficking. The results obtained during this thesis provide a good platform for further investigations into the role of Kifap3. The results hint towards a role for this protein in munc18c delivery to the plasma membrane. Experiments to be performed in order to test this hypothesis should include the production of non-interacting mutants of Kifap3 and/or munc18c. The subcellular location of munc18c could be assessed using fluorescently tagged vectors and microscopy, or by the use of immunohistochemistry. This could be performed with both the full length proteins and a non-interacting mutant, in order to see if disruption of munc18c:Kifap3 interactions affect the subcellular location of munc18c. Glucose transport assays could then also determine the effect of this interaction on insulin mediated glucose transport. Again, any further information may provide possibility

In conclusion, this thesis has made some important and exciting discoveries about insulin signalling and GLUT4 vesicle trafficking. It has further elucidated the mechanics of the signalling pathway and the vesicle trafficking machinery: the interactions between the proteins involved and their role in the cells response to insulin. Hopefully, the findings from this work will lead to additional research in this area, which may unearth possible treatments for diseases such as type II diabetes in the future.

APPENDIX 1

Biochemical Journal
Published on 24 October 2007
Insulin-triggered repositioning of munc18c on syntaxin4 in GLUT4 signalling

BJ www.biochemj.org

BJ Signal

Biochem. J. (2008) 410, 255–260 (Printed in Great Britain) doi:10.1042/BJ20070802

Insulin-triggered repositioning of munc18c on syntaxin-4 in GLUT4 signalling

Natalie P. SMITHERS[1], Conrad P. HODGKINSON[1], Matt CUTTLE and Graham J. SALE[2]

School of Biological Sciences, University of Southampton, Biomedical Sciences Building, Bassett Crescent East, Southampton SO16 7PX, U.K.

One of the most important actions of insulin is the stimulation of the uptake of glucose into fat and muscle cells. Crucial to this response is the translocation of GLUT4 (glucose transporter-4) to the plasma membrane. The insulin-stimulated GLUT4 vesicle docking at the plasma membrane requires an interaction between VAMP-2 (vesicle-associated membrane protein-2) on the GLUT4 vesicle and syntaxin-4 in the plasma membrane. In the basal state, munc18c is thought to preclude GLUT4 vesicle docking by inhibiting this interaction. Here, we have used FCS (fluorescence correlation spectroscopy) in single living cells to show that munc18c binds to syntaxin-4 in both the basal and insulin-stimulated states. We show that munc18c contains two binding sites for syntaxin-4, one of which is disrupted by insulin, while the other is activated by insulin. Insulin-triggered repositioning of munc18c on syntaxin-4 in this way in turn allows syntaxin-4 to adopt its 'open' conformation and bind VAMP-2, resulting in the docking of the GLUT4 vesicle at the cell surface. The results also demonstrate the utility of using FCS in intact single living cells to elucidate cell signalling events.

Key words: fluorescence correlation spectroscopy (FCS), glucose transporter-4 (GLUT4), glucose uptake, insulin, munc18c, vesicle-associated membrane protein (VAMP).

INTRODUCTION

The most important action of insulin is the regulation of glucose homoeostasis. Activation of PKCζ (protein kinase C ζ) and PKB (protein kinase B; also called Akt) leads to the translocation of GLUT4 (glucose transporter-4) from an intracellular vesicle to the plasma membrane. The GLUT4 vesicle contains the v-SNARE [vesicle SNARE (soluble *N*-ethylmaleimide-sensitive factor-attachment protein receptor)] VAMP-2 (vesicle-associated membrane protein 2) and membrane binding requires interaction with the t-SNARE (target membrane SNARE) syntaxin-4. In the basal state, the v- and t-SNARE interaction is precluded by accessory proteins such as munc18c. In unstimulated cells, the association between munc18c and syntaxin-4 is stronger than that between VAMP-2 and syntaxin-4. This blocks the GLUT4 vesicle from docking to the plasma membrane. Upon insulin stimulation, the situation reverses, the association between munc18c and syntaxin-4 weakens considerably and is out-competed by the syntaxin-4 VAMP-2 interaction and thus the GLUT4 vesicle docks at the cell surface. However, the details of this mechanism, whereby insulin weakens the syntaxin-4–munc18c interaction, are poorly understood [1–4].

The present study utilized FCS (fluorescence correlation spectroscopy) to investigate interactions between munc18c and syntaxin-4 in intact living cells. FCS analysis indicated that munc18c did not dissociate from syntaxin-4 in response to insulin. Rather, insulin triggered the repositioning of munc18c on syntaxin-4 via an additional binding site, thus allowing VAMP-2–syntaxin-4 interaction and GLUT4 vesicle docking at the plasma membrane.

EXPERIMENTAL

Plasmid constructs

The full-length syntaxin-4 clone was supplied in a pCMVSport 6 vector (Invitrogen). The full-length syntaxin-4 sequence was amplified by PCR by using Pfu DNA polymerase and the sequence-specific forward primer 5′-ATGCGCGACAGGACCCAC-3′ and reverse primer 5′-TGGTATTGGCAACCTATT-3′. The DNA product from this reaction was then used as a template for further amplification by PCR by using Pfu DNA polymerase and the forward primer (containing the EcoRI restriction site) 5′-GCGGT**GAATTC**ATGCGCGACAGGACCCAC-3′ and reverse primer (containing the KpnI restriction site) 5′-TAGTGGTATTGGCAACCTA**CCATGGT**GGCG-3′. Other constructs were described by Hodgkinson et al. [5,6]. Digestion of the PCR products by EcoRI and KpnI then allowed ligation in frame with the EYFP (enhanced yellow fluorescent protein) epitope of the pEYFP-N2 vector (BD Biosciences).

Transient transfection

CHO (Chinese-hamster ovary; CHO-K1) cells were purchased from A.T.C.C. (A.T.C.C. number CCL-61; Manassas, VA, U.S.A.) and maintained at 37°C and 5% CO_2 on 25 cm^2 tissue culture dishes in HAM-12 medium supplemented with 10% (v/v) fetal bovine serum and 1% (v/v) glutamine. CHO cells were transfected using Polyfect transfection reagent (Qiagen) as per the manufacturer's instructions and serum-starved 24 h prior to FCS measurements. 3T3-L1 adipocytes were obtained and cultured as described previously [7,8]. For electroporation, 3T3-L1 adipocytes were detached from culture dishes by incubation with 0.25% trypsin (0.5 mg/ml), and 5×10^6 cells were mixed with 5 μg of plasmid in the solution provided for the cell line Nucleofector kit V (Amaxa, Cologne, Germany). The plasmid was then introduced into the 3T3-L1 adipocytes by electroporation with the use of a Nucleofector (Amaxa) instrument according to the T-20 program. For immunoblotting, cells were extracted into 200 μl of lysis buffer [62.5 mM Tris, pH 7.4, and 1% (w/v) SDS].

Abbreviations used: CHO cell, Chinese-hamster ovary cell; EYFP, enhanced yellow fluorescent protein; FCS, fluorescence correlation spectroscopy; GLUT4, glucose transporter-4; GST, glutathione transferase; PKCζ, protein kinase C ζ SM protein, Sec/Munc18 protein; SNARE, soluble *N*-ethylmaleimide-sensitive factor-attachment protein receptor; t-SNARE, target membrane SNARE; VAMP, vesicle-associated membrane protein; v-SNARE, vesicle SNARE.

[1] These authors contributed equally to this work.

[2] To whom correspondence should be addressed (email G.J.Sale@soton.ac.uk).

FCS and confocal microscopy

FCS and confocal microscopy were carried out with a Leica × 63 water-immersion objective and Leica SP2 confocal laser-scanning microscope (Leica). Samples were excited with a 514 nm Ar/Kr laser at low-average laser power. Cells were first washed twice with 1 ml of prewarmed Krebs–Ringer buffer (10 mM Hepes, pH 7.4, 136 mM NaCl, 4.7 mM KCl and 1.25 mM $MgSO_4$). Cells were then incubated with 2 ml of the same buffer. A prebleaching illumination period of 160 s was used prior to data collection. Correlation curves of 600 s were collected from cells and traces were analysed with the Leica FCS software. Experiments were performed at room temperature to reduce the mobility of the cells. When required, cells were stimulated with 100 nM insulin in Krebs–Ringer buffer for 20 min. Data were collected from six individual cells both before and after insulin stimulation. Values are expressed as means ± S.E.M. The presence of the overexpressed proteins was confirmed by detection of the fluorescence by microscopy and subsequent Western blotting of the cell extract (SySy; results not shown).

GST (glutathione transferase) pull-down protocol

BL21 cells were used to express the GST-tagged syntaxin-4 by using a standard protocol supplied by Amersham Biosciences. BL21 cells overexpressing GST-tagged syntaxin-4 were lysed using Bugbuster (Novagen) and clarified extracts were incubated with glutathione beads (Amersham Biosciences). After several washes with PBS, the glutathione bead syntaxin-4 complex was exposed to cell extracts prepared from CHO cells overexpressing Xpress-tagged munc18c constructs. After 4 h of constant agitation at 4 °C, complexes were washed three times with PBS and then resuspended in a small volume of PBS.

Immunoprecipitation

Cells were extracted into lysis buffer [50 mM Tris, pH 7.5, 150 mM NaCl and 1 % (v/v) Sigma Protease and Phosphatase Inhibitor cocktails] to give a 500 μl final volume (500 μg). Co-immunoprecipitation was carried out by incubating 500 μg of cell lysate with a monoclonal Xpress antibody (5 μl; Invitrogen) and Protein G–Protein A beads (50:50; 20 μl; Sigma). After 5 h continuous gentle agitation at 4 °C, the beads were collected by pulse spin and then washed three times with lysis buffer, after which they were resuspended in PBS.

Immunoblotting

Samples were resolved by SDS/PAGE [7,8] and transferred to a nitrocellulose filter. The membranes were probed with various primary antibodies followed by incubation with horseradish peroxidase-conjugated secondary antibodies. Primary antibodies [GST (NEB), munc18c (BD Biosciences), Living Colours antibody (SySy), syntaxin-4 (SySy), Xpress (Invitrogen) and 80K-H (BD Biosciences)] were used according to the manufacturer's instructions. Blots were developed using the ECL® system according to the manufacturer's instructions (Amersham Biosciences).

RESULTS

The FCS results from the present study were fitted using a three-dimensional Gaussian triplet calculation (Leica software) and the τ_{DI} value was calculated in microseconds. τ_{DI} represents the average time the EYFP-tagged construct spends in the observation volume and thus can be called a diffusion coefficient. A larger diffusion coefficient corresponds to a longer time spent in the observation volume and hence relates to a slower-moving molecule. Knowledge of the average speed of the protein of interest *in vivo* provides valuable insights into its behaviour.

Table 1 Action of insulin on the diffusion coefficients of munc18c and syntaxin-4 in CHO cells

The indicated EYFP-tagged constructs were expressed in the presence or absence of the indicated interactor. Cells were serum-starved for 24 h and stimulated with or without 10^{-7} M insulin for 20 min, FCS data were collected and diffusion coefficients were measured (microseconds). Results are the means ± S.E.M. for three separate experiments each using six separate cells. *$P < 0.01$ compared with absence of the interactor. MFL, munc18c full-length; M295, munc18c 295.

EYFP	Interactor	No insulin	Insulin
MFL		526 ± 41	592 ± 78
MFL	Syntaxin-4	795 ± 69*	804 ± 61*
M295		576 ± 64	489 ± 36
M295	Syntaxin-4	619 ± 34	821 ± 32*
Syntaxin-4		459 ± 54	491 ± 71
Syntaxin-4	MFL	720 ± 59*	789 ± 88*

Table 2 Action of insulin on the diffusion coefficients of munc18c and syntaxin-4 in 3T3-L1 adipocytes

The indicated EYFP-tagged constructs were expressed in the presence or absence of the indicated interactor. Cells were serum-starved for 24 h and stimulated with or without 10^{-7} M insulin for 20 min, FCS data were collected and diffusion coefficients were measured (microseconds). Results are the means ± S.E.M. for three separate experiments each using six separate cells. *$P < 0.01$ compared with absence of the interactor. MFL, munc18c full-length; M295, munc18c 295.

EYFP	Interactor	No insulin	Insulin
MFL		480 ± 25	507 ± 17
MFL	Syntaxin-4	776 ± 71*	772 ± 27*
M295		501 ± 69	561 ± 58
M295	Syntaxin-4	493 ± 62	748 ± 57*

To investigate insulin-triggered interactions between munc18c, syntaxin-4 and other proteins *in vivo* within intact cells, one or two of the proteins, or non-binding constructs, were expressed. In all experiments, cells were serum-starved 24 h prior to data collection and were bleached for 120 s prior to data collection in order to provide optimal signal-to-noise ratio for FCS (this typically being 10–100 fluorescent molecules in the focal volume). Levels of the constructs were determined by immunoblotting. Analysis of the immunoblots showed that expression levels were similar for all the constructs used in the present study (results not shown). CHO cells and 3T3 L1 adipocytes were employed in the present study. CHO cells possess GLUT4 storage vesicles, which translocate to the plasma membrane in response to insulin and have been frequently used to investigate the mechanism whereby insulin stimulation promotes GLUT4 translocation to the plasma membrane. 3T3 L1 adipocytes were utilized as a truly insulin-responsive cell type. The two cell types yielded similar results.

Insulin did not affect the τ_{DI} value of the EYFP-tagged full-length munc18c construct when expressed alone (Tables 1 and 2). When the EYFP-tagged munc18c construct was co-expressed with syntaxin-4, the diffusion coefficient of EYFP-tagged full-length munc18c was markedly increased compared with the single transfection both before and after insulin stimulation (Tables 1 and 2). The effects of co-expressing syntaxin-4 were highly statistically significant, with P values of <0.01, and indicate that munc18c binds syntaxin-4 both in the presence and absence of insulin. Example FCS traces are shown in Figure 1.

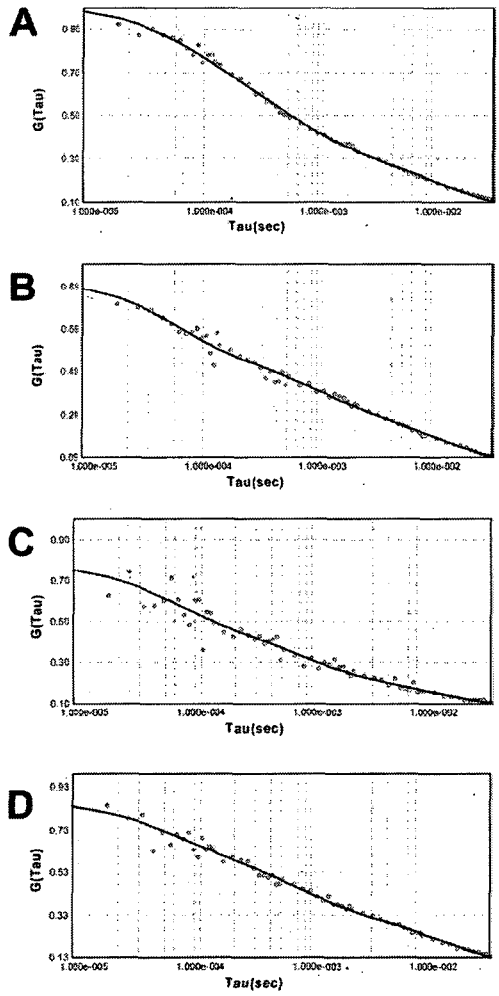

Figure 1 Example FCS traces showing that syntaxin-4 reduces the diffusion coefficient of munc18c 295, but not full-length munc18c, in an insulin-dependent manner

Syntaxin-4 was expressed with the EYFP-tagged full-length munc18c construct (**A**, **B**) or the EYFP-tagged munc18c 295 construct (**C**, **D**), which lacks the well-characterized syntaxin-4-binding site. Cells were serum-starved for 24 h, stimulated with (**B**, **D**) or without (**A**, **C**) 10^{-7} M insulin for 20 min and FCS data were collected. Note the shift to the right of the curve in (**D**) compared with that in (**C**), demonstrating an insulin-stimulated increase in the diffusion coefficient of the EYFP-tagged munc18c 295 construct; this corresponds to a reduction in mobility of the EYFP-tagged munc18c 295 construct. When full-length munc18c was employed, insulin stimulation did not shift the curve. The original FCS traces are shown.

To confirm this, we next determined the diffusion coefficient of EYFP-tagged syntaxin-4. Insulin stimulation had no effect on the diffusion coefficient of EYFP-tagged syntaxin-4 (Table 1). However, when full-length munc18c was co-expressed, the diffusion coefficients for EYFP-tagged syntaxin-4 were again markedly increased both before and after insulin stimulation (Table 1). These increases are virtually identical with those for the EYFP-tagged full-length munc18c construct in the EYFP-tagged full-length munc18c and syntaxin-4 transfections. Again, insulin had no effect on the diffusion coefficients.

Table 3 Insulin increases the mobility of munc18c in an 80K-H-dependent manner in CHO cells

The indicated EYFP-tagged munc18c constructs were expressed in the presence or absence of 80K-H. Cells were serum-starved for 24 h and stimulated with or without 10^{-7} M insulin for 20 min. FCS data were collected, diffusion coefficients were measured and the effect of stimulation by insulin on the mobility (speed) of the EYFP construct was determined. Each value is the ratio of the diffusion coefficients (absence of insulin/presence of insulin). Results are the means ± S.E.M. for three separate experiments, each using six separate cells. *$P < 0.01$ compared with no 80K-H. MFL, munc18c full length; M295, munc18c 295; M338, munc18c 338.

	Effect of insulin on mobility	
EYFP	No 80K-H	80K-H
MFL	0.83 ± 0.07	1.75 ± 0.18*
M295	1.1 ± 0.01	1.96 ± 0.27*
M338	0.83 ± 0.06	0.98 ± 0.06

To further define the binding of munc18c to syntaxin-4, we employed a truncation construct of munc18c, namely munc18c 295, which lacks the N-terminal 295 amino acids. GST pull-down assays in our laboratory showed that this construct is unable to bind to syntaxin-4 when expressed in the non-insulin-responsive Cos-1 cell line (results not shown). This is in accordance with other published data [9] that showed that the N-terminal 139 amino acids of munc18c bind to syntaxin-4. The diffusion coefficient for the EYFP-tagged munc18c 295 was not significantly affected by insulin stimulation (Tables 1 and 2). The co-expression of syntaxin-4 with EYFP-tagged munc18c 295 had no statistically significant effect on the diffusion coefficient of the EYFP-tagged munc18c 295 construct in the basal state. In contrast, insulin stimulation caused a major increase in the diffusion coefficient of the EYFP-tagged munc18c 295 construct (Tables 1 and 2; Figure 1). This effect was highly significant with a P value of <0.01 and indicated that munc18c 295 only binds syntaxin-4 in the insulin-stimulated state. These results suggest that munc18c has two binding sites for syntaxin-4. One of them lies between residues 1 and 295, as has been shown previously, and the other lies between residues 295 and 592 and binds syntaxin-4 in the presence of insulin.

To further confirm that insulin was working in the cells and to help validate the FCS approach, the interaction of munc18c with 80K-H was analysed. 80K-H is believed to be an upstream regulator of munc18c that is crucial for delivering an insulin signal to the GLUT4 translocation machinery [5,6]. Co-expression of EYFP-tagged full-length munc18c with 80K-H resulted in insulin eliciting a major increase in the mobility of the full-length EYFP-tagged munc18c of approx. 2-fold ($P < 0.01$; Tables 3 and 4). To test whether this effect was dependent on the ability of 80K-H to bind munc18c, a truncation construct of munc18c, namely EYFP-tagged munc18c 338, was employed. This construct is unable to bind 80K-H and inhibits insulin-stimulated GLUT4 translocation to a greater extent than full-length munc18c. As with the EYFP-tagged full-length munc18c, insulin did not affect the diffusion coefficient of EYFP-tagged munc18c 338 when expressed alone. Importantly, when EYFP-tagged munc18c 338 and 80K-H were co-expressed, insulin was no longer able to trigger a change in the speed of the munc18c construct (Tables 3 and 4). As a control, a less truncated version of munc18c was employed,

Table 4 Insulin increases the mobility of munc18c in an 80K-H-dependent manner in 3T3-L1 adipocytes

The indicated EYFP-tagged munc18c constructs were expressed in the presence or absence of 80K-H. Cells were serum-starved for 24 h and stimulated with or without 10^{-7} M insulin for 20 min. FCS data were collected, diffusion coefficients were measured and the effect of stimulation by insulin on the mobility (speed) of the EYFP construct was determined. Each value is the ratio of the diffusion coefficients (absence of insulin/presence of insulin). Results are the means ± S.E.M. for three separate experiments each using six separate cells. *$P < 0.01$ compared with no 80K-H. MFL, munc18c full length; M295, munc18c 295; M338, munc18c 338.

	Effect of insulin on mobility	
EYFP	No 80K-H	80K-H
MFL	1.06 ± 0.04	2.17 ± 0.48*
M295	1.12 ± 0.16	2.51 ± 0.37*
M338	1.05 ± 0.36	1.16 ± 0.10

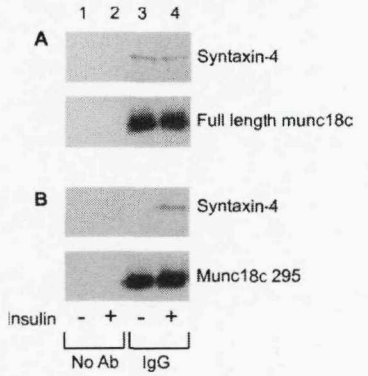

Figure 2 Syntaxin-4 interacts with munc18c 295 in an insulin-dependent manner and with full-length munc18c in an insulin-independent manner

CHO cells, overexpressing Xpress-tagged full-length munc18c (**A**) or Xpress-tagged munc18c 295 (**B**), were serum-starved for 24 h and then incubated for 20 min in the presence or absence of 100 nM insulin. Xpress-tagged munc18c proteins were immunoprecipitated from cell lysates (0.5 mg of protein) and the immunoprecipitates were washed extensively. Proteins in the immunocomplex were immunoblotted with an anti-syntaxin-4 antibody (upper panels, lanes 3 and 4) or anti-munc18c antibody as a control (lower panels, lanes 3 and 4). Control immunoprecipitations with an equal amount of cell lysate and Protein A/G beads but omitting the antibody were also performed (lanes 1 and 2). The results shown are representative of two independent experiments.

namely EYFP-tagged munc18c 295. This construct still has the ability to bind 80K-H and, like the full-length munc18c, to inhibit GLUT4 translocation when overexpressed. Insulin did not affect the mobility of the EYFP-tagged munc18c 295 construct when expressed alone. However, when EYFP-tagged munc18c 295 and 80K-H were co-expressed, insulin stimulation caused an approx. 2-fold increase in the speed of EYFP-tagged munc18c 295.

To further test the nature of the interactions between munc18c and syntaxin-4, co-immunoprecipitation experiments were performed. For this, Xpress-tagged munc18c 295 or full-length munc18c constructs were expressed in CHO cells and the cells were incubated with and without insulin. Only with the insulin-stimulated cells did syntaxin-4 co-immunoprecipitate with the Xpress-tagged 295 construct, whereas with both unstimulated and insulin-stimulated cells, syntaxin-4 co-immunoprecipitated with the Xpress-tagged full-length munc18c construct (Figure 2). As expected, 80-KH co-immunoprecipitated with munc18c 295

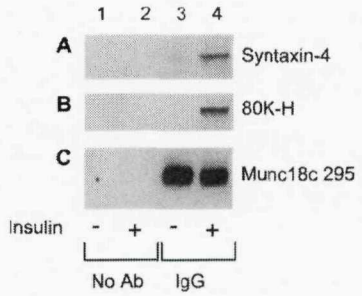

Figure 3 Immunoprecipitates of munc18c 295 from insulin-stimulated, but not unstimulated, cells contain 80K-H

CHO cells, overexpressing Xpress-tagged munc18c 295, were serum-starved for 24 h and then incubated for 20 min in the presence or absence of 100 nM insulin. Xpress-tagged munc18c 295 was immunoprecipitated from cell lysates (0.5 mg of protein) and the immunoprecipitates were washed extensively. Proteins in the immunocomplex were immunoblotted with either antibodies against syntaxin-4 (**A**), 80K-H (**B**) or munc18c (**C**) as a control (lanes 3 and 4). Control immunoprecipitations with an equal amount of cell lysate and Protein A/G beads but omitting the antibody were also performed (lanes 1 and 2). The results are representative of two independent experiments.

and syntaxin-4 from insulin-stimulated but not unstimulated cells (Figure 3). Crucially, these co-immunoprecipitation data support, by a different method, the FCS data.

The above results establish that full-length munc18c can bind syntaxin-4 both in the presence and absence of insulin, whereas munc18c 295 can only bind syntaxin-4 in the presence of insulin. Munc18c 295 lacks the well-established binding site for syntaxin-4 located in the N-terminus of the protein. The results above thus indicate that munc18c contains a second syntaxin-4-binding site. To help define the nature of the second syntaxin-binding site, further co-immunoprecipitation experiments were performed by more extensively truncating munc18c. For this, various Xpress-tagged munc18c truncation constructs were expressed in CHO cells and the cells were incubated with insulin. Cell extracts were then incubated with GST-tagged syntaxin-4 glutathione beads. As expected, the Xpress-tagged munc18c 295 construct was pulled down by the GST-tagged syntaxin-4 glutathione beads. In contrast, the Xpress-tagged munc18c 308, 326 and 338 constructs were not pulled down by the GST-tagged syntaxin-4 glutathione beads (Figure 4). This indicates that key residues involved in forming the second binding site are located between amino acids 295 and 308 of munc18c.

DISCUSSION

Insulin regulates glucose homoeostasis predominantly by causing a rapid increase in glucose uptake in muscle and adipose cells via the translocation of the GLUT4 vesicle to the cell surface. GLUT4 vesicle trafficking is similar to that seen in synaptic vesicles. The GLUT4 vesicle contains the v-SNARE VAMP-2, which binds to its cognate t-SNARE receptor syntaxin-4 in the plasma membrane [10–12]. Insulin regulates the VAMP-2–syntaxin-4 binding by virtue of accessory proteins, the most important of which is munc18c.

There have, however, been few studies conducted to elucidate the exact role of munc18c in GLUT4 vesicle exocytosis. munc18c has been shown to inhibit GLUT4 vesicle exocytosis and yet to be also essential for this process. *In vitro* assays have shown that in the basal state munc18c binds to syntaxin-4 with higher affinity than

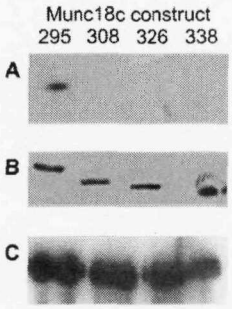

Figure 4 Munc18c 295, but not munc18c 308, 326 or 338, interacts with syntaxin-4

CHO cells, overexpressing the Xpress-tagged munc18c constructs, were serum-starved for 24 h and then incubated for 20 min in the presence of 100 nM insulin. GST-tagged syntaxin-4 was produced in bacteria and, after purification, coupled with glutathione beads. The GST-tagged syntaxin-4 glutathione beads were exposed to the CHO cell extracts (0.5 mg of protein) containing the Xpress-tagged munc18c constructs. After incubation, the complexes were washed extensively. Complexes were probed with an anti-Xpress antibody (**A**) and an anti-GST antibody to show equal loading (**C**). Cell extracts (20 μg) were probed with an anti-Xpress antibody to confirm expression of the constructs (**B**).

VAMP-2. This prevents VAMP-2 from binding to syntaxin-4 and hence inhibits GLUT4 vesicle docking at the plasma membrane [11,13,14]. These same *in vitro* assays also showed that when insulin stimulation decreases the binding strength of munc18c towards syntaxin-4, the VAMP-2 interaction with syntaxin-4 becomes relatively stronger. This allows the GLUT4 vesicle to bind to the plasma membrane. Due to the *in vitro* nature of these assays, the mechanistic detail *in vivo* remained uncategorized. Several scenarios would fit these data *in vivo*. Either munc18c would dissociate from syntaxin-4 in response to insulin or weaker binding association would not cause munc18c dissociation but rather allow syntaxin-4 to undergo a conformational change allowing syntaxin-4 to bind VAMP-2.

In our study, FCS has been utilized to investigate munc18c biology in intact living cells. Co-expression of EYFP-tagged full-length munc18c with syntaxin-4 resulted in a significant increase in the diffusion coefficient of the EYFP-tagged full-length munc18c in the absence of insulin stimulation. This slow down in the mobility of munc18c is expected as munc18c is known to bind syntaxin-4. The insulin-independent binding between munc18c and syntaxin-4 was confirmed using EYFP-tagged syntaxin-4 in the presence and absence of co-expression of munc18c. If insulin caused munc18c to physically dissociate from syntaxin-4, then insulin stimulation would be expected to increase the mobility of the EYFP-tagged full-length munc18c. However, the diffusion coefficient of EYFP-tagged munc18c did not change in response to insulin. The same result was seen when the diffusion coefficient of EYFP-tagged syntaxin-4 was measured in the presence of munc18c. These *in vivo* results clearly show that munc18c is not released from syntaxin-4 in response to insulin. Munc18c belongs to the nSec1 family of proteins. Yeast Sec1 proteins have been the most heavily studied. Several mechanisms appear to be used for interaction between Sec1 proteins and syntaxins. Sec1 only binds to the yeast syntaxin Sso1p when the complete SNARE complex is formed [15]. The structure of the neuronal SM protein (Sec/Munc18 protein), nSec1, bound to the closed conformation of syntaxin 1a has been interpreted as an intermediate required to convert syntaxin into the 'open' conformation, which then assembles with the other SNAREs to form the fusogenic SNARE complex [16]. An indirect syntaxin-binding mode describes the interaction of the yeast vacuolar SM protein, Vps33p, which is part of a large protein complex that binds to the cognate syntaxin, Vam3p [17]. Indeed, null mutations in the genes for the SM proteins cause dramatic reductions in vesicle exocytosis, suggesting that these proteins are essential for normal SNARE function [18]. The munc18c–syntaxin-4 complex has been shown to be specifically required for insulin-stimulated GLUT4 vesicle fusion, and munc18c has been described as a positive fusogenic protein [19]. Our FCS data agree with these findings. If munc18c is not actually released by syntaxin-4, some change in munc18c must allow syntaxin-4 to bind VAMP-2.

To test whether munc18c has a binding site for syntaxin-4 distinct from the well-known site in the N-terminal portion of the protein, the EYFP-tagged munc18c 295 construct, which lacks the site, was employed. The mobility of the EYFP-tagged munc18c 295 construct was similar in the presence and absence of co-expressed syntaxin-4 in the absence of insulin. This indicates that, unlike full-length munc18c, the munc18c 295 construct does not associate with syntaxin-4 in the basal state and that the N-terminal region is responsible for binding syntaxin-4 in the basal state. Upon insulin stimulation of cells co-expressing the EYFP-tagged munc18c 295 construct and syntaxin-4, there was a marked increase in the diffusion coefficient of the EYFP-tagged munc18c 295 construct. This indicates that the munc18c 295 construct was able to associate with syntaxin-4 in the insulin-stimulated state and that munc18c contains a second binding site for syntaxin-4 that is outside the N-terminal region. Thus insulin may trigger a conformational change in munc18c that results in it repositioning on syntaxin-4 and in turn allowing syntaxin-4 to adopt its 'open' conformation and bind VAMP-2. Very recent data from D'Andrea-Merrins et al. [20] support our view that munc18c has more than one binding site on syntaxin-4.

To analyse how the insulin signal may be delivered to munc18c to induce such a conformational change, experiments were conducted with 80K-H. Recent evidence suggests that 80K-H links insulin signalling to the machinery controlling GLUT4 exocytosis through an insulin-triggered association with munc18c [5,6]. For this, EYFP-tagged full-length munc18c was expressed in the presence and absence of 80K-H. While insulin did not affect the mobility of EYFP-tagged full-length munc18c when expressed alone, in the presence of 80K-H, insulin induced a large increase in the mobility of the EYFP-tagged full-length munc18c. Use of various constructs of munc18c showed that this increase in speed of munc18c was critically dependent on the presence of an intact 80K-H-binding site on munc18c. These results indicate that 80K-H interacts with munc18c in intact living cells. How then does insulin trigger 80K-H to increase the speed of munc18c if, as shown above, munc18c remains associated with syntaxin-4? One way that the mobility of munc18c can increase is if there is a decrease in the tethering of the syntaxin-4 complex with other known interactors, such as synip or tomosyn or other scaffolding proteins. In this model, insulin would break or reduce these interactions. This model is shown in Figure 5. However, we did not observe an increase in mobility of syntaxin-4 when cells co-expressing munc18c and syntaxin-4 were stimulated with insulin. This is probably because the availability of the other interactors was limiting and because most of the overexpressed syntaxin-4 was not tethered in the first place. Tyrosine phosphorylation of munc18c has been shown to promote VAMP-2 binding to syntaxin-4 and this provides a further mechanism of delivering an insulin signal to munc18c [21].

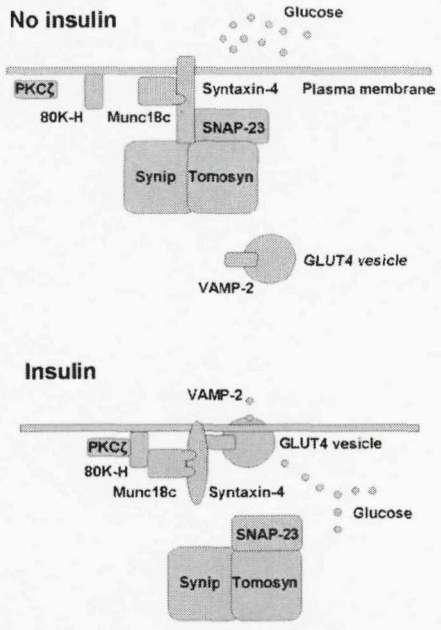

Figure 5 Hypothetical model showing how insulin triggers the repositioning of munc18c on syntaxin-4

Upstream signalling molecules including PKCζ and 80K-H relay the insulin signal to munc18c. Activated munc18c then repositions itself on syntaxin-4, thereby triggering syntaxin-4 to adopt *the 'open' formation enabling it to bind VAMP-2 of the GLUT4 vesicle. Breakage of interactions* between syntaxin-4 and other known interactors, such as synip, tomosyn, SNAP-23 or other scaffolders, may account for the observed increase in munc18c mobility.

The above conclusions, based on differences in the diffusion coefficients between *full-length munc18c* and *munc18c* 295 (Tables 1 and 2), suggest that in unstimulated cells the latter does not interact with syntaxin-4, whereas association is enhanced with syntaxin-4 in insulin-stimulated cells. This is a critical result that raises the concept that reorganizing the molecular interaction between munc18c and syntaxin-4 serves as a gating mechanism that permits interaction between SNARE proteins. To underpin this finding it was important to substantiate these interactions by another approach. For this Xpress-tagged munc18c 295 or full-length munc18c, constructs were expressed in CHO cells. If the proposition holds, then only in insulin-stimulated cells should syntaxin-4 co-immunoprecipitate with munc18c 295. Western blots in Figure 2 show that this was indeed the case. Additionally, if the proposition is correct, full-length munc18c should not undergo any change in association with syntaxin-4 upon insulin treatment. Again, this was found to be the case (Figure 2). These results corroborate the repositioning hypothesis.

In conclusion, we have identified that insulin does not trigger the release of munc18c from syntaxin-4 in intact single living cells. Rather munc18c appears to contain two binding sites for syntaxin-4, one of which is disrupted by insulin and the other exposed by insulin. Thus insulin may elicit a repositioning of munc18c on syntaxin-4, which in turn allows syntaxin-4 to adopt its 'open' conformation and bind VAMP-2.

This work was funded by grants from the BBSRC (Biotechnology and Biological Sciences Research Council) and Diabetes UK.

REFERENCES

1 Ishiki, M. and Klip, A. (2005) Minireview: recent developments in the regulation of glucose transporter-4 traffic: new signals, locations, and partners. Endocrinology **146**, 5071–5078
2 *Kanzaki, M., Mora, S., Hwang, J. B., Saltiel, A. R. and Pessin, J. E. (2004) Atypical protein* kinase C (PKCζ/λ) is a convergent downstream target of the insulin-stimulated phosphatidylinositol 3-kinase and TC10 signaling pathways. J. Cell Biol. **164**, 279–290
3 Patel, N., Huang, C. and Klip, A. (2006) Cellular location of insulin-triggered signals and implications for glucose uptake. Pflugers Arch. **451**, 499–510
4 *Watson, R. T. and Pessin, J. E. (2001) Subcellular compartmentalization and trafficking of* the insulin-responsive glucose transporter, GLUT4. Exp. Cell Res. **271**, 75–83
5 Hodgkinson, C. P., Mander, A. and Sale, G. J. (2005) Identification of 80K-H as a protein involved in GLUT4 vesicle trafficking. Biochem. J. **388**, 785–793
6 Hodgkinson, C. P., Mander, A. and Sale, G. J. (2005) Protein kinase-ζ interacts with *munc18c* role in GLUT4 trafficking. Diabetologia **48**, 1627–1636
7 Sale, E. M., Atkinson, P. G. and Sale, G. J. (1995) Requirement of MAP kinase for differentiation of fibroblasts to adipocytes, for insulin activation of p90 S6 kinase and for insulin or serum stimulation of DNA synthesis. EMBO J. **14**, 674–684
8 Arnott, C. H., Sale, E. M., Miller, J. and Sale, G. J. (1999) Use of an antisense strategy to dissect the signalling role of protein-tyrosine phosphatase α. J. Biol. Chem. **274**, 26105–26112
9 Grusovin, J., Stoichevska, V., Gough, K. H., Nunan, K., Ward, C. W. and Macaulay, S. L. (2000) Definition of a minimal munc18c domain that interacts with syntaxin 4. Biochem. J. **350**, 741–746
10 Kawanishi, M., Tamori, Y., Okazawa, H., Araki, S., Shinoda, H. and Kasuga, M. (2000) Role of SNAP23 in insulin-induced translocation of GLUT4 in 3T3-L1 adipocytes. Mediation of complex formation between syntaxin4 and VAMP2. J. Biol. Chem. **275**, 8240–8247
11 Kanda, H., Tamori, Y., Shinoda, H., Yoshikawa, M., Sakaue, M., Udagawa, J., Otani, H., Tashiro, F., Miyazaki, J. and Kasuga, M. (2005) Adipocytes from Munc18c-null mice show increased sensitivity to insulin-stimulated GLUT4 externalization. J. Clin. Invest. **115**, 291–301
12 Chang L, Chiang S. H. and Saltiel, A. R. (2004) Insulin signaling and the regulation of glucose transport. Mol. Med. **10**, 65–71
13 Thurmond, D. C., Ceresa, B. P., Okada, S., Elmendorf, J. S., Coker, K. and Pessin, J. E. (1998) Regulation of insulin-stimulated GLUT4 translocation by Munc18c in 3T3L1 adipocytes. J. Biol. Chem. **273**, 33876–33883
14 Tamori, Y., Kawanishi, M., Niki, T., Shinoda, H., Araki, S., Okazawa, H. and Kasuga, M. (1998) Inhibition of insulin-induced GLUT4 translocation by Munc18c through interaction with syntaxin4 in 3T3-L1 adipocytes. J. Biol. Chem. **273**, 19740–19746
15 Togneri, J., Cheng, Y. S., Munson, M., Hughson, F. M. and Carr, C. M. (2006) Specific *SNARE complex binding mode of the Sec1/Munc-18 protein, Sec1p. Proc. Natl. Acad.* Sci. U.S.A. **103**, 17730–17735
16 Misura, K. M., Scheller, R. H. and Weis, W. I. (2000) Three-dimensional structure of the neuronal-Sec1–syntaxin 1a complex. Nature **404**, 355–362
17 Seals, D. F., Eitzen, G., Margolis, N., Wickner, W. T. and Price, A. (2000) A Ypt/Rab *effector complex containing the Sec1 homolog Vps33p is required for homotypic vacuole* fusion. Proc. Natl. Acad. Sci. U.S.A. **97**, 9402–9407
18 Hosono, R., Hekimi, S., Kamiya, Y., Sassa, T., Murakami, S., Nishiwaki, K., Miwa, J., Taketo, A. and Kodaira, K. I. (1992) The unc-18 gene encodes a novel protein affecting the kinetics of acetylcholine metabolism in the nematode *Caenorhabditis elegans*. *J. Neurochem.* **58**, 1517–1525
19 Thurmond, D. C. and Pessin, J. E. (2000) Discrimination of GLUT4 vesicle trafficking from fusion using a temperature-sensitive Munc18c mutant. EMBO J. **19**, 3565–3575
20 D'Andrea-Merrins, M., Chang, L., Lam, A. D., Ernst, S. A. and Stuenkel, E. L. (2007) Munc18c interaction with syntaxin 4 monomers and SNARE complex intermediates in GLUT4 vesicle trafficking. J. Biol. Chem. **282**, 16553–16566
21 Oh, E. and Thurmond, D. C. (2006) The stimulus-induced tyrosine phosphorylation of Munc18c facilitates vesicle exocytosis. J. Biol. Chem. **281**, 17624–17634

Received 15 June 2007/17 October 2007; accepted 24 October 2007
Published as BJ Immediate Publication 24 October 2007, doi:10.1042/BJ20070802

REFERENCES

6. References

Actis Dato S.M., Rebolledo O.R. (2000)
Lipoprotein glycation and glycoxidation: their importance in diabetes mellitus
Medicina (B Aires). 2000;60(5 Pt 1):645-56

Adio S., Reth J., Bathe F., Woehlke G. (2006)
Review: regulation mechanisms of Kinesin-1.
J Muscle Res Cell Motil. 27(2):153-60.

Ai H., Ralston E., Lauritzen H.P., Galbo H., Ploug T. (2003)
Disruption of microtubules in rat skeletal muscle does not inhibit insulin- or contraction-stimulated glucose transport.
Am J Physiol Endocrinol Metab. 2003 Oct;285(4):E836-44

Aizawa H., Sekine Y., Takemura R., Zhang Z., Nangaku M., Hirokawa N. (1992)
Kinesin family in murine central nervous system.
J Cell Biol. 119(5):1287-96

Andrade M.A., Petosa C., O'Donoghue S.I., Müller C.W., Bork P. (2001)
Comparison of ARM and HEAT protein repeats.
J Mol Biol. 25;309(1):1-18

Antonin W., Dulubova I., Arac D., Pabst S., Plitzner J., Rizo J., Jahn R.
The N-terminal domains of syntaxin 7 and vti1b form three-helix bundles that differ in their ability to regulate SNARE complex assembly.
J Biol Chem. 2002 Sep 27;277(39):36449-56

Bandyopadhyay, G., Sajan, M. P., Kanoh, Y., Standaert, M. L., Quon, M. J., Lea-Currie, R.,Sen, A. and Farese, R. V. (2002)
PKC-zeta mediates insulin effects on glucose transport in cultured preadipocyte-derived human adipocytes.
J. Clin. Endocrinol. Metab. 87, 716–723

Bandyopadhyay G., Standaert M.L., Galloway L., Moscat J., Farese R.V. (1997)
Evidence for involvement of protein kinase C (PKC)-zeta and noninvolvement of diacylglycerol-sensitive PKCs in insulin-stimulated glucose transport in L6 myotubes.
Endocrinology. 138(11):4721-31.

Bandyopadhyay, G., Standaert, M. L., Sajan, M. P., Kanoh, Y., Miura, A., Braun, U., Kruse, F., Leitges, M. and Farese, R. V. (2004)
Protein kinase C-lambda knockout in embryonic stem cells and adipocytes impairs insulin stimulated glucose transport.
Mol. Endocrinol. 18, 373–383

Bandyopadhyay, G., Standaert, M.L., Kikkawa, U., Ono, Y., Moscat, J., Farese, R.V. (1999).
Effects of transiently expressed atypical (□□), conventional (□□) and novel (□□) protein kinase C isoforms on insulin-stimulated translocation of epitope-tagged GLUT4 glucose transporters in rat adipocytes: specific interchangeable effects of protein kinases C-λ and C-ζ.
Biochem. J. 337, 461-470

Bandyopadhyay G., Standaert M.L., Zhao L., Yu B., Avignon A., Galloway L., Karnam P., Moscat J., Farese R.V. (1997)
Activation of protein kinase C (alpha, beta, and zeta) by insulin in 3T3/L1 cells. Transfection studies suggest a role for PKC-zeta in glucose transport.
J Biol Chem. 272(4):2551-8.

Banta L..M.., Vida T..A.., Herman P..K.., Emr S..D. (1990)
Characterization of yeast Vps33p, a protein required for vacuolar protein sorting and vacuole biogenesis
Mol Cell Biol. Sep;10(9):4638-49.

Beeson, M., Sajan, M.P., Dizon, M., Grebenev, D., Gomez-Daspet, J., Miura, A., Kanoh, Y., Powe, J., Bandyopadhyay, G., Standaert, M.L., Farese, R.V. (2003)
Activation of protein kinase C-zeta by insulin and phosphatidylinositol-3,4,5-(PO4)3 is defective in muscle in type 2 diabetes and impaired glucose tolerance: amelioration by rosiglitazone and exercise
Diabetes. 52(8):1926-34

Bennett M.K., Calakos N., Scheller R.H. (1992)
Syntaxin: a synaptic protein implicated in docking of synaptic vesicles at presynaptic active zones.
Science. 10;257(5067):255-9

Bloomgarden Z.T. (2000)
Obesity and diabetes.
Diabetes Care. 23(10):1584-90. Review.

Braiman L., Alt A., Kuroki T., Ohba M., Bak A., Tennenbaum T., Sampson S.R. (2001)
Activation of protein kinase C zeta induces serine phosphorylation of VAMP2 in the GLUT4 compartment and increases glucose transport in skeletal muscle.
Mol Cell Biol. 21(22):7852-61.

Brewer, D. (2006.)
Are alpha-glucosidase inhibitors effective for control of type 2 diabetes?
Am Fam Physician. 2006 Feb 1;73(3):433-4. Review.

Brule S., Rabahi F., Faure R., Beckers J.F., Silversides D.W., Lussier J.G. (2000)
Vacuolar system-associated protein-60: a protein characterized from bovine granulosa and luteal cells that is associated with intracellular vesicles and related to human 80K-H and murine beta-glucosidase II.
Biol Reprod. 62(3):642-54.

Bracher A., Weissenhorn W. (2002)
Structural basis for the Golgi membrane recruitment of Sly1p by Sed5p.
EMBO J. 21(22):6114-24

Cao X., Ballew N., Barlowe C. (1998)
Initial docking of ER-derived vesicles requires Uso1p and Ypt1p but is independent of SNARE proteins.
EMBO J. 17(8):2156-65.

Carr C.M., Grote E., Munson M., Hughson F.M., Novick P.J.
Sec1p binds to SNARE complexes and concentrates at sites of secretion.
J Cell Biol. 1999 Jul 26;146(2):333-44.

Chang, L., Chiang, S.H., Saltiel, A.R. (2004).
Insulin signaling and the regulation of glucose transport.
Mol Med. 10 65-71.

Chen Y.A., Scheller R.H. (2001)
SNARE-mediated membrane fusion.
Nat Rev Mol Cell Biol. 2001 Feb;2(2):98-106. Review

Chestukhin A., Litovchick L., Muradov K., Batkin M., Shaltiel S. (1997)
Unveiling the substrate specificity of meprin beta on the basis of the site in protein kinase A cleaved by the kinase splitting membranal proteinase.
J Biol Chem. 1997 Feb 7;272(6):3153-60.

Chou, M.M., Hou, W., Johnson, J., Graham, L.K., Lee, M.H., Chen, C.S., Newton, A.C., Schaffhausen, B.S., Toker, A. (1998)
Regulation of protein kinase C zeta by PI 3-kinase and PDK-1.
Curr Biol. 1998 Sep 24;8(19):1069-77

Chou, W.H. and Messing, R.O. (2005).
Protein kinase C isozymes in stroke.
Trends Cardiovasc Med. 2005 Feb;15(2):47-51

Cole D.G., Chinn S.W., Wedaman K.P., Hall K., Vuong T., Scholey J.M. (1993)
Novel heterotrimeric kinesin-related protein purified from sea urchin eggs.
Nature. 1993 Nov 18;366(6452):268-70.

Conesa-Zamora, P., Lopez-Andreo, M.J., Gomez-Fernandez, J.C., Corbalan-Garcia, S. (2001)
Identification of the phosphatidylserine binding site in the C2 domain that is important for PKC alpha activation and in vivo cell localization.
Biochemistry. 2001 Nov 20;40(46):13898-905.

Corbalan-Garcia, S. and Gomez-Fernandez, J.C. (2006)
Protein kinase C regulatory domains: the art of decoding many different signals in membranes.
Biochim Biophys Acta. 2006 Jul;1761(7):633-54

Cormont, M., Bortoluzzi, M.N., Gautier, N., Mari, M., van Obberghen, E., Le Marchand-Brustel, Y. (1996)
Potential role of Rab4 in the regulation of subcellular localization of Glut4 in adipocytes.
Mol Cell Biol. 1996 Dec;16(12):6879-86.

Cormont, M., Tanti JF, Zahraoui A, Van Obberghen E, Tavitian A, Le Marchand-Brustel Y. (1993)
Insulin and okadaic acid induce Rab4 redistribution in adipocytes.
J Biol Chem. 1993 Sep 15;268(26):19491-7.

Coughlin S.R., Barr P.J., Cousens L.S., Fretto L.J., Williams L.T. (1988)
Acidic and basic fibroblast growth factors stimulate tyrosine kinase activity in vivo.
J Biol Chem. 1988 Jan 15;263(2):988-93

Currie, R.A., Walker, K.S., Gray, A., Deak, M., Casamayor, A., Downes, C.P., Cohen, P., Alessi, D.R. and Lucocq, J. (1999)
Role of phosphatidylinositol 3,4,5-trisphosphate in regulating the activity and localization of 3-phosphoinositide-dependent protein kinase-1.
Biochem J. 1999 February 1; 337(Pt 3): 575–583.

D'Andrea-Merrins M., Chang L., Lam A.D., Ernst S.A., Stuenkel E.L. (2007)
Munc18c interaction with syntaxin 4 monomers and SNARE complex intermediates in GLUT4 vesicle trafficking.
J Biol Chem. 2007 Jun 1;282(22):16553-66.

Darsow T., Rieder S.E., Emr S.D. (1997)
A multispecificity syntaxin homologue, Vam3p, essential for autophagic and biosynthetic protein transport to the vacuole.
J Cell Biol. 1997 Aug 11;138(3):517-29.

Deneka M., Neeft M., van der Sluijs P. (2003)
Regulation of membrane transport by rab GTPases.
Crit Rev Biochem Mol Biol. 2003;38(2):121-42.

Diamant, M., Heine, R.J. (2003).
Thiazolidinediones in type 2 diabetes mellitus: current clinical evidence.
Drugs. 2003;63(13):1373-405

Drenth J.P., Martina J.A., Te Morsche R.H., Jansen J.B., Bonifacino J.S. (2004)
Molecular characterization of hepatocystin, the protein that is defective in autosomal dominant polycystic liver disease.
Gastroenterology. 2004 Jun;126(7):1819-27

Drenth J.P., Tahvanainen E., te Morsche R.H., Tahvanainen P., Kaariainen H., Hockerstedt K., van de Kamp J.M., Breuning M.H., Jansen J.B. (2004)
Abnormal hepatocystin caused by truncating PRKCSH mutations leads to autosomal dominant polycystic liver disease.
Hepatology. 2004 Apr;39(4):924-31

Drenth J.P., te Morsche R.H., Smink R., Bonifacino J.S., Jansen J.B. (2003)
Germline mutations in PRKCSH are associated with autosomal dominant polycystic liver disease.
Nat Genet. 2003 Mar;33(3):345-7

Dulubova I., Sugita S., Hill S., Hosaka M., Fernandez I., Sudhof T.C., Rizo J.A.
Aconformational switch in syntaxin during exocytosis: role of munc18.
EMBO J. 1999 Aug 16;18(16):4372-82.

Dulubova I., Yamaguchi T., Arac D., Li H., Huryeva I., Min S.W., Rizo J., Sudhof T.C.
Convergence and divergence in the mechanism of SNARE binding by Sec1/Munc18-like proteins.
Proc Natl Acad Sci U S A. 2003 Jan 7;100(1):32-7.

Durán, A., Serrano, M., Leitges, M., Flores, J. M., Picard, S., Brown, J.P., Moscat, J. and Diaz-Meco, M.T. Emoto M, Langille SE, Czech MP. (2004).

The atypical PKC-interacting protein p62 is an important mediator of RANK activated osteoclastogenesis.

Developmental Cell Vol.6 Issue2 pages 303-309

Elferink, L.A., Trimble, W.S., Scheller, R.H. (1989)
Two vesicle-associated membrane protein genes are differentially expressed in the rat central nervous system.
J Biol Chem. 1989 Jul 5;264(19):11061-4

Emoto M., Langille S.E., Czech M.P. (2001)
A role for kinesin in insulin-stimulated GLUT4 glucose transporter translocation in 3T3-L1 adipocytes.
J Biol Chem. 2001 Apr 6;276(14):10677-82

Eyster C.A., Duggins Q.S., Gorbsky G.J., and Olson A.L.. (2006)
Microtubule Network Is Required for Insulin Signaling through Activation of Akt/Protein Kinase B. Evidence That Insulin Stimulates Vesicle Docking/Fusion But Not Intracellular Mobility.
The Journal Of Biological Chemistry Vol. 281, NO. 51, pp. 39719–39727,

Fant X., Merdes A., Haren L. (2004)
Cell and molecular biology of spindle poles and NuMA.
Int Rev Cytol. 2004;238:1-57

Farese R. V. (2002)
Function and dysfunction of aPKC isoforms for glucose transport in insulin-sensitive and insulin-resistant states.
Am. J. Physiol. Endocrinol. Metab. 283, E1–E11/

Fasshauer D., Antonin W., Margittai M., Pabst S., Jahn R. (1999)
Mixed and non-cognate SNARE complexes. Characterization of assembly and biophysical properties.
J Biol Chem. 1999 May 28;274(22):15440-6

Fasshauer D., Bruns D., Shen B., Jahn R., Brunger AT. (1997)
A structural change occurs upon binding of syntaxin to SNAP-25
J Biol Chem. 1997 Feb 14;272(7):4582-90.

Fasshauer D., Eliason W.K., Brunger A.T., Jahn R. (1998)
Identification of a minimal core of the synaptic SNARE complex sufficient for reversible assembly and disassembly.
Biochemistry. 1998 Jul 21;37(29):10354-62

Felber J.P., Golay A. (2002)
Pathways from obesity to diabetes.
Int J Obes Relat Metab Disord. 2002 Sep;26 Suppl 2:S39-45. Review.

Finegood D.T. (2003)
Obesity, inflammation and type II diabetes.
Int J Obes Relat Metab Disord. 2003 Dec;27 Suppl 3:S4-5. Review.

Fletcher L.M., Welsh G.I., Oatey P.B., Tavare J.M. (2000)
Role for the microtubule cytoskeleton in GLUT4 vesicle trafficking and in the regulation of insulin-stimulated glucose uptake.
Biochem J. 2000 Dec 1;352 Pt 2:267-76.

Forbes J.M., Fukami K., Cooper M.E. (2007)
Diabetic nephropathy: where hemodynamics meets metabolism.
Exp Clin Endocrinol Diabetes. 2007 Feb;115(2):69-84.

Foster L.J., Yaworsky K., Trimble W.S., Klip A. (1999)
SNAP23 promotes insulin-dependent glucose uptake in 3T3-L1 adipocytes: possible interaction with cytoskeleton.
Am J Physiol. 276(5 Pt 1):C1108-14.

Frevert E.U., Kahn B.B. (1997)
Differential effects of constitutively active phosphatidylinositol 3-kinase on glucose transport, glycogen synthase activity, and DNA synthesis in 3T3-L1 adipocytes.
Mol Cell Biol. 1997 Jan;17(1):190-8.

Ginkel L.M., Wordeman L. (2000)
Expression and partial characterization of kinesin-related proteins in differentiating and adult skeletal muscle.
Mol Biol Cell. 2000 Dec;11(12):4143-58

Goh K.C., Lim Y.P., Ong S.H., Siak C.B., Cao X., Tan Y.H., Guy G.R. (1996)
Identification of p90, a prominent tyrosine-phosphorylated protein in fibroblast growth factor-stimulated cells, as 80K-H.
J Biol Chem. 1996 Mar 8;271(10):5832-8

Goldberg I.J., Dansky H.M. (2006)
Diabetic vascular disease: an experimental objective.
Arterioscler Thromb Vasc Biol. 2006 Aug;26(8):1693-701.

Goldstein LS, Philp AV.
The road less traveled: emerging principles of kinesin motor utilization.
Annu Rev Cell Dev Biol. 1999;15:141-83

Gotte M., Gallwitz D. (1997)
High expression of the yeast syntaxin-related Vam3 protein suppresses the protein transport defects of a pep12 null mutant.
FEBS Lett. 1997 Jul 7;411(1):48-52.

Govers R., Coster A.C., James D.E. (2004)
Insulin increases cell surface GLUT4 levels by dose dependently discharging GLUT4 into a cell surface recycling pathway.
Mol Cell Biol. 2004 Jul;24(14):6456-66

Greenberg, A.S., McDaniel, M.L. (2002)
Identifying the links between obesity, insulin resistance and beta-cell function: potential role of adipocyte-derived cytokines in the pathogenesis of type 2 diabetes.
Eur J Clin Invest. 2002 Jun;32 Suppl 3:24-34

Grusovin J., Macaulay S.L. (2003)
Snares for GLUT4--mechanisms directing vesicular trafficking of GLUT4.
Front Biosci. May 1;8:d620-41. Review.

Grusovin, J., Stoichevska, V., Gough, K.H., Nunan, K., Ward, C.W., Macaulay, S.L. (2000).
Definition of a minimal munc18c domain that interacts with syntaxin-4.
Biochem J. 350 741–746.

Guilherme A., Emoto M., Buxton J.M., Bose S., Sabini R., Theurkauf W.E., Leszyk J., Czech M.P. (2000)
Perinuclear localization and insulin responsiveness of GLUT4 requires cytoskeletal integrity in 3T3-L1 adipocytes.
J Biol Chem. 2000 Dec 8;275(49):38151-9.

Gurkan C., Lapp H., Alory C., Su A.I., Hogenesch J.B., Balch W.E. (2005)
Large-scale profiling of Rab GTPase trafficking networks: the membrome.
Mol Biol Cell. 2005 Aug;16(8):3847-64.

Gustavsson J., Parpal S., Karlsson M., Ramsing C., Thorn H., Borg M., Lindroth M., Peterson K.H., Magnusson K.E., Stralfors P. (1999)
Localization of the insulin receptor in caveolae of adipocyte plasma membrane.
FASEB J. 1999 Nov;13(14):1961-71.

Halachmi N. and Lev Z. (1996)
The Sec1 family: a novel family of proteins involved in synaptic transmission and general secretion.
J Neurochem. 1996 Mar;66(3):889-97

Hanada M., Feng J., Hemmings B.A. (2004)
Structure, regulation and function of PKB/AKT-a major therapeutic target.
Biochim Biophys Acta. 2004 Mar 11;1697(1-2):3-16. Review.

Hanson P.I., Roth R., Morisaki H., Jahn R., Heuser J.E. (1997)
Structure and conformational changes in NSF and its membrane receptor complexes visualized by quick-freeze/deep-etch electron microscopy.
Cell. 1997 Aug 8;90(3):523-35

Harrison S.D., Broadie K., van de Goor J., Rubin G.M. (1994)
Mutations in the Drosophila Rop gene suggest a function in general secretion and synaptic transmission.
Neuron. 1994 Sep;13(3):555-66

Hata Y. and Sudhof T.C. (1995)
A novel ubiquitous form of Munc-18 interacts with multiple syntaxins. Use of the yeast two-hybrid system to study interactions between proteins involved in membrane traffic.
J Biol Chem. 1995 Jun 2;270(22):13022-8

Haustein E., Schwille P. (2003)
Ultrasensitive investigations of biological systems by fluorescence correlation spectroscopy.
Methods. 2003 Feb;29(2):153-66

Hers I., Bell C.J., Poole A.W., Jiang D., Denton R.M., Schaefer E., Tavare J.M. (2002)
Reciprocal feedback regulation of insulin receptor and insulin receptor substrate tyrosine phosphorylation by phosphoinositide 3-kinase in primary adipocytes.
Biochem J. 2002 Dec 15;368(Pt 3):875-84.

Hodgkinson C.P., Mander A., Sale G.J. (2005)
Identification of 80K-H as a protein involved in GLUT4 vesicle trafficking.
Biochem J. 2005 Jun 15;388(Pt 3):785-93.

Hodgkinson C.P., Mander A., Sale G.J. (2005)
Protein kinase-zeta interacts with munc18c: role in GLUT4 trafficking.
Diabetologia. 2005 Aug;48(8):1627-36. Epub 2005 Jun 29.

Hodgkinson C.P., Sale E.M. and Sale G.J. (2002)
Characterization of PDK2 activity against protein kinase B gamma.
Biochemistry 41, 10351–10359

Hosono R., Hekimi S., Kamiya Y., Sassa T., Murakami S., Nishiwaki K., Miwa J., Taketo A., Kodaira K.I. (1992)
The unc-18 gene encodes a novel protein affecting the kinetics of acetylcholine metabolism in the nematode Caenorhabditis elegans.
J Neurochem. 1992 Apr;58(4):1517-25.

Hu S.H., Latham C.F., Gee C.L., James D.E., Martin J.L. (2007)
Structure of the Munc18c/Syntaxin4 N-peptide complex defines universal features of the N-peptide binding mode of Sec1/Munc18 proteins.
Proc Natl Acad Sci U S A. 2007 May 22;104(21):8773-8.

Huang J., Imamura T., Babendure J.L., Lu J.C., Olefsky J.M. (2005)
Disruption of microtubules ablates the specificity of insulin signaling to GLUT4 translocation in 3T3-L1 adipocytes.
J Biol Chem. 2005 Dec 23;280(51):42300-6.

Idris I., Gray S., Donnelly R. (2001)
Protein kinase C activation: isozyme-specific effects on metabolism and cardiovascular complications in diabetes.
Diabetologia. 2001 Jun;44(6):659-73. Review.

Ishiki M., Klip A. (2005).
Minireview: recent developments in the regulation of glucose transporter-4 traffic: new signals, locations, and partners.
Endocrinology. 146, 5071-8.

Ishikawa Y., Otsu K., Oshikawa J. (2005)
Caveolin; different roles for insulin signal?
Cell Signal. 2005 Oct;17(10):1175-82.

Jahn, R., Grubmuller H. (2002)
Membrane fusion.
Curr Opin Cell Biol. 2002 Aug;14(4):488-95

Jahn R., Südhof T.C. (1999.)
Membrane fusion and exocytosis.
Annu. Rev. Biochem. 68 863-911

James D. E. (2003.)
MUNC-ing around with insulin action.
J. Clin. Invest. 115 219-221

Jiang Z.Y., Zhou Q.L., Coleman K.A., Chouinard M., Boese Q., Czech M.P. (2003)
Insulin signaling through Akt/protein kinase B analyzed by small interfering RNA-mediated gene silencing.
Proc Natl Acad Sci U S A. 2003 Jun 24;100(13):7569-74..

Kahn B.B. and Flier J.S (2000)
Obesity and insulin resistance.
Clin Invest. 2000 August 15; 106(4): 473–481.

Kanai M., Goke M., Tsunekawa S., Podolsky D.K. (1997)
Signal transduction pathway of human fibroblast growth factor receptor 3. Identification of a novel 66-kDa phosphoprotein.
J Biol Chem. 1997 Mar 7;272(10):6621-8.

Kanda H., Tamori Y., Shinoda H., Yoshikawa M., Sakaue M., Udagawa J., Otani H., Tashiro F., Miyazaki J., Kasuga M. (2005)
Adipocytes from Munc18c-null mice show increased sensitivity to insulin-stimulated GLUT4 externalization.
J Clin Invest. Feb;115(2):291-301.

Kanoh Y., Sajan M.P., Bandyopadhyay G., Miura A., Standaert M.L. and Farese R.V. (2003).
Defective Activation of Atypical Protein Kinase C ζ and λ by Insulin and Phosphatidylinositol-3,4,5-$(PO_4)_3$ in Skeletal Muscle of Rats Following High-Fat Feeding and Streptozotocin-Induced Diabetes.
Endocrinology Vol. 144, No. 3 947-954

Kanzaki M., Mora S., Hwang J.B., Saltiel A.R., Pessin J.E. (2004).
Atypical protein kinase C (PKCzeta/lambda) is a convergent downstream target of the insulin-stimulated phosphatidylinositol 3-kinase and TC10 signaling pathways.
J. Cell. Biol. 164 279-90.

Kanzaki M., Pessin J.E. (2001)
Insulin-stimulated GLUT4 translocation in adipocytes is dependent upon cortical actin remodeling.
J Biol Chem. 2001 Nov 9;276(45):42436-44.

Kanzaki M., Pessin J.E. (2003).
Insulin Signaling: GLUT4 Vesicles Exit via the Exocyst.
Current Biology 13, R574–R576

Karylowski O., Zeigerer A., Cohen A., McGraw T.E. (2004)
GLUT4 is retained by an intracellular cycle of vesicle formation and fusion with endosomes.
Mol Biol Cell. 2004 Feb;15(2):870-82.

Katagiri H., Terasaki J., Murata T., Ishihara H., Ogihara T., Inukai K., Fukushima Y., Anai M., Kikuchi M., Miyazaki J. et al. (1995)
A novel isoform of syntaxin-binding protein homologous to yeast Sec1 expressed ubiquitously in mammalian cells
J Biol Chem. 1995 Mar 10;270(10):4963-6

Kavalali E.T. (2002)
SNARE interactions in membrane trafficking: a perspective from mammalian central synapses.
Bioessays. 2002 Oct;24(10):926-36. Review.

Kawanishi M., Tamori Y., Okazawa H., Araki S., Shinoda H., Kasuga M. (2000)
Role of SNAP23 in insulin-induced translocation of GLUT4 in 3T3-L1 adipocytes: mediation of complex formation between Syntaxin4 and VAMP2.
J Biol Chem. 275 8240-7.

Kirpichnikov D., McFarlane S.I., Sowers J.R. (2002)
Metformin: an update.
Ann Intern Med. 2002 Jul 2;137(1):25-33

Kondo S., Sato-Yoshitake R., Noda Y., Aizawa H., Nakata T., Matsuura Y., Hirokawa N. (1994)
KIF3A is a new microtubule-based anterograde motor in the nerve axon.
J Cell Biol. 1994 Jun;125(5):1095-107.

Krichevsky O. and Bonnet G. (2002)
Fluorescence correlation spectroscopy: the technique and its applications.
Rep. Prog. Phys. 65 (2002) 251–297

Kuroki K., Kobayashi S., Shiroishi M., Kajikawa M., Okamoto N., Kohda D., Maenaka K. (2007)
Detection of weak ligand interactions of leukocyte Ig-like receptor B1 by fluorescence correlation spectroscopy.
J Immunol Methods. 2007 Mar 30;320(1-2):172-6.

Lakämper S., Meyhöfer E. (2006)
Back on track - on the role of the microtubule for kinesin motility and cellular function.
J Muscle Res Cell Motil. 2006;27(2):161-71.

Larson D.R., Ma Y.M., Vogt V.M., Webb W.W. (2003)
Direct measurement of Gag-Gag interaction during retrovirus assembly with FRET and fluorescence correlation spectroscopy.
J Cell Biol. 2003 Sep 29;162(7):1233-44

Latham C.F., Hu S.H., Gee C.L., Armishaw C.J., Alewood P.F., James D.E., Martin J.L. (2007)
Crystallization and preliminary X-ray diffraction of the Munc18c-syntaxin4 (1-29) complex.
Acta Crystallogr Sect F Struct Biol Cryst Commun. 2007 Jun 1;63(Pt 6):524-8.

Latham C.F., Lopez J.A., Hu S.H., Gee C.L., Westbury E., Blair D.H., Armishaw C.J., Alewood P.F., Bryant N.J., James D.E., Martin J.L. (2006)
Molecular Dissection of the Munc18c/Syntaxin4 Interaction: Implications for Regulation of Membrane Trafficking.
Traffic 7 1408–1419.

Latham C.F, Meunier F.A. (2006)
Munc18a: Munc-y business in mediating exocytosis.
Int J Biochem Cell Biol. 2006 Nov 30

Le Bot N, Antony C, White J, Karsenti E, Vernos I.
Role of xklp3, a subunit of the Xenopus kinesin II heterotrimeric complex, in membrane transport between the endoplasmic reticulum and the Golgi apparatus.
J Cell Biol. 1998 Dec 14;143(6):1559-73.

Le Good J.A., Ziegler W.H., Parekh D.B., Alessi D.R., Cohen P., Parker P.J. (1998).
Protein kinase C isotypes controlled by phosphoinositide 3-kinase through the protein kinase PDK1.
Science. 1998 Sep 25;281(5385):2042-5

Li A., Davila S., Furu L., Qian Q., Tian X., Kamath P.S., King B.F., Torres V.E., Somlo S. (2003)
Mutations in PRKCSH cause isolated autosomal dominant polycystic liver disease.
Am J Hum Genet. 2003 Mar;72(3):691-703.

Li L., Omata W., Kojima I., Shibata H. (2001)
Direct interaction of Rab4 with syntaxin 4.
J Biol Chem. 2001 Feb 16;276(7):5265-73.

Li Y.M., Mitsuhashi T., Wojciechowicz D., Shimizu N., Li J., Stitt A., He C., Banerjee D., Vlassara H. (1996)
Molecular identity and cellular distribution of advanced glycation endproduct receptors: relationship of p60 to OST-48 and p90 to 80K-H membrane proteins.
Proc Natl Acad Sci U S A. 1996 Oct 1;93(20):11047-52.

Lian J.P., Stone S., Jiang Y., Lyons P., Ferro-Novick S. (1994)
Ypt1p implicated in v-SNARE activation
Nature. 1994 Dec 15;372(6507):698-701

Liao G., Gundersen G.G. (1998)
Kinesin is a candidate for cross-bridging microtubules and intermediate filaments. Selective binding of kinesin to detyrosinated tubulin and vimentin.
J Biol Chem. 1998 Apr 17;273(16):9797-803

Lippincott-Schwartz J., Snapp E., Kenworthy A. (2001)
Studying protein dynamics in living cells.
Nat Rev Mol Cell Biol. 2001 Jun;2(6):444-56.

Liu L.Z., Zhao H.L., Zuo J., Ho S.K., Chan J.C., Meng Y., Fang F.D., Tong P.C. (2006).
Protein kinase C ζ mediates insulin-induced glucose transport through actin remodeling in L6 muscle cells.
Mol. Biol. Cell. 17 2322-30

Liu X.J., Yang C., Gupta N., Zuo J., Chang Y.S., Fang F.D. (2007)
Protein kinase C-zeta regulation of GLUT4 translocation through actin remodeling in CHO cells.
J Mol Med. 2007 Aug;85(8):851-61

Lizunov V.A, Matsumoto H., Zimmerberg J., Cushman S.W., Frolov V.A. (2005)
Insulin stimulates the halting, tethering, and fusion of mobile GLUT4 vesicles in rat adipose cells.
J Cell Biol. 2005 May 9;169(3):481-9.

Lupashin V.V., Waters M.G. (1997)
t-SNARE activation through transient interaction with a rab-like guanosine triphosphatase.
Science. 1997 May 23;276(5316):1255-8

Macaulay S.L., Grusovin J., Stoichevska V., Ryan J.M., Castelli L.A., Ward C.W. (2002)
Cellular munc18c levels can modulate glucose transport rate and GLUT4 translocation in 3T3L1 cells.
FEBS Lett. 2002 Sep 25;528(1-3):154-60.

Macaulay S.L., Hewish D.R., Gough K.H., Stoichevska V., MacPherson S.F., Jagadish M., Ward C.W. (1997)
Functional studies in 3T3L1 cells support a role for SNARE proteins in insulin stimulation of GLUT4 translocation.
Biochem J. 1997 May 15;324 (Pt 1):217-24.

Macaulay S.L., Rea S., Gough K.H., Ward C.W., James D.E. (1997)
Botulinum E toxin light chain does not cleave SNAP-23 and only partially impairs insulin stimulation of GLUT4 translocation in 3T3-L1 cells.
Biochem Biophys Res Commun. 1997 Aug 18;237(2):388-93

Malide D., Dwyer N.K., Blanchette-Mackie E.J., Cushman S.W. (1997)
Immunocytochemical evidence that GLUT4 resides in a specialized translocation post-endosomal VAMP2-positive compartment in rat adipose cells in the absence of insulin.
J Histochem Cytochem. 1997 Aug;45(8):1083-96.

Manning B.D., Snyder M. (2000)
Drivers and passengers wanted! the role of kinesin-associated proteins.
Trends Cell Biol. 2000 Jul;10(7):281-9. Review

Levin M.K and Carson J.H. (2004)
Fluorescence correlation spectroscopy and quantitative cell biology
Di.erentiation (2004) 72:1–10

Milburn C.C., Deak M., Kelly S.M., Price N.C., Alessi D.R., Van Aalten D.M. (2003).
Binding of phosphatidylinositol 3,4,5-trisphosphate to the pleckstrin homology domain of protein kinase B induces a conformational change.
Biochem J. 2003 Nov 1;375(Pt 3):531-8

Min J., Okada S., Kanzaki M., Elmendorf J.S., Coker K.J., Ceresa B.P., Syu L.J., Noda Y., Saltiel A.R., Pessin J.E. (1999).
Synip A Novel Insulin-Regulated Syntaxin 4–Binding Protein Mediating GLUT4 Translocation in Adipocytes.
Mol Cell. 6 751-60.

Misura K.M., Scheller R.H., Weis W.I. (2000)
Three-dimensional structure of the neuronal-Sec1-syntaxin 1a complex.
Nature. 2000 Mar 23;404(6776):355-62

Molero J.C., Whitehead J.P., Meerloo T., James D.E. (2001)
Nocodazole inhibits insulin-stimulated glucose transport in 3T3-L1 adipocytes via a microtubule-independent mechanism.
J Biol Chem. 2001 Nov 23;276(47):43829-35. Epub 2001 Sep 24.

Moscat J. and Diaz-Meco M. T. (2000)
The atypical protein kinase Cs. Functional specificity mediated by specific protein adapters.
EMBO Rep. 1, 399–403

Muresan V., Abramson T., Lyass A., Winter D., Porro E., Hong F., Chamberlin N.L., Schnapp B.J. (1998)
KIF3C and KIF3A form a novel neuronal heteromeric kinesin that associates with membrane vesicles.
Mol Biol Cell. 1998 Mar;9(3):637-52.

Nawale R.B., Mourya V.K., Bhise S.B. (2006)
Non-enzymatic glycation of proteins: a cause for complications in diabetes.
Indian J Biochem Biophys. 2006 Dec;43(6):337-44

Neely K.A., Quillen D.A., Schachat A.P., Gardner T.W., Blankenship G.W. (1998)
Diabetic retinopathy.
Med Clin North Am. 1998 Jul;82(4):847-76

Oh E., Spurlin B.A., Pessin J.E., Thurmond D.C. (2005)
Munc18c heterozygous knockout mice display increased susceptibility for severe glucose intolerance.
Diabetes. 2005 Mar;54(3):638-47.

Oh E., Thurmond D.C. (2006)
The stimulus-induced tyrosine phosphorylation of Munc18c facilitates vesicle exocytosis.
J Biol Chem. 2006 Jun 30;281(26):17624-34.

Ohno S. and Nishizuka Y. (2002)
Protein kinase C isotypes and their specific functions.
J. Biochem. 132, 509–511

Olson A.L., Trumbly A.R., Gibson G.V. (2001)
Insulin-mediated GLUT4 translocation is dependent on the microtubule network.
J Biol Chem. 2001 Apr 6;276(14):10706-14.

Oma Y., Kino Y., Sasagawa N. and Ishiura S.
Intracellular Localization of Homopolymeric Amino Acid-containing Proteins Expressed in Mammalian Cells.
The Journal Of Biological Chemistry 279(20) 21217–21222, 2004

Omata W., Shibata H., Li L., Takata K., Kojima I. (2000)
Actin filaments play a critical role in insulin-induced exocytotic recruitment but not in endocytosis of GLUT4 in isolated rat adipocytes.
Biochem J. 2000 Mar 1;346 Pt 2:321-8

Oyler G.A., Higgins G.A., Hart R.A., Battenberg E., Billingsley M., Bloom F.E., Wilson M.C. (1989)
The identification of a novel synaptosomal-associated protein, SNAP-25, differentially expressed by neuronal subpopulations.
J Cell Biol. 1989 Dec;109(6 Pt 1):3039-52.

Parlati F., McNew J.A., Fukuda R., Miller R., Sollner T.H., Rothman J.E. (2000)
Topological restriction of SNARE-dependent membrane fusion.
Nature. 2000 Sep 14;407(6801):194-8

Patel N., Huang C., Klip A. (2006).
Cellular location of insulin-triggered signals and implications for glucose uptake.
Eur J Physiol. 451, 499–510

Peifer M., Berg S., Reynolds A.B. (1994)
A repeating amino acid motif shared by proteins with diverse cellular roles.
Cell. 1994 Mar 11;76(5):789-91.

Pelham H.R.(2001)
SNAREs and the specificity of membrane fusion.
Trends Cell Biol. 2001 Mar;11(3):99-101. Review

Pesavento P.A., Stewart R.J., Goldstein L.S. (1994)
Characterization of the KLP68D kinesin-like protein in Drosophila: possible roles in axonal transport.
J Cell Biol. 1994 Nov;127(4):1041-8

Pittas AG., Joseph N.A., Greenberg A.S. (2004).
Adipocytokines and insulin resistance.
J Clin Endocrinol Metab. 2004 Feb;89(2):447-52.

Poirier M.A., Hao J.C., Malkus P.N., Chan C., Moore M.F., King D.S., Bennett M.K. (1998)
Protease resistance of syntaxin.SNAP-25.VAMP complexes. Implications for assembly and structure.
J Biol Chem. 1998 May 1;273(18):11370-7.

Poirier M.A., Xiao W., Macosko J.C., Chan C., Shin Y.K., Bennett M.K. (1998).
The synaptic SNARE complex is a parallel four-stranded helical bundle.
Nat Struct Biol. 1998 Sep;5(9):765-9.

Puls A., Schmidt S., Grawe F. and Stabel S.
Interaction of protein kinase C ζ with ZIP, a novel protein kinase C-binding protein.
*Proc. Natl. Acad. Sci. USA*Vol. 94, pp. 6191–6196, June 1997 Cell Biology

Rea S., Martin L.B., McIntosh S., Macaulay S.L., Ramsdale T., Baldini G., James D.E. (1998)
Syndet, an adipocyte target SNARE involved in the insulin-induced translocation of GLUT4 to the cell surface.
J Biol Chem. 1998 Jul 24;273(30):18784-92.

Rice L.M., Brennwald P., Brunger A.T. (1997)
Formation of a yeast SNARE complex is accompanied by significant structural changes.
FEBS Lett. 1997 Sep 22;415(1):49-55

Rizo J., Sudhof T.C. (2002)
Snares and Munc18 in synaptic vesicle fusion.
Nat Rev Neurosci. 2002 Aug;3(8):641-53. Review.

Rudich A., Klip A. (2003).
Push/pull mechanisms of GLUT4 traffic in muscle cells.
Acta Physiol Scand 178 297–308.

Said G. (2007)
Diabetic neuropathy-a review.
Nat Clin Pract Neurol. 2007 Jun;3(6):331-40

Sajan M.P., Rivas J., Li P., Standaert M.L., and Farese R.V. (2006).
Repletion of Atypical Protein Kinase C following RNA Interference-mediated Depletion Restores Insulin-stimulated Glucose Transport.
J. Biol. Chem. 281 17466-17473

Sajan M.P., Standaert M.L., Miura M., Bandyopadhyay G., Vollenweider P., Franklin D.M., Lea-Currie R. and Farese R.V. (2004)
Impaired Activation of Protein Kinase C-ζ by Insulin and Phosphatidylinositol-3,4,5-$(PO_4)_3$ in Cultured Preadipocyte-Derived Adipocytes and Myotubes of Obese Subjects
The Journal of Clinical Endocrinology & Metabolism Vol. 89, No. 8 3994-3998

Sano H., Kane S., Sano E., Lienhard G.E. (2005)
Synip phosphorylation does not regulate insulin-stimulated GLUT4 translocation.
Biochem Biophys Res Commun. 2005 Jul 8;332(3):880-4.

Sato T., Iwaki M., Shimogaito N., Wu X., Yamagishi S., Takeuchi M. (2006)
TAGE (toxic AGEs) theory in diabetic complications.
Curr Mol Med. 2006 May;6(3):351-8

Schoch S., Deak F., Konigstorfer A., Mozhayeva M., Sara Y., Sudhof T.C., Kavalali E.T. (2001)
SNARE function analyzed in synaptobrevin/VAMP knockout mice
Science. 2001 Nov 2;294(5544):1117-22

Schulze K.L., Littleton J.T., Salzberg A., Halachmi N., Stern M., Lev Z., Bellen H.J. (1994)
rop, a Drosophila homolog of yeast Sec1 and vertebrate n-Sec1/Munc-18 proteins, is a negative regulator of neurotransmitter release in vivo
Neuron. 1994 Nov;13(5):1099-108

Scott B.L., Van Komen J.S., Irshad H., Liu S., Wilson K.A., McNew J.A. (2004)
Sec1p directly stimulates SNARE-mediated membrane fusion in vitro
J Cell Biol. 2004 Oct 11;167(1):75-85

Semiz S., Park J.G., Nicoloro S.M., Furcinitti P., Zhang C., Chawla A., Leszyk J., Czech M.P. (2003)
Conventional kinesin KIF5B mediates insulin-stimulated GLUT4 movements on microtubules.
EMBO J. 2003 May 15;22(10):2387-99

Shigematsu S., Khan A.H., Kanzaki M., Pessin J.E. (2002)
Intracellular insulin-responsive glucose transporter (GLUT4) distribution but not insulin-stimulated GLUT4 exocytosis and recycling are microtubule dependent.
Mol Endocrinol. 2002 May;16(5):1060-8.

Signor D., Wedaman K.P., Rose L.S., Scholey J.M. (1999)
Two heteromeric kinesin complexes in chemosensory neurons and sensory cilia of Caenorhabditis elegans.
Mol Biol Cell. 1999 Feb;10(2):345-60

Smart E.J., Graf G.A., McNiven M.A., Sessa W.C., Engelman J.A., Scherer P.E., Okamoto T., Lisanti MP.
Caveolins, liquid-ordered domains, and signal transduction.
Mol Cell Biol. 1999 Nov;19(11):7289-304. Review.

Soldatos G., Cooper M.E. (2006)
Advanced glycation end products and vascular structure and function.
Curr Hypertens Rep. 2006 Dec;8(6):472-8.

Sollner, T., Whiteheart, S.W., Brunner, M., Erdjument-Bromage, H., Geromanos, S., Tempst, P., Rothman, J.E. (1993)
SNAP receptors implicated in vesicle targeting and fusion.
Nature. 1993 Mar 25;362(6418):318-24

Spurlin B.A., Park S.Y., Nevins A.K., Kim J.K., Thurmond D.C. (2004)
Syntaxin 4 transgenic mice exhibit enhanced insulin-mediated glucose uptake in skeletal muscle.
Diabetes. 2004 Sep;53(9):2223-31.

Spurlin B.A., Thomas R.M., Nevins A.K., Kim H.J., Kim Y.J., Noh H.L., Shulman G.I., Kim J.K., Thurmond D.C. (2003)
Insulin resistance in tetracycline-repressible Munc18c transgenic mice.
Diabetes. 2003 Aug;52(8):1910-7.

Standaert M.L., Bandyopadhyay G., Perez L., Price D., Galloway L., Poklepovic A., Sajan M.P., Cenni V., Sirri A., Moscat J., Toker A., Farese R.V. (1999)
Insulin activates protein kinases C-zeta and C-lambda by an autophosphorylation-dependent mechanism and stimulates their translocation to GLUT4 vesicles and other membrane fractions in rat adipocytes.
J Biol Chem. 1999 Sep 3;274(36):25308-16.

Sutton R.B., Fasshauer D., Jahn R., Brunger A.T. (1998)
Crystal structure of a SNARE complex involved in synaptic exocytosis at 2.4 A resolution.
Nature. 1998 Sep 24;395(6700):347-53

Schwille P. and Haustein E.
Fluorescence Correlation Spectroscopy : An Introduction to its Concepts and Applications

Tamori Y., Kawanishi M., Niki T., Shinoda H., Araki S., Okazawa H., Kasuga M. (1998)
Inhibition of insulin-induced GLUT4 translocation by Munc18c through interaction with syntaxin4 in 3T3-L1 adipocytes.
J Biol Chem. 1998 Jul 31;273(31):19740-6.

Tan A.L., Forbes J.M., Cooper M.E. (2007)
AGE, RAGE, and ROS in diabetic nephropathy.
Semin Nephrol. 2007 Mar;27(2):130-43.

Tellam J.T., Macaulay S.L., McIntosh S., Hewish D.R., Ward C.W., James D.E. (1997)
Characterization of Munc-18c and syntaxin-4 in 3T3-L1 adipocytes. Putative role in insulin-dependent movement of GLUT-4.
J Biol Chem. 1997 Mar 7;272(10):6179-86.

Tellam J.T., McIntosh S., James D.E. (1995)
Molecular identification of two novel Munc-18 isoforms expressed in non-neuronal tissues.
J Biol Chem. 1995 Mar 17;270(11):5857-63.

Titu M.A., Gilbert S.P. (1999)
The diversity of molecular motors: an overview.
Cell Mol Life Sci. 1999 Oct 15;56(3-4):181-3

Thornalley P.J. (1998).
Cell activation by glycated proteins. AGE receptors, receptor recognition factors and functional classification of AGEs.
Cell Mol Biol 44 1013-23.

Thurmond D.C., Ceresa B.P., Okada S., Elmendorf J.S., Coker K., Pessin J.E. (1998)
Regulation of insulin-stimulated GLUT4 translocation by Munc18c in 3T3L1 adipocytes.
J Biol Chem. 1998 Dec 11;273(50):33876-83.

Thurmond D.C., Kanzaki M., Khan A.H., Pessin J.E. (2000)
Munc18c function is required for insulin-stimulated plasma membrane fusion of GLUT4 and insulin-responsive amino peptidase storage vesicles.
Mol Cell Biol. 2000 Jan;20(1):379-88.

Tsakiridis T., McDowell H.E., Walker T., Downes C.P., Hundal H.S., Vranic M., Klip A. (1995)
Multiple roles of phosphatidylinositol 3-kinase in regulation of glucose transport, amino acid transport, and glucose transporters in L6 skeletal muscle cells.
Endocrinology. 1995 Oct;136(10):4315-22.

Tsuru M., Katagiri H., Asano T., Yamada T., Ohno S., Ogihara T., Oka Y. (2002)
Role of PKC isoforms in glucose transport in 3T3-L1 adipocytes: insignificance of atypical PKC.
Am J Physiol Endocrinol Metab. 2002 Aug;283(2):E338-45.

Ungermánn C. and Wickner W. (1998)
Vam7p, a vacuolar SNAP-25 homolog, is required for SNARE complex integrity and vacuole docking and fusion
EMBO J. 1998 Jun 15;17(12):3269-76

VanRheenen S.M., Cao X., Lupashin V.V., Barlowe C., Waters M.G. (1998)
Sec35p, a novel peripheral membrane protein, is required for ER to Golgi vesicle docking.
J Cell Biol. 1998 Jun 1;141(5):1107-19

Verhage M., Maia A.S., Plomp J.J., Brussaard A.B., Heeroma JH., Vermeer H., Toonen R.F., Hammer R.E., van den Berg T.K., Missler M., Geuze H.J., Südhof T.C. (2000)
Synaptic assembly of the brain in the absence of neurotransmitter secretion.
Science. 2000 Feb 4;287(5454):864-9

Verhage M., Maia A.S., Plomp J.J., Brussaard A.B., Heeroma J.H., Vermeer H., Toonen R.F., Hammer R.E., van den Berg T.K., Missler M., Geuze H.J., Sudhof T.C. (2000)
Synaptic assembly of the brain in the absence of neurotransmitter secretion.
Science. 2000 Feb 4;287(5454):864-9

Verhey K.J., Rapoport T.A. (2001)
Kinesin carries the signal.
Trends Biochem Sci. 2001 Sep;26(9):545-50

Vilinsky I., Stewart B.A., Drummond J., Robinson I., Deitcher D.L. (2002)
A Drosophila SNAP-25 null mutant reveals context-dependent redundancy with SNAP-24 in neurotransmission.
Genetics. 2002 Sep;162(1):259-71

Volchuk A., Wang Q., Ewart H.S., Liu Z., He L., Bennett M.K., Klip A. (1996)
Syntaxin 4 in 3T3-L1 adipocytes: regulation by insulin and participation in insulin-dependent glucose transport.
Mol Biol Cell. 1996 Jul;7(7):1075-82.

Vukojevic V., Pramanik A., Yakovleva T., Rigler R., Terenius L., and Bakalkin G. (2005)
Study of molecular events in cells by fluorescence correlation spectroscopy
CMLS, Cell. Mol. Life Sci. 62 (2005) 535–550

Walther Z., Vashishtha M., Hall J.L. (1994)
The Chlamydomonas FLA10 gene encodes a novel kinesin-homologous protein.
J Cell Biol. 1994 Jul;126(1):175-88.

Washbourne P., Thompson P.M., Carta M., Costa E.T., Mathews J.R., Lopez-Bendito G., Molnar Z., Becher M.W., Valenzuela C.F., Partridge L.D., Wilson M.C. (2002)
Genetic ablation of the t-SNARE SNAP-25 distinguishes mechanisms of neuroexocytosis.
Nat Neurosci. 2002 Jan;5(1):19-26

Watson R.T., Kanzaki M., Pessin J.E. (2004)
Regulated membrane trafficking of the insulin-responsive glucose transporter 4
in adipocytes.
Endocr Rev. 2004 Apr;25(2):177-204

Watson R.T. and Pessin J.E. (2001).
Subcellular compartmentalization and trafficking of the insulin-responsive glucose transporter, GLUT4.
Experimental Cell Research 271, 75–83.

Wei M.L., Bonzelius F., Scully R.M., Kelly R.B., Herman G.A. (1998)
GLUT4 and transferrin receptor are differentially sorted along the endocytic pathway in CHO cells.
J Cell Biol. 1998 Feb 9;140(3):565-75.

Whitehead J.L., Wang S.Y., Bost-Usinger L., Hoang E., Frazer K.A., Burnside B. (1999)
Photoreceptor localization of the KIF3A and KIF3B subunits of the heterotrimeric microtubule motor kinesin II in vertebrate retina.
Exp Eye Res. 1999 Nov;69(5):491-503.

Woodman P. (1998)
Vesicle transport: more work for the Rabs?
Curr Biol. 1998 Mar 12;8(6):R199-201

Wordeman L. (2005)
Microtubule-depolymerizing kinesins.
Curr Opin Cell Biol. 2005 Feb;17(1):82-8

Yamada E., Okada S., Saito T., Ohshima K., Sato M., Tsuchiya T., Uehara Y., Shimizu H., Mori M. (2005)
Akt2 phosphorylates Synip to regulate docking and fusion of GLUT4-containing vesicles.
J Cell Biol. 2005 Mar 14;168(6):921-8.

Yamagishi S., Nakamura K., Matsui T. (2006)
Advanced glycation end products (AGEs) and their receptor (RAGE) system in diabetic retinopathy.
Curr Drug Discov Technol. 2006 Mar;3(1):83-8

Yamagishi S., Ueda S., Okuda S. (2007)
A possible involvement of crosstalk between advanced glycation end products (AGEs) and asymmetric dimethylarginine (ADMA), an endogenous nitric oxide synthase inhibitor in accelerated atherosclerosis in diabetes.
Med Hypotheses. 2007 Mar 16; [Epub ahead of print]

Yamamoto M., Toya Y., Schwencke C., Lisanti M.P., Myers M.G. Jr, Ishikawa Y. (1998)
Caveolin is an activator of insulin receptor signaling.
J Biol Chem. 1998 Oct 9;273(41):26962-8.

Yamaguchi T., Dulubova I., Min S.W., Chen X., Rizo J., Sudhof T.C. (2002)
Sly1 binds to Golgi and ER syntaxins via a conserved N-terminal peptide motif.
Dev Cell. 2002 Mar;2(3):295-305.

Yamazaki H., Nakata T., Okada Y., Hirokawa N. (1995)
KIF3A/B: a heterodimeric kinesin superfamily protein that works as a microtubule plus end-directed motor for membrane organelle transport.
J Cell Biol. 1995 Sep;130(6):1387-99.

Yamazaki H., Nakata T., Okada Y., Hirokawa N. (1996)
Cloning and characterization of KAP3: a novel kinesin superfamily-associated protein of KIF3A/3B.
Proc Natl Acad Sci U S A. 1996 Aug 6;93(16):8443-8.

Yang B., Gonzalez L. Jr, Prekeris R., Steegmaier M., Advani R.J., Scheller R.H. (1999)
SNARE interactions are not selective. Implications for membrane fusion specificity.
J Biol Chem. 1999 Feb 26;274(9):5649-53.

Yang C., Coker K.J., Kim J.K., Mora S., Thurmond D.C., Davis A.C., Yang B., Williamson R.A., Shulman G.I., Pessin J.E. (2001)
Syntaxin 4 heterozygous knockout mice develop muscle insulin resistance.
J Clin Invest. 2001 May;107(10):1311-8.

Yang J.T., Laymon R.A., Goldstein L.S. (1989)
A three-domain structure of kinesin heavy chain revealed by DNA sequence and microtubule binding analyses.
Cell. 1989 Mar 10;56(5):879-89.

Yang Z., Goldstein L.S. (1998)
Characterization of the KIF3C neural kinesin-like motor from mouse.
Mol Biol Cell. 1998 Feb;9(2):249-61.

Yang Z., Hanlon D.W., Marszalek J.R., Goldstein L.S. (1997)
Identification, partial characterization, and genetic mapping of kinesin-like protein genes in mouse.
Genomics. 1997 Oct 1;45(1):123-31

Yang Z., Makita Z., Horii Y., Brunelle S., Cerami A., Sehajpal P., Suthanthiran M., Vlassara H. (1991)
Two novel rat liver membrane proteins that bind advanced glycosylation endproducts: relationship to macrophage receptor for glucose-modified proteins.
J Exp Med. 1991 Sep 1;174(3):515-24

Yu C., Cresswell J., Loffler M.G., Bogan J.S. (2007)
The glucose transporter 4-regulating protein TUG is essential for highly insulin-responsive glucose uptake in 3T3-L1 adipocytes.
J Biol Chem. 2007 Mar 9;282(10):7710-22

Zerial M., McBride H. (2001)
Rab proteins as membrane organizers.
Nat Rev Mol Cell Biol. 2001 Feb;2(2):107-17. Review.

Zhou Q.L., Park J.G., Jiang Z.Y., Holik J.J., Mitra P., Semiz S., Guilherme A., Powelka A.M, Tang X., Virbasius J., Czech M.P. (2004)
Analysis of insulin signalling by RNAi-based gene silencing.
Biochem Soc Trans. 2004 Nov;32(Pt 5):817-21.

Zimmerman B.R. (1997).
Sulfonylureas.
Endocrinology and metabolism clinics of North America1997;26:511-522.